Partial saturation as a means of liquefaction mitigation in granular soil.

Copp, Darren Mark

PARTIAL SATURATION AS A MEANS OF LIQUEFACTION MITIGATION IN GRANULAR SOIL

Ph.D. Thesis by

DARREN MARK COPP B.SC (WALES), M.SC. (WALES)

March 2003

Supervisor : Professor G.N. Pande

Department of Civil Engineering

University of Wales, Swansea

ProQuest LLC.
789 East Eisenhower Parkway
P.O. Box 1346
Ann Arbor, MI 48106 – 1346

DECLARATION

I declare that this work has not previously been accepted in substance for any degree, nor is it being concurrently submitted in candidature for any degree.

Candidate _____

Signed _____

Date _____

STATEMENT 1

This thesis is the results of my own investigations, except where otherwise stated. Other sources are acknowledged by specific reference. A bibliography of these references is appended.

Candidate _____

Signed _____

Date _____

STATEMENT 2

I hereby consent for this thesis, if accepted, to be available for photocopying and for inter-library loan, and for the title to be made available to outside organisations.

Candidate _____

Signed _____

Date _____

ACKNOWLEDGEMENTS

Firstly, I wish to express my appreciation to **Professor Gyan Pande** for giving me the opportunity to complete this Ph.D., for his suggestions in the process, and for his forbearance from a very early stage.

To my parents, **Arthur** and **Sandra**, who I believe I constantly surprised with my desire to succeed, a simple 'thank you' would not be enough. The tremendous sacrifices that they have made in order that I could continue with this work have always been hugely appreciated.

To my great aunt and uncle, **Esther** and **Hubert**, who have been a constant source of inspiration for many, many years.

This thesis would not have been possible without the tremendous ability of the technicians at the Faculty of Engineering at Swansea University. Firstly, I must mention **Mr. Ian Evans**, who is one of the most skilled individuals I have ever met, and whose efforts meant that the practical phase of this work could be completed with total confidence.

Also, to **Mr. Clive Francis**, **Mr. Steve Jones**, and **Mr. Paul Tregembo**, who were always ready to assist with magnificent contributions when I had Ian doing other things! A special 'thank you' goes to **Mr. Tony Jolly**, who made his computer system available to me during the early months of my research, and who also made contributions during the later stages. Finally, to **Mr. Brian Lewis**, who has since retired as a technician, but will be remembered for his invaluable contribution, once again during the earliest stages of this work.

To the technicians in **Chemical Engineering**, particularly **Mr. Gary Tuckett**, many thanks for getting the oscillating box ready in good time.

Thanks also go to **Dr. Bob Allen**, who was always ready to encourage me in any way he could, to the ever-industrious **Mrs. Lucik Jenkins**, and also to **Mrs. Lynette Jones**, who always seemed to know when a smile was needed.

To my business partner **Graham**, to his wife **Alyson**, and to their children **Richard** and **Kelly**, I appreciate your patience with me while I've been dividing my time between Audacia Ltd. and my Ph.D.

A big thank you must go to my good friend **Terry Griffiths** who, despite his own wide-reaching commitments in the world of snooker, was still able to take the time out to understand what I was attempting to achieve, and was always willing to provide any moral and professional support that he could.

Finally, a very special tribute must go to the many, many children who I have helped with their snooker over the past six years. I have always asked for determination, effort, and a will to succeed from them; sometimes, I've not been able to exude these important qualities myself. They have all been a constant source of inspiration to me, and I am privileged to be able to call them my friends.

SUMMARY

Liquefaction of loose sand deposits has been a widely-researched branch of geotechnical engineering after it first came to prominence during the Niigata/Alaskan earthquakes of 1964.

Since then, engineers have developed various methods of liquefaction mitigation, in which soil improvement techniques are employed in order that the local development of those criteria which affect a soil's liquefaction susceptibility are inhibited. The most important of these criteria is rises in excess pore-water pressure, which reduces the effective stress, thereby reducing its shear strength.

This thesis proposes the use of partially saturated soil as a means of liquefaction mitigation, as opposed to the more invasive methods, which are currently advocated in the geotechnical engineering industry. Partial saturation induces matric suction within a given soil mass. The matric suction, being a tensile stress, increases the effective stress and thereby increases the shear strength of the soil. Furthermore, partial saturation reduces the bulk modulus of pore pressure resulting in a lesser rise in pore pressure. For validating the above hypothesis, a series of undrained one-way stress-controlled cyclic tests have been conducted.

A newly-formulated method of preparing loose, partially saturated sand specimens for triaxial testing has been proposed. Experimental studies indicate that even a slightest decrease in the degree of saturation leads to considerable reduction in the generation of pore-water pressure. A series of tests on a partially saturated loose sand bed in a sinusoidally-oscillating box have confirmed the observations made in the triaxial tests.

GENERAL NOTATION

This Section gives the general notation, and typical units and dimensions, of variables and constants which have been used in this work.

Symbol	General Description	Units/Dimensions
a, $a(t)$	Acceleration	m/s^2
B	Skempton Pore-Water Pressure Parameter	Dimensionless
c'	Effective Cohesion	kPa or kN/m^2
D_r	Relative Density	Dimensionless
E	Young's Modulus	kPa or kN/m^2
e	Void Ratio	Dimensionless
e_c	Critical Void Ratio	Dimensionless
e_0	Initial Void Ratio	Dimensionless
G	Shear Modulus	kPa or kN/m^2
G_{max}	Maximum Shear Modulus	kPa or kN/m^2
G_s	Specific Gravity of Soil Particles	Dimensionless
g	Acceleration due to Gravity	m/s^2 or ft/sec^2
h	Volumetric Coefficient of Solubility	Dimensionless
K_0	Coefficient of Earth Pressure at Rest	Dimensionless
M	Total Mass of Soil	[M]
M_a	Total Mass of Air (often assumed negligible)	[M]
M_s	Total Mass of Solids	[M]
M_w	Total Mass of Water	[M]
n	Porosity	Dimensionless
p, p'	Stress Invariants	kPa or kN/m^2
p'_0	Effective Normal Stress	kPa or kN/m^2
q	Stress Invariant	kPa or kN/m^2
R_S	Radius of Curvature of the Contractile Skin	[L]
r_0	Excess Pore-Water Pressure Ratio	Dimensionless
$r_{0,10}$	Excess Pore-Water Pressure Ratio after 10 Cycles	Dimensionless
S_r	Degree of Saturation	Dimensionless

S_{r0}	Initial Degree of Saturation	Dimensionless
S_{su}	Steady State Strength of a Soil	kPa or kN/m^2
T	Surface Tension	Nm^{-1}
t	Time	s
u_a	Pore-Air Pressure	kPa or kN/m^2
u_{a0}	Initial Pore-Air Pressure	kPa or kN/m^2
u_{af}	Pore-Air Pressure at Failure	kPa or kN/m^2
u_a-u_w	Matric Suction	kPa or kN/m^2
u_e, u_{excess}	Excess Pore-Water Pressure	kPa or kN/m^2
u_w	Pore-Water Pressure	kPa or kN/m^2
$u_{w, max}$	Maximum Pore-Water Pressure	kPa or kN/m^2
u_{wf}	Excess Pore-Water Pressure at Failure	kPa or kN/m^2
V	Volume (Total)	[L]^3
V_a	Volume of Pore-Air	[L]^3
V_d	Volume of Dissolved Gas in a Liquid	[L]^3
V_s	Volume of Solids	[L]^3
V_v	Volume of Voids	[L]^3
V_w	Volume of Pore-Liquid (normally Water)	[L]^3
v	Specific Volume	Dimensionless
v_s	Shear Wave Velocity	m/s ([L][T]$^{-1}$)
w	Moisture Content	Dimensionless
z	Depth within a Soil or Rock Layer	m
γ	Unit Weight	kN/m^3
γ_{xz}	Shear Strain	Dimensionless
ε_c	Cyclic Shear Strain	Dimensionless
ε_x, ε_z	Normal Strains	Dimensionless
θ	Angle of Principal Shear Stress from Vertical	Degree (°)
θ_w	Volumetric Water Content	Dimensionless
ν	Poisson's Ratio	Dimensionless
ρ	Bulk Density	kg/m^3
ρ_d	Dry Density	kg/m^3
ρ_s	Density of Solids	kg/m^3

$\rho_{saturated}$	Saturated Density	kg/m^3
ρ_w	Density of Water	kg/m^3
σ	Total Overburden Stress	kPa or kN/m^2
σ'	Total Effective Stress	kPa or kN/m^2
σ'_0	Initial Effective Overburden Stress	kPa or kN/m^2
σ_1	Major Principal Stress	kPa or kN/m^2
σ_2	Intermediate Principal Stress	kPa or kN/m^2
σ'_{3c}	Minor Principal Stress (Effective)	kPa or kN/m^2
σ_a	Confining or All-Round (Ambient) Pressure	kPa or kN/m^2
σ_c	Normal Stress during Consolidation	kPa or kN/m^2
σ_{dc}	Applied Deviatoric Stress	kPa or kN/m^2
σ_{ff}	Total Normal Stress on Failure Plane at Failure	kPa or kN/m^2
σ_{mc}	Mean Principal Stress during Consolidation	kPa or kN/m^2
σ_z	Geostatic Stress at Depth 'z'	kPa or kN/m^2
τ_{cyc}	Cyclic Shear Stress	kPa or kN/m^2
τ_{ff}	Shear Stress on Failure Plane at Failure	kPa or kN/m^2
τ_{hv}	Shear Stress on Horizontal and Vertical Planes	kPa or kN/m^2
τ_p	Peak Shear Stress	kPa or kN/m^2
τ_s	Static Shear Stress	kPa or kN/m^2
τ_{max}	Maximum Shear Stress	kPa or kN/m^2
ϕ'	Effective Angle of Internal Friction	Degree (°)
ϕ^b	Angular Value in Extended Failure Criterion	Degree (°)
χ	Unification Variable for Partially Saturated Soil	Dimensionless
ψ'	Slope of the Drained Failure Envelope	Dimensionless
ψ_L	Slope of the Flow Liquefaction Surface	Dimensionless

CONTENTS

CHAPTER 1

INTRODUCTION

1.1 OPENING REMARKS

1.1.1 Outline

Of all the topics currently residing under the generic title of Geotechnical Earthquake Engineering, those relating to the phenomenon of liquefaction have arguably received the most attention over the last 35 years. Workers around the world have researched the subject both experimentally and numerically throughout that time, although a common approach has yet to transpire.

The importance of liquefaction, and the destruction it is able to cause, first came to prominence following an analysis of the aftermath of the Alaska and Niigata earthquakes in 1964 (e.g. Seed and Idriss, 1967). In both cases, the liquefaction-induced damage included numerous failures in structural foundations and natural slopes, as well as loss of human life. Clearly, with respect to this last point, a unified theory of liquefaction assumes a high importance and, as part of the requirements of this particular thesis, an attempt is made to bring many of the theoretical standpoints together.

Various numerical models have been presented in the literature in an attempt to understand the process of liquefaction. Many have addressed the characteristics of liquefaction (e.g. Castro and Poulos, 1977; Tsatsanifos and Sarma, 1982), rather than directing attention toward mitigation, although there have been some noteworthy attempts to forward analytical models (e.g. Pyke, 1979; Kagawa and Leland, 1981) for a mathematical description of the liquefaction process. Experimental research has also had a significant effect on the understanding of liquefaction (e.g. Finn et. al., 1971; Yoshimi and Tokimatsu, 1977), while rigorous examination of the role of the soil characteristics has also been considered (e.g. Wong et. al. 1975; Blazquez et. al. 1980). This work will incorporate and, where applicable, adapt and actively comment on the published findings from all of the above areas.

In recent years, more attention has been given to prevention or, at least, the reduction of the detrimental effects of liquefaction on the environment. The procedures currently being employed in the field in order to reduce liquefaction hazards will be discussed, and an innovative method involving partially saturated soils will be presented. Such soils have themselves been the subject of much

academic debate as their importance in geotechnical engineering is now being realised, and here an attempt is made to exploit the properties of partially saturated soils in the key area of liquefaction mitigation.

It is known that liquefaction is most common in non-cohesive, saturated soil deposits in the loose condition, which are then subjected to transient or cyclic loadings. The deposits are assumed to be in the undrained state, an observation which, although not true in the field, may be approximated as such due to the relatively short time intervals involved. The reproduction of such conditions in the laboratory provides an invaluable reference for evaluating the success of partially saturated samples with respect to liquefaction mitigation. This thesis offers a comprehensive account of two such experimental programmes.

Much of the relevant work on the possible beneficial effects of partially saturated soils in this field has been undertaken by Pietruszczak and Pande, in particular their role in developing the constitutive relations for such soils (Pietruszczak and Pande, 1996). Their analytical research in evaluating the undrained response of partially saturated soils will be expanded upon here.

One of the major challenges which needs to be overcome with experimental work in Geotechnical Engineering is that of sampling, but it is especially true in studies into liquefaction since the liquefaction potential of a given element of soil is highly dependent on its in-situ stress state. This work will present a new development in the preparation of loose, partially saturated samples of soil. This new development was employed throughout the first experimental phase of the research described in this thesis. The success of this new method will be discussed fully.

Finally, the most widely reported source of liquefaction in the field is the earthquake, although artificial processes such as blasting may also induce its effects. While this work is not intended to focus upon the seismological evolution of liquefaction, it is accepted that a fundamental comprehension of the physical nature of earthquakes is required for this course of study. The mechanisms behind the earthquake assume great importance in any basic understanding of the processes behind liquefaction phenomena.

1.1.2 The Scope of the Work

The primary objective of this thesis is to provide a rudimentary insight into how partially saturated soils might be employed by the Geotechnical Engineering industry in its continuing research into effective and efficient methods of liquefaction mitigation. The developments contained here are not designed to be a complete description of the undrained behaviour of partially saturated soils. For that, the reader is directed to the excellent reference works currently existing on this subject (e.g. Fredlund and Rahardjo, 1993).

As this work encompasses new developments in Geotechnical Engineering, some refinement in the ideas presented is inevitable. This thesis is not intended to be a state-of-the-art account of liquefaction mitigation or evaluation. However, the motivation for the work originates from previous research conducted by Pietruszczak and Pande (1996), and the developments described within are intended to be logical continuations of this important numerical work.

This thesis is meant to portray a systematic development by the author from basic concepts and ideas regarding liquefaction, through modifications of existing specimen preparation methods and subsequent experimental research.

1.1.3 The Layout of the Work

This thesis contains seven Chapters, each of which is meant to be a natural progression from the previous one, although each Chapter is structured so that it may be considered in isolation, with some reference to earlier Chapters and Sections.

Chapter 1 - Introduction

Chapter 1 contains a basic introduction to the thesis, and presents the structure of the work in full. Although integral to the understanding of the manner in which the material is presented in the thesis, it was not meant to occupy an inordinate amount of space in this work. Therefore, the introduction was kept as concise as possible, while still relaying vital information to the reader.

Chapter 2 – Liquefaction

Chapter 2 concentrates on the development of the phenomenon of liquefaction, from earliest references, through to modern advances. This Chapter introduces many of the concepts which will be widely used throughout this thesis. Other topics within liquefaction have been included for the sake of completeness, in order that those concepts which are more appropriate in terms of the aims of this thesis may be better understood. An illustrative case study, focusing on the catastrophic effects caused by liquefaction during the Hyogo-ken Nanbu earthquake of 1995, has also been included in this Chapter.

Chapter 3 – Modifications to the Triaxial Apparatus

The first stage of the experimental research concentrated on the preparation of loose, partially saturated specimens for subsequent testing in the triaxial apparatus. The required modifications included a complete redesigning of the system that was available to the author for the purposes of this research. Also, a new method of specimen preparation is proposed in which the accepted sequence of steps normally followed in order to produce a reconstituted granular soil specimen is effectively reversed. The method of employing zeolite to produce a partially saturated sand specimen is explored before, finally, the reliability of the new method is assessed.

Chapter 4 – Triaxial Test Results

Chapter 4 focuses on the results of the triaxial test programme conducted using the modifications described in Chapter 3. A total of 24 stress controlled, one-way cyclic, undrained tests were conducted on cylindrical Hostun sand specimens having a cross-sectional diameter of 38mm, and length 76mm. Hostun sand was chosen for this experimental stage as it has been demonstrated that the nature of the soil renders it more susceptible to liquefaction (e.g. Doanh et. al., 1999). The results of these tests provided important information regarding the viability of employing partially saturated soil as a means of liquefaction mitigation.

Chapter 5 – The Oscillating Box

Chapter 5 takes the research a stage further, by introducing dynamic motion to a partially saturated soil stratum. Here, the results of a test programme involving a single-degree-of-freedom system, called the oscillating box, are described in full. Similar work has been conducted by Yoshimi and Tokimatsu (1977), in order to assess the liquefaction susceptibility of soil having a surface loading. This work was summarised by Rollins and Seed (1990). Swansea Bay sand as opposed to Hostun sand was used for this current programme, in an attempt to broaden the scope of the work. The programme was effective in confirming those conclusions stated at the end of Chapter 4.

Chapter 6 – Closing Remarks

Although each Chapter which contains a presentation of results, whether experimental or numerical, has a Section focusing of the conclusions of such work, Chapter 6 has been included in order to bring all of these conclusions together into one, all-encompassing summary of the research conducted for the purposes of this thesis. Recommendations for future research are also presented.

As can be seen from this very basic outline, the author has intended to present the work in a logical manner, moving from simple concepts, through experimental work, and onto application with real-time situations.

CHAPTER 2

LIQUEFACTION

2.1 LIQUEFACTION EXPLAINED

2.1.1 Introduction and Historical Background

Soil liquefaction is a naturally-occurring phenomenon during which the inherent strength of a given soil element or stratum is significantly reduced by earthquake (transient) shaking, producing vertically propagating shear waves. Artificially-induced rapid loadings, of which blasting is a common example, may also be considered. Throughout this work, however, earthquakes will always be considered as the primary source of shaking.

Historically, Hazen (1920) used the word 'liquefies' in reference to the failure of the Calaveras Dam in California. The first qualitative account of the phenomenon was presented by Casagrande (1936), although the term 'liquefaction' was first employed by Mogami and Kabu (1953). Terzaghi (1956) applied the phrase 'spontaneous liquefaction' to describe the sudden change of loose granular deposits into flows, due to a slight disturbance. A comprehensive summary of the terminology used in liquefaction analysis was presented by Marcuson (1978). A thorough résumé of the liquefaction phenomenon, particularly with reference to clean sands and silty sands, is provided by Ishihara (1993).

As an important branch of geotechnical engineering, liquefaction first came to prominence both during and after the earthquakes which adversely affected Alaska and Niigata in 1964 (e.g. Yamada, 1966; Kawakami and Asada, 1966; Watanabe, 1966), from which emerged many examples of the devastating effects of liquefaction-induced damage, including spectacular slope and foundation failures (although liquefaction is not essential for slope failures), and flotation of buried structures. Since that period, liquefaction has become one of the most widely studied topics in modern geotechnical engineering.

Despite extensive study by researchers all over the world, a unified method of analysis has yet to transpire. This, at least in part, is due to the fact that the term 'liquefaction' has been used to describe many different, though related, phenomena (Kramer 1996). The term 'liquefaction' has historically been used in relation to a variety of processes that involve soil deformations caused by monotonic, transient, or repeated disturbance of saturated cohesionless soils under undrained conditions.

However, irrespective of the terminology used, the defining feature of all liquefaction-related phenomena is the generation of deleterious excess pore-water pressures within the soil matrix.

It is important to recognise that liquefaction occurs only in saturated soils, within which the pore spaces between the particles constituting the fabric of the soil are completely filled with water. Conversely, the mere fact that a soil is susceptible to liquefaction does not necessarily mean that liquefaction will occur. The initiation of liquefaction requires a disturbance that is strong enough to trigger it.

In order to formulate a qualitative understanding of the processes involved in liquefaction, it is essential that the critical components of the overall condition of the soil, prior to the occurrence of an earthquake, are fully understood. In many situations, a soil deposit may be treated as a continuum. On the microscopic scale, such a deposit consists of groups of discrete particles. Each particle will be in contact with some of its immediate neighbours in the group, though not necessarily all of them.

Contact forces exist between the particles. These forces are produced by the weight of the overlying particles, and the resulting friction gives the soil its strength.

Liquefaction will occur when the structure of a loosely bound, saturated sand distorts and collapses due to a rapidly applied loading, such as that which occurs during a seismic disturbance. On collapsing, the constituent particles of the soil deposit will attempt to shift into a denser, more stable configuration. Under normal circumstances, this process would squeeze water out from the pore spaces but, due to the relatively short duration of the most significant earthquake loading, there is insufficient time for this to occur i.e. drainage of water is effectively prevented.

Thus, the water remains constrained within the pore spaces which, as a result of the incompressibility of the pore water, restricts the soil particles from moving closer together. In response, the pore-water pressure rises, thereby pushing the soil particles apart and subsequently reducing the number of contact forces in the soil structure. The strength of the soil deposit, as described above, is reduced accordingly.

If the excess pore-water pressure rises further, particularly to a level approaching the stress exerted by the overlying soil, then friction forces will be lost as more particles lose contact with their neighbours, and the soil will begin to exhibit behaviour more appropriate to a viscous liquid rather that a solid (Figure 2.1). In this extreme condition, 'liquefaction' can be said to have occurred in the soil deposit.

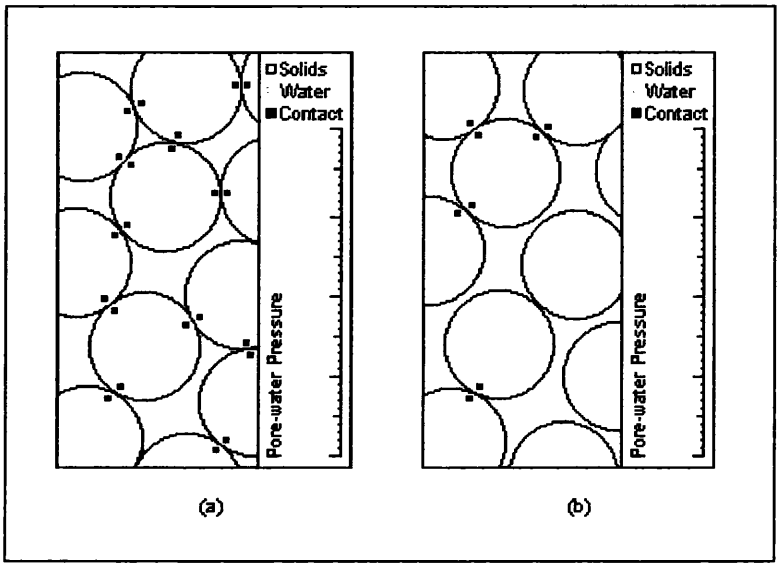

***Figure 2.1** – Generation of Excess Pore-Water Pressure within a Granular Soil*

This concept can be reinforced by reference to the classic effective stress equation, normally written as:

$$\sigma' = \sigma - u \qquad [2.1]$$

where σ is the total overburden stress, u is the excess pore-water pressure, and σ' is the effective vertical stress i.e. that portion of the total stress which is transmitted directly through the soil skeleton. According to this equation, which is one of the cornerstones of geotechnical engineering and which has been repeatedly verified through laboratory testing, the effective stress falls as the excess pore-water pressure rises, provided the total overburden stress remains constant. Should the excess pore-water pressure reach the same value as the total overburden pressure, the effective stress will become zero. The soil will then

have lost all of its shear strength, and its behaviour will be similar to that of a viscous liquid. The soil can then be said to have 'liquefied'.

The liquefaction condition, and the associated loss of strength in the soil deposit, are temporary. On cessation of the rapid loading, excess pore-water pressures are permitted to dissipate, and the soil particles will be able to settle into a denser, more stable configuration. In the liquefied state, however, the soil has negligible shear resistance, and deformations large enough to cause severe structural damage through ground failures can readily occur.

The natural resistance of a given soil deposit to liquefaction depends on such factors as the degree of cohesion between the soil particles, the extent to which drainage of the pore-water is restricted, and the looseness of the soil prior to the earthquake. The natural liquefaction resistance of soils was the subject of NCEER (National Center for Earthquake Engineering Research) workshops which were held in both 1996 and 1998; a summary of the research conducted at these workshops is presented by Youd and Idriss (eds., 1997), and Youd et. al. (2001). The following areas were reviewed:

- Standard and Cone Penetration tests
- Shear wave velocity measurements
- Earthquake magnitude scaling factors (Seed and Idriss, 1982)
- Correction factors for overburden stresses and sloping ground
- Input values for earthquake magnitude and peak acceleration.

The use of the cone penetration test (CPT) resistance as an indicator of liquefaction susceptibility/resistance is receiving increased recognition. Zhang (1998) reports on the feasibility of using mathematical methods to interpret the data from CPT tests, in order that the liquefaction resistance of a given soil deposit may be reliably quantified. Comparisons indicate that the rate of success of this method can exceed that of the conventional method proposed by Stark and Olsen (1995). More recently, Juang et. al. (2000, a & b) have addressed the topic of the determination the earthquake-induced liquefaction potential by means of CPT data from 225 field records.

With regard to the second of the subjects discussed at the workshops, an empirical equation for assessing the liquefaction resistance of soils based upon the shear wave velocity, v_s, was proposed by Juang et. al. (2001). A treatment

which also considered the possibility of using the shear wave velocity as a viable parameter in the assessment of liquefaction resistance was presented by Andrus and Stokoe (2000). There, the writers reaffirmed the findings of Boulanger et. al. (1997) that thin strata of low v_s value may not be detected if the measurement interval of the liquefaction resistance is too large. Another concern is that measurements are made at small strains, whereas excess pore-water pressure build-up and liquefaction are medium- to high-strain phenomena (e.g. Jamiolkowski and Lo Presti, 1990; Roy et. al. (1996)).

Factors influencing the amount of post-liquefaction deformation in the soil deposit include the distributed loads from surface and sub-surface structures, the slope of the affected ground, and the depth, thickness, and areal extent of the liquefied layer. Once again, the looseness of the soil prior to liquefaction is significant, and this is normally expressed in geotechnical engineering in terms of the void ratio, *e*. Vaid and Thomas (1995) present the results from an empirical study of the post-liquefaction behaviour of sand in the triaxial test. This required a comprehensive investigation of both the static and cyclic behaviour which takes the sand to the liquefied state prior to the assessment of its post-cyclic behaviour.

As stated previously, the unifying feature in all liquefaction-related phenomena is the generation of excess pore-water pressures. Such phenomena may be divided into two main groups: *Cyclic Mobility* and *Flow Liquefaction.* Both of these processes are capable of producing catastrophically large permanent deformations during earthquakes. A wide variety of references, including technical information and case studies, are provided with the descriptions in order that the reader may gain a deeper insight into these important processes

Without changes in the pore-water pressure, and therefore changes in the effective stress, neither of these important processes can occur. Brief qualitative descriptions of both of these related though distinct phenomena are given here, although a more comprehensive treatment of the initiation of liquefaction will be given later in this Chapter.

Cyclic Mobility

Cyclic mobility, which can occur in either dense or loose (→ negatively dilatant) sands, does *not* involve a loss in undrained shear strength. The deformations produced by cyclic mobility, which occur primarily on virtually level ground adjacent to bodies of water, develop incrementally during earthquake shaking. The term generally assigned to these deformations is *lateral spreading*.

Sand boils are a consequence of level-ground liquefaction, in which the seismically-induced excess pore-water pressures dissipate through the upward movement of water through the soil. If the upward hydraulic gradient reaches some critical value, which is a function of both the specific gravity, G_s, and the void ratio, e, of the soil, gravitational forces will be cancelled out by the upward seepage forces, and the effective stress on any plane will be zero. Consequently, the vertical effective stress will drop to zero, leading to loss of all undrained shear strength, and a quick condition is then said to exist within the soil. The upward water velocity may be sufficiently high to eject solid particles onto the surface. These so-called 'sand boils' are normally accompanied by excessive vertical settlement of the affected soil, and subsequent flooding of low-lying land. Sand boils, which have been reproduced under laboratory conditions (e.g. Fiegel and Kutter, 1994), are of little engineering significance in the free field, although they are reliable indicators of high subsurface excess pore-water pressures having existed.

There are three combinations of initial conditions and cyclic loading conditions which generally produce cyclic mobility in a given specimen. These will be discussed later in this Chapter.

Flow Liquefaction

Flow liquefaction occurs in a given element or stratum of soil when the *static* shear stress is *greater than* the shear strength of the *liquefied* soil. In field conditions, these shear stresses are provided by gravity, and will generally remain constant until such time as significant strains develop. The large deformations produced by flow liquefaction (termed *flow failures*) are driven by the static shear stresses. The cyclic stresses may simply bring the soil to an unstable state, such that its strength drops sufficiently to allow the static stresses

to produce the flow failure. Flow failures form suddenly, develop quickly, and tend to affect a wider area than is normally the case with cyclic mobility.

Flow liquefaction may be triggered in a variety of ways, other than the seismic scenario. Hryciw et. al. (1990) discuss the initiation of flow liquefaction as a result of geophysical exploration, while Fellenius (1955) highlights a notable case of flow liquefaction in Sweden caused by train traffic. The near-collapse of the Lower San Fernando Dam in 1971, was caused by an underwater landslide initiated by sudden increases in pore-water pressures during the San Fernando Earthquake. Had the dam collapsed completely, the damage to the populated areas below the dam might have been incalculable. A further analysis of this dam slide, focusing on the steady-state strength parameters, is provided by Castro et. al. (1992).

Zeng and Arulanandan (1995) investigated the stability of soil slopes based on experimental data obtained from a centrifuge test programme. The failure mechanisms which occurred during the tests closely resembled those which occurred in the field. Excess pore-water pressures were generated in a sand seam sandwiched between two silt layers; this contributed to the observed lateral sliding. The writers also demonstrated that the slope angles were significantly reduced following the conclusion of each test. The experimental results were in accordance with the lateral sliding observed at Valdez during the Alaska earthquake of 1964 (Seed, 1968). For further information on centrifuge modelling, the reader is referred to Section 2.5.

Liquefaction may also be initiated by a monotonic loading, such as the flow slides described by, for example, Kramer (1988), and Anderson and Bjerrum (1971). Kramer and Seed (1988) provide a comprehensive account of the initiation of liquefaction in laboratory tests. The study of liquefaction under monotonic loading has contributed greatly to the understanding of seismically induced liquefaction phenomena. This is due to the fact that, in monotonic tests, the effective stress conditions under which liquefaction is initiated have been formally identified.

One further case study of monotonic flow liquefaction reported in the literature is that of the static flow failure of the north dike of the Wachusett Dam in 1907 (Olson et. al., 2001). There, liquefaction occurred on the upstream slope of the dike on the first filling of the reservoir. Using 'back-calculation' methods,

the writers were able to establish that the estimated shear strength was comparable with other flow liquefaction case histories reported in the literature.

Back-calculation is gaining widespread acceptance as a reliable method for analysing the liquefaction effects from older earthquakes. Martin and Clough (1994) present an outline of the method, and apply it to the liquefaction damage caused by the 1886 Charleston earthquake in South Carolina. The writers conclude that the magnitude and peak acceleration of this particular event has been overestimated in the literature which, in turn, has implications for seismic design practices in the Charleston area.

2.1.2 Liquefaction and the Built Environment

Generally, liquefaction is only destructive when some ground failure or ground displacement occurs at a susceptible location. Therefore, predicting the occurrence of liquefaction does not assume as high a priority as improving the susceptible soil in order to reduce the often-unpredictable capability of liquefaction to cause structural damage. This Section outlines some of the more destructive liquefaction-induced phenomena.

Lateral Spreads

A lateral spread will occur when the liquefaction of a subsurface layer of soil induces horizontal movement of the soil at the surface. Horizontal displacements in lateral spreads can be as much as several metres. Lateral spreads generally develop on slopes of less than 2 or 3°, and will tend to move toward a free face, such as a river channel or section of coastline (Figure 2.2). Lateral spreads are especially damaging to pipelines; every pipeline failure that occurred in the city of San Francisco during the 1906 earthquake occurred in areas where lateral spreads were prevalent (e.g. Youd and Hoose, 1978). Surface structures can also be affected by lateral spreads. For example, during the 1964 Alaska earthquake, more than 200 bridges were damaged, some beyond repair, by the spreading of surficial deposits.

A new empirical method, called the EPOLLS (Empirical Prediction of Liquefaction-Induced Lateral Spreading) model, was developed by Rauch and Martin (2000) for predicting ground surface displacements due to the lateral

spreading phenomenon. More recently, Berrill et. al. (2001) present a case study on the effect of lateral spreading on the piled foundations on the Landing Road Bridge, Whakatane, New Zealand, during the 1997 Edgecumbe earthquake. There, liquefaction occurred in the most recently sedimented sands. Average settlement of the liquefied ground was approximately 400mm. The presence of wood chippings in the river bank material suggests a remedy for such vulnerable bridges, which involves the placement of a 'crushing zone' of weak material behind piles which are likely to be affected by lateral spreading. Such a zone may cushion the forces exerted on such structures by liquefied soil.

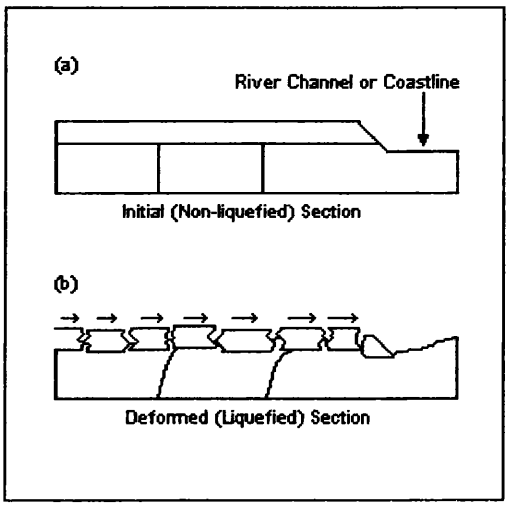

***Figure 2.2** – Lateral Spreading*

Ground Oscillation

Liquefaction in deep soils may 'decouple' the layers nearer the surface from the affected subsurface soils. In this case, the surficial layers may 'float', allowing the surface soil to oscillate both horizontally and vertically (Figure 2.3). The decoupled layer oscillates at a different frequency from the surrounding ground, causing ground fissures and the fracture of rigid structures, for example pipelines, roads, and pavements.

Bartlett and Youd (1995) present an empirical model for predicting the amount of horizontal ground displacement resulting from liquefaction-induced lateral spread. Two general types of lateral spread were differentiated:

- lateral spread toward a free face; and
- lateral spread down gentle slopes where a free face is absent.

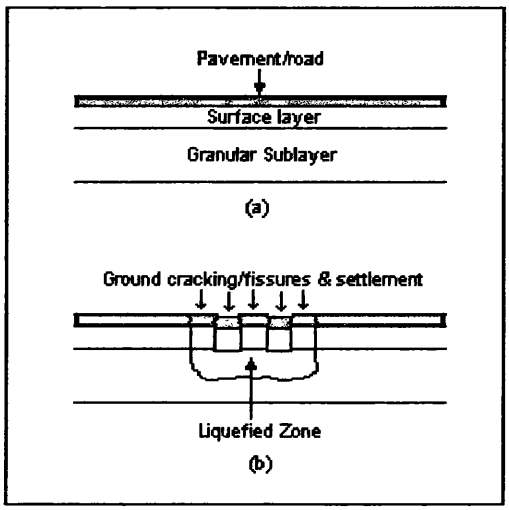

***Figure 2.3** – Ground Oscillation*

For 'free face' conditions, the analysis showed that the ground displacement is strongly correlated with the height and proximity of the free face. Similarly, displacement associated with ground slope conditions is correlated with the slope of the surface, and generally occurs in the direction of the maximum topographical gradient.

Kokusho (1999) presents the results from an extensive series of tests conducted to investigate the formation of 'water-films' on liquefied sand, and their subsequent effect on the phenomenon of lateral spreading. The writer concludes that an overlying water-film can be readily formed just after the complete liquefaction of the sand, directly beneath a less permeable of soil, for example a fine silt or clay. The maximum thickness and duration of the water-film may be approximated as being inversely proportional to the density of the sand, which indicates that the effects of a water-film may be more pronounced for looser soils, such as those under investigation in this thesis. Kokusho (1999) also concludes that the water–film tends to outlast liquefaction settlement in each soil sub-layer, suggesting that it may affect the soil stability for longer than the liquefaction time period.

Flow Failures

Such flows, which are among the most devastating liquefaction-induced phenomena, usually develop in slopes with inclines greater than 3° (Figure 2.4). Flow failures generally displace large masses of soil laterally by tens of metres. Flows may comprise completely liquefied soil of zero bearing strength, or blocks of intact material riding on a layer of liquefied soil, which form as outlined above in the description of *Ground Oscillation.*

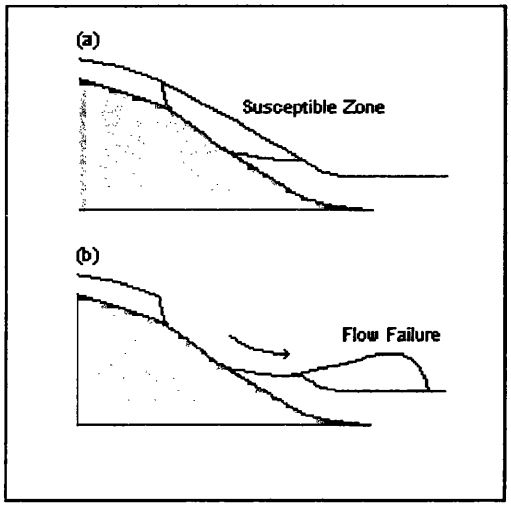

Figure 2.4 *– Flow Failure*

Meneses-Loja and Ishihara (2000) report on laboratory tests where flow failure was induced by the superimposition of a cyclic stress on a monotonic load. The superimposed stress was designed to simulate the minor seismic shaking, following the strong shaking, that is still acting on the liquefied sand. The test results were validated for Japanese Toyoura sand prepared by moist tamping. A comprehensive account of the moist tamping method, as used in specimen preparation, is presented by Ladd (1978). Further details regarding the moist tamping method in specimen preparation are provided by Vasquez-Herrera and Dobry (1989). A full description of the method is given in Chapter 3, which deals with the method of specimen preparation for the triaxial test programme outlined in this thesis.

Flow failures are often initiated by rainfall and, in this instance, are termed 'flowslides'. Flowslides are slope failures which are characterised by a

rise in excess pore-water pressure, the development of fluid-like motion, and the gradual disintegration of the sliding mass. Research into this particular cause of flowslides has been discussed by, for example, Wang and Sassa (2001), who used a small flume to conduct a series of tests in which the relationship between sliding distance and excess pore-water pressure generation was examined.

Settlement

As previously discussed, the pore-water pressures within a loose granular soil will rise during earthquake shaking. During dissipation of these pressures, the soil will consolidate, and structures at the surface will subside. In certain instances, the rate of consolidation may vary at given points beneath a structure, causing differential settlement and damage, such as the cracking of masonry.

Loss of Shear Strength

As the excess pore-water pressure rises, the shear strength of the soil supporting a structure will fall (Figure 2.5). During full liquefaction, all shear strength will be lost. In this case, the structure may settle as described above, or may tilt, as occurred spectacularly in the residential area of Kawangishicho in Niigata, Japan, in 1964, where several four-storey apartment buildings tipped backward, without structural collapse, by as much as 60°. Here, liquefaction first developed at depth, then spread vertically through the overlying layers. Thus, the loss of strength beneath the apartments was gradual, causing the buildings to slowly settle and tip.

The dynamic analysis of the stability of foundations on saturated granular soils, along with associated liquefaction phenomena, was investigated by Pietruszczak and Oulapour (1999), using a numerical approach similar to that adopted by Pietruszczak (1994).

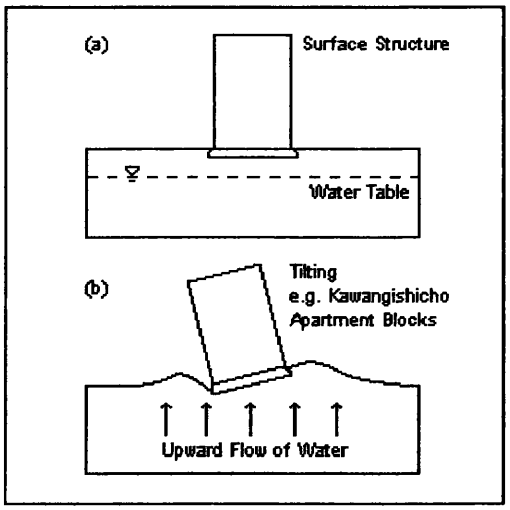

***Figure 2.5** – Loss of Shear Strength*

Wave-Induced Liquefaction

Liquefaction may also be caused within submerged sand beds through wave-induced disturbances, as described by Sassa and Sekiguchi (2001). There, the writers describe finite element analyses of wave-induced liquefaction of sand beds. This form of liquefaction is of importance due to its potential effects on submarine pipelines, and on the performance of coastal defence structures such as breakwaters.

2.1.3 Evaluation of Liquefaction Hazards

When assessing the liquefaction susceptibility at a particular site, the following three questions must be answered as fully as possible:

(a) Is the soil under consideration susceptible to liquefaction, taking into account such factors as granularity, void ratio, age of the deposit, etc.?

(b) Will liquefaction actually be triggered if the soil is susceptible?

(c) If liquefaction is triggered, will appreciable damage occur?

If the answer to all three of these questions is 'yes', then clearly a problem exists. There are several criteria by which liquefaction susceptibility can be judged, and these are described later in this Chapter.

In general, liquefaction is restricted to certain hydrological and geological environments, primarily recently deposited sands and coarse silts in areas with high ground-water levels. Gravel has also been observed to liquefy under certain conditions. Generally, the looser and younger the deposit, and the higher the water table, the higher the susceptibility of the soil to liquefaction. In areas where ground-water levels change significantly, liquefaction susceptibility may also change.

Several methods are used to evaluate the susceptibility of a given soil deposit to liquefaction. Four of the most commonly used criteria are outlined below (Kramer 1996).

Geological

The type of geological process which produces a given soil deposit can have a significant influence on its susceptibility to liquefaction (Youd and Hoose, 1977). The four most common deposits are:

a) fluvial or alluvial – formed by sedimentation in rivers or lakes,
b) colluvial – deposition of eroded material or debris,
c) aeolian – deposits formed by wind action, and
d) man-made – for example, hydraulic filling.

These processes, particularly the first three, sort particles into uniform grain sizes and deposit them in the loose state, thus making the deposit susceptible to liquefaction. The tendency for these deposits to densify results in increased pore-water pressures and reduced soil strength, as discussed earlier.

These three main methods of deposition tend to produce rounded particles. Friction between rounded particles is less than that normally associated with angular particles, and so a deposit so formed will have a lower shear strength and so be inherently weaker with, therefore, a higher susceptibility to liquefaction.

Compositional

Soils whose structure consists of similarly-sized particles are more susceptible to liquefaction than those which are well-graded. Also, fine-grained soils containing plate-like particles generally exhibit sufficient cohesion, due to their colloidal nature, to inhibit liquefaction, although liquefaction of non-plastic silts has been

reported (e.g. Ishihara 1984). Thevanayagam and Mohan (2000) explored the possibilities of introducing a new set of intergranular and interfine state variables to characterise the mechanical behaviour of silty soils. The writers conclude that the constitutive behaviour of a silty sand specimen at any void ratio e_s was similar to that of the host sand at the same void ratio.

A coarse-grained soil containing fine-grained particles within its voids will be less susceptible to liquefaction due to the reduced tendency for subsequent densification and increase of excess pore-water pressures.

Clays, with the exception of 'quick' clays, are not susceptible to liquefaction, although a fine-grained soil may be prone to significant strength loss, and possibly liquefaction, if it satisfies each of the following four criteria (Wang, 1979):

a) Fraction finer than 0.005 mm is less than 15%
b) liquid limit less than 35%
c) natural water content greater than 0.9 of the liquid limit, and
d) liquidity index less than 0.75

Strain-softening in a fine-grained soil may also produce effects resembling liquefaction under certain conditions.

Historical

Observations and reports of liquefaction during earthquakes can provide useful and detailed information, particularly when planning new sites for development. For example, it is known that liquefaction will often recur at a given location when the hydrological and geological conditions remain largely unchanged. Kramer (1996) suggests that a deposit which has liquefied at some time in the past may therefore do so again, and research into the liquefaction damage caused by previous earthquakes is therefore an important consideration when attempting to evaluate the susceptibility at a particular site.

Investigations following earthquakes have shown that the effects of liquefaction are generally confined to an area within some determinable distance from the source of the disturbance (e.g. Ambraseys, 1988). As might be reasonably expected, the distance at which the effects of liquefaction may be observed increases significantly with increasing earthquake magnitude.

As a result of such efforts, detailed maps indicating areas at risk from liquefaction are now available for practicing geotechnical engineers.

State

Liquefaction susceptibility depends as much on the initial state of the soil under consideration as any of the criteria previously described. When describing the state of the soil deposit, several parameters may be used. Among the most common are the relative density, D_r, and the initial effective stress level.

The importance of relative density, and its ability to be defined in terms of the void ratio, e, of the deposit, has already been alluded to. It has been demonstrated by several investigators (e.g. Castro 1969; Kramer and Seed 1988) that the higher the initial shear stress on a given deposit, the greater the liquefaction potential, and the smaller the disturbance required to liquefy the soil.

Within the state criteria, there exist two important concepts which are now qualitatively described.

(1) Critical Void Ratio

Casagrande, in an important and celebrated series of tests, the results from which were published in 1936, discovered that soil specimens, whether initially loose (⇒ contractive behaviour) or dense (⇒ dilative behaviour), and tested at a given confining pressure, approached a given density (Figure 2.6), and that the relationship between this density and the initial confining pressure was uniquely defined. He expressed this density in terms of the *critical void ratio*, e_c.

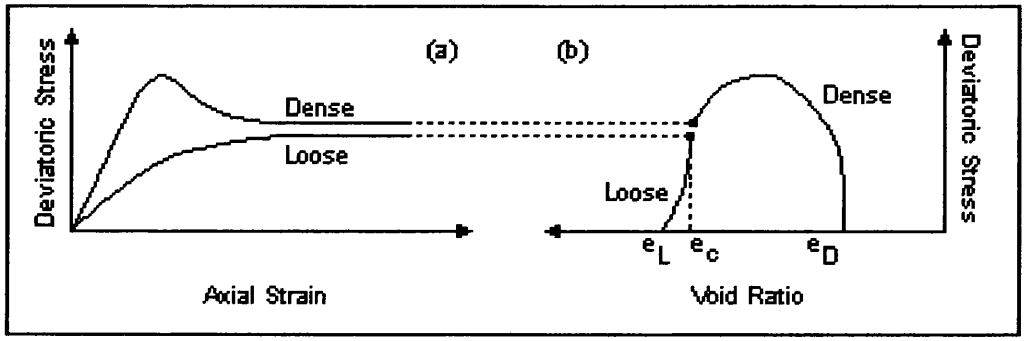

Figure 2.6 *– Graphical Explanation of the Critical Void Ratio*

By defining the state of the soil in terms of the effective confining pressure and the critical void ratio, Casagrande was able to establish the boundary between the loose and dense states (Figure 2.7). This boundary is called the *Critical Void Ratio (CVR)* line.

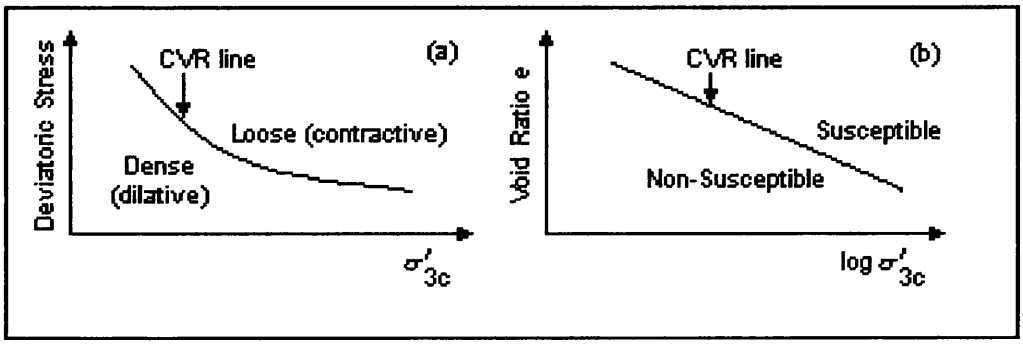

***Figure 2.7** – The Critical Void Ratio (CVR) Line*

As the CVR line provides the boundary between loose and dense states, it follows that the CVR line (as shown in Figure 2.7 above) may also be employed to determine whether or not a particular saturated soil is susceptible to liquefaction. If a particular soil plots above the CVR line (i.e. high void ratio ⇒ low density), then that soil might be considered a liquefaction risk. For soils below the CVR line (i.e. low void ratio ⇒ high density), the soil is not generally considered to be a liquefaction risk. Measurements from field investigations have produced various anomalies in this theory. For example, post-failure studies on sites where liquefaction has been induced have produced initial states that have plotted significantly below the CVR line. Casagrande (1976) attributed this discrepancy to shortcomings in the sample preparation technique, and also the difficulties in employing strain-controlled tests in liquefaction analysis. In this connection, this discussion returns to details presented earlier in this Section.

(2) Critical State, or Steady State of Deformation

The steady state of deformation (Castro and Poulos, 1977) is described as one in which a liquefied soil mass flows continuously under constant shear stress and constant effective confining pressure at constant volume and constant velocity.

The steady state of deformation is termed the *critical state* in later work. This special state is reached only at large strains.

The locus of points describing the relationship between the void ratio, e, the effective confining pressure, σ', and the shear stress, τ, within the critical state, is termed the *Steady State Line* (SSL). The SSL is a curve plotted in 3-dimensional e-σ'-τ space. Any 2-dimensional representation of the SSL line may be obtained by keeping the third quantity constant. For example, using the 2-dimensional projection on the e-σ' plane, the susceptibility of the soil to liquefaction may be determined, in a similar way to the procedure used with the CVR line.

Soils whose states plot below the SSL are not susceptible to liquefaction, whereas a soil whose state plots above the SSL will only be susceptible to liquefaction if, and only if, the static shear stress exceeds the steady state ($\Rightarrow$ residual) strength. However, it should be noted that cyclic mobility may occur in soils whose states plot anywhere in e-σ'-τ space. In other words, both loose and dense soils may be affected by cyclic mobility.

The applicability of the SSL is limited in so far as its position in e-σ'-τ space tends to depend upon the compositional characteristics of the soil in question. For example, the slope of the SSL is influenced by particle angularity. Also, soils with rounded particles will generally have flatter SSL's which, in turn, leads to difficulties when attempting to evaluate the steady state strength.

In this last respect amongst others, it may be argued that the measurement of such quantities as the relative density and void ratio is of limited use in the evaluation of the liquefaction susceptibility of soils. However, both the relative density and void ratio have continued to be used extensively as reliable indicators of liquefaction susceptibility for the practicing engineer.

2.2 LIQUEFACTION IN FIELD AND LABORATORY RESEARCH

2.2.1 Introduction

Extensive research has been conducted in recent years to evaluate the behaviour of those in-situ soils which are susceptible to liquefaction. Much of this work has involved subjecting representative soil samples to the same conditions in the laboratory as they would experience in the field. The underlying problem here is interpretation of the degree to which the results obtained in the laboratory can be applied to the field situation.

Many investigators have had much to say regarding the subject of sample preparation for laboratory testing purposes. For example, Ladd (1977) identifies three properties of a given sand sample which will affect the cyclic strength when an in-situ sample is to be extracted for testing in the laboratory. They are:

(a) differences in grain and interparticle contact orientation;

(b) variations in void ratio within an individual specimen; and

(c) the segregation of the particles.

Peck (1979) states that, in soil mechanics, no laboratory evidence can reasonably be considered adequate until such time as there is sufficient field experience to establish whether the phenomena observed in the laboratory are indeed representative of those which operate in the field. The writer adds that it must also be determined whether predictions based on laboratory results are indeed fulfilled in the field.

Most investigators agree that the amount of field evidence available to verify laboratory results is inadequate, although new techniques, such as the use of downhole arrays to monitor the consequences of earthquake shaking, are now available (e.g. Elgamal et. al., 1996).

In all instances, it is accepted that the primary forces acting on a given element of in-situ soil during earthquakes are those resulting from the upward propagation of shear waves emanating from the underlying bedrock (e.g. Seed and Peacock, 1971). The effect of these forces is that a given representative element of soil is subjected to the sequence of cyclic stress applications as shown in Figure 2.8 on the next page.

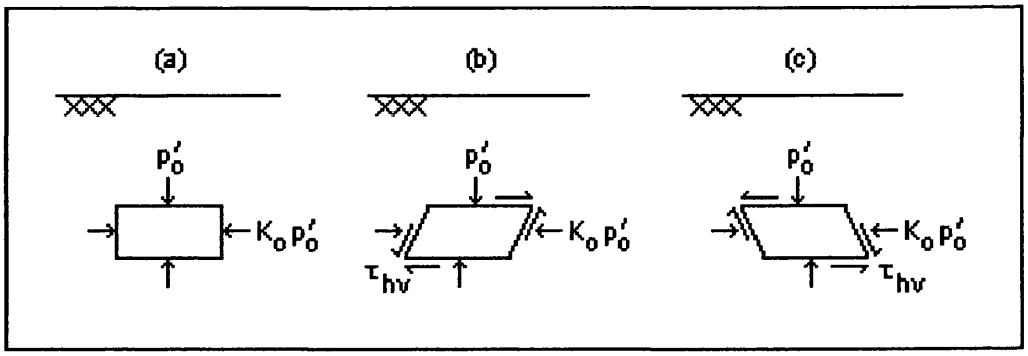

***Figure 2.8** - Idealised Field Loading Conditions*

Before shaking, the soil element will be acted upon by the principal stresses p'_0 and $K_0 p'_0$, where p'_0 is the effective normal stress, and K_0 is the coefficient of lateral earth pressure at rest, as shown in Figure 2.8(a). During shaking, a component of shear stress τ_{hv}, which is present on both the horizontal and vertical planes, will deform the element and will reverse directions many times during the earthquake to produce the cyclic loading (Figures 2.8(b) and 2.8(c)).

The magnitude of shear stress will not remain constant, but will vary during the period of shaking. However, by estimating the energy levels present during the earthquake, it is possible to convert the irregular pattern of shear stress applications to an equivalent number of uniform stress cycles. This important principle is used extensively when testing laboratory samples.

The purpose of the test procedure is to determine the magnitude of τ_{hv} which will cause liquefaction in a representative sample, for varying values of the effective normal stress p'_0. The likelihood of liquefaction occurring may then be assessed by direct comparison of the cyclic stress as determined by the laboratory test, and the cyclic stress developed by the earthquake shaking (Seed and Peacock, 1971).

2.2.2 Triaxial Compression Tests

In the laboratory tests conducted to date in the field of liquefaction, the triaxial test is by far the most commonly used in order to determine the liquefaction characteristics of a saturated sand. The widespread availability of the triaxial test, and the ease with which stresses and excess pore-water pressures can be measured, makes it the most logical choice in the vast majority of cases.

In the compression test, as described by Seed and Peacock (1971), the soil specimen is normally consolidated under an all-round pressure σ_a, which produces the stress state shown in Figure 2.9(a) below. Referring to Figure 2.8 earlier, this will reproduce a condition in which $K_0 = 1$. Note also that, initially, τ=0 i.e. there is no shear stress present. The specimen is then subjected to an increase of $\sigma_{dc}/2$ in the axial stress, and a simultaneous reduction in the lateral stress by the same amount, Figure 2.9(b).

The normal stress on a 45° plane in the specimen is then unchanged, but a shear stress of $\sigma_{dc}/2$ is developed on the same plane.

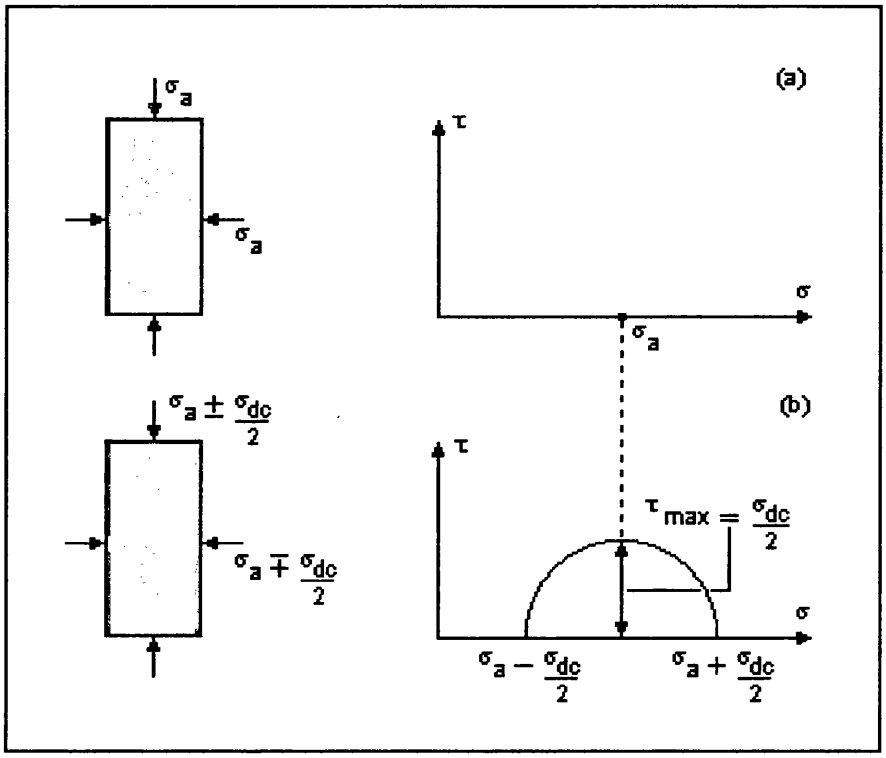

Figure 2.9 *– Cyclic Loading Triaxial Compression Test*

If the stress changes are now reversed so that the direction of stress application on the 45° plane is also reversed, the normal stress will remain constant, as will the magnitude of the shear stress $\sigma_{dc}/2$. Now, however, the direction of the shear stress will have rotated through 90° so that, as the above process of stress application is repeated, a cyclic shear stress of $\sigma_{dc}/2$ is established.

It should be noted here that identical effective stress conditions may also be obtained by keeping the lateral stress constant, and cycling the axial stress by $\pm\sigma_{dc}$. This principle forms the basis of the triaxial tests described later in this thesis.

In such triaxial compression tests, the results are generally expressed in terms of the ratio of two quantities, both of which are controlled by the investigator. These are

(a) the confining pressure, σ_a; and

(b) the applied deviatoric stress, σ_{dc}.

This ratio is expressed as $\sigma_{dc}/2\sigma_a$, or, in terms of the preceding theory, τ_{max}/σ_a.

2.2.3 Comparison of Triaxial and Field Conditions

Peacock and Seed (1968) have highlighted various differences between the conditions present in the field and those used in triaxial compression tests in the laboratory. These differences are summarised below.

(a) Stress Orientation – In triaxial compression tests, the major principal stress can act in only one of two directions – horizontal or vertical. Generally, in the field, the major principal stress is initially in the vertical position, then moves through some angle, θ, to the right and left of the initial position. The behaviour of granular materials when subjected to rotation of their principal axes is not fully understood. Joer et. al. (1998) conclude that cyclic rotation induces a general tendency to compaction of the specimen under consideration. In consequence, continued rotation of the principal axes may lead to liquefaction of the specimen.

(b) Consolidation Conditions – Sand samples in standard triaxial tests may be consolidated under hydrostatic stress conditions whereas, in the field, the soil element is initially consolidated under K_0 conditions i.e. the effective minor principal stress is K_0 times the effective major principal stress.

(c) Strain Conditions – Deformations in the field are assumed to occur under plane-strain conditions. In the triaxial test

configuration, deformations can occur in all three principal stress directions.

(d) Symmetry – Cyclic stress conditions are considered symmetric in the field. In the triaxial test, however, the intermediate principal stress is equal to the major principal stress during *lateral* compression, but equal to the minor principal stress during *axial* compression.

In addition to these important considerations, there are various problems inherent in the triaxial test which must also be outlined (Seed and Peacock, 1971).

(a) Unless special precautions are taken, friction between the loading cap and the top of the triaxial sample, and also between the cell base and the bottom of the sample, can cause stress concentrations leading to premature failure of the test specimen (e.g. Castro, 1969). This, in turn, produces a deviation from the desirable condition of uniform stress and strain. It should be noted here that the friction between the end caps and the specimen is necessary for the transmission of the axial load to the specimen. (Bishop and Henkel, 1957).

(b) During lateral compression of the specimen, the sample will tend to 'neck' prior to failure, which produces difficulties in determining the stress concentrations in the sample. For loose samples, in which liquefaction and large strain deformations occur almost simultaneously, this effect is not likely to be particularly significant, although it can have a detrimental effect on the observed behaviour of dense samples, leading to larger deformations than might otherwise be expected.

It should be clear from the preceding discussion that there are various problems with employing triaxial test specimens for the interpretation of field data. In this connection, specimen preparation is another area in which various investigators have been active (e.g. Ladd, 1977; Peck, 1979; Nemat-Nasser and Takahashi, 1984). Although there is agreement that many problems exist when attempting to reproduce a laboratory sample with the same void ratio, particle orientation, etc., as might be expected in the field, there is as yet no clear consensus on how these problems might be overcome in order that laboratory test results may be

considered truly representative of field data. In consequence, there has been a tendency in recent years to concentrate on developing numerical models for the evaluation of liquefaction (e.g. Elgamal et. al., 1999; Hicks and Boughrarov, 1998; Bouckovalas et. al., 1984; Dikmen and Ghaboussi 1984; Kagawa and Leland, 1981; Ghaboussi and Dikmen, 1981; Christian, 1980; Pyke, 1979).

With these restrictions in mind, it may appear that there is little value in employing the triaxial test for research into liquefaction. However, the triaxial test allows for relatively simple and direct measurement of stress, strain, and pore-water pressure measurement, all of which are essential components in any modelling of the liquefaction process. To date, no other practical test has yet been developed which approaches this versatility in data recovery and, as a result, the triaxial test has been used for the initial and crucial experimental phase of this thesis.

It is the opinion of the author that a clear correlation between laboratory testing and field results is of critical importance in the desirable development of a unified theory of liquefaction. There is an obvious need to be able to reproduce field conditions accurately under laboratory conditions. As a result, this thesis will present details for minor modifications of the triaxial apparatus in order that loose sand samples may be prepared with the minimum of interference from the investigator. Details of these modifications will be presented in Chapter 3; for the moment, it is sufficient to state that the author considers the lack of balance between empirical and computational research is counter-productive to a clear understanding of the liquefaction process.

2.2.4 Relationship Between Triaxial and Simple Shear Theory

In simple shear ($\Rightarrow$ field) tests, the conditions inducing liquefaction are expressed in terms of the ratio τ_{max}/σ'_0, whereas those in the triaxial test are expressed in terms of τ_{max}/σ_a. Therefore, it is clearly of benefit to determine a relationship between τ_{max}/σ'_0 and τ_{max}/σ_a. Such a relationship has been expressed by Seed and Peacock (1971), and is outlined here for the purpose of demonstrating that the results from triaxial tests may be simply adapted to interpret field observations.

The relationship depends on the value of K_0, the coefficient of lateral stress at rest, and also on the particular criterion controlling the initiation of liquefaction. Four criteria are considered:

(a) The stress ratio $(\tau/\sigma_c)_{max}$, which is the (maximum) ratio of the *shear* stress developed during cyclic loading to the *normal* stress during the consolidation phase on any plane within the sample.

(b) The stress ratio $(\Delta\tau/\sigma_c)_{max}$, which is the (maximum) ratio of the *change* in shear stress on any plane during cyclic loading to the *normal* stress on that plane during the consolidation phase.

(c) The stress ratio τ_{max}/σ_{mc}, which is the ratio of the *maximum* shear stress produced in a sample during cyclic loading to the *mean* principal stress on the sample during initial consolidation.

(d) The stress ratio $\Delta\tau_{max}/\sigma_{mc}$, which is the ratio of the *maximum* change in the shear stress on any one plane during cyclic loading to the *mean* principal stress on the sample during consolidation.

These four criteria were considered in turn by Seed and Peacock (1971) to produce simple relationships between the simple shear and triaxial conditions.

There are, as might be expected, other possible criteria which can be used to define the onset of liquefaction. Those summarised below offer a demonstrative selection of the practical options.

(a) The stress ratio $(\tau/\sigma_c)_{max}$

In a simple shear test, this ratio is approximately expressed by:

$$\left(\frac{\tau}{\sigma_c}\right)_{\max} \approx \frac{\tau_{hv}}{K_0 . p'_0} \qquad [2.2]$$

In the triaxial compression test, the relation becomes:

$$\left(\frac{\tau}{\sigma_c}\right)_{\max} = \frac{\tau_{\max}}{\sigma_a} = \left(\frac{\sigma_{dc}}{2\sigma_a}\right)_{triaxial} \qquad [2.3]$$

Thus, for the same conditions in the sample and the same failure criteria:

$$\left(\frac{\tau_{hv}}{K_0.p'_0}\right)_{ss} \cong \left(\frac{\sigma_{dc}}{2\sigma_a}\right)_{triaxial} \Rightarrow \left(\frac{\tau_{hv}}{p'_0}\right)_{ss} \cong K_0\left(\frac{\sigma_{dc}}{2\sigma_a}\right)_{triaxial} \quad [2.4]$$

where the subscript 'ss' denotes the 'simple shear' condition. K_0 approximates to 0.4 for a normally consolidated sample, indicating significantly lower values in the triaxial test data for subsequent analysis of results obtained from the field.

(b) The stress ratio $(\Delta\tau/\sigma_c)_{max}$

Under simple shear conditions, we have:

$$\left(\frac{\Delta\tau}{\sigma_c}\right)_{\max} \cong \frac{\tau_{hv}}{K_0.p'_0} \quad [2.5]$$

In a triaxial compression test:

$$\left(\frac{\Delta\tau}{\sigma_c}\right)_{\max} = \frac{\tau_{\max}}{\sigma_a} = \left(\frac{\sigma_{dc}}{2\sigma_a}\right)_{triaxial} \quad [2.6]$$

Thus, for failure at the same condition:

$$\left(\frac{\tau_{hv}}{K_0.p'_0}\right)_{ss} \cong \left(\frac{\sigma_{dc}}{2\sigma_a}\right)_{triaxial} \Rightarrow \left(\frac{\tau_{hv}}{p'_0}\right)_{ss} \cong K_0\left(\frac{\sigma_{dc}}{2\sigma_a}\right)_{triaxial} \quad [2.7]$$

which gives the same result as in (a) above.

(c) The stress ratio τ_{max}/σ_{mc}

Again, under simple shear conditions:

$$\tau_{\max} = \left(\tau_{hv}^2 + \left[\frac{p'_0(1-K_0)}{2}\right]^2\right)^{1/2} \quad [2.8]$$

while the mean principal stress during consolidation, σ_{mc}, is given by:

$$\sigma_{mc} = \frac{p'_0 (1 + 2K_0)}{3} \qquad [2.9]$$

After algebraic manipulation of [2.8] and [2.9], we have that:

$$\left(\frac{\tau_{hv}}{p'_0}\right)_{ss} = \left[\left(\frac{\tau_{max}}{\sigma_{mc}}\right)_{triaxial}\left(\frac{1+2K_0}{3}\right)^2 - \left(\frac{1-K_0}{2}\right)^2\right]^{1/2} \qquad [2.10]$$

In a triaxial compression test, we have that:

$$\left(\frac{\tau_{max}}{\sigma_{mc}}\right) = \left(\frac{\sigma_{dc}}{2\sigma_a}\right) \qquad [2.11]$$

so that, for failure:

$$\left(\frac{\tau_{hv}}{p'_0}\right)_{ss} = \left[\left(\frac{\sigma_{dc}}{2\sigma_a}\right)_{triaxial}\left(\frac{1+2K_0}{3}\right)^2 - \left(\frac{1-K_0}{2}\right)^2\right]^{1/2} \qquad [2.12]$$

Relationships calculated for different values of K_0 are given below:

$K_0 = 0.5$: $$\left(\frac{\tau_{hv}}{p'_0}\right)_{ss} = 0.25\left(\frac{\sigma_{dc}}{2\sigma_a}\right)_{triaxial} \qquad [2.13]$$

$K_0 = 0.6$: $$\left(\frac{\tau_{hv}}{p'_0}\right)_{ss} = 0.54\left(\frac{\sigma_{dc}}{2\sigma_a}\right)_{triaxial} \qquad [2.14]$$

$K_0 = 0.8$: $$\left(\frac{\tau_{hv}}{p'_0}\right)_{ss} = 0.83\left(\frac{\sigma_{dc}}{2\sigma_a}\right)_{triaxial} \qquad [2.15]$$

$K_0 = 1.0$: $$\left(\frac{\tau_{hv}}{p'_0}\right)_{ss} = 1.00\left(\frac{\sigma_{dc}}{2\sigma_a}\right)_{triaxial} \qquad [2.16]$$

(d) The stress ratio $\Delta\tau_{max}/\sigma_{mc}$

For simple shear conditions:

$$\frac{\Delta\tau_{\max}}{\sigma_{mc}} = \frac{3\tau_{hv}}{p'_0\left(1+2K_0\right)} \qquad [2.17]$$

In the triaxial compression test:

$$\frac{\Delta\tau_{\max}}{\sigma_{mc}} = \frac{\tau_{\max}}{\sigma_a} = \frac{\sigma_{dc}}{2\sigma_a} \qquad [2.18]$$

Thus, for failure:

$$\left(\frac{\tau_{hv}}{p'_0}\right)_{ss} = \frac{1+2K_0}{3}\left(\frac{\sigma_{dc}}{2\sigma_a}\right)_{triaxial} \qquad [2.19]$$

In each of the cases (a)-(d) above, the failure relation connecting simple shear and triaxial test conditions may be expressed in the form:

$$\left(\frac{\tau_{hv}}{p'_0}\right)_{ss} = \left(\frac{\sigma_{dc}}{2\sigma_a}\right)_{triaxial} \qquad [2.20]$$

Values of $\psi(K_0)$ for different values of K_0 for each of the four failure criteria given above are listed in Table 1.1 below. ψ represents the constants established in Equations [2.4], [2.7], [2.12] and [2.19] respectively.

	Liquefaction Criteria			
K_0	$(\tau/\sigma_c)_{max}$	$(\Delta\tau/\sigma_c)_{max}$	τ_{max}/σ_{mc}	$\Delta\tau_{max}/\sigma_{mc}$
0.4	0.4	0.4		0.60
0.5	0.5	0.5	0.25	0.67
0.6	0.6	0.6	0.54	0.73
0.7	0.7	0.7		0.80
0.8	0.8	0.8	0.83	0.87
0.9	0.9	0.9		0.93
1.0	1.0	1.0	1.00	1.00

Table 1.1 *– Liquefaction Criteria*

2.3 MITIGATION OF LIQUEFACTION HAZARDS

2.3.1 Introduction

It can be seen from the details already presented in this Chapter that, in order to minimise the risk to structures and utilities from the often-catastrophic effects of liquefaction, effective soil improvement techniques need to be employed. The ultimate goal of mitigation techniques would be the reduction of the tendency for excess pore-water pressures to build up during earthquake shaking, to the point where any liquefaction phenomena may be successfully inhibited.

It should, however, be carefully noted that, while it is possible to assess a particular site's potential for liquefaction, its occurrence (in terms of time, place, and severity) is no more predictable than the seismic motion that triggers it.

The practicing engineer's knowledge of liquefaction and, in particular, liquefaction hazards, has been greatly improved through the mapping of the liquefaction potential on a regional scale. Superimposing a liquefaction opportunity map onto a liquefaction susceptibility map produces a map of liquefaction potential. Liquefaction opportunity is a primarily a function of both the intensity of the earthquake shaking, and also the frequency (occurrence) of the seismic events. Liquefaction susceptibility, as already outlined, depends on such internal factors as the depth of the water table, and the type and density of the soil in question. Areas which have high levels of liquefaction opportunity in addition to a high liquefaction susceptibility will clearly have a high liquefaction potential. Should either the opportunity or susceptibility be high, while the other is low, then the site will have an intermediate liquefaction potential. Sites with low opportunity and susceptibility will clearly have a low liquefaction potential.

Liquefaction potential maps now exist for many of the regions around the world which are currently known to be, or which have been in the past, prone to liquefaction hazards. Those regions which have been successfully mapped include California, through which the San Andreas transform fault runs, and the eastern seaboard of Japan, which lies on the seismically active zone where the Pacific plate subducts the Eurasian plate.

The California Division of Mines and Geology (CDMG) (1992) has mapped those sites throughout the state which have been deemed prone to liquefaction hazards. These maps are used in conjunction with individual

properties known to exist at a hazard zone, such as initial shear stresses on representative elements of soil. For the purposes of the CDMG, these zones are defined as areas meeting one or more of the following criteria:

(a) areas known to have experienced liquefaction during previous earthquakes;

(b) all areas of uncompacted fill containing saturated or nearly saturated liquefaction-susceptible material. Areas which can expect to become saturated, possibly due to seasonal changes in the height of the water table, are also included here;

(c) areas where the existing geotechnical and geological data suggests that the soils are potentially liquefiable; and

(d) areas underlain with saturated, geologically young sediments, perhaps younger than 10,000 years old.

Such maps allow positive identification of those sites which have both high and low liquefaction susceptibilities, thus enabling the engineer to make an informed choice regarding the technique to be used in the mitigation.

The two most commonly used methods for preventing large increases in excess pore-water pressures, as currently used in engineering practice, are:

(a) improvement of a site's drainage capacity; and

(b) reduction of the void ratio of the soil.

Clearly, both of these measures will lead to some degree of settlement in the soil, and so neither would be satisfactory for sites where structures currently exist. Incorporating a method for liquefaction mitigation at a site which has a structure present is more expensive than those methods which can be used in the free-field situation.

For a structure, either existing or under construction, the choices for liquefaction mitigation which would bring minimal damage include:

(a) the strengthening of the structure to resist the predicted ground movements, for example through lateral spreading of liquefied soil; and

(b) appropriate selection of foundation type and depth, including modifications to the foundations of existing structures, so that the structure is not adversely affected by ground movements.

In addition to the techniques described here, a new method of liquefaction mitigation, which utilises the physical characteristics of a partially saturated soil, will be proposed later in this thesis. It will be seen that this innovative procedure has some advantages over those described in this Chapter, and it is anticipated that, with sufficient refinement, the use of partially saturated soils as a viable mitigation procedure may be successfully employed on a wider scale.

However, it should be noted that while the study of the effectiveness of partial saturation as a means of liquefaction mitigation remains the primary focus of this thesis, no attempt has been made to compare the success (or otherwise) of the method with existing mitigation processes.

Also, the permanence of soil in the partially saturated condition should be considered. Again, this thesis does not provide any insights into this aspect, although it is recognised that partially saturated soils will be affected by the flow of water through the soil, resulting in a changes in the height of the water table at a given site. It is to be expected that the more stable the water table at a particular location, the more likely that any partially saturated soil below the water table will remain in that condition.

2.3.2 Mitigation of Liquefaction in the Field

Improvement of Drainage

If pore-water pressures are permitted to rise in a closed system, such as that which is assumed to exist in a subsurface soil during an earthquake, or in a triaxial test with the backpressure/pore-water pressure valve closed, then any excess pore-water pressures induced as a result of loading on the system will not be permitted to dissipate.

For a granular soil, a drain is made from a material of higher void ratio, in order that excess pore-water pressures may dissipate more quickly. For example, if a given stratum of sand is considered susceptible to liquefaction, then a gravel drain may be installed vertically through the stratum in order to allow rapid dissipation of predicted pore-water pressures. To install the drain, a steel casing is driven in through the sand, gravel is in-filled from the top of the casing, and then tamped while the casing is finally removed.

Drains may also consist of a network of high discharge-capacity pipes, such as those installed on St. Lucia, which proved very effective against liquefaction damage during the earthquake of June 8th 1999. Water expelled from the sand as a result of the rise in pore-water pressures entered the pipes radially, and flowed upward into a reservoir constructed above the water table. The total length of the drains used in this particular project exceeded 150,000 metres. Such drains may be installed in half the time of stone or gravel columns, and at around one-third of the cost. Further information regarding drains of this type, including details of drainage procedures installed in St. Lucia, can be obtained from the Geotechnics America Inc. website.

Kerwin and Stone (1997) review the installation of stone/gravel drains at marina facilities at King Harbor, Redondo Beach, California, following the Northridge earthquake of 1994. The area had suffered extensive damage through lateral spreading and differential settlement of structures. The reconstructed facilities contained stone/gravel columns, which were installed by a vibratory displacement method. This procedure had the additional effect of densifying the soil in the immediate vicinity of the columns, thereby providing further protection against liquefaction phenomenon.

While the use of gravel columns can significantly increase the drainage of a sand stratum, the liquefaction behaviour of a sand/gravel composite soil is less clearly understood. Evans and Zhou (1995) present the data from a test programme conducted to investigate the effect of gravel content on the liquefaction resistance of such composites. The writers conclude that liquefaction resistance of sand/gravel composites may increase with increasing gravel content.

Dynamic Compaction

Among the more obvious soil improvement techniques in use is that of dynamic compaction, in which a heavy weight (normally composed of steel or concrete) is dropped from a height of up to 100 feet onto the susceptible soil below. Although economical, the dynamic compaction method has the disadvantage of being highly invasive, and the irreversible volume changes produced tend to result in settlement of the surrounding ground surface. With some techniques, additional soil is introduced at the surface to minimize this effect.

This method is based on the principle that the stiffness of a granular soil is higher when the particles are packed closely together rather than when they remain in a loose state. An increase in stiffness results in decreased strains in response to the earthquake motion. Thus, the scope for the increase of excess pore-water pressures, as outlined in Section 2.2, is reduced.

A comprehensive account of a case study, involving the successful use of dynamic compaction, is provided by Bevan (1997).

Vibroflotation

The technique of vibrating a granular soil in order to reduce its void ratio, thereby increasing its density, is widely used in laboratory testing. The vibroflotation method employs this principle in the field of liquefaction mitigation; a vibrating probe, or vibroflot, is inserted into the sand to depths of 80 to 100 feet. The vibrations cause the grain structure around the vibroflot to collapse, thereby desifying the nearby soil. In order to treat a wide area of soil considered to be susceptible to liquefaction, the vibroflot is used in a grid pattern.

At the start of the process, the vibroflot is lowered to the bottom of a borehole, previously drilled in the deposit (Kramer 1996). It is then withdrawn, still vibrating, at a rate of around 30cm per minute. The vibrations produce localised areas of liquefaction, which causes the soil around the vibroflot to densify.

As the vibroflot is withdrawn, new granular material is introduced into the borehole through the tip of the vibroflot. Normally, this material consists of gravel which, due to its high void ratio, permits the drainage of excess pore-water pressures at later times.

Vibro-replacement is a highly efficient combination of vibroflotation and the insertion of a gravel backfill (as described above), which provides an extra degree of reinforcement to the densified soil in the form of an effective drain.

Compaction Piles

Compaction piles, which are normally made of pre-stressed concrete, are driven into the soil to a depth of around 60 feet. Installation of the piles, which is normally done in a grid pattern, both densifies and reinforces the susceptible soil.

Compaction Grouting

Compaction grouting is a relatively new technique in which a slow-flowing viscous mix of sand, water, and cement is injected under pressure into a granular soil. The grout forms a 'bulb' which displaces sand particles and thereby densifies the surrounding soil. The advantage of compaction grouting is that the mix does not have to be injected vertically, a property employed successfully in the ongoing project to stabilise the Leaning Tower of Pisa. Although not susceptible to liquefaction, the ground beneath the Tower did not have sufficient bearing strength to prevent the inclination of the structure from increasing over time. Rather than disturb the ground close to the Tower, which is clearly undesirable, the grout was injected from as much as 50 metres away, at an angle which allowed the reaction between the injected mix and the soil beneath the tower to be controlled. Since injection, the Tower has been stabilised, and a small fraction of the lean has been corrected.

A grout mass may commonly have a diameter of 1 metre (Warner, 1982). Therefore, neglecting heave at the surface, the total void volume of the soil will be reduced by the volume of the grout mass. The grout itself might have a slump of no more than 2.5 cm, due to its viscosity. Spacings of grout masses range between 1 m and 4.5 m, depending on the subsurface conditions. The looser the soil, the closer the grout masses will generally tend to be.

A comprehensive case study involving the use of compaction grouting in liquefaction control is provided by Baez and Henry (1993), while further descriptions of the grouting method with explicit reference to foundations engineering are provided by Stilley (1982). More recently, Boulanger and Hayden (1995) reviewed the available case history data on the treatment of liquefiable soils by compaction grouting, providing observations that are useful in evaluating the effectiveness of future compaction grouting applications.

Blasting

Densification of subsurface granular soil by blasting is achieved by detonation of charges, placed in boreholes. The boreholes are vertical, and the charges may be between 3m and 6m apart. The boreholes are backfilled with further granular material before the charges are detonated.

On detonation, the ground surface heaves, and subsurface air and water are expelled through the resulting fractures. The soil then settles into a denser configuration than existed previously, thus increasing the resistance to liquefaction phenomena.

The main disadvantages of blasting are the strong vibrations produced, which may have unwanted consequences for nearby structures, while the storage of the hazardous explosives is expensive. Further accounts of the use of blasting in liquefaction mitigation are provided by Solymar and Reed (1986) and Hachey et. al. (1994).

Gohl et. al. (2000) provide a description of explosive compaction, a method used in various projects for the past 70 years. Explosive compaction involves placing an explosive charge at depth, and then detonating the charge. Normally, several charges are fired at one time, with slight delays between the detonation of each charge. The purpose of this delay is to enhance the effect of cyclic loading while, at the same time, minimising the peak acceleration. Explosive compaction produces volume changes which can be as much as three times larger than those that might occur with strong earthquake motions, with final average densities often greater than 70%. Environmental and vibration control issues do not constrain the employment of explosive compaction, provided that appropriate explosives, controlled storage, and delayed detonation sequences are observed.

Reinforced Earth Technique

Krishnaswamy and Isaac (1995) report on a laboratory study of small-sized sand samples, in which it was demonstrated that the liquefaction resistance of sand deposits could be markedly increased by the reinforced earth technique. Such reinforcement utilises woven geotextiles, nonwoven geotextiles, and coir (natural fabric). The woven geotextile employed by the writers was polypropylene of mass 209g/m^2, and thickness 0.50mm. The nonwoven geotextile was so-called 'needle-punched' polypropylene of mass 460g/m^2 and thickness 3.90mm. Finally, the coir had a mass of 1000g/m^2 and thickness 7.00mm. The geotextiles were either placed laterally inside the specimens, or placed around its exterior. In all cases, the resistance of the sand specimens to liquefaction was increased.

2.4 THE INITIATION OF LIQUEFACTION

2.4.1 Monotonic Loading

The conditions that exist at the onset of liquefaction may best be observed when a specimen of granular soil is subjected to monotonically increasing stresses. Figure 2.11 below shows the response of an isotropically-consolidated specimen of very loose saturated sand. The specimen is then subjected to stress-controlled compression in an undrained triaxial test.

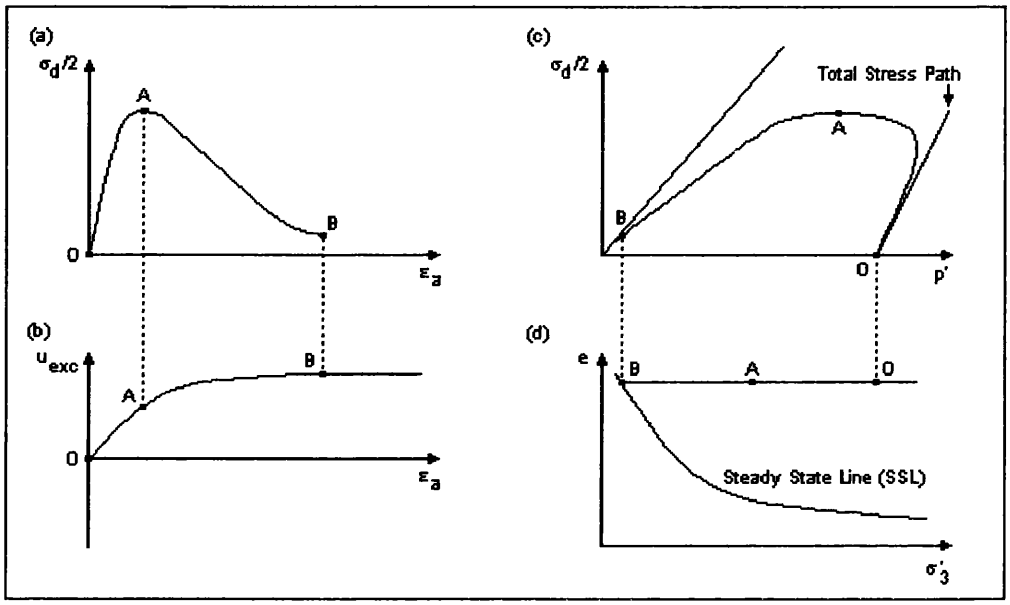

***Figure 2.11** – Monotonic Loading*

Prior to the commencement of the test (Point *O,* Figure 2.11 above), the specimen has zero shear stress ((a) and (c), where $q = 0$), and is in drained equilibrium with the confining pressure σ'_{3c} i.e. the excess pore-water pressure is also zero (b). From (d), it can be seen that the initial state of the specimen plots high above the SSL, confirming its very loose state and subsequent contractive behaviour.

As the axial load is applied ($q > 0$), the shearing resistance of the specimen begins to be mobilized, and excess pore-water pressures start to be generated. The shearing resistance reaches its maximum value at Point *A*, where the specimen is most unstable. Beyond Point *A*, the particle matrix begins to

collapse, and the axial strain may increase from around 1% to 20% in as little as a fraction of a second. Flow liquefaction is initiated at Point *A*.

Pore-water pressures will also continue to increase beyond point *A*, reaching a maximum value when the shear stress on the specimen becomes constant (Point *B*). Beyond Point *B*, the specimen is in the critical state, within which the effective stress within the specimen has dropped to almost zero. In this condition, the specimen is exhibiting *flow liquefaction*, since the static shear stress required for equilibrium (Point *A*) is greater than the shear (residual) strength of the liquefied soil. Point *B* is called the *steady state point*.

The position and shape of the stress path in Figure 2.11(c) is primarily determined by the effective confining pressure on the specimen. Figure 2.12 overleaf shows stress paths for five specimens, initially at the same void ratio, but subjected to differing confining pressures.

Specimens 'A' and 'B' both plot below the SSL, and therefore they will exhibit dilative behaviour on the applications of a shear stress. Specimens 'C', 'D', and 'E' all plot above the SSL, and so each will exhibit contractive characteristics on shearing. Flow liquefaction is initiated at the top of the stress paths (Figure 2.12(a)). It has been shown that the locus of points describing the stress state on the initiation of liquefaction is a straight line which, when extrapolated, passes through the origin of the stress space (e.g. Vaid and Chern, 1983). This locus is termed the *flow liquefaction surface* (FLS), and it describes the conditions at which flow liquefaction will be triggered. The literature sometimes describes the flow liquefaction surface as the *instability line* (e.g. Lade, 1999). It should also be noted that the line joining the steady state point to the flow liquefaction surface is horizontal since liquefaction cannot occur beneath this level. The intercept of this horizontal line on the q-axis is referred to as the *steady state strength* of the soil, S_{su}.

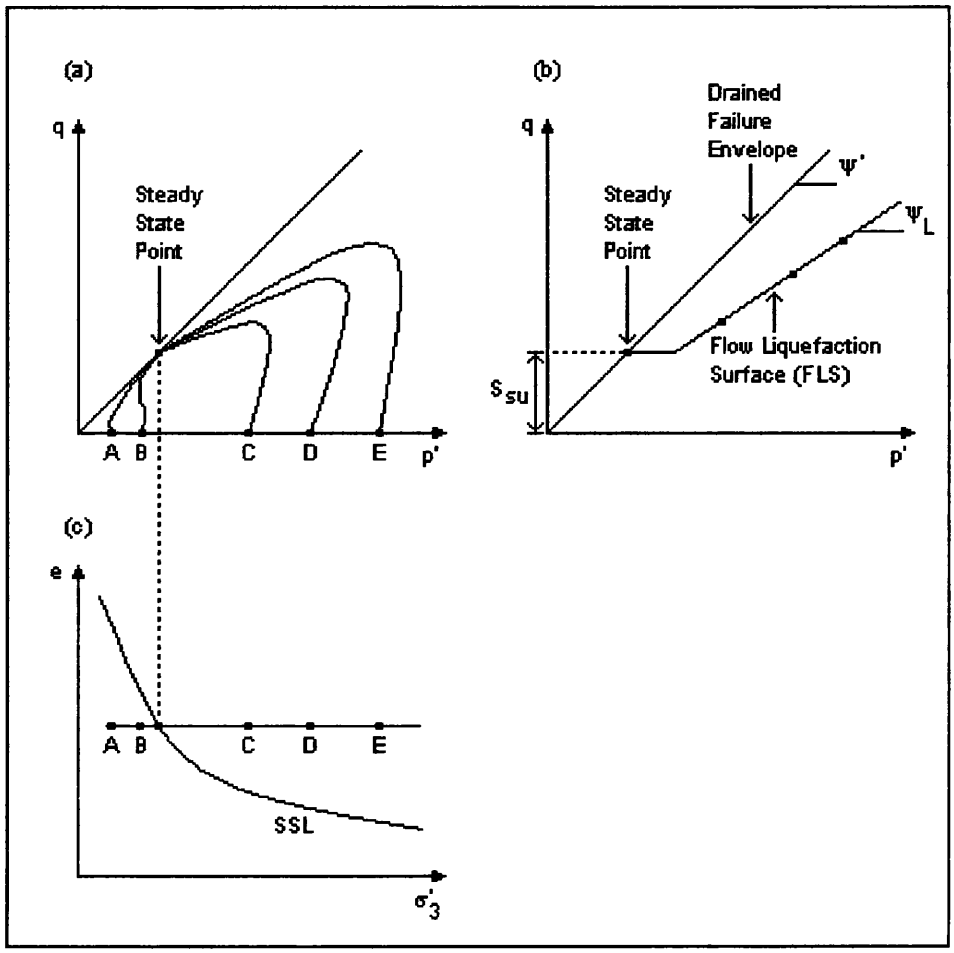

Figure 2.12 – Comparison of Various Monotonic Loadings

The slope of the FLS is approximately $^2/_3$ that of the drained failure envelope (e.g. Kramer, 1996) i.e. $\psi_L = (2/3)\psi'$, although the slope of the FLS may increase if specimens are tested under anisotropic conditions rather than isotropic ones, as is the case here. There is sufficient evidence in the literature to suggest that the FLS may apply to both monotonic and cyclic loading (e.g. Vaid and Chern, 1983), although it is not known at present whether liquefaction is initiated *exactly* at the FLS for cyclic as well as monotonic loading.

If the stress state in a given element of soil under undrained conditions reaches the FLS, then flow liquefaction will inevitably occur. The shearing strength of the soil will then be reduced to its residual value. In cases where the initial shear stress on the specimen is such that the point defining its stress state and the steady state point are in close proximity, then it may be possible that only a small, undrained disturbance would be sufficient to trigger liquefaction.

An important series of triaxial tests was conducted in the mid-1960's by Gonzalo Castro, a student of Casagrande's. Both static (⇒ monotonic) and cyclic tests were performed on specimens that were isotropically-consolidated, whilst anisotropically-consolidated specimens were only subjected to static loadings (Castro, 1969). Three different types of constitutive behaviour were observed, with each type being dependent on the initial state of the soil (Figure 2.13 below).

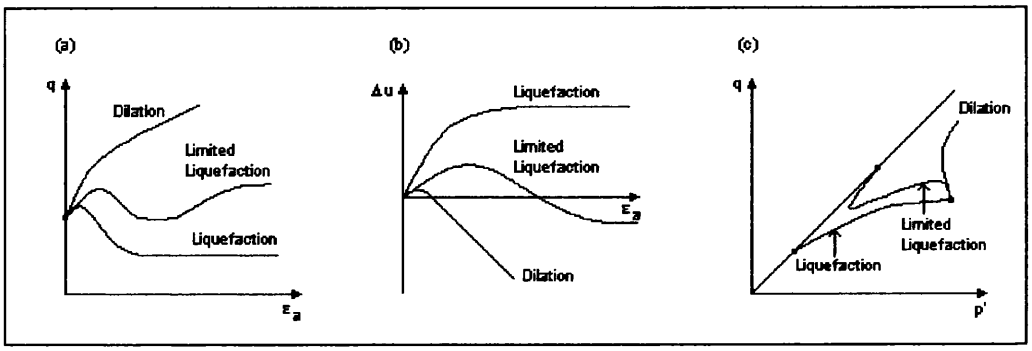

***Figure 2.13** – Liquefaction, Limited Liquefaction, and Dilation*

For dense specimens (i.e. low void ratio), the soil matrix initially contracted before dilating with increasing shear stress and effective confining pressure. For medium dense specimens, the peak strength was exceeded at low strain following a short period of contraction. A brief phase of strain-softening preceded dilation of the specimen at intermediate strains and beyond. Castro (1969) observed that very loose specimens exhibited a peak undrained strength at minimal shear strains, before failing rapidly at large strains and at low effective confining pressure. The writer termed these three types of behaviour 'dilation', 'limited liquefaction', and 'liquefaction' respectively.

Therefore, a monotonic test in which the initial conditions are such that flow liquefaction is eventually induced, may be said to consist of two distinct phases. In the first phase, which occurs at low values of strain, excess pore-water pressures of sufficient magnitude are generated such that the stress path is brought to the FLS. At this point, the specimen becomes unstable, and flow liquefaction is thereby initiated at the start of the second phase. Here, the pore-water pressure builds up swiftly as the specimen strains rapidly to the critical

state condition. At the critical state, the specimen continues straining at constant shear stress and constant volume. Since the change in volumetric strain within an element is directly proportional to the change in excess pore-water pressure within that element, it follows that, at the critical state, there can be no further increases in excess pore-water pressure.

The concepts of the critical state and the flow liquefaction surface provide a basis from which liquefaction may be understood.

2.4.2 Cyclic Loading

In the previous sub-Section, the method by which information pertaining to the initiation of liquefaction may be extracted from undrained monotonic triaxial tests was demonstrated. In addition, there has been significant progress reported in the literature with regard to cyclic testing, and this will be further discussed later in this thesis.

Figure 2.14 below shows the responses of two loose, saturated sand specimens, as might be obtained from standard stress-controlled undrained laboratory tests. The specimens have been anisotropically consolidated, and are both in drained equilibrium under some static shear stress, τ_s. Both specimens are loaded in the undrained condition. Note that τ_s is greater than S_{su}, the steady state strength, which is the defining condition for the occurrence of flow liquefaction.

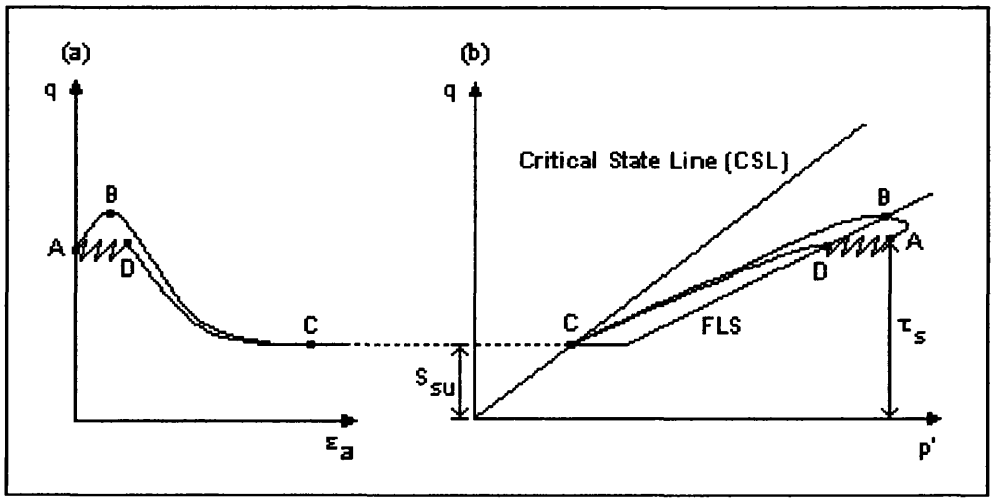

***Figure 2.14** – Response of Loose, Saturated Sand to Monotonic & Cyclic Loading*

The first specimen is loaded monotonically until the peak shearing resistance is mobilized at Point *B*. As discussed earlier, flow liquefaction is now initiated, and the specimen collapses through instability. Large strains are quickly induced in the specimen, which is now at the steady state (Point *C*). Beyond Point *C*, the specimen will continue straining under constant shear stress and constant volume, and so is in the *critical state*.

The critical state line, or CSL, represents those states of stress existing in the soil specimen at the onset of the critical state. The slope of the critical state line, which passes through the origin, is a function of the effective angle of internal friction, ϕ', and will be used in the analysis of the results of the triaxial test programme conducted for the purposes of the current research.

The second specimen is loaded cyclically. On each cycle, a small shear stress is applied, resulting in an increase in the axial strain. On removal of the stress in the second half of the cycle, some, but not all, of the strain is recovered. Therefore, even for the small strains described here, the specimen does not behave perfectly elastically, a fact confirmed by the fully non-linear response of a similar specimen to a monotonic load.

As the number of cycles increases, the stress path for the specimen moves to the left. This is due to the increases in pore-water pressure brought about by the plastic straining of the specimen. The effective confining stress (p') then falls according to the classical effective stress equation. As in the monotonic test, the specimen becomes unstable when it reaches Point *D* on the flow liquefaction surface, whereupon it rapidly converges to the steady state.

2.4.3 Flow Liquefaction, Cyclic Mobility, and the FLS

It was stated in Section 2.1 that flow liquefaction would develop in a given specimen if the static shear stress were greater than the shear strength of the liquefied soil. The static shear stress, which is caused by gravity, is the initial stress condition of the soil, whilst the shear strength of the liquefied soil is the steady state strength, S_{su}. Therefore, a given soil is susceptible to liquefaction if its initial state plots anywhere in the shaded area shown in Figure 2.15 overleaf.

An undrained disturbance of sufficient magnitude is now required to move the effective stress path from its initial point within the shaded area, and on to the flow liquefaction surface (FLS).

Cyclic mobility, which can affect both loose and dense saturated soils, does not involve a loss in shear strength in those soils. However, incremental shear strains are induced. Soils whose initial states lie within the shaded area of Figure 2.15 are susceptible to cyclic mobility. Soils with initial states which plot above the FLS will converge rapidly to the critical state line.

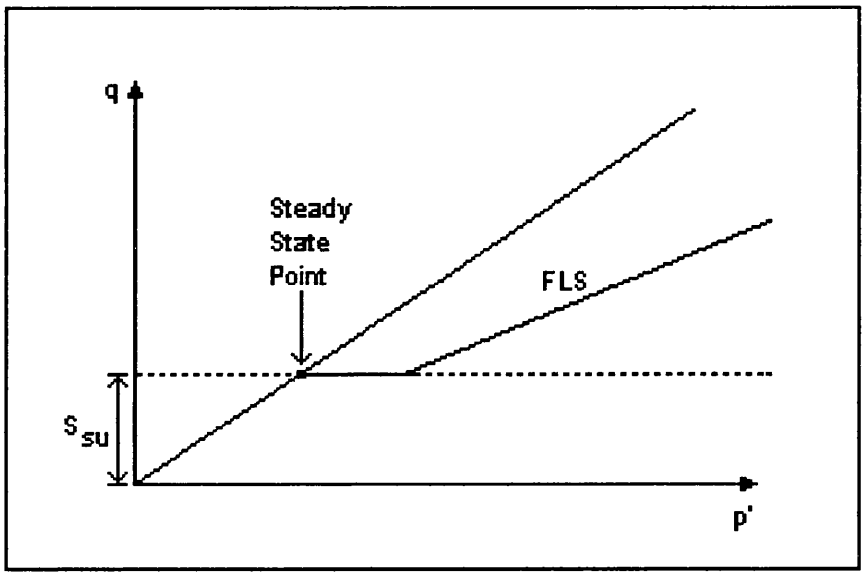

Figure 2.15 *– Flow Liquefaction Surface (from Kramer, 1996)*

Given that τ_{cyc} is the maximum amplitude of the cyclic shear stress application, and τ_s is the initial static shear stress on the soil specimen, there exist three combinations of initial conditions and cyclic loading conditions which normally produce cyclic mobility. These are:

(a) $\tau_s + \tau_{cyc} < S_{su}$, and $\tau_s - \tau_{cyc} > 0$

(b) $\tau_s + \tau_{cyc} > S_{su}$, and $\tau_s - \tau_{cyc} > 0$

(c) $\tau_s + \tau_{cyc} < S_{su}$, and $\tau_s - \tau_{cyc} < 0$

Each of these cases will now be discussed in detail.

(a) $\tau_s + \tau_{cyc} < S_{su}$, and $\tau_s - \tau_{cyc} > 0$

These conditions indicate that, firstly, there is no exceedance of the steady state strength and, secondly, there is no shear stress reversal by ensuring that $q > 0$ at all times. Here, the effective stress path moves to the left as the number of cyclic stress applications is increased until the drained failure envelope is reached, indicating significant increases in the pore-water pressure and a corresponding decrease in the effective confining stress. At this point, further stress applications will merely move the stress path back and forth along the drained failure envelope (between points A and A').

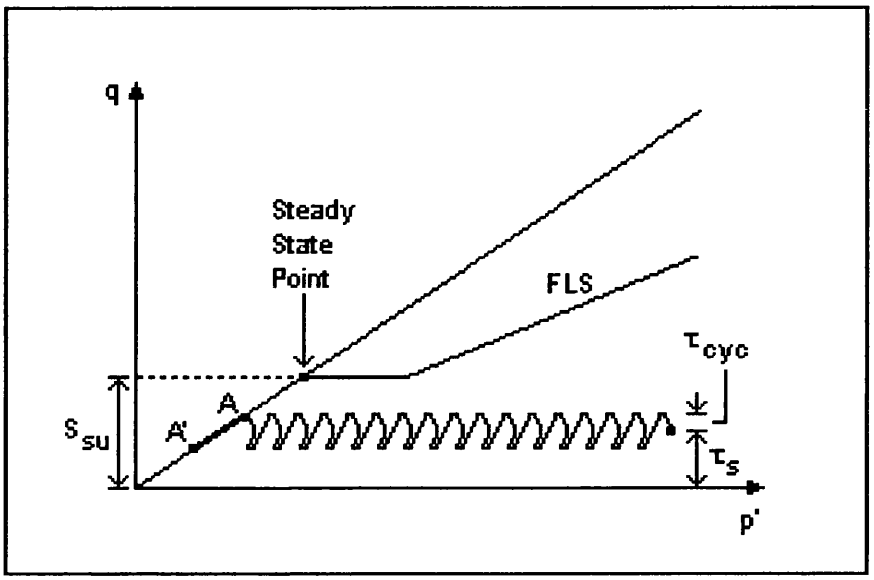

Figure 2.16 *- $\tau_s + \tau_{cyc} < S_{su}$, and $\tau_s - \tau_{cyc} > 0$ (from Kramer, 1996)*

(b) $\tau_s + \tau_{cyc} > S_{su}$, and $\tau_s - \tau_{cyc} > 0$

Again, there is no stress reversal as $q > 0$ but, in this case, the steady state strength is exceeded at intervals during the application of the cyclic shear stress, τ_{cyc}. The cyclic shear stresses will increase the pore-pressure in the specimen, resulting in the stress path moving once more to the left and away from the initial state. The specimen will be unstable on reaching the FLS; this may occur more than once during the application of the cyclic shear stresses. In these instances, significant strains may develop, although the stress path will still move toward the drained failure surface whilst being contained below the FLS. The stress path

will once again move between two points on the drained failure surface i.e. the specimen is stable.

This situation is shown in Figure 2.17 overleaf. Note that the stress path in this case remains constrained by the FLS as the steady state point is approached.

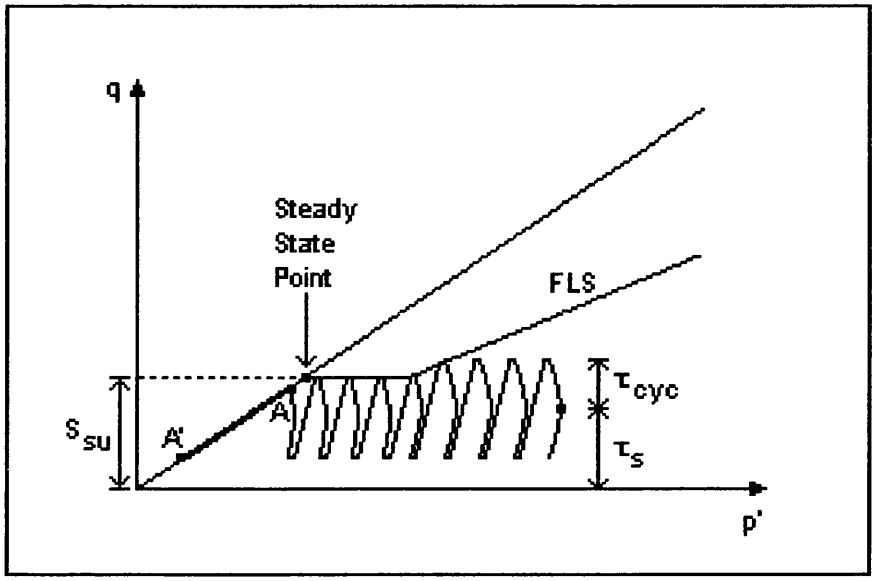

Figure 2.17 *- $\tau_s + \tau_{cyc} > S_{su}$, and $\tau_s - \tau_{cyc} > 0$ (from Kramer, 1996)*

(c) $\tau_s + \tau_{cyc} < S_{su}$, and $\tau_s - \tau_{cyc} < 0$

Here, the steady state strength is not exceeded at any time (Figure 2.18), although stress reversal does occur ($q < 0$). Each cycle will now include both *compressional* (above the p' axis) and *extensional* (below the p' axis) phases. It has been demonstrated in the literature that the rate of pore pressure generation increases with increased degree of stress reversal. This is explained (e.g. Mohamad and Dobry, 1986) by the larger cyclic strains generated in the extension part of the cycle. This indicates that, with this combination of conditions, the effective stress path will move more quickly to the left than was the case with either (a) and (b) above. On reaching the drained failure envelope, the stress path will oscillate between the compressional and extensional parts.

Mohamad and Dobry (1986) also state that, for contractive specimens, the resistance to liquefaction increases with increasing τ_s if there is stress reversal, *and* if the peak strength τ_p ($= \tau_s + \tau_{cyc}$) is smaller than the steady state strength, S_{su}.

If τ_s is greater than S_{su}, then liquefaction resistance can either increase or decrease with increasing τ_s. If there is no shear stress reversal, the liquefaction resistance will always decrease with increasing τ_s. For dilative specimens, liquefaction resistance will always increase with increasing τ_s. A partially-contractive sand under cyclic loading behaves like a contractive sand for small accumulated failure strains, and like a dilative sand for large accumulated failure strains. Liquefaction resistance is sometimes termed 'cyclic strength' in the literature.

During each stress cycle, the stress path will pass through the point $q = 0$. Thus, liquefaction can only occur with this particular combination of conditions, as no other combination takes the stress path across the origin. However, it does not mean that the soil has zero shear stress at these points. If a monotonic load is applied when the stress path reaches $q = 0$, the specimen will dilate until the maximum shear resistance is mobilized.

The state of *initial* liquefaction was defined by Seed and Lee (1966) as that point at which the total increase in pore-water pressure within the soil was equal to the effective confining pressure (i.e. $u_{excess} = \sigma'_{3c}$).

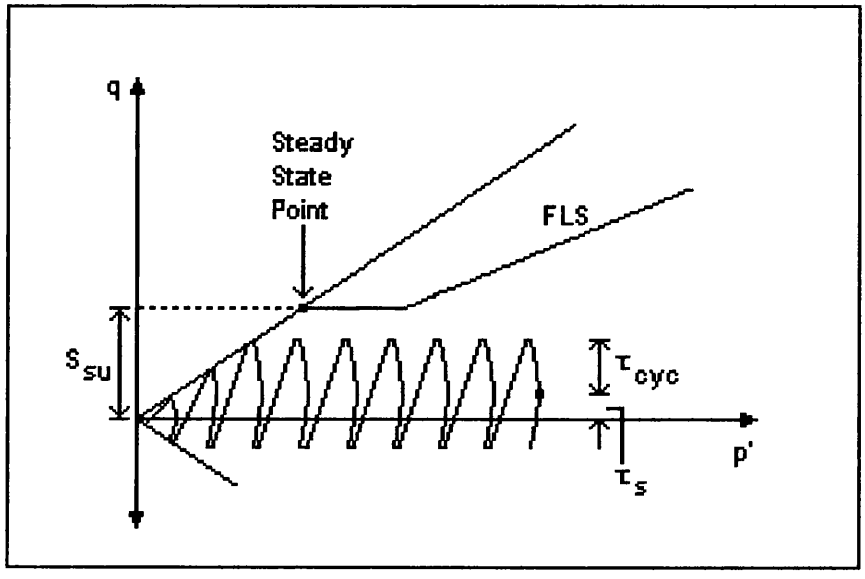

Figure 2.18 *- $\tau_s + \tau_{cyc} < S_{su}$ and $\tau_s - \tau_{cyc} < 0$ (from Kramer, 1996)*

2.5 EXPERIMENTAL RESEARCH AND NUMERICAL MODELLING

2.5.1 Introduction

In the 38-year period since the earthquakes in Niigata and Alaska, many attempts have been made to quantify the liquefaction process, and hence to describe that process in a truly mathematical form. This is clearly desirable since, in the absence of a numerical model which successfully predicts field observations, the development of a universally-accepted algorithm is not possible.

The primary purpose of such an algorithm would be to analyse the subsurface conditions prior to the occurrence of liquefaction. These conditions might include the nature and depth of soil layers, consolidation history, upper and lower limits of the water table, etc. An input motion (earthquake) may then be introduced into the model by means of an accelerogram, which is a computer input file consisting of ground acceleration values. Depending on the sophistication of the model, it should then be possible to examine the progress of liquefaction through the soil, and to assess any surface and subsurface damage that this liquefaction may cause.

A model of this depth would positively complement the experimental research on, for example, representative soil samples recovered from the area in question for the purpose of determining the liquefaction susceptibility at that particular site. The recovery of field specimens is a science in itself, and the process by which a sand sample from the field may be returned to the laboratory in a totally undisturbed state has yet to be determined. The absence of such a description, quite clearly, immediately introduces a correction factor into any results obtained through laboratory research, even before the specimen has been placed into the testing apparatus. Further correction factors may be required in respect of the unwanted but totally necessary manipulation of the specimen during the setting-up phase. Finally, any discrepancy in the stress conditions that the specimen might experience in the field in comparison with the laboratory test must also be taken into account. It should be seen, therefore, that the results obtained from the testing of sand specimens in the laboratory, while not completely arbitrary, must always be considered as somewhat inaccurate.

This Section will discuss the latest advances in experimental research, and also the current methods by which specimens are extracted from the field, as

well as examining the latest and also most notable developments in the numerical modelling of the liquefaction process.

2.5.2 Extraction of Field Specimens

The successful removal of undisturbed sand specimens from the field is a problem not only in liquefaction analysis, but also in other areas of geotechnical engineering. Such problems are not associated with sand alone. For example, a clay sample will swell on sampling due to the removal of the in-situ confining stresses. However, for the purposes of this work, only those difficulties associated with sand specimens will be considered.

An undisturbed soil specimen may be loosely defined as one in which the degree of saturation, in-situ void ratio, structure, or stress history remains unaltered from the commencement of extraction to the start of the laboratory test. These criteria, and their respective importance in the context of stress-strain development in the laboratory specimen, are discussed further by Hofmann (1997).

Initially, it should be noted that sand is a granular material. Due to the relatively large size of sand particles, no form of cohesion between the particles exists, such as the electrostatic force which is present between neighbouring colloidal particles in a clay. Any attempt to remove sand from its natural state will result in irreversible rearrangement of the soil structure, which is clearly undesirable for any subsequent programme of testing in the laboratory.

By convention, tube sampling is used to extract clay samples from the ground, but it has been amply demonstrated that this method, when applied to sand, will densify loose specimens and loosen dense specimens (e.g. Seed et. al., 1982; Yoshimi et. al., 1994).

Changes in arrangement and orientation of sand particles can have significant consequences for the value of the cyclic strength, as determined in the laboratory. Ladd (1977) concluded that variations in the cyclic strength of more than 100% can occur when testing reconstituted specimens of sand, prepared by different methods. As outlined earlier, Ladd states that, after an evaluation of the soil fabric studies presented in the literature, these cyclic strength discrepancies are related to three variances in the fabric of the sand, namely:

(i) differences in grain and interparticle contact orientation;

(ii) variations in void ratio within an individual specimen; and

(iii) the segregation of the particles.

However, Ladd (1977) acknowledges that the cyclic stress-strain development of in-situ specimen is relatively similar to that of a reconstituted specimen prepared by pluviating (pouring) the sand through water (e.g. Finn et. al. 1971 a & b; Lee and Seed 1967), Seed and Lee 1966). This is an important observation, and will be exploited later in this work where the preparation of loose, reconstituted sand specimens by a new method is rigorously discussed.

In addition to Ladd's conclusions, Mulilis (1975) proposes that the method of densification may also have a considerable bearing on the measurement of cyclic strength on a reconstituted specimen.

Two types of soil fabric are identified, both of which may influence the mechanical response of a sand specimen when attempting to model the cyclic stress-strain development (Nemat-Nasser and Takahashi, 1984). These are:

(i) inherent anisotropy; and

(ii) induced anisotropy.

Inherent anisotropy originates in the method used for the sample preparation and natural deposition, while induced anisotropy is produced by plastic flow induced by the applied (cyclic) loading. Both of these forms of anisotropy affect the cyclic stress-strain behaviour of a soil specimen (e.g. Oda, 1972).

One of the most commonly used methods of loose sand sampling is that of in-situ freezing (e.g. Sego et. al., 1999; Seed et. al., 1992; Davila et. al., 1992; Broms, 1980). Yoshimi et. al. (1994) describe a method of obtaining undisturbed in-situ samples of saturated clean sand by freezing it in-situ using a single freezer pipe. The writers contend that tests indicate the method can yield high-quality specimens that retain the density and undrained cyclic strength of the in-situ sand. The liquefaction resistance of the frozen samples correlates well with that determined by the standard penetration test for the in-situ sand.

In recent research, the ground-freezing technique was applied at six sites during the Canadian Liquefaction Experiment (CANLEX) in the mid-1990's. Among the primary objectives of the CANLEX project was the evaluation of the in-situ undrained response of various sand masses, thereby permitting a model for the direct linking of field and laboratory data. The in-situ soil was frozen

using liquid nitrogen. A 1m radius of soil was frozen, with the samples extracted no further than 0.4m from the centre of the frozen zone.

As part of the CANLEX project, undisturbed samples of tailings sand were recovered after freezing in-situ (Fourie et. al., 2001). Examination of the frozen cores of the undisturbed tailings indicated that the specimens were not fully saturated. This situation was confirmed by both physical measurements and laboratory tests, during which gas was recovered from the sample cores. Following a chromatographical analysis, the gas was confirmed to be mainly air, although a small amount of microbial gas was also present. Undrained triaxial compression tests were conducted on the undisturbed tailings specimens. Occluded air pockets were found to have a marked effect on the response to undrained loading of the pore-water pressure within the specimens. Air in the occluded state does not exist as small bubbles within the pore fluid, but as much larger enclosures contained within an otherwise fully saturated soil matrix. It was suggested by the writers that the liquefaction resistance of the tailings sand was increased by the presence of such occluded air pockets. A comprehensive summary of the work conducted as part of the CANLEX project is presented by Robertson et. al. (1995).

Hofmann (1998) elaborates on the necessary requirements to ensure that the site may be frozen without disturbing the soil structure. Consequently:

(i) freezing the soil mass should not attract water into the site; and

(ii) the freezing mechanism must be selected and installed so as to cause minimum disturbance the soil structure.

Similarly, there may be certain site characteristics that would either inhibit the freezing process, or disturb the soil mass during freezing. These include:

(i) the overburden stresses involved (Konrad and Morganstern, 1980);

(ii) drainage conditions (e.g. Hoffman et. al. 1998);

(iii) salinity and groundwater temperatures (e.g. Hashemi and Sliepcevich (1973), Sanger and Sayles (1979)); and

(iv) grain-size distribution (Davila et. al. 1992).

It was found that specimens which were thawed under 90% of the in-situ effective stress and pore-water pressure conditions underwent an average decrease in the void ratio of 0.02, while those thawed under a nominal effective

stress and then consolidated to the in-situ stress value underwent an average void ratio decrease of 0.08. Thawing via the former method therefore preserves the void ratio to within 2% of the in-situ value, and so it may be concluded that degree of saturation, structure, and stress history will also be preserved.

Despite the success of the method, the cost associated with ground freezing can be prohibitive. For example, for the six sites used by the CANLEX project, the cost of freezing per site averaged between $40K and $50K (Canada). However, at the time of writing, no other method of specimen extraction has been developed which retains the structure of the sample for subsequent laboratory testing.

2.5.3 Experimental Research

In general, experimental research into liquefaction has failed to keep pace with numerical modelling. This is due mainly to the fact that experimental testing is frequently time consuming and expensive, while models prepared for analysis on computer will tend to be faster and more versatile. However, it is important that experimental research continues to keep pace with numerical work, since liquefaction presents a purely physical problem to investigators and engineers.

The tests carried out on potentially-liquefiable soil in the laboratory may be split into four categories:

(i) triaxial tests;

(ii) simple shear tests;

(iii) shaking table tests; and

(iv) centrifuge tests.

2.5.4 The Triaxial Test

Of the four categories of test outlined above, the triaxial test is the most commonly used, due to its wide availability and greater simplicity in testing procedures (Seed and Peacock, 1971). An account of the idealized conditions within the cyclic triaxial test is given in Section 2.2, while a graphical description is provided in Figure 2.9.

Essentially, the proliferation of the triaxial test in practical liquefaction analysis is due to the relatively straight-forward method of measuring excess pore-water pressure. Accurately monitoring changes in excess pore-water pressures are crucial in any assessment of liquefaction, and the triaxial test provides this. In turn, this ensures that effective stress analyses are possible since the confining stress and axial stress can be controlled. Stress-controlled tests are most prevalent in liquefaction research, although strain-controlled tests, which require some modifications of the triaxial apparatus, are also occasionally employed for certain investigations.

The various relationships between the value of $\sigma_{dc}/(2\sigma_a)$ causing liquefaction under triaxial conditions and τ_{hv}/σ'_0 resulting in field liquefaction is covered at length in Section 2.2. However, apart from this difference in stress conditions, there are several other considerations (Seed and Peacock, 1971) which need to be taken into account when conducting triaxial tests for the purpose of liquefaction analysis. These are as follows:

(i) Under field loading conditions, the direction of the *major* principal stress may assume various angles from the vertical while, in the stress-controlled cyclic triaxial compression test, the same stress will switch from 0° to 90° on each stress cycle.

(ii) The *intermediate* principal stress has a value equal to the *major* principal stress during one half of the stress cycle, and equal to the *minor* principal stress during the other half of the stress cycle. In the field, the intermediate principal stress has a value corresponding to plane strain conditions.

(iii) Friction can exist between the specimen, the loading cap, and the porous disk at the specimen's base. Such stress concentrations can lead to premature failure of the soil specimen (Castro, 1969).

(iv) During the lateral compression part of the stress cycle (in which the major principal stress is provided by the confining pressure in the triaxial cell), the sample will tend to 'neck' as failure approaches. In this state, accurate determination of the stress conditions is difficult. However, necking is more common in

dense rather than loose samples, and may not therefore be very significant in a given liquefaction test programme.

The combined effect of these limitations is that a given soil specimen will liquefy or fail at lower stress values than those that might be expected under field conditions.

In more recent research, Yamamuro et. al. (1999) performed drained and undrained cyclic triaxial compression tests on silty sand. Their tests were conducted on cylindrical specimens of 97mm diameter and 97mm height. This large diameter ensured that the stress levels required to cause liquefaction of the sample were small. In addition, the end platens were lubricated so that friction was reduced and uniform strains effected. Silty sand was used in this research as the presence of fines (around 5-8%) in a sand specimen can increase the potential for *static* liquefaction in certain circumstances.

Norris et. al. (1997) used the results from three series of triaxial tests to propose an effective stress approach that allows the assessment of the entire undrained stress-strain curves, including peak and residual strength values, and the undrained stress path of a monotonic test, from drained triaxial tests.

More recently, Polito and Martin (2001) investigated the effects of non-plastic silts on the liquefaction resistance of various sand-silt combinations. A total of 300 triaxial tests were performed. The writers concluded that the mechanical behaviour of a sand-silt mix could not be assessed in terms of the silt content alone; the amount of silt present in relation to the amount of sand present needed to be considered. Further research was recommended.

Investigations have also been conducted by Yamamuro and Covert (2001) with respect to liquefaction in sands possessing a high silt content.

2.5.5 The Simple Shear Test

While the triaxial test is the most widely used in liquefaction analysis, the simple shear apparatus is better suited to simulating the field conditions induced in a horizontal sand layer during an earthquake. The effects of cyclic shear loading have been rigorously analysed by, for example, Silver and Seed (1971, a & b). In the aforementioned work, a series of cyclic strain-controlled tests is conducted on dry sand specimens, for a pre-determined range of small cyclic shear strain

amplitudes. The effects on the volumetric strain of the specimens, as well as on the shear modulus, are presented.

The simple shear (or shear box) test involves the relative horizontal motion of the top of the specimen and its base. In general, the base remains stationary, whilst the upper portion of the specimen moves laterally at a constant rate. Also, a normal stress of constant magnitude is applied through the top of the specimen.

Boulanger and Seed (1995) conducted a programme of laboratory tests in which the liquefaction behaviour of sand subjected to bidirectional monotonic and cyclic simple shear loading conditions was investigated by means of a new bi-directional simple shear apparatus.

The primary disadvantage of the cyclic shear test over the cyclic triaxial test is the extra complication, and therefore extra expense, required for the experimental set-up (e.g. Seed and Lee, 1966). However, the simple shear test continues to be used for the determination of the essential parameters in liquefaction analysis (e.g. Kovacs and Leo, 1981, Dyvik et. al., 1981), although it was not employed for any of the tests presented in this thesis.

2.5.6 The Shaking Table Test

The shaking table test has been used, and continues to be used, by many investigators attempting to simulate field conditions in the laboratory (e.g. Yoshimi and Tokimatsu, 1977; Finn et. al., 1971). For example, Yoshimi and Tokimatsu (1977) tested various soil/structure models in a transparent box of length 140cm, width 20cm, and height 40cm. The model moved with random oscillations in one horizontal direction, thus simplifying the motion produced by an earthquake, and the width of the 'building' resting on the surface of the sand was exactly equal to the width of the box. This permitted simulation of plane strain conditions. In these tests, measurements of pore-water pressure within the soil mass were made at various times, enabling contours of pore-water pressure development to be plotted.

The two-phase instability of saturated soils under plane strain conditions is discussed by Iai and Bardet (2001).

2.5.7 The Centrifuge Test

Arguably the most complex method of liquefaction analysis is the centrifuge test. The test has become more dependable as accumulated experience has been re-applied to the modelling process. The result is that the centrifuge test has become a powerful experimental tool for liquefaction study.

In simple terms, the centrifuge consists of a box within which the soil to be tested is placed. Sand specimens are prepared by pouring sand from a funnel through sieves and into the centrifuge (Ko and Dewoolkar, 1999). This method produces homogeneous, uniform specimens with repeatable densities, a principle that was used during the experimental work outlined in this thesis. Saturation of the specimen is provided by saturation under vacuum through the sand which is flushed with carbon dioxide (CO_2), and confirmed by measuring the velocities of *p*-waves propagating through the soil specimen (Wilson et. al, 1997).

The use of the centrifuge is gaining widespread acceptance among investigators. Madabhushi and Schofield (1993) investigated the dynamic behaviour of a tower structure, founded on a saturated sand bed, and subjected to model earthquakes by means of a centrifuge. Excess pore-water pressures were generated, and the effective stress in the sand was reduced. When the initial natural frequency of the tower-soil system exceeded the driving frequency of the model earthquake, the reduction in effective stress caused a degradation in the soil stiffness. When the initial natural frequency of the tower-soil system was less than or equal to the driving frequency of the model earthquake, the rise in excess pore-water pressures did not cause any significant change in the natural frequency of the tower-soil system.

Fiegel and Kutter (1994) present results from four centrifuge model tests, in which the response of layered soil deposits to model earthquake shaking was investigated. The layered soil consisted of fine saturated sand overlain by a layer of silt. The data indicated that, during liquefaction, a water interlayer or very loose zone of soil may develop at the sand-silt interface, due to the difference in permeabilities between the two soils. In each layered model test, sand boils were observed at the surface of the silt layer. These boils were found to be concentrated in the thinnest zones of the overlying silt layer, which ultimately fissured and provided vents for the excess pore-water pressures generated in the fine sand below.

Pilgrim (1998) conducted a centrifuge test programme to research the response of sand slopes to model earthquakes. Taboda-Urtuzuastegui and Dobry (1998) discuss the use of the centrifuge to study earthquake-induced lateral spreading in sands. Adalier et. al. (1998) used a centrifuge to model the performance of various liquefaction mitigation techniques under an embankment. The liquefaction mitigation techniques investigated were:

- densification of the sand layer;
- solidification of the sand layer by meant of a cement;
- gravel drains; and
- sheet-pile enclosures.

The range and variety of investigation summarised here clearly illustrates the versatility of the centrifuge in liquefaction analyses. Wilson et. al. (2000) performed a series of centrifuge tests on pile-supported structures, in order to evaluate their dynamic response during seismic loadings. Ellis et. al. (2000) employed a centrifuge to investigate the effect of the viscosity of the pore fluid on the damping, stiffness, and liquefaction characteristics of sands subjected to a modelled seismic response. The specimens used in these tests were 38mm in diameter and 79mm in height, similar dimensions to the specimens used for the triaxial test programme outlined in Chapters 3 and 4 of this thesis.

2.5.8 Numerical Modelling

It has already been stated that a general approach to the explanation of liquefaction and related phenomena has been slow to emerge. It is in the area of the numerical modelling of liquefaction that this undesirable situation is most conspicuous. Although this thesis does not focus primarily on such difficulties, a short description of the developments in liquefaction research is included here for completeness.

Scientific interest in liquefaction came to the fore in the aftermath of the earthquakes at Niigata and Alaska in 1964. This 'new' phenomenon needed 'new' phraseology and mathematics to describe it. However, despite the introduction of a new terminology, it must be remembered that liquefaction is merely a consequence of the constitutive behaviour of soil (Jefferies, 1999), and

as such investigations into stress characteristics and strain characteristics should not, in the opinion of the author, be undertaken separately.

Since the fundamental component of any liquefaction failure is the deleterious rise in excess pore-water pressures, effective stress analyses naturally have a greater value than total stress analyses. Among the early models were those proposed by Finn et. al. (1977), Kagawa and Leland (1981), and Dikmen and Ghaboussi (1984), who also presented constitutive relations for dry or saturated sands in simple shear (1975). Each of these models proposed solutions for describing the response of a saturated sand to earthquake shaking.

More recently, advances in finite element analysis have permitted investigators to further research the effective stress response of a soil stratum being disturbed by earthquake shaking. For example, Hicks and Boughrarov (1998) utilise the finite element technique to investigate the possible causes of liquefaction failure, during construction, of the Nerlerk underwater berm in the Canadian Beaufort Sea. The numerical analysis demonstrated that the most likely cause of liquefaction was movement of the clay layer underlying the berm. Elgamal et. al. (1999) use the power of the finite element method to describe constitutive behaviour.

The constitutive behaviour of any soil deposit or element under shear loading is inherently non-linear. Such behaviour is characterised by the decrease in shear modulus with increasing shear strain. Consequently, models which have a greater emphasis on non-linear aspects of liquefaction phenomena have also drawn attention. For example, Pyke (1979) proposes a model for the non-linear response of a soil stratum under the action of irregularly-applied cyclic loadings, such as those which exist during earthquakes. Also, Bouckovalas et. al. (1984) present a non-linear model for calculating permanent strains and stresses in sand caused by cyclic loadings.

For further details on the advances in the numerical modelling of the liquefaction phenomenon, the reader is directed to the literature.

2.6 CASE STUDY: THE HYOGO-KEN NANBU EARTHQUAKE OF 1995

2.6.1 Introduction

This Section contains a brief account of the widespread liquefaction-induced damage caused by the Hyogo-Ken Nanbu earthquake, which struck the Kobe-Osaka area of Japan on January 17th 1995. No technical information is included in this case study, although the reader should still be able to gain an intuitive feel for the implications from the devastation, both human and material, from such a phenomenon.

Further information regarding the effects of the Hyogo-Ken Nanbu earthquake may be readily obtained from the literature (e.g. Comartin, et. al., 1995; Iwasaki, 1995; O'Rourke, 1995; Sitar (ed.), 1995; Somerville, 1995). Elgamal et. al. (1996) analyzed numerical predictions for the site. Davis and Berrill (1998) investigated the energy dissipation during liquefaction at the heavily-affected Port Island site. In addition, Arulanandan et. al. (2000) utilized the observed performance of the Port Island facility in order to establish the feasibility of using computer simulations for the determination of earthquake-induced site response and liquefaction-induced deformations at a level-ground site. Desai (2000) employed a so-called disturbed-state concept and energy dissipation techniques in analyzing the liquefaction of Port Island.

The epicentre of the Hyogo-Ken Nanbu earthquake, which had a duration of approximately 17 seconds, was located at the northern tip of Awaji Island, approximately 20km from the city of Kobe in the prefecture of Hyogo, and measured 6.9 on the Richter Scale. Kobe is part of a huge metropolitan area, which extends around Osaka Bay to Osaka itself, approximately 45km east of the epicentre. As of March 31st 1995, estimations were that nearly 6,000 people had died, with over 26,000 injured. Approximately 80,000 houses had been destroyed. The financial cost of the earthquake is currently estimated at 200 billion US dollars.

Prior to the earthquake, Kobe was Japan's second busiest port, and the fourth largest container port in the world, handling around 53 million metric tonnes of foreign trade in 1990. The port employed 17% of Kobe's work force, and contributed nearly 40% of the city's gross industrial product. The following sections contain a concise report of the immense liquefaction damage to the port

facilities, from which the huge importance of the subject within geotechnical engineering should be appreciated.

Further and more detailed information relating to the Hyogo-Ken Nanbu earthquake, including the behaviour of dams, slopes, structural fills, and lifeline system can be found online at *www.ce.berkeley.edu.*

2.6.2 Introduction to Liquefaction Effects

The city of Kobe is constrained within a narrow strip of land between Osaka Bay to the south, and a mountainous region to the north. Expansion of the port facilities after 1963 led to the extensive development of man-made islands in Osaka Bay. These islands were constructed using weathered granite, or *Masa*, which was the most readily available local material. SPT data (e.g. Elgamal et. al., 1996) from the site indicated a very low blow count down to a depth of 19m, around five to six blows per foot of penetration. Such a low value is typical of a location where the susceptibility to liquefaction is high. Compaction of the fill was generally only applied where the material was placed above the water level.

The earthquake at Kobe was monitored by a four-accelerometer downhole array, with shear stresses and strains being estimated using simple techniques down to a depth of 83m. During the shaking phase, peak accelerations of 0.5*g* throughout the depths 16-83m were recorded. Earlier liquefaction studies in the area using a simplified procedure (Seed and Idriss, 1982) had suggested that there was sufficient resistance to liquefaction for ground accelerations below 0.2*g* for an earthquake of magnitude 8+. Therefore, the pre-earthquake estimates for the acceleration were much lower than the actual values. Extensive investigation of the site following the earthquake revealed evidence ground fissures, and surface settlements of as much as 0.7m. Such observations are highly indicative of lateral spreading.

Toward the end of the shaking phase, there was noticeable de-amplification of the surface accelerations, due possibly to the liquefaction-induced reduction in the stiffness of the soil, caused as described previously by the development of excess pore-water pressures at shallow depths. Below 16m, there was negligible de-amplification, indicating minimal reductions in soil-stiffness below this depth.

The effects of liquefaction from the Hyogo-Ken Nanbu earthquake were experienced up to 3km inland from Osaka Bay, and extended right around the Bay as far as Sakai, south of Osaka. Evidence of liquefaction away from the shoreline included small amounts of differential ground settlement, ground fissures and sand boils. Some of the most severe damage was located at the Rokko and Port Islands, where lateral spreads were initiated as well as along the mainland shoreline, and where significant ground settlement occurred. Although liquefaction had a relatively small influence on structural devastation in the area, damage to underground utilities was extensive.

Land-use on both Port and Rokko Island includes port facilities with cranes and container yards, apartment complexes, industrial warehouses, and commercial buildings. Port Island also includes as amusement park, a monorail, and high-rise buildings such as the Portopia Hotel. Port Island was constructed in two phases, with Phase I consisting of nearly 440 hectares being reclaimed between 1965 and 1981. Phase II, which began in 1996, involved the development of a further 390 hectares. The work was scheduled for completion in 1996, one year after the Hyogoken-Nanbu earthquake. Rokko Island has an area of 580 hectares; construction and filling was completed in 1992, twenty years after work was begun.

As previously outlined, the fills beneath the surface of these islands consists of a decomposed granite, which is collapsible in its natural state. Beneath Port Island, grain size varies between 2mm and 40mm, a mean grain size between 0.2 and 6mm, and a fines content between 5% and 30%. The fill beneath Rokko Island was similar apart from a Miocene sediment that was mixed with the granite, which therefore contains a higher percentage of fines than the fill on Port Island (Matsui, 1994).

The most common liquefaction-induced damage on both Port and Rokko Islands involved lateral spreads, and ground settlements within the interiors of the islands. Lateral spreads with displacements as great as 2-3m pushed outward against quay walls at most localities on the islands, resulting in 181 of the 187 shipping berths being severely damaged.

Depressions, or grabens, as deep as 4m and in areas as much as 30m wide formed behind the quay walls, where many of the cranes used for hauling freight were located. The bases of these structures were destroyed by the lateral

movement of the ground, and were tilted through differential settlement and subsidence. As a result, Kobe was effectively closed to international shipping, which naturally had widespread and detrimental financial implications for the economy of the city.

2.6.3 Details of Liquefaction Damage at Kobe

The map (below) of the Kobe-Osaka region shows some of the areas where significant liquefaction damage was experienced. The numbers on the map correspond with the details of a small selection of sites, listed below, around Kobe and Osaka where liquefaction damage was most pronounced.

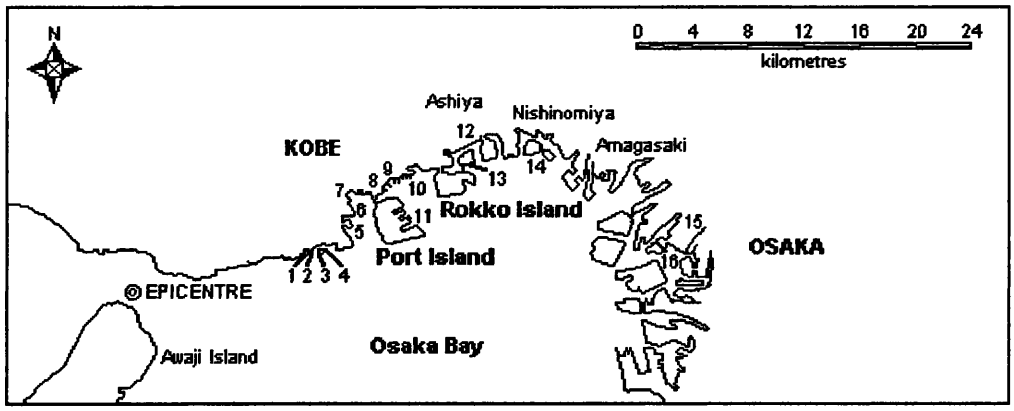

***Figure 2.19** - Map of Kobe-Osaka Region*

(1) Nippon Gatx Tank Farm

Of the several dozen tanks used to store substances such as ethelyne glycol and alcohol, none were founded on piles, and many had tilted following the earthquake. Around the tanks, there was ample evidence of sand boils and ground fissures having occurred.

(2) Minami-Komaecho

The walls on the southern side of Minami-Komaecho were constructed with concrete buttresses, and suffered differential displacements of between 10 and 15cm. However, the walls on the eastern side of Minami-Komaecho had no concrete buttresses, and experienced both horizontal and vertical displacements

of up to 2m. This indicates the benefit of buttressed quay walls with regard to reduction of liquefaction damage. Ground fissures and sand boils were also observed at Minami-Komaecho.

(3) Hanshin Silo Complex

One of the silos at this installation collapsed due to the effects of liquefaction and damaged adjacent crane structures. In addition, several silos at the western end of the complex suffered structural damage, where parts of the silo skins had buckled and sheared.

(4) Karumojima-cho

Situated about 4km to the west of Port Island, Karumojima-cho is estimated to have suffered peak accelerations of 0.7g. Extensive liquefaction damage, including differential settlements and sand boils, occurred on and around man-made fills. The quay walls which extend along both sides of the channel on the north side of Karumojima-cho were severely damaged by lateral deformations. As might be expected, there was also damage to structures situated along the quay walls.

(5) Tsukiji-cho and Hyogo Piers

At the eastern ends of Hyogo Piers Nos. 1 and 2, there was sufficient displacement of the quay walls to bring the buildings and surrounding apron slabs below water level. All quay walls around the perimeter of Tsukiji-cho suffered damage to some appreciable degree.

(6) Kawasaki Heavy Industries

Located to the north of the Hyogo Piers is the Kawasaki Heavy Industries complex and, as at Hyogo, buildings settled sufficiently in the vertical direction to drop the surrounding apron slabs below the water level. The quay walls around the buildings were laterally displaced, causing extensive damage to cranes and other structures.

(7) Harbor Land Ferry Terminal

The terminal building for the Harbor Land Ferry is situated to the north of the Kawasaki Heavy Industries installation, to the northwest of Port Island. Damage to the building was caused by differential settlements of up to 0.5m, while the lateral spreading toward the water was as much as 10m. As a result, a supporting column in the building was displaced between 0.5 and 1.0m, causing internal damage to the building.

(8) Onohama-cho

At Onohama-cho, there was severe damage to the south end of Shinko Pier No.5, including the dropping the foundation for a crane and many of the surrounding apron slabs below the water level. There was also damage to surrounding quay walls.

(9) Maya-ohashi Bridge

The Maya-ohashi Bridge section of the Harbor expressway spans the channel between Onohama-cho and Maya Futo. The eastern (Maya Futo) end of the bridge is elevated over a spit of land which suffered lateral spreading. Differential settlements of up to 1m occurred in the piers supporting the bridge in the middle of the spit, resulting in some vehicles falling from the highway.

(10) Maya Futo

Maya Futo would appear to be an exception to much of the surrounding port facility, in that the four piers extending southward were designed with strong pile foundations in order to resist much of the severe damage caused by seismic loading. As a result, the quay walls experienced minimal damage, although there was some evidence of liquefaction at the surface, including sand boils and cracking in asphalt pavements.

(11) Port Island Ferry Terminal Building

The larger of the two terminal buildings at Port Island was constructed on a pier-supported grid of perimeter walls and connected beams. This system was strongly tied together, resulting in negligible differential horizontal movements. The seaward end of the building lay within a graben that was liquefaction

induced, and away from the seaward end the terminal was intersected by open ground fissures caused by lateral spreading. In general, the terminal building performed well against the liquefaction- induced effects experienced elsewhere in the area.

(12) Higashi-Kobe Ferry Pier

The most notable damage at Higashi-Kobe at the eastern two of four berths with loading ramps for cars and passengers. As was common throughout the Kobe region during the earthquake, the quay walls were pushed outward, and grabens up to 10m wide and 3m deep had formed. Those ramps which straddled the grabens were destroyed. The ramps were supported on piles which were exposed due to liquefaction effects and which, during inspection after the earthquake, were shown to be inadequately installed.

(13) Higashinada Power Station Fuel Tanks

The Power Station is located on a man-made island, near to the north side of Rokko Island, on which accelerations of as much as 0.7g were experienced and on which liquefaction-induced effects were again present. Fissures formed within the Power Station complex, pavements cracked, and the ground was subjected to differential settlement. A group of pile-supported fuel tanks, which were constructed approximately 50m from the quay walls, experienced little damage, although the ground beneath one of the tanks had settled 28cm.

(14) Nishinomiya Bridge

This bridge, which runs through the residential and industrial district of Nishinomiya collapsed due to liquefaction-induced effects. Residential areas of Nishinomiya also suffered differential settlement and extensive damage to underground utilities, such as water and gas.

(15) Osaka Ferry Terminal

Peak ground accelerations in the vicinity of the Osaka Ferry Terminal, approximately 25km from the epicentre of the earthquake, were estimated to be as high as 0.3g. The terminal is located on a man-made island which suffered

damage due to differential settlements, sand boils, and ground fissures up to 5 cm wide.

(16) Tempoyama Park

Tempoyama park is situated on a man-made hillside directly to the east of the Osaka Ferry Terminal building. Liquefaction of the fill beneath the hillside caused extensive lateral spreads all direction, effectively destroying the park.

2.6.4. Summary

Performance of Man-Made Islands

The deficient performance of foundations in waterfront areas on the man-made islands was extensive, with sometimes catastrophic lateral spreading behind quay walls being a major contributing factor to the destruction of the port's facilities. However, there was minimal damage to those structures that were supported on deep foundations, indicating that the effects of liquefaction were not pronounced at appreciable depths, even in man-made fills. In a very few cases, strong foundations withstood the strong ground motions and associated lateral displacements with little damage to the foundation itself or the structure being supported.

Performance of Shallow Foundations

In many instances, shallow foundations performed poorly, with overlying structures being pulled apart at points of weakness, such as joints and doorways. In those instances where the foundation consisted of a grid of interconnected perimeter-wall footings and grid beams, such as at the Port Island Ferry Terminal building, performance against the minor effects of liquefaction, such as sand boils and minimal lateral spread, was satisfactory.

The effects of the Hyogo-Ken Nanbu earthquake in terms of liquefaction damage, are not uncommon. However, due to the importance of the city of Kobe to world shipping, the devastation caused by liquefaction phenomena meant that researchers and investigators were given renewed impetus to study the causes

and effects of liquefaction with increased rigour. As a result, the aftermath of the Hyogo-Ken Nanbu earthquake, as it relates to liquefaction phenomena, has become the most extensively researched event of recent times.

This Chapter has alluded to other work where the real-time occurrence of liquefaction in the field has been studied. The reader is directed to these numerous and excellent references for further insights into the effects of liquefaction in geotechnical engineering.

CHAPTER 3

MODIFICATIONS TO THE TRIAXIAL APPARATUS

3.1 OVERVIEW OF THE PRACTICAL RESEARCH

3.1.1 Introduction

Having discussed liquefaction phenomena at some length in Chapter 2, attention is now turned to the practical research upon which this thesis is based. It has already been described how the mitigation of liquefaction might be achieved in the field, using methods such as compaction grouting and vibroflotation. In addition to these methods, a new technique employing partially saturated soils is formally proposed here. The research outlined in this Chapter focuses on exploiting those particular properties of a partially saturated soil which may be of significant value in the ongoing investigations into liquefaction mitigation, with the aim that such properties, if deemed successful, provide a sound basis upon which further research may be undertaken.

All tests whose details are included in this Chapter and Chapter 4 were conducted using Hostun sand in one-way cyclic stress-controlled tests employing the standard triaxial apparatus. In the course of this research, this apparatus was modified by the author to permit the preparation of loose, partially saturated specimens of Hostun sand. This new technique of specimen preparation is also outlined here for the first time. The test programme was structured to allow a full investigation not only of the success of these modifications, but also into the potential of liquefaction mitigation using partially saturated sand specimens.

A brief outline of the theory of partially saturated soils, and the terminology employed therein, is also included in this Chapter. This is presented for completeness only, and the reader is directed to the literature for further excellent work in this important and expanding area of geotechnical research (e.g. Pietruszczak and Pande, 1995; Karstunen and Pande, 1994; Fredlund and Rahardjo, 1993; Fredlund and Morganstern, 1976 and 1977).

3.1.2 Effective Stress in Partially Saturated Soil

In Chapter 2, the important concepts relating to liquefaction phenomena were introduced. These principles were based on a two-phase soil specimen, in which the soil particles, sand in this case, interacted with a continuous liquid phase. Then, the degree of saturation, S_r, which is the ratio of the volume of water in the specimen to the volume of voids, will have a value of 1.00.

If the water phase remains continuous but now small air bubbles are introduced into the soil matrix, then the degree of saturation will fall to a value less than 1.00. At the same time, the soil specimen will become a three-phase system, in which soil (solids), liquid (water) and gas (air) are all interacting. In a rigorous analysis of such a system, a fourth phase, namely the 'contractile skin', which forms the boundary between the water and air phases, may be introduced (Fredlund and Morganstern, 1977). A rigorous examination of this four-phase system is presented by Fredlund and Morganstern (1993).

In a saturated soil specimen (where the degree of saturation, S_r, = 1.00), the effective stress is expressed as:

$$\sigma' = \sigma - u_w \qquad [3.1]$$

where σ' is the effective stress, σ is the applied normal stress, and u_w is the pore-water pressure. The subscript 'w' denotes 'water'. For a saturated soil, it has been demonstrated that only a single-valued effective stress, or one stress-state variable, is required to describe its mechanical behaviour. In this case, the stress-state variable is simply $(\sigma - u_w)$.

In the two-phase system, air is not present. The situation becomes more complicated for a three-phase system (in which the aforementioned contractile skin is taken to be a part of the water phase). In this case, the air introduced into the soil matrix will have its own pressure, u_a. It is important to note that the magnitudes of u_w and u_a are generally not the same, and only approach each other when the degree of saturation, S_r, approaches 1.00. In a partially saturated soil, the pore-water pressure, u_w, will be negative with respect to the pore-air pressure, u_a. The stress-state variable which expresses the difference between the pore-air and pore-water pressures, $(u_a - u_w)$, is termed the *matric suction*. The matric suction, as the name suggests, is a *tensile* stress which increases the initial shear strength of the soil matrix under consideration.

The pressure difference between u_a and u_w causes the contractile skin to curve (thereby forming a meniscus), in accordance with Kelvin's classical capillary model $(u_a - u_w) = 2T/R_S$ (Fredlund and Rahardjo, 1993), where T is the surface tension, and R_S is the radius of curvature of the contractile skin. As the

matric suction increases, so the R_S decreases. Conversely, as the matric suction goes to zero, R_S increases to infinity, resulting in a flat air-water interface.

The matric suction is an important quantity in the analysis of partially saturated soil, since it was realised that a change in the value of the matric suction did not result in the same change in the effective stress as did a change in a further stress-state variable, the net normal stress (σ - u_a) (e.g. Bishop and Blight, 1963). Note that the net normal stress is denoted here by (σ - u_a). This is because an incremental change in the net normal stress will not produce a similar rise in the pore-water pressure, u_w, in a partially saturated soil. Primarily, this is due to the change in the net normal stress forcing the pore-water further into the air occlusions, causing the pore-air pressure to rise. The net normal stress is therefore given by the increase in applied normal stress, σ, minus this incremental change in the pore-air pressure, u_a.

The conclusion that a change in the matric suction did not produce the same change in the effective stress as did a change in the net normal stress led to the recommendation that these two stress state variables, (u_a - u_w) and (σ - u_a) must be used in an independent manner when analysing the effective stress behaviour of a partially saturated soil specimen.

However, both before and after this recommendation, attempts were being made to couple both stress-state variables for a partially saturated soil into a single-valued equation for the effective stress. The most frequently-quoted work in this area was undertaken by Bishop (1959), who proposed the following form for the effective stress equation for a partially saturated soil:

$$\sigma' = (\sigma - u_a) + \chi(u_a - u_w) \qquad [3.2]$$

where χ is a variable relating to the degree of saturation of the soil specimen. The value of χ varies between 0.00 and 1.00, and will approach 1.00 for a fully saturated granular soil. In this case, u_a=0 and Equation [3.2] reduces to the classic effective stress equation for a saturated soil as expressed by Equation [3.1]. Later research indicated that the value of χ was influenced by the soil type under investigation, and that the relationship between χ and the degree of saturation was not linear (e.g. Donald, 1961; Blight, 1961).

Despite this and other efforts in a similar vein, experimental research has shown that the effective stress in a partially saturated soil is not single-valued. In addition, there would appear to be a dependence of the stress path followed. Morganstern (1979) stated that Bishop's equation had limited significance in the light of these theoretical concerns, citing that the difference in the value of χ when determined for volume change analysis was dissimilar to that determined for shear strength investigations. In addition, since χ is dependent upon the soil type, then it becomes a soil property rather than an independent variable.

From this brief discussion, it should be clear to the reader that the effective stress in a partially saturated soil is not single-valued, and must be determined by the use of two independent stress-state variables, the net normal stress (σ - u_a) and the matric suction (u_a - u_w).

3.1.3 Shear Strength in Partially Saturated Soil

As already explained, the stress state of a soil can be determined by the use of two independent state variables, (σ - u_a) and (u_a - u_w). This sub-Section discusses how shear strength may also be determined using these variables.

For a fully saturated soil, the shear strength is given by the Mohr-Coulomb failure criterion and the concept of effective stress (Terzaghi, 1936):

$$\tau_{ff} = c' + (\sigma_f - u_w)_f \tan\phi' \qquad [3.3]$$

where τ_{ff} is the shear stress on the failure plane at the time of failure of the soil specimen, c' is the effective cohesion, $(\sigma_f - u_w)_f$ is the effective normal stress on the failure plane at failure, σ_{ff} is the total normal stress on the failure plane at failure, u_{wf} is the excess pore-water pressure at failure, and ϕ' is the effective angle of internal friction. The Mohr-Coulomb failure criterion has been satisfactorily employed in engineering practice with saturated soils for many years. Graphically, the Mohr-Coulomb failure criterion is represented by a straight-line envelope, as shown in Figure 3.1 overleaf. This envelope gives possible combinations of shear stress (τ_{ff}), and effective normal stress $(\sigma_f - u_w)_f$, acting on the failure plane at failure. Those stress states (i.e. those combinations of τ_{ff} and $(\sigma_f - u_w)_f$) which plot below the line will not induce failure in the soil

specimen. Those stress states plotting above the failure envelope will always produce the failure condition.

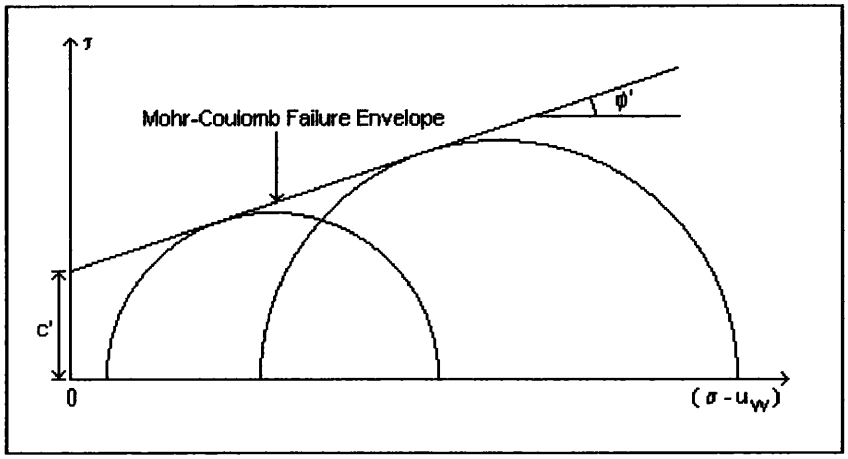

***Figure 3.1** – Graphical Representation of the Mohr-Coulomb Failure Criterion*

The formulation of a failure criterion for an unsaturated soil may be achieved in terms of the independent stress state variables described earlier (Fredlund et. al., 1978). The resulting equation is similar to that in [3.3], but an extra term has been included in order to incorporate the matric suction in the soil sample at failure. This 'extended' Mohr-Coulomb failure criterion may be written as:

$$\tau_{ff} = c' + (\sigma_f - u_a)_f \tan\phi' + (u_a - u_w)_f \tan\phi^b \qquad [3.4]$$

where τ_{ff} is the shear strength on the failure plane at failure, c' is the effective cohesion, which is the intercept on the shear stress axis when both the net normal stress and the matric suction at failure are zero, $(\sigma_f - u_a)_f$ is the net normal stress on the failure plane at failure, u_{af} is the pore-air pressure on the failure plane at failure, ϕ' is the angle of internal friction associated with the net normal stress, $(u_a - u_w)_f$ is the matric suction on the failure plane at failure, and ϕ^b is an angular value relating to the rate of increase in shear strength relative to the matric suction.

The extended Mohr-Coulomb failure criterion for a partially saturated soil will approach the classic Mohr-Coulomb failure criterion (Equation [3.3]) as the degree of saturation, S_r, of the partially saturated soil approaches unity. Then, the excess pore-water pressure, u_w, approaches the pore-air pressure, u_a, and the matric suction (u_a - u_w) goes to zero.

3.1.4 Partially Saturated Soil in Liquefaction Mitigation

It is proposed by the author that partially saturated soils may be employed in the process of liquefaction mitigation. Existing methods used in engineering practice for this purpose are described briefly in Section 2.3, and will not be repeated here. The mechanical behaviour of partially saturated soils has received considerable attention in the literature, and the reader is directed to these works for more technical information (e.g. Pietruszczak and Pande, 1995; Fredlund and Rahardjo, 1993; Sills et. al., 1991; Wheeler, 1988; Wood, 1979).

In previous studies (Copp, 1996), the author has attempted to produce a partially saturated soil specimen from a saturated soil specimen, employing methods which have received limited examination in the literature. Among these was the proposal that electrolysis may be used in order to remove pore water from the saturated soil specimen, in order to leave a partially saturated soil specimen. In summary, this method had very limited success, with arguably the most noticeable effect being the rapid degeneration of the electrodes during the electrolysing process. This degeneration is clearly visible in Figure 3.2 below. The lateral black marker to the right indicates the depth to which the electrodes were inserted into the soil matrix (i.e. to a depth of 110 mm).

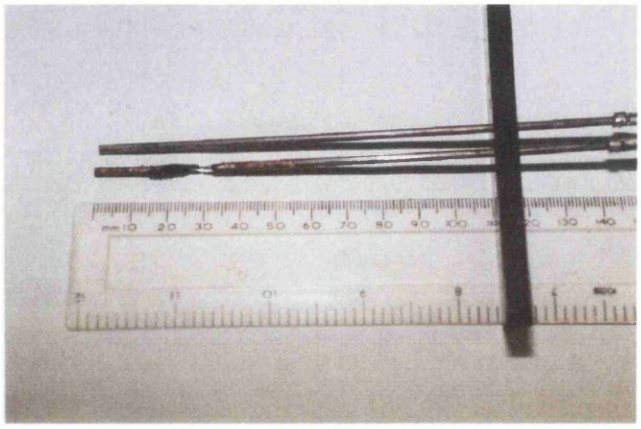

***Figure 3.2** – Degeneration of Electrodes During Electrolysis of Pore-Water*

It is well understood that the matric suction, a tensile stress which is inherent in a partially saturated soil, will increase that soil's shear strength. The greater the value of the matric suction, the higher the shear strength of the specimen. When the degree of saturation approaches zero, the shear strength of the specimen will approach the drained shear strength.

It has already been seen that a partially saturated soil specimen will have a pore water pressure that is negative relative to the pore air pressure. This pore water pressure, according to the Mohr-Coulomb failure criterion, will increase the shear strength of the soil. Also, it was demonstrated in Chapter 2 that changes in excess pore-water pressure are produced by changes in shear strain. The clear conclusion is that the smaller the increment of shear strain, the smaller the change in excess pore-water pressure, and so the higher the resistance to liquefaction phenomena. These observations form the basis for the proposal that the introduction of partial saturation into an otherwise saturated soil matrix will reduce the susceptibility of that soil to liquefaction.

3.1.5 The Theory of Backpressuring

Any investigation into the mechanical response of a partially saturated soil to an applied load implies the use of specimens whose degree of saturation is less than 1.00. In this work, specimens were first brought to their lowest degree of saturation through the irreversible reactions associated with the use of water and the chemical zeolite, and then backpressured. Backpressuring is a means of increasing the degree of saturation within a specimen, in order that the mechanical response of such specimens at various degrees of saturation may be compared. Zeolite will be discussed later in this Section.

The process of backpressuring specimens to achieve differing degrees of saturation is a consequence of Henry's Law. Henry's Law states that the mass of gas which is dissolved in a fixed quantity of liquid is directly proportional to the pressure of the gas occlusions contained in that liquid. For the purposes of this work, the liquid is pore-water, while the gas occlusions are the air pockets created by the reaction between zeolite and water.

Water molecules form a loosely-bound lattice structure. This structure contains openings, refereed to as a 'cage' (Rodebush and Busswell, 1958), within

which air may be dissolved. The 'cage' occupies approximately 2% of the total volume of the water, a percentage also termed as the volumetric coefficient of solubility, h, which is the ratio of the maximum volume of dissolved gas in a liquid, V_d, to the volume of the liquid, V_w. Thus, for air at room or ambient temperature, h has the value 0.02. More precisely, for air at 20°C, h has the value 0.01868 (Dorsey, 1940).

Therefore, by increasing the pressure of the pore-water, the pore-air occlusions will be compressed according to Boyle's Law, which states that, for a given volume of gas at a given pressure, a change in the gas pressure will result in a change in the gas volume, such that the product of the gas pressure and gas volume remain constant. Boyle's Law may be expressed mathematically as:

$$u_{a1}V_{a1} = u_{a2}V_{a2} \qquad [3.5]$$

where u_{a1} and u_{a2} are the absolute pore-air pressures at conditions '1' and '2' respectively, and V_{a1} and V_{a2} are the pore-air volumes at these pressures.

Pore-air will then dissolve into the pore-water, according to Henry's Law as stated earlier. The equation for the change in pore-air pressure, Δu_a, required to saturate a soil specimen which has an initial degree of saturation S_{r0}, is given by (Lowe and Johnson, 1993):

$$\Delta u_a = \frac{(S_r - S_{r0})(1-h)}{1-[S_r(1-h)]} u_{a0} \qquad [3.6]$$

where Δu_a is the increase in pore-air pressure required to saturate the specimen, S_{r0} is the initial degree of saturation, S_r is the final degree of saturation, h is the volumetric coefficient of solubility, and u_{a0} is the absolute initial pore-air pressure. For the purposes of this work, $S_r = 1.00$, and so Equation [3.6] reduces to the following:

$$\Delta u_a = \frac{(1-S_{r0})(1-h)}{h} u_{a0} \qquad [3.7]$$

It will be seen later that Equation [3.7] gives a reliable estimate of the increase in pore-air pressure, induced through the backpressure process, required to completely saturate the soil specimens used for the purposes of this research.

During the backpressuring process, the matric suction in the specimen, $(u_a - u_w)$ reduces, since the dissolution of pore air into the pore water reduces the volume of air present. The degree of saturation, S_r, approaches unity, and the extended Mohr-Coulomb failure criterion (Equation [3.4]) approaches the classic criterion as expressed by Equation [3.3].

Backpressuring by increasing the pore-water pressure requires infusion of water into the specimen. The specimen is therefore being backpressured under drained conditions. Since the volume of water increases, a greater volume of water is made available for the dissolution of the pore air. This is clearly of benefit, while the slight volume change that the specimen undergoes during the process, due to the infusion of water, is not deemed to be significant.

The procedure by which backpressure was applied to the specimens prepared for the current research is outlined later in this Chapter.

3.1.6 Zeolite

'Zeolite' is the generic name ascribed to a number of microporous crystalline solids. They are also often referred to as 'molecular sieves'. Zeolites can occur naturally, but they may also be manufactured by synthetic processes for specific purposes.

The basic zeolite structure is tetrahedral, with either a silicon or aluminium atom at the centre of the tetrahedron, and an oxygen atom at each of the four corners. These tetrahedra may then link together to form loosely-bound framework structures such as channels, cavities, and cages, into which small molecules may enter and be absorbed. Also, the loosely-bound nature of the frameworks permit other ions to be readily substituted into the structures. For example, the inclusion of sodium or potassium in a framework structure may replace calcium or magnesium, which are both constituents of 'hard' water. Thus, zeolite may be employed as a water softener. Approximately 130 framework structures are currently known to exist.

Zeolites are able to act as catalysts for certain chemical reactions, and it is this property which is of interest in the current work. Through the process of ion-exchange, water molecules enter the framework structure of the zeolite. The two hydrogen atoms in the water molecule are absorbed by the zeolite, while the single oxygen atom is released.

In a soil matrix, within which zeolite has been incorporated, this free oxygen forms the gas occlusions which reduce the degree of saturation, S_r, of the soil specimen. For the purposes of the research detailed in this thesis, the zeolite used had silicon as the tetrahedral atom, and possessed a cavity-structure which permitted hydrogen atoms to be absorbed to the sides of the zeolite framework while oxygen atoms were released into the pore water.

Figure 3.3 below shows the physical result of the reaction between zeolite and water in sand. Cavities can clearly be seen just above the centre of the specimen. Other cavities were also present, but were too small to be shown clearly in this photograph. Note also the small aggregations of the white zeolite powder within the soil structure.

***Figure 3.3** – The Effect of Zeolite in Producing Oxygen Pockets in a Saturated Soil*

Figure 3.4 *– Visual Confirmation of the Generation of Air Pockets*

Figure 3.4 above illustrates the problems associated with introducing larger aggregations of zeolite, rather than a true powder form, into a soil structure. A small fissure can be seen in the specimen, running vertically downwards from the cavity near the centre of the specimen. However, the main point to note in this photograph is the presence of an aggregation of zeolite *inside* the aforementioned cavity. The fact that this aggregation remains intact, and has not reacted with water to produce oxygen, indicates that there is a gas phase (oxygen) present but no water inside this cavity. The photograph was taken approximately four minutes after the formation of the cavity.

The unique properties of zeolites have created a worldwide market in which several million tonnes of the chemical in its various forms are used in industrial applications such as petrochemical cracking, and the separation and

removal of solvents. Referring to topical issues, zeolites may also be used to remove ozone-depleting CFC's (chlorofluorocarbons), exhaust gases, and other atmospheric pollutants.

While a full description of the chemical reaction involved when zeolite and water come into contact is beyond the scope of this current work, it is known that zeolites generally produce harmless by-products, a property which promotes their positive use in the wider environment. For example, zeolites are used to reduce both energy consumption and toxic waste, while the by-products of these processes, while varied in nature, are not harmful to the environment.

It is important to state that, when zeolite is used on a granular material such as a sand in a test programme, the sand should be carefully washed after the test has been concluded. That mass of zeolite which does not react with water (such as that inside the oxygen occlusion illustrated in Figure 3.4) is still in the powder form, and will remain within the soil matrix even when necessary drying of the sand particles has been effected. In addition, the by-products of the ion-exchange processes will also be present within the soil matrix.

For further information on zeolites and their use, the reader is directed to the website of the British Zeolite Association (*www.bza.org*).

3.2 MODIFICATIONS TO THE TRIAXIAL APPARATUS

3.2.1 The Upper Platen, Plug, and Key

The overall objective of the research detailed in this thesis was to investigate the success of partial saturation as a means of liquefaction mitigation in a granular soil. Therefore, two problems existed. Firstly, the method of obtaining a partially saturated specimen of sand needed consideration and, secondly, the preparation of a loosely packed granular matrix had to be addressed. The significance of a loose soil matrix on liquefaction susceptibility has been outlined earlier in Chapter 2.

For producing a loose specimen, the literature often makes reference to the so-called 'moist tamping' method (e.g. Ladd, 1978; Ishihara, 1993) which, while having significant merit in preparing saturated specimens in the laboratory, is of limited benefit in tests on, and the preparation of, partially saturated samples. In the moist tamping method, five, six, or seven equal pre-weighed portions of oven-dried sand are mixed with de-aired water at around 5% water content. A membrane is stretched tightly around the interior face of a pre-assembled split-mould, which is in turn attached to the base pedestal of the triaxial apparatus. Each portion of the moist sand is pluviated through a funnel to a pre-determined height in five, six, or seven 'lifts', depending on the number of sand portions being used. At the end of each lift being placed, the sand is lightly tamped with a flat-bottomed tamper. The capillary effect between moist particles means that the sand can be tamped into a very loose matrix, well in excess of the maximum void ratio, e_{max}, of the dry sand. The amount of tamping energy required for preparation of the initial structure of the specimen depends upon the objectives of the particular test being undertaken. In general, if a very loose specimen is required, the tamping energy will be very low. However, in this instance, the subsequent saturation of the specimen produces volume contractions which are unduly large, and the resulting reduction in the diameter of the specimen produces vertical wrinkles in the specimen membrane. Normally, the tamping energy is such that the volume contraction would be around 5% for a loose specimen prepared by this method. There is, therefore, a recommended maximum void ratio for specimens prepared by the moist tamping method.

For denser specimens, a greater amount of tamping energy needs to be applied to the specimen. This can be done, for example, by increasing the number of tampings

during the compaction of each lift, rather than increase the downward pressure for individual tampings.

Once all lifts have been placed and tamped, the specimen is enclosed by the membrane, upper platen, and rubber O-rings. A vacuum of 10-20kPa is generally applied to the specimen to ensure stability while the split-mould is removed. Carbon dioxide gas is percolated through the specimen, which is then flushed through with de-aired water. During this final saturation process, volume reduction takes place due to the collapse of the initial structure of the specimen. This effect was alluded to earlier in this review of the moist tamping method. The estimated void ratio after saturation under the vacuum pressure is taken to be the initial void ratio, e_0, of the specimen. Consolidation is then performed to a desired confining stress.

This method, while effective, did not match with the author's objectives of developing a system which allowed the reproduction of loose sand specimens in the triaxial apparatus, by means which approximated the physical processes which were present in the field. The moist tamping method was also deemed by the author to have the disadvantage of introducing significant scope for disturbance to the specimen, particularly when the membrane, upper platen, and O-rings, were being manipulated.

Therefore, a new method of preparing the loose specimens needed to be implemented into the triaxial apparatus which was available to the author for the purposes of the current research. In conducting the extensive literature review for this thesis, it was noted that many of the problems in testing a loose sand sample generated from the difficulties in extracting quality samples from the field. For example, freezing the sub-surface soil in liquid nitrogen for subsequent thawing and testing in the laboratory was perceived as one viable solution to this problem (e.g. Sego et. al, 1999). This method was reported to produce samples of satisfactory condition and quality, but the costs of such work were prohibitive, ranging between $40,000 and $50,000 (Canada) per site (see Chapter 2).

Attention was therefore turned to the possibility of modifying the triaxial apparatus itself, in particular the technique of in-situ specimen preparation, so that loosely bound, cylindrical sand specimens of 38mm diameter and 76mm length may be prepared with the minimum of sample disturbance by the investigator. It was recognised that such a method would have to be reproducible for application on other triaxial systems. In addition it was desirable, in the opinion of the author, to develop a specimen preparation procedure which resembled, as closely as possible, the methods

by which those deposits in the field, which are equally susceptible to liquefaction, are produced. This concern has already been discussed with reference to moist tamping.

It was realised that the main difficulty with the triaxial apparatus for preparing reconstituted specimens of sand was the nature of the rubber membrane, which completely surrounds the sample, necessarily protecting it from the ambient working pressure within the triaxial cell itself (e.g. Bishop and Henkel, 1957). In a clay sample, which in its natural state is always fully saturated, there is sufficient inherent cohesion present, due to the colloidal nature of the particles, to permit the membrane to be applied to the clay sample with minimum disturbance to those particles. However, for sand, no such cohesion exists, and thus it was concluded that, for any new method to work effectively, the preparation of the specimen had to be the *concluding* element of this crucial setting-up process, rather than the *initial* element. As widely reported in the literature, the scenario where the specimen or sample is prepared prior to the rubber membrane being set in place is the most commonplace method of specimen preparation which exists at the time of writing.

To this end, the author designed a new system, within which homogeneous samples could be prepared in the loose state (with scope for densification, if required), with virtually no likelihood of disturbance from a competent investigator. The system centred on the redesigning of the solid upper platen, which is universally employed in triaxial testing. At present, this platen does little more than to seal the upper end of the specimen, and to transmit the applied load, via a single ball bearing, through to the fixed framework of the triaxial apparatus. The proposed system maintains these vital functions, as well as allowing for the preparation of a loose sand specimen. An engineering diagram of this modified upper platen and plug (the plug is threaded into the platen prior to testing) is provided in Figure 3.5 on the next page, while the complete arrangement is shown in its working state in Figures 3.6 and 3.7.

The modified upper platen and plug illustrated here were both manufactured from an abrasion-resistant and rigid polyurethane, which has the 'TUFSET' trademark. These essential properties allowed for the durability of the arrangement, a very important criterion given the possibility of the failure of the thread with sustained use. Also, the proposed arrangement and the classic upper platen both had the same weight, namely 0.3N, which prevented the need for an additional correction to the standard theories relating to triaxial testing. Figure 3.8 shows the similarities between the modified upper platen (left), and that used in classic triaxial tests (right).

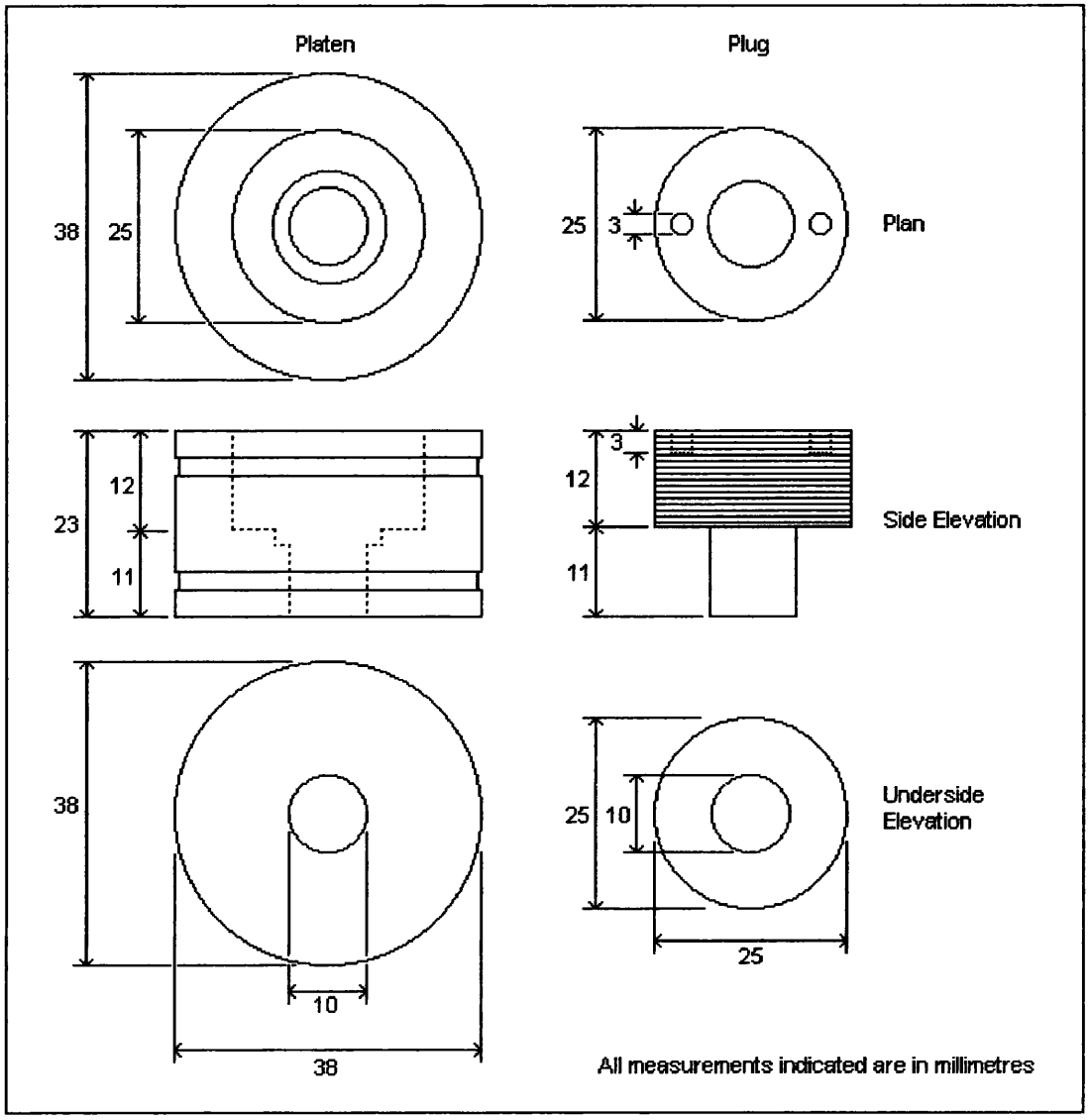

***Figure 3.5** – Modified Upper Platen and Plug*

The general principle was that, with the plug removed, sand could be passed through the modified upper platen and into the space contained by the rubber membrane and the lower platen which, in the work described throughout this thesis, was a fully-saturated porous stone of low porosity. The membrane was attached to the modified upper platen *prior* to the preparation of the specimen, and the whole system was held in the vertical position by a specially-manufactured clamp, the design of which is described later in this Section. The clamp was designed to prevent any disturbance of the specimen when the plug is replaced into the upper platen prior to testing.

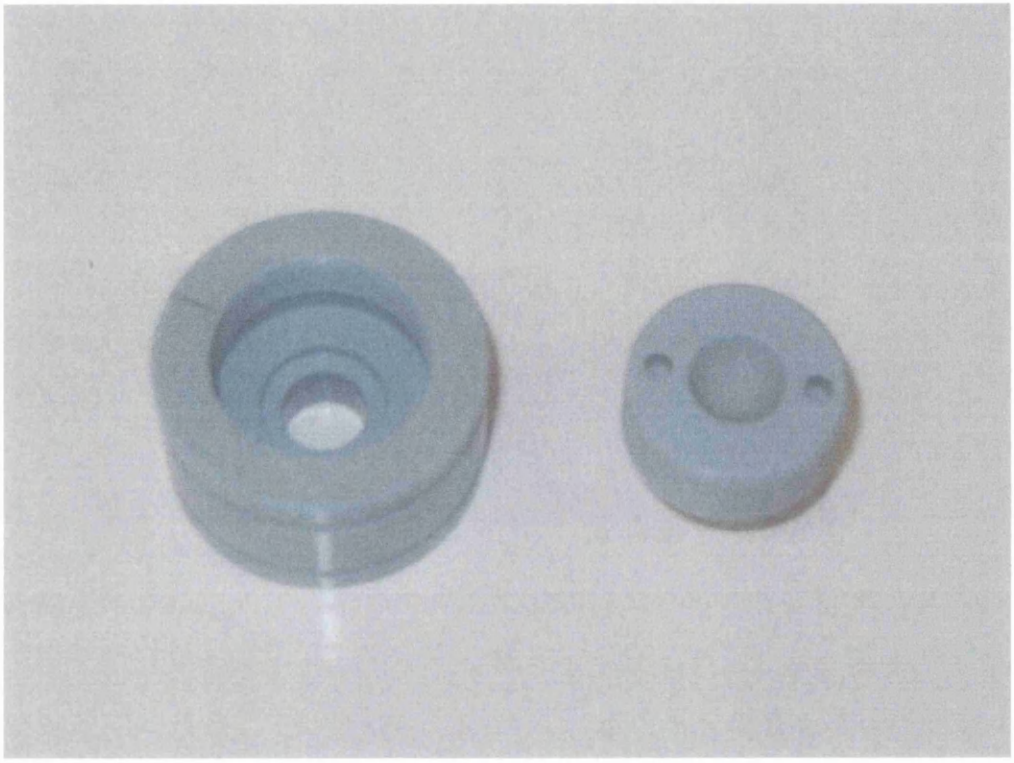

Figure 3.6 *– Modified Upper Platen and Plug (Plan View)*

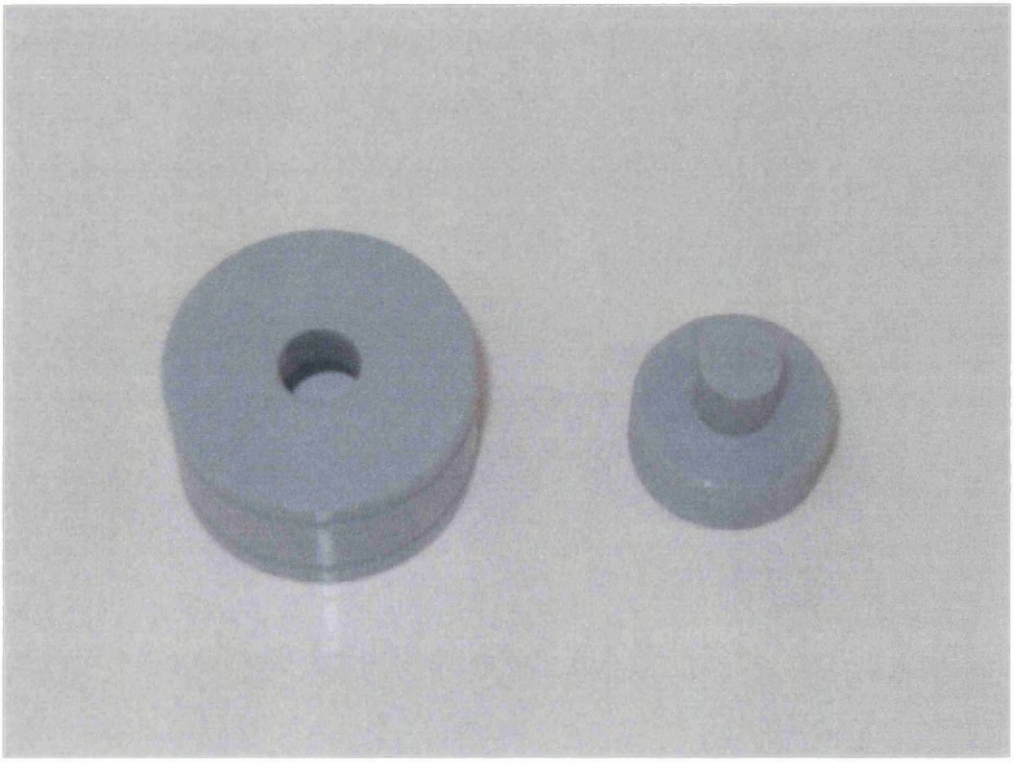

Figure 3.7 *– Modified Upper Platen and Plug (Underside View)*

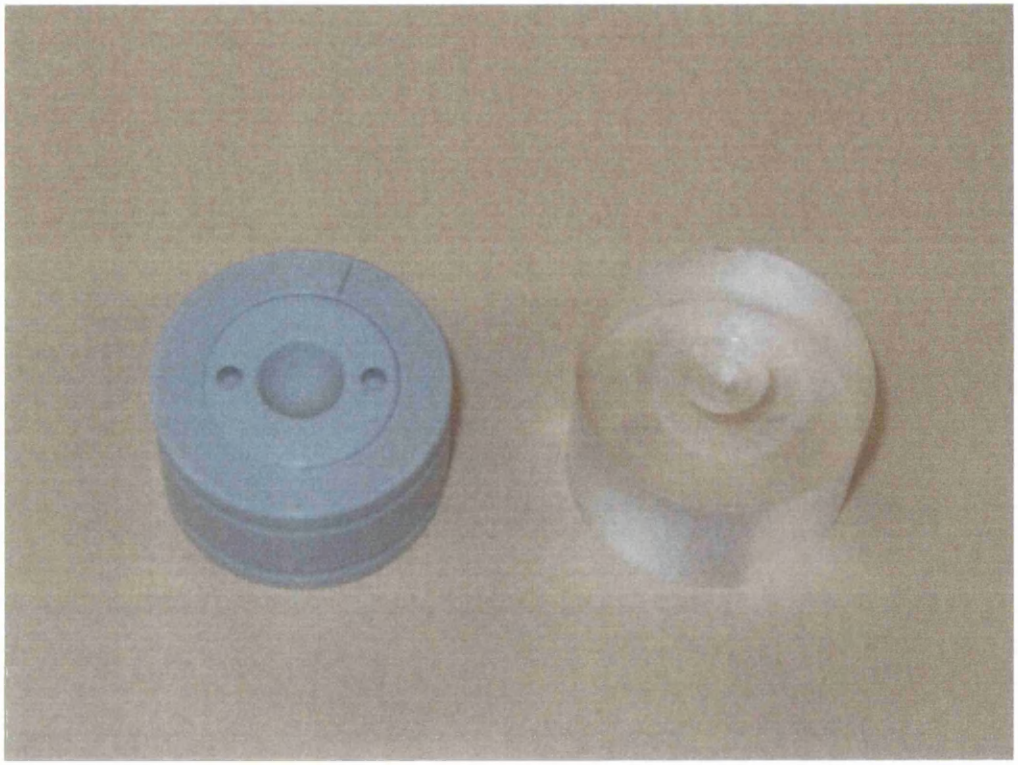

Figure 3.8 *– Visual Comparison Between Modified and Classic Upper Platens*

As discussed earlier, the membrane provides the primary reason why preparation of loose sand specimens tends to fail when the classic upper platen is used. Modern membranes normally have two vertical creases, the nature of which means that the sand specimen will inevitably be disturbed when attempting to place the upper platen in position prior to testing. The modifications to the upper platen described here permit the specimen to be prepared without the necessity of such disturbances, irrespective of whether or not the membrane contains such creases.

When preparing and testing sand specimens, the determination of the void ratio and degree of saturation is of great importance. Although the initial void ratio, e_0, was not measured directly in any test described in this thesis, it was determined by establishing the specific gravity, G_s, of the prepared specimens and the moisture content, w, of representative specimens. Using these quantities and the standard phase relations, the void ratio could be determined for each specimen. It was found that the proposed platen-and-plug arrangement did indeed produce specimens possessing an initial void ratio normally associated with very loose sand specimens, a situation assisted by the sieving of the sand prior to any specimen preparation, so that fines such as silt and clay were removed.

All essential measurements relating to the upper platen and plug have been included in Figure 3.5, with the exception of the small notch inside the platen, as indicated on the side elevation in Figure 3.5. The purpose of this notch was to house an insulating rubber O-ring of appropriate diameter. However, thicknesses of such O-rings may vary, and so this measurement is left to the best judgement of any future investigators, depending on equipment that is available. The thread on the exterior of the upper part of the plug was matched by a thread of similar gauge on the inside of the platen.

Two external rubber O-rings, which are an essential component of the triaxial test set up, were accommodated by the two narrow grooves which ran around the entire perimeter of the upper platen. Intervening between these O-rings and the platen was the rubber membrane, which totally surrounded the specimen. The positioning of these O-rings is also a problem in classic triaxial tests on sand, as the 'snap-back' which occurs when the O-rings are placed in position can cause significant movement in the granular particles constituting the sensitive soil matrix.

The plug was inserted into and extracted from the platen by means of a 'key', made from the same material from the rest of the arrangement. The key had two aluminium prongs, which fitted inside the plug via the small holes indicated on the plan and side elevations as shown in Figure 3.5 and Figure 3.6. When fitted, the key permitted the plug to be inserted with a clockwise movement, and removed with an anticlockwise movement. The key is shown, again with all essential measurements, in Figure 3.9 and Figure 3.10 on the coming pages.

The key had four small grooves on its outer perimeter, to allow the investigator some grip when inserting or removing the plug. A small degree of downward pressure should be applied to the key when being used, to ensure that the key and plug remain in the fullest possible contact with each other during use. Care should also be taken to ensure that the plug is not threaded too far into the platen. Initially, there is very little resistance between the plug and platen, and as such it is only at the very end of the travel of the plug that any appreciable resistance is encountered. Once complete, the investigator should remove the key, and continue with the next stage of the test set-up. With the key removed, a steel ball bearing was placed in the semi-spherical indentation at the top of the plug before the triaxial cell was placed into position.

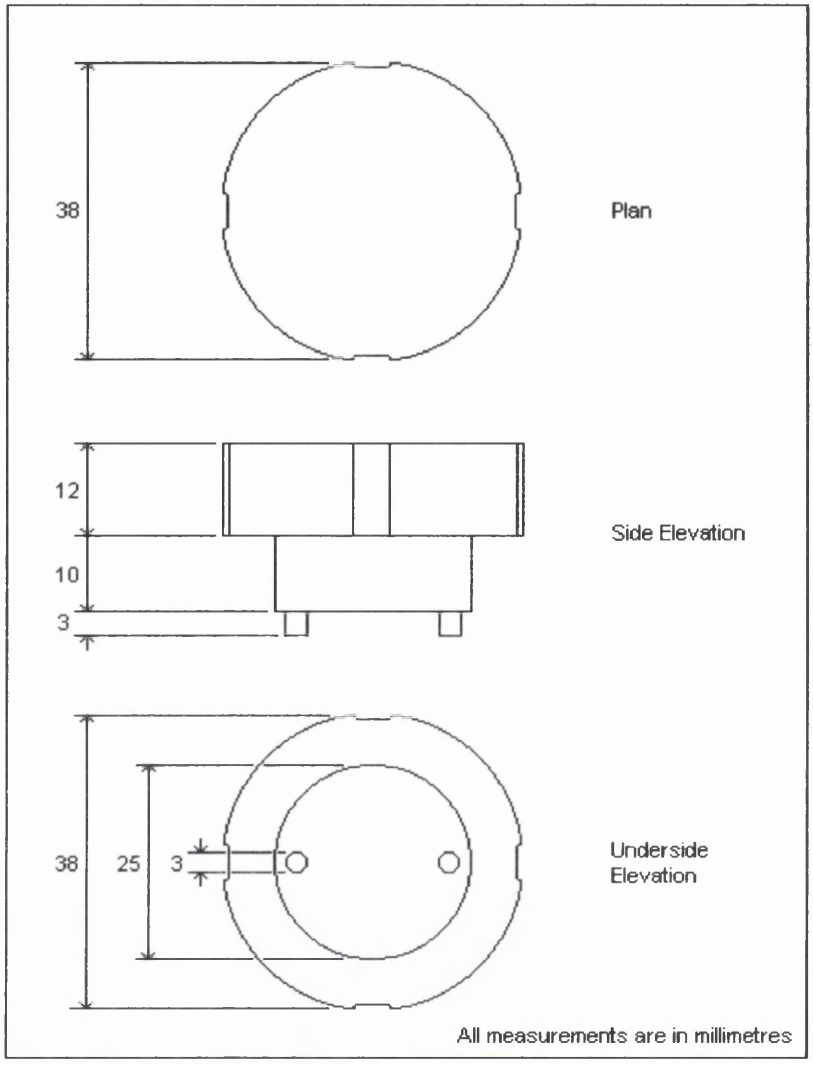

Figure 3.9 *– Diagram of Key for Modified Upper Platen and Plug*

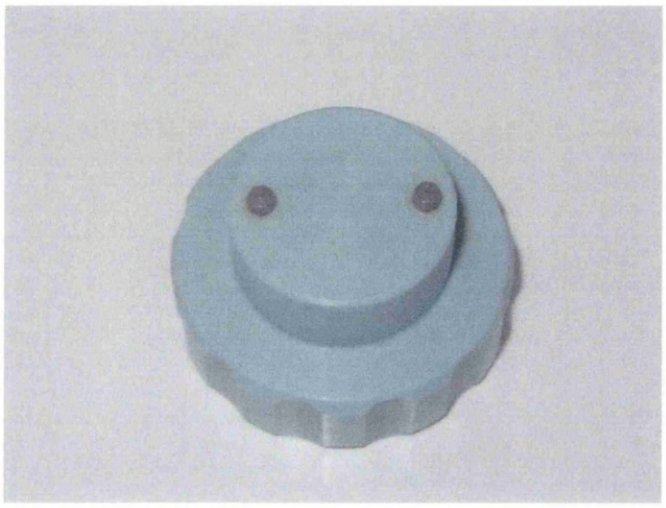

Figure 3.10 *– Key for Modified Upper Platen and Plug*

3.2.2 The Clamp and Lock

The necessity of holding the modified arrangement vertically when preparing the sand specimen through the upper platen required the use of a clamp and lock, which was employed during the preparation stage, and then removed when the specimen was ready for testing.

Traditionally, the preparation of a sand specimen, no matter what its void ratio or degree of saturation, has been achieved by means of a three-piece metal sheath, or split-mould, around the top of which the rubber membrane is folded. It should therefore be clear that, in positioning the upper platen, membrane, and rubber O-rings, disturbance of the soil matrix is virtually unavoidable. Such a system, therefore, would have to be improved upon by way of any proposed changes.

The clamp and lock that was designed by the author, and used throughout the triaxial testing programme described in this thesis, is illustrated in Figures 3.11, 3.12, and 3.13. The clamp and lock were both manufactured from aluminium, an ideal material for durability and economy. The clamp was secured on one side of the triaxial frame by means of the 20mm diameter hole, and was rotated in the horizontal plane as necessary. The diameters of the vertical members of the triaxial frame may vary from system to system; any difference from the 20mm diameter quoted here would obviously have to incorporated into any final design. The collar, which maintained the position and height of the clamp, is described later in this Section.

The two bolts securing the lock to the body of the clamp were 3mm in diameter, and were of sufficient length to ensure that the lock could not be loosened by hand. For example, in the system used for the triaxial tests outlined in this thesis, the bolts were 30mm in length. A third bolt secured the clamp onto to frame of the triaxial apparatus. This bolt was 6mm in diameter, and should ideally be between 20mm and 25mm in length. In the clamp used for this work, the bolt was 20mm in length.

At the commencement of the specimen preparation, the lock was detached from the clamp. The clamp was then positioned with the 39mm hole directly over the centre of the triaxial pedestal. With the lower porous stone having previously been adequately de-aired in boiling water, the membrane and stone were placed over the pedestal. Two O-rings were placed loosely over the membrane, for subsequent positioning at the end of the preliminary set-up process. The modified upper platen, with the plug removed, was secured to the free end of the membrane, and the two

rubber O-rings at this end are correctly positioned. The upper platen was then placed inside the clamp, with the lower rubber O-ring resting on the lip. The lock was secured, and the clamp was tightened to the triaxial frame. Any slack in the membrane was taken up at the pedestal, and the final two O-rings were placed in position once this had been done. This set-up process is described and illustrated in more detail later in this Section. Note that the investigator may safely disturb the system as much as necessary in order to position it correctly during the set-up process, since no granular material has, as yet, been introduced.

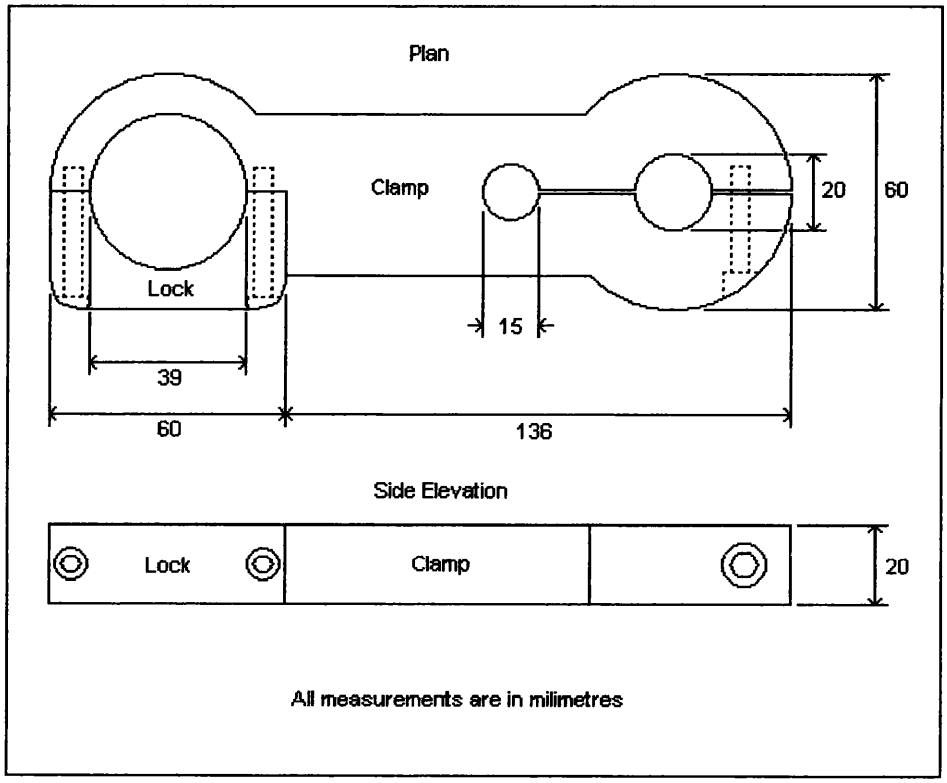

Figure 3.11 *– Diagram of Clamp and Lock Used With Modified Upper Platen*

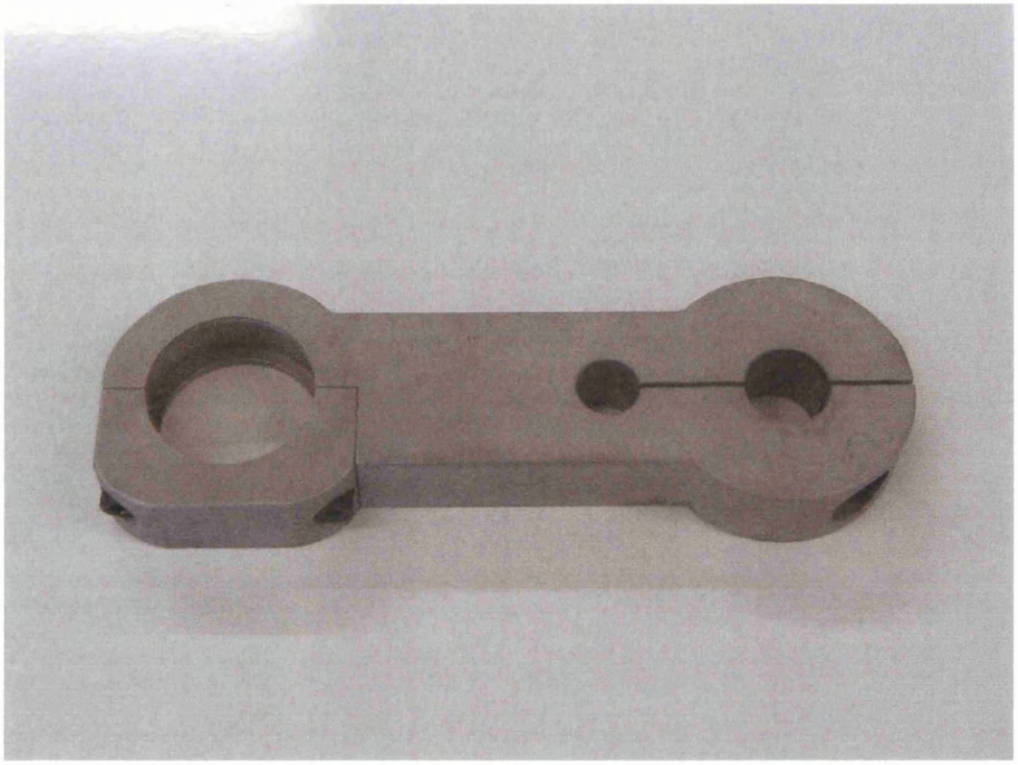

Figure 3.12 – *Clamp and Lock Used With Modified Upper Platen*

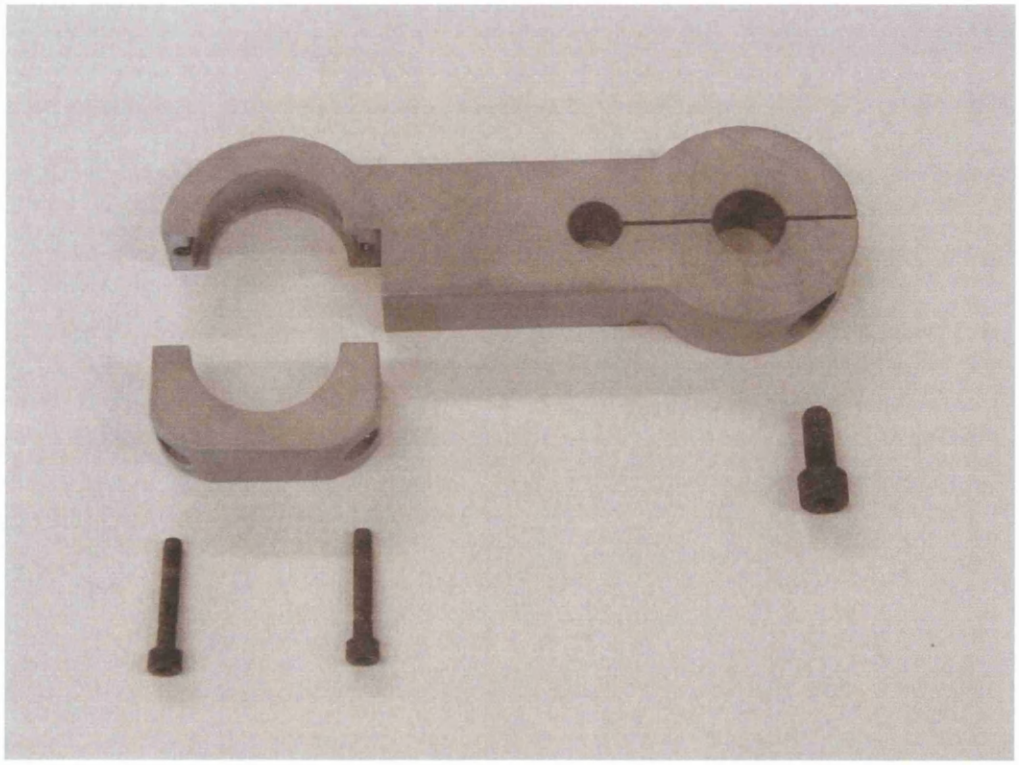

Figure 3.13 – *Components of Clamp and Key*

3.2.3 The Collar

The purpose of the collar was to maintain the height and position of the clamp and lock during the process of specimen preparation. The collar also contained a 'stop', which prevented the clamp from travelling any further than the ideal position for the preparation of the sand specimen. This, as described earlier, was such that the clamp's 39mm hole was directly above the centre of the triaxial pedestal.

The collar, as with the clamp and lock, was manufactured from aluminium. One bolt of length 20mm was employed to secure the collar to the triaxial frame. The insertion point of the bolt is clearly indicated on the side elevation in Figure 3.14 below.

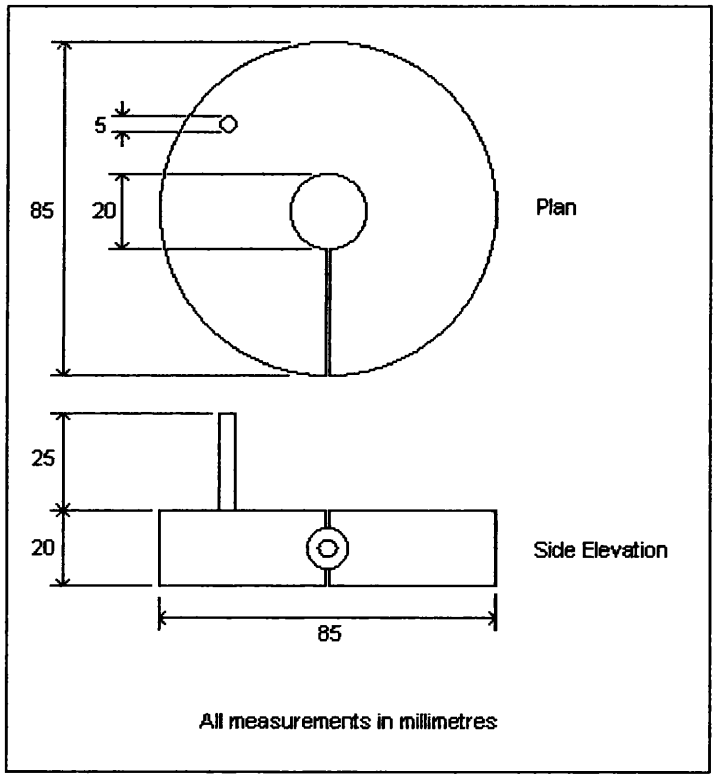

***Figure 3.14** – Diagram of Collar*

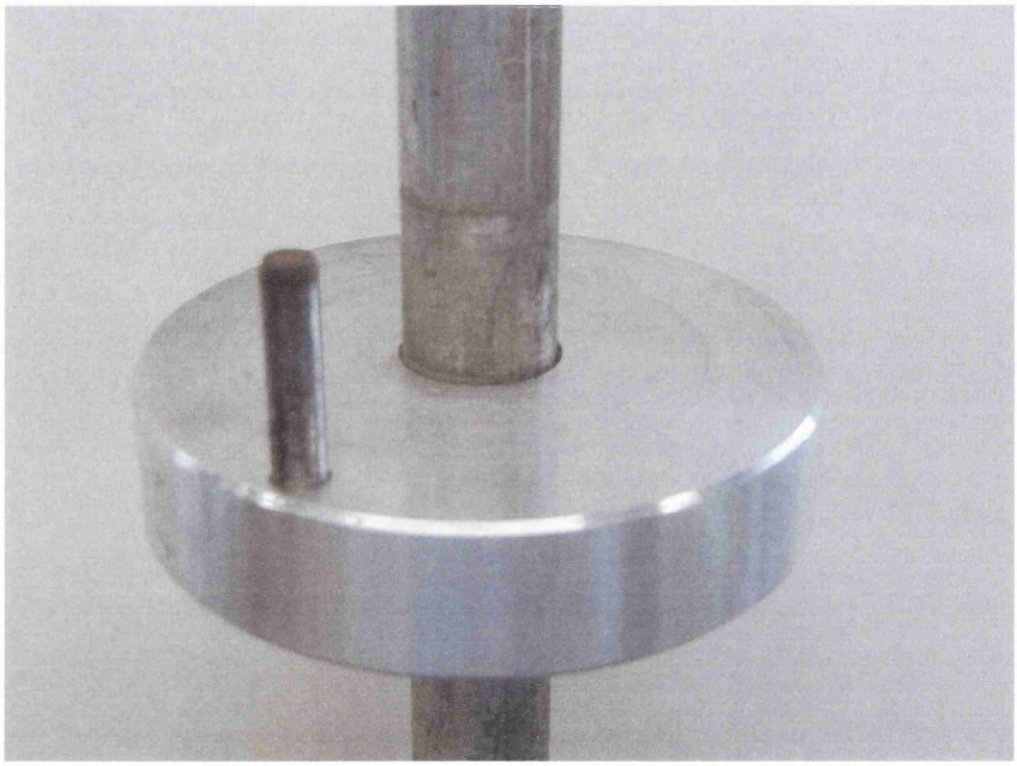

Figure 3.15 *– Collar in Position on Frame of Triaxial Apparatus*

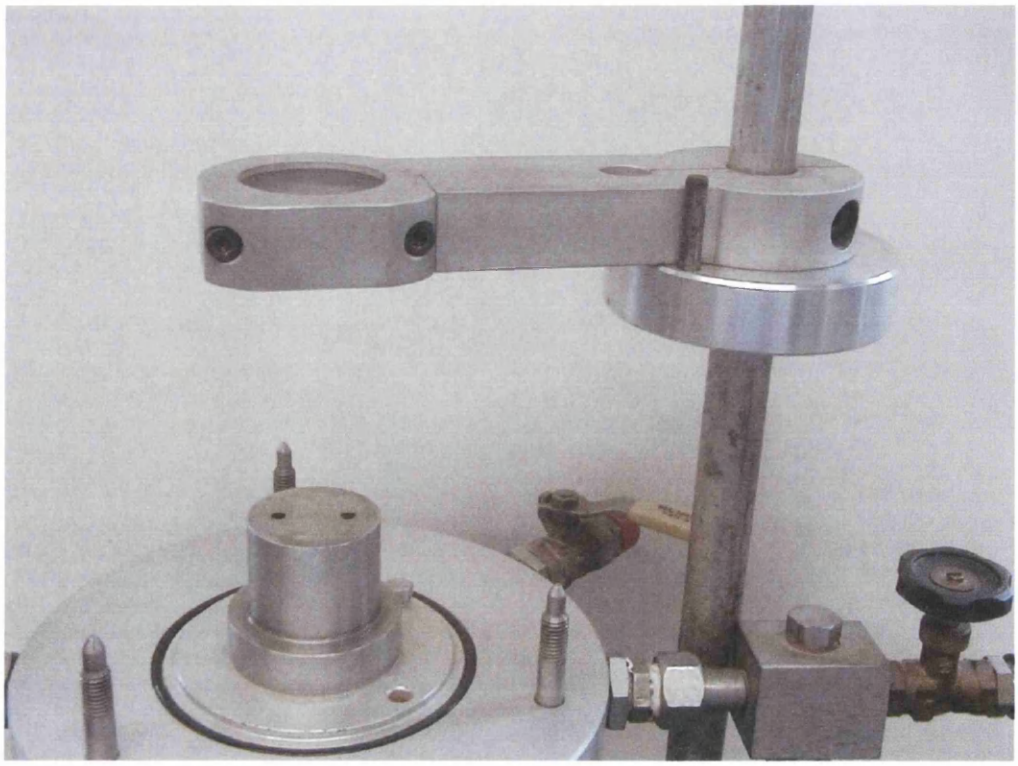

Figure 3.16 – The Clamp and Collar in Place

Figure 3.15 shows the collar, while Figure 3.16 illustrates the clamp and collar in place when attached to the fixed framework of the triaxial apparatus. Note that the 39mm diameter hole, formed when the lock is secured, is directly over the centre of the triaxial pedestal. Tightening the clamp to the framework ensured that the clamp did not rotate away from this position during the preparation of the sand specimen, whist the stop provided a permanent guide for the position of the clamp, providing the collar is not removed.

3.2.4 The Modified Triaxial System

Prior to the commencement of the triaxial testing programme, it was realised by the author that the available triaxial apparatus was not adequate for the proposed investigations. In summary, the original equipment lacked:

- a facility for measurement of pore-water pressure;
- a facility for separating the compressed air system from the water;
- a facility for the process of backpressuring the sand specimen; and
- a facility for de-airing the water used in testing.

A simplified diagram of the original apparatus is shown in Figure 3.17 below.

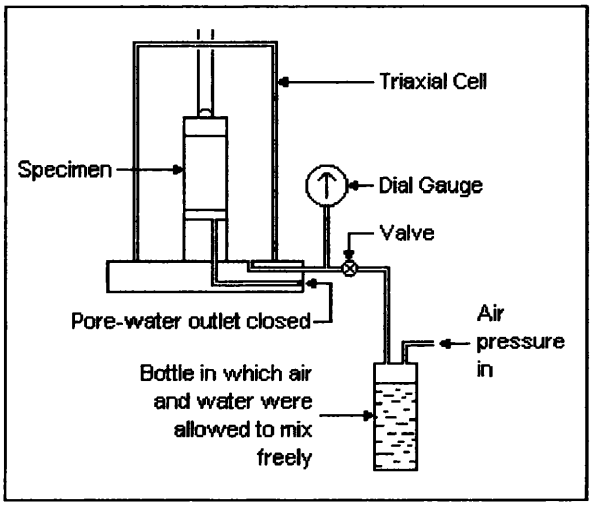

Figure 3.17 *– Original Triaxial Set-Up*

Referring to Figure 3.17, it can be seen that the pore-water pressure outlet was closed. The pore-water pressure, which is one of the most fundamental indicators of the onset

of liquefaction, therefore could not be measured, and so the apparatus was deemed unsatisfactory from this standpoint alone.

As there was no pore-water connection present, there was also no scope for backpressuring the specimen to be tested. Backpressuring, as explained earlier in this Chapter, is a very important procedure when the degree of saturation needs to be controlled. The determination of the degree of saturation has a high priority in any series of tests on partially saturated specimens, and so the existing apparatus needed to be appropriately modified.

In addition, the triaxial cell itself was pressured internally from a single bottle in which compressed air and water were permitted to mix freely. Although the water, which provides the confining pressure, is not in contact with the specimen at any time, it is still generally undesirable to have a situation where the water to be used in the testing programme can come into contact with air under pressure.

Finally, there was no capacity for establishing the change in volume of any specimen under test. In a compression test, such as those detailed extensively in the current work, the volume change is determined by measuring the quantity of pore fluid that is expelled from the specimen, and so any device for measuring the volume change would have to be connected to the pore-water pressure outlet.

Having discussed the drawbacks of this system, it should be noted that the applied axial load and axial displacement were measured by means of a transducers and a data logger. This method of measuring axial load, although not as accurate as a proving ring as it only measured in whole newtons (N), did provide the degree of automation that would be required for cyclic-stress testing. This conclusion was reached after the author's investigations into the feasibility of manually controlling the applied load during stress-controlled triaxial tests. The method of logging the result electronically would, therefore, be retained in any modified apparatus. However, a proving ring would also be used during the test programme in order to remove total reliance on one single method for estimating the applied cyclic load.

After considering all of the changes that would be needed in order to conduct research into the liquefaction susceptibility of partially saturated sand specimens, the author's design for the new system is shown in Figure 3.18. It is important to note that, for the purposes of clarity, this is not a scale diagram, and the size of the accumulators has been underestimated. Also, the proving ring has not been included, although it was correctly secured above the triaxial cell prior to testing.

A brief description will now be given of this system and, for future investigators, its operation with respect to triaxial specimens.

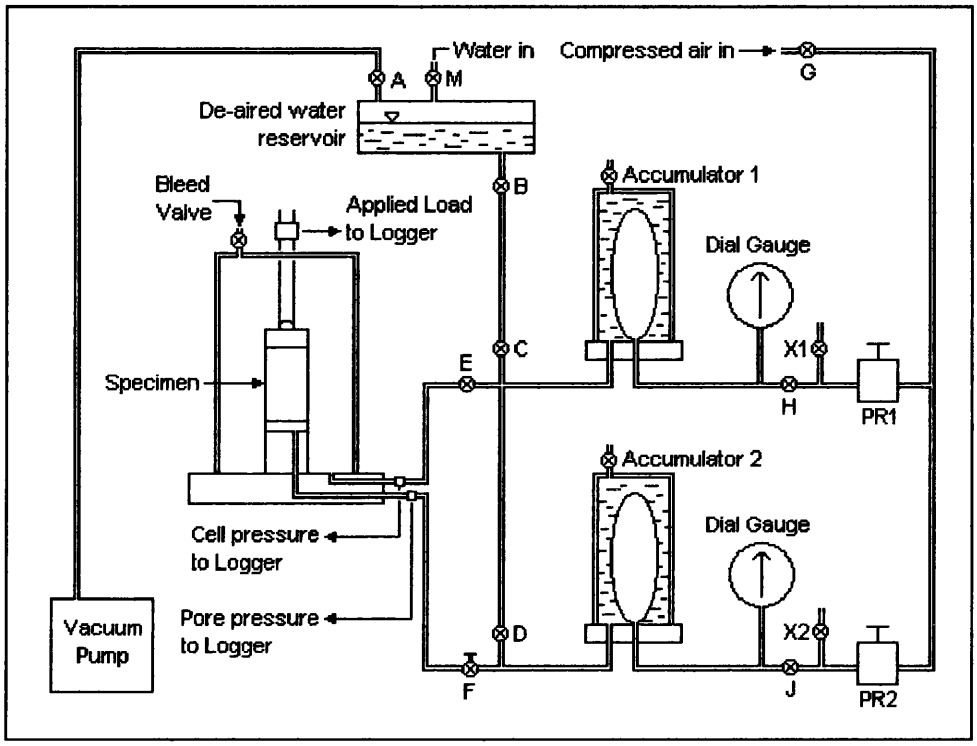

Figure 3.18 *– Modified Triaxial Set-Up*

Initially, it was required that the two air-water accumulators were filled with distilled, de-aired water. An accumulator is merely a pressure-resistant container within which a durable rubber bladder is secured. The distilled water in the reservoir was de-aired by closing valves *B* and *M*, opening valve *A*, and allowing the water to be exposed to vacuum. At this point, the de-airing process was isolated from the remainder of the system. The rate of de-airing, and the magnitude of the vacuum that the water is exposed to, is left to the requirements of the investigator, since the efficiency of the vacuum pump will need to be taken into consideration. However, for this system, it was found that 2.5 atmospheres of vacuum pressure applied to the water produced complete de-airing in approximately 2 hours, using this particular vacuum pump. De-airing was deemed to be complete when air bubbles were no longer observed to rise from any point in the body of the water.

With de-airing complete, the vacuum pump was switched off, and valves *A*, *E*, and the 'T'-valve *F* were closed. Valves *B*, *C*, and *D*, were opened so that de-aired

water could flow from the reservoir and into the accumulators. The reservoir was the highest component of the system, as indicated in Figure 3.18, thereby allowing water to flow freely under a head pressure, provided the air above the reservoir water was slowly brought back to atmospheric equilibrium via the vacuum pump. At this point in the process, the bleed valves on top of the accumulators were also opened, to allow the air outside the bladders to be expelled by the infusion of the de-aired water. The water emerging from the bleed valves was allowed to flow freely for ten seconds before the valves were finally closed. At this time, valves *B*, *C*, and *D* were also closed.

It was necessary to re-fill the reservoir with distilled water, in order to complete the filling of the accumulators. To effect this, valve *B* was closed and, with valve *M* remaining open, more distilled water was poured into the reservoir by means of a funnel. When sufficient water has been added, valve *M* was closed, valve *A* was opened, and the de-airing process was repeated. Once complete, valves *B*, *C*, and *D* were opened, in order that the filling of the accumulators could continue.

With the triaxial specimen in place using the modifications described earlier in this Section, water was infused into the triaxial cell by opening valves *E*, *G*, and *H*, and adjusting the pressure regulator *PR1* so that compressed air filled the bladder inside accumulator *1*. The compressed air produced inflation of the bladder, forcing de-aired, distilled water into the triaxial cell. The pressure was adjusted by means of the regulator until the pressure was equal to the required confining pressure. A transducer connected to the data logger recorded the magnitude of this pressure, as did the dial gauge, although it was observed by the author that there was a slight discrepancy between the two values due to the energy required in expanding the bladder. Thus, the magnitude of the pressure as recorded by the data logger was taken as the cell (confining) pressure, while the reading on the dial gauge served as a useful visual guide during the backpressuring process.

Throughout the triaxial testing programme, it was necessary to infuse water into the triaxial specimen itself. To achieve this, valves *B*, *C*, and *D*, were opened, and the 'T' valve, *F*, was opened very slightly (approximately $^1/_{16}$ of a rotation) to allow the rate of infusion to be kept to a minimum. This was important since rapid filling of the pores in the specimen might have caused unwanted and irreversible disturbances in the soil particles. The valve *D* was closed when water emerged from the unplugged modified upper platen, as described earlier in this Section. This provided a continuous

channel of distilled, de-aired water between the specimen and accumulator *2*, even though this accumulator was not being directly used to saturate the specimen.

If backpressuring was required, then the cell pressure and the pore-water pressure were increased at the same rate, until the required value of the pore-water pressure needed for the backpressuring process was reached. Normally this rate would be very slow and difficult to judge effectively, but the work was assisted by means of the dial gauges, which provided important information on the relative magnitudes of these two pressures. Ideally, the cell pressure was kept between 3 and 5 kPa higher that the pore-water pressure. This allowed a nominal *effective* confining pressure to be applied to the specimen, preventing any significant rearrangements and reorientations of the soil particles. If the pore-water pressure was permitted to rise above the confining pressure, then irreversible disturbance of the soil particles would have inevitably occurred. The dial gauges and pressure regulators are shown in their working configuration in Figure 3.19 below. Note the close proximity of the dial gauges, an essential consideration when attempting to maintain a nominal effective stress on the soil specimen during backpressuring.

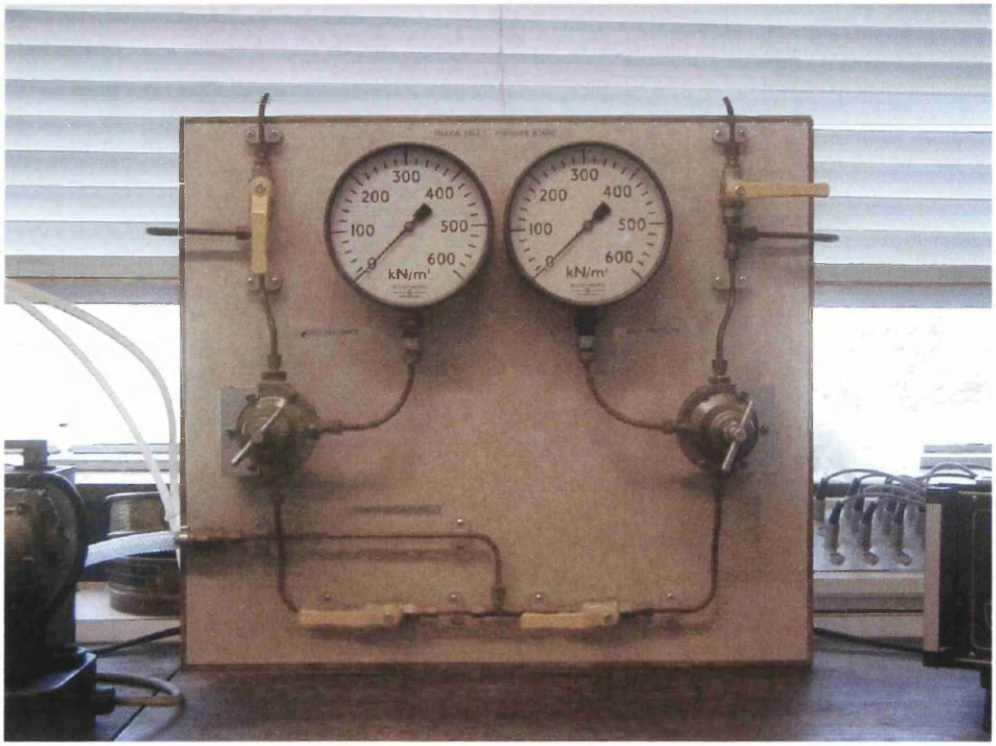

Figure 3.19 *– Dial Gauges and Pressure Regulators*

During the backpressuring process, valves *E* and *F* were kept open. Valves *B*, *C*, and *D*, were all closed during this period. Once backpressuring had been completed, the required effective confining pressure could be applied. This was achieved by keeping valves *E* and *F* and open, and increasing the air pressure using regulator *PR1* until the required effective confining pressure was reached. For example, if the difference between the confining pressure and pore-water pressure during back-pressuring of the specimen was 3 kPa, and the effective confining pressure required for testing was 100 kPa, then the cell pressure would need to have been increased by 97 kPa to reach this value. In fact, it was more usual that the cell pressure would have needed to be increased by an increment slightly higher than this value, in order to take account of the energy lost in expanding the bladder inside accumulator *1*. The value of the pore-water pressure as recorded on the data logger should be referred to, rather than the dial gauge reading, in order to reach the correct effective confining (cell) pressure.

If a drained test was to be conducted on the specimen, then valve *F* would have needed to be kept open throughout the test. This allowed any potential rise in pore-water pressure, brought about by the compression of the specimen, to be dissipated through the system to reach equilibrium with the pore water in accumulator *2*. The drained parameters of the specimen could then be determined. If an undrained test was to be performed, as was the case throughout the testing programme outline in this work, then valve *F* would have needed to be closed immediately prior to testing. Any increase in the pore-water pressure would then not be permitted to dissipate, allowing the undrained parameters and pore-water pressure increases within the specimen to be established during testing.

At the conclusion of testing, data logging was discontinued. In an undrained test, valve *F* would now need to be opened whereas, in a drained test, it will already be open. In either case, the pore-water pressure would need to reach pressure equilibrium with the water in accumulator *2*. The water pressure was brought to the atmospheric value, with valve *J* open, through the pressure regulator *PR2*. Any excess air pressure remaining in the system could be removed by opening the exhaust valve *X2*.

With the pore-water pressure now in equilibrium with atmospheric pressure, the cell pressure was dissipated through the pressure regulator *PR1* with valves *E* and *H* open. Here, any excess air pressure remaining in the system was removed by opening the exhaust valve *X1*.

Finally, that water which had provided the effective confining pressure in the system was removed by opening the bleed valve at the top of the triaxial cell. The water then drained back to accumulator *2* under atmospheric pressure.

The modified triaxial apparatus is shown in Figure 3.20 below. Note the presence of a proving ring as a check against the logged readings of the axial load.

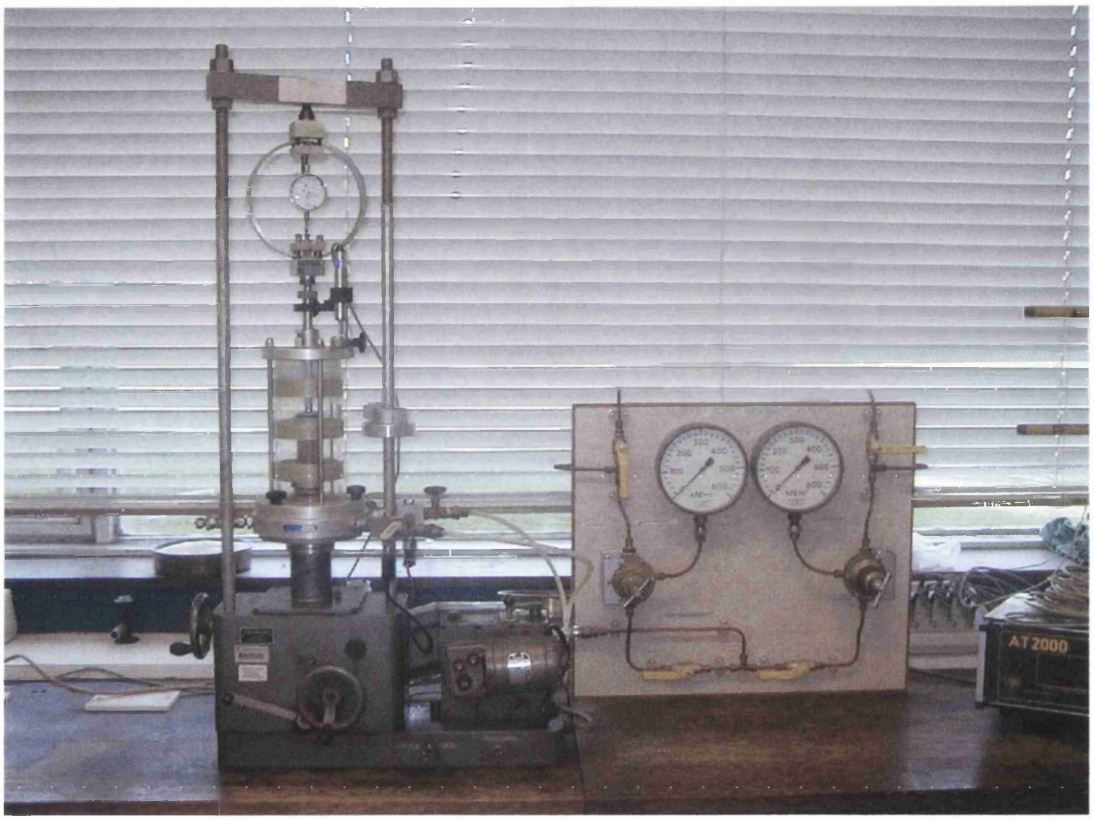

Figure 3.20 *– The Full Triaxial Apparatus*

3.2.5 Maintenance of the Modified Triaxial System

With any triaxial system, effective maintenance is a vital component of the success of any testing programme conducted upon it. This sub-Section provides an account of how this particular system was maintained.

It was critically important, due to the compressibility of air and the incompressibility of water, that the accumulators were always completely filled with de-aired water prior to any test being carried out. Therefore, in preparation for each triaxial test being conducted, any air that had, by some means, become trapped in either or both accumulators, was removed by opening valves *B*, *C*, and *D*, and the

bleed valves on the top of each accumulator, while valves *A*, *E*, *F*, and *M* remained closed. Clearly, the air above the reservoir water must be in atmospheric equilibrium for the water to flow. The accumulators were bled in this way for about 15 seconds each. This was deemed sufficient time for any unwanted air in the accumulators to be removed.

The water was kept in its required de-aired state by re-applying a vacuum between test sessions. As outlined previously, a vacuum pressure of 2.5 atmospheres de-aired the distilled water in the reservoir in approximately 2 hours. This rate of de-airing will change depending on the efficiency of the de-airing system used. Water can be added to the reservoir, while de-airing is not being employed, through valve *M* with valve *B* closed.

It is not uncommon for air to become trapped around the interior of the system's tubing close to the transducers. This is clearly undesirable, as the compressibility of any such air can seriously affect the results of any triaxial tests conducted using this apparatus. Therefore, the transducer connections were bled prior to each test being conducted. Being a smaller enclosure than the accumulator, the time required for bleeding is that much less. However, this process is no less critical. The transducer connections were bled by opening valves *E* and *F*, and allowing water to flow from the reservoir under a head pressure. The bleed valve on the appropriate transducer connection was opened and, in this manner, air was successfully removed from the system.

When using granular specimens such as those comprising sand or even coarse silt, it was important to ensure that no grains were permitted to fall into either the cell-water entry point, or through the pore-water entry point. Both of these entry points can be clearly seen in Figure 3.18 on the pedestal of the triaxial apparatus. Any grains falling into these entry points can cause constrictions, which may affect any readings obtained during subsequent testing.

It was also essential that the porous platen or stone upon which the triaxial specimen was prepared was fully de-aired before testing. Any air pockets present in this stone during a test might be forced up into the sample during, for example, backpressuring, or flushed back down the system into the transducer connections or accumulators during the removal of the pore-water pressure. The stone was de-aired prior to testing by maintaining it in boiling water for approximately ten minutes.

All of the above procedures were completed prior to each triaxial test described herein. It was recognised by the author that failure to follow these precautions might have compromised the objectives of the test programme.

In between testing periods, a continuous channel of de-aired water was maintained between the reservoir and the pedestal of the triaxial apparatus. This was done to remove any air from the interior of the triaxial pedestal (as shown in Figure 3.18). Such air could have had a negative effect on the quality of any results obtained using this system. Thus, every effort was made to maintain a thin layer of water on the triaxial pedestal.

Regular calibration of the axial displacement transducer, load transducer, and both pressure transducers, was a vital consideration when attempting to ensure the quality of the results obtained from the triaxial test programme described in the next Chapter. On calibration, the datum values of each of the three transducers, as given by the data logger, were recorded. If, after subsequent testing, the datum value of any transducer differed from the original datum value by more than 0.002% of the stated full-scale gain of that particular transducer, then re-calibration was carried out. Calibration of the cell pressure and pore-water pressure transducers was conducted by means of a compressor, and cross-referenced against known values. Calibration of the load transducer was conducted through a proving ring, while calibration of the axial displacement transducer was achieved by means of a vernier scale.

3.3 SPECIMEN PREPARATION AND BACKPRESSURING

3.3.1 Specimen Preparation

Having discussed at length the nature and benefits of the modified upper platen as used in the testing programme described later in Chapter 4, attention is now turned to the method of preparation of homogeneous, isotropic sand specimens for which these modifications were introduced. The existing methods by which samples are extracted from the field and brought to the laboratory for subsequent testing are well documented in Chapter 2, as well as elsewhere in the literature, and will not be repeated here.

The previous Section gave a brief description of the setting-up of the modified upper platen and clamp arrangement. A visual and sequential description is provided by Figure 3.21, Figure 3.22, Figure 3.23, and Figure 3.24.

In Figure 3.21, the de-aired porous stone is placed on the triaxial pedestal. The membrane is then wrapped around the pedestal, thereby enclosing the porous stone. The upper end of the membrane is, at this point, unsecured. The lock has been removed from the clamp, in readiness for the later stages of the set-up procedure. Two O-rings have been placed loosely around the membrane, also for a later stage.

Figure 3.22 shows the modified upper platen in position, with the plug removed and two O-rings occupying the grooves that run round the exterior of the platen. Also, any excess membrane has been taken up at the base of the pedestal, leaving a smooth boundary running parallel with the top of the platen. This is important since, immediately prior to testing, it will be necessary to bring the loading ram of the triaxial cell in contact with the ball bearing on top of the platen, and the investigator's view must not be obscured for this vital and delicate process.

In Figure 3.23, the platen can be seen inserted into the clamp. The purpose of the lip on the inside of the 39mm diameter hole can now be understood. The O-rings sit inside this lip, preventing any vertical motion of the platen during the specimen preparation phase. It is now possible to rectify any twists in the membrane through rotation of the lower, unsecured end of the membrane.

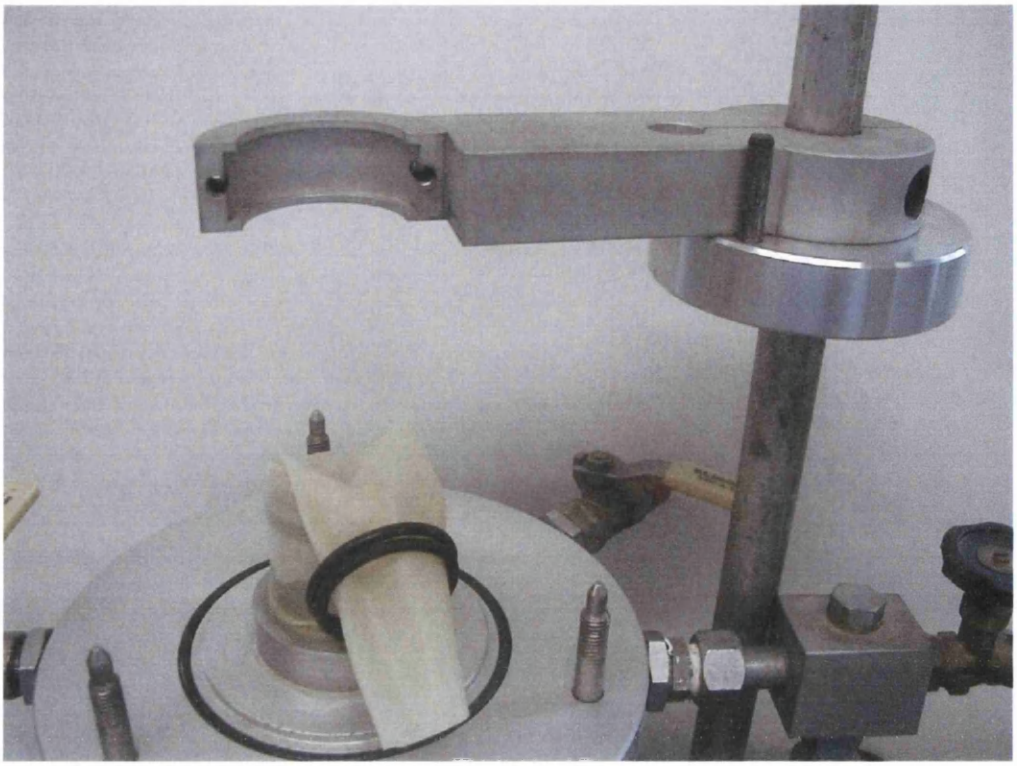

Figure 3.21 *– Set-Up Stage 1*

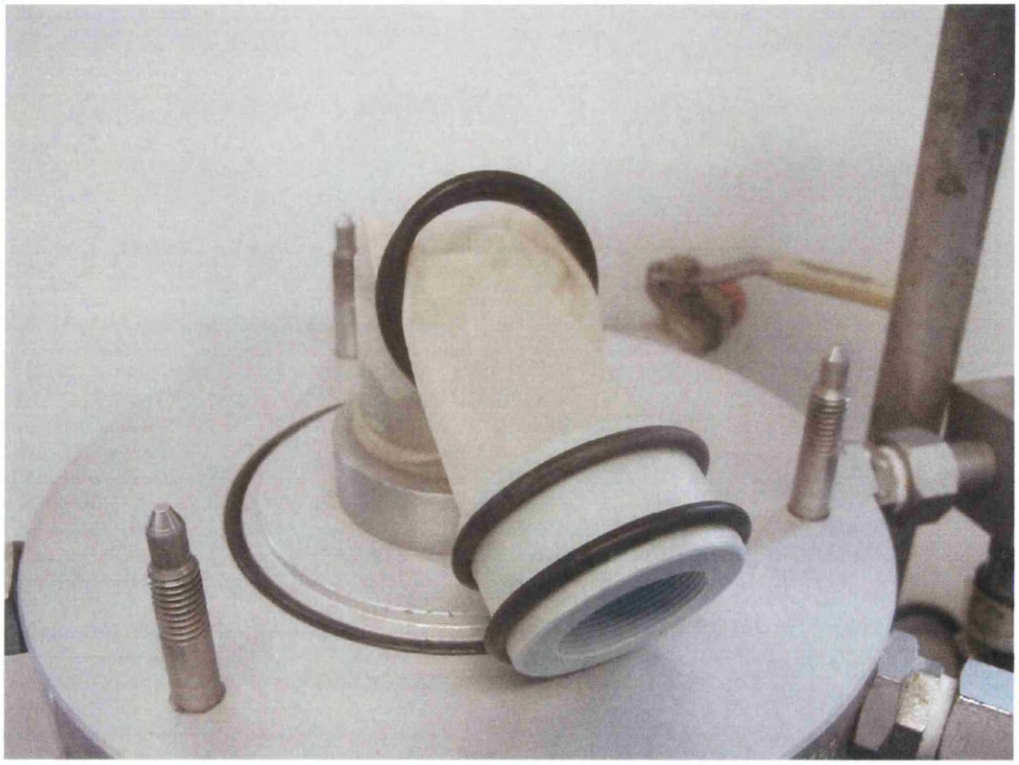

Figure 3.22 *– Set-Up Stage 2*

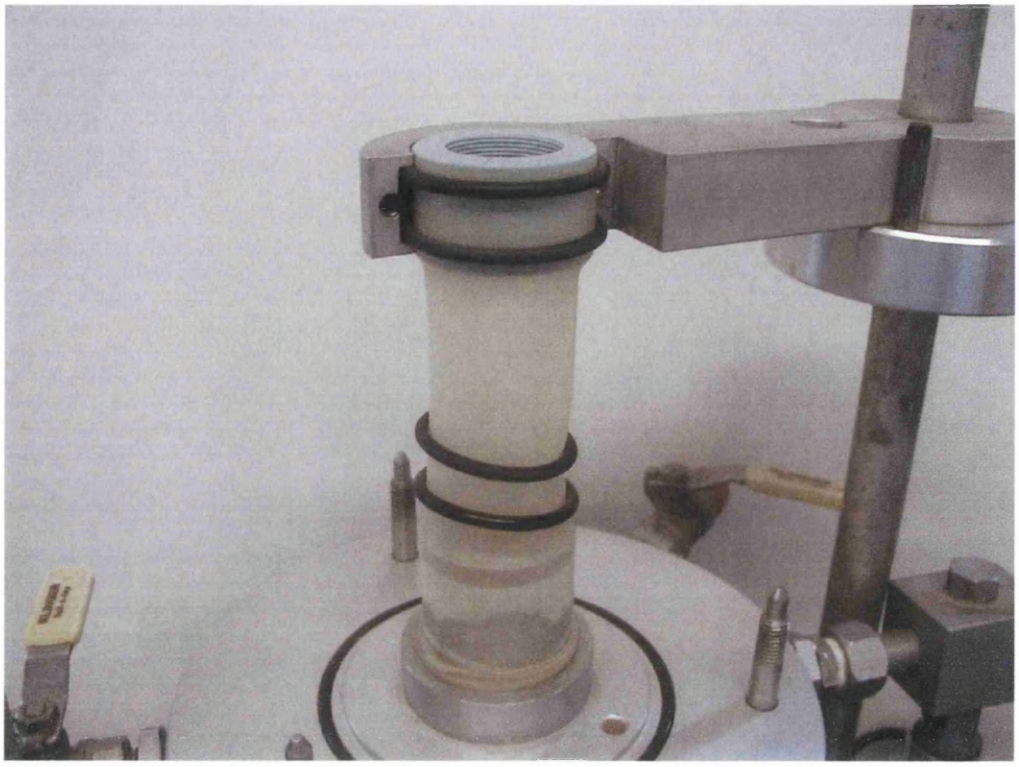

Figure 3.23 – *Set-Up Stage 3*

Figure 3.24 – *Set-Up Stage 4*

Finally, in Figure 3.24, the lock is set in position, and the O-rings are secured to the base of the triaxial pedestal. The platen is now unable to move either laterally or vertically. This has positive implications for the quality of any specimen prepared by this method. There is no further requirement for contact with the membrane, which would restrict any potential for disturbance of the soil matrix.

It is now possible to prepare the sand specimen. In the triaxial tests outlined in this work, Hostun sand was employed. This particular sand is known for its ability to liquefy, despite its fine-grained nature. It's uniformity and lack of fines, however, does allow for a sound estimation of the void ratio, a critical component of the analysis described later in this Section.

Preparation of the Hostun sand specimen was achieved by passing the sand through a funnel, which was situated inside the hole in the modified upper platen vacated by the plug (Figure 3.25). A similar method has been outlined by Bishop and Henkel in their celebrated text (1957). There, a rubber bung was used instead of a modified platen. However, this method has the disadvantage of a high potential for disturbance of the soil particles during the removal of the rubber bung and the placement of the classic platen. The method describe here seeks to minimise these inherent difficulties by combining the means of specimen preparation and load transmission into a single component, namely the modified upper platen.

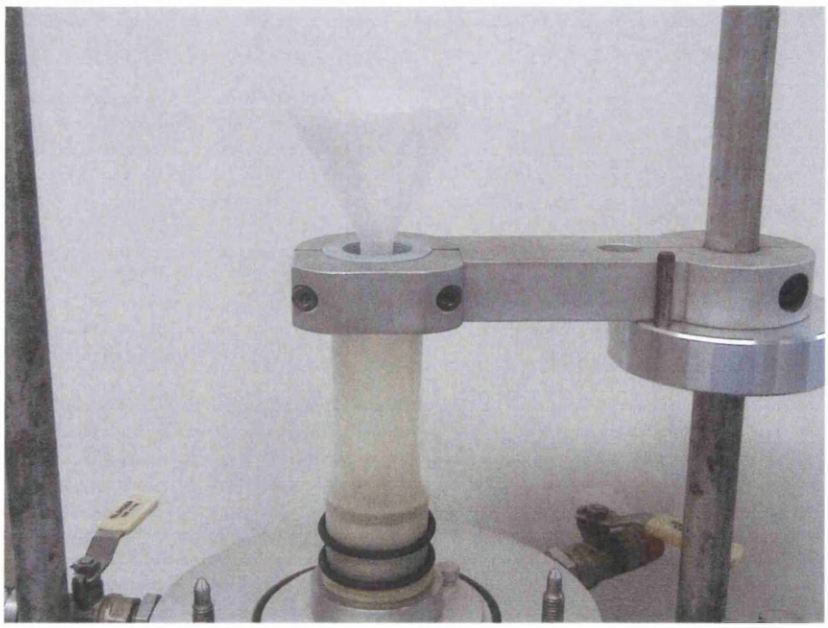

***Figure 3.25** – Arrangement With Funnel Inserted*

During preparation, dry sand was gently poured through the funnel, which then rested on the top of the saturated porous disc. In its saturated state, a thin layer of de-aired water was always present on the upper surface, and so the first sand particles entering through the funnel were wetted immediately. Further sand particles introduced through the funnel and into the mould formed by the membrane rested upon those particles already present. There was no densification or compaction, unless deliberately induced by the author by vibration or some other means, and so the sand remained in a loose state. This process satisfied one of the objectives outlined by the author earlier in this work, that the method of specimen preparation should, as closely as possible, follow those methods employed in engineering practice. The mould, when completely filled with sand, is shown in Figure 3.26. Note that the membrane appears more opaque, due to the presence of the sand, but the overall shade has changed little due to the pale colour of the Hostun sand used.

Figure 3.26 *– Mould Completely Filled With Loose Hostun Sand*

At this point, infusion of water into the specimen could take place. This was achieved, as described earlier and with reference to Figure 3.18, by closing valve *E*, opening valves *B*, *C*, and *D*, and opening valve the 'T'-valve *F* by $^{1}/_{16}$ of a rotation so that a continuously flowing channel of de-aired, distilled water was maintained between the reservoir and the base of the triaxial specimen.

With this slow rate of infusion, disturbance of the sand particles by the upward flow of water was kept to an absolute minimum. The time interval required for successful infusion is approximately 3 hours. This rate of infusion equated to an upward flow of water at a rate of approximately 0.007 mm/sec. A typical grain of Hostun sand is 0.5mm in diameter, which means that the infused water surrounded a single sand grain in approximately 70 seconds. Such a slow rate could not produce a hydraulic gradient of sufficient magnitude to disturb the sand particles. Figures 3.27 to 3.30 illustrate the infusion process.

The presence of water inside the membrane is indicated by a gradual darkening of the sand. The upper boundary of the dark region indicates the height to which the water has reached, including capillarity effects. Note that the region filled in successive 45-minute periods gets narrower. This is because the height difference between the top of the infused region, and the datum level inside the reservoir, is constantly decreasing. Therefore, the head pressure under which the water flows also decreases, resulting in a slight decrease in the rate of infusion.

Infusion was deemed to be complete when water emerged through the base of the modified upper platen. This was done by inspection, with the funnel removed. At this point, the 'T'-valve *F* was closed, preventing any further flow of water into the specimen. However, it was more advantageous to allow water to continue to flow upward into the upper platen, to ensure that the upper portion of the specimen is saturated to the fullest degree. Any excess water may then be removed from the interior of the platen with a syringe.

The plug was subsequently threaded into the upper platen by means of the key, as described earlier. The lock on the clamp was then removed. Finally, the clamp was carefully loosened from the triaxial framework. Vigilance was needed here to ensure that the loosening of the clamp did not simultaneously produce an unwanted rotation of the specimen. However, rotation of the *clamp* was required to free the specimen, but this was done after all other steps had been completed. To do otherwise could have seriously compromised the sensitive soil structure. With the key replaced into the upper platen and held in position *without* downward pressure being applied by the investigator, the clamp was slowly swung away. The key was removed, and the loose Hostun sand specimen was then be in its correct vertical position, with the seating for the ball bearing being precisely positioned in line with the axis of the loading ram of the triaxial cell. Figures 3.31 and 3.32 illustrate these final steps.

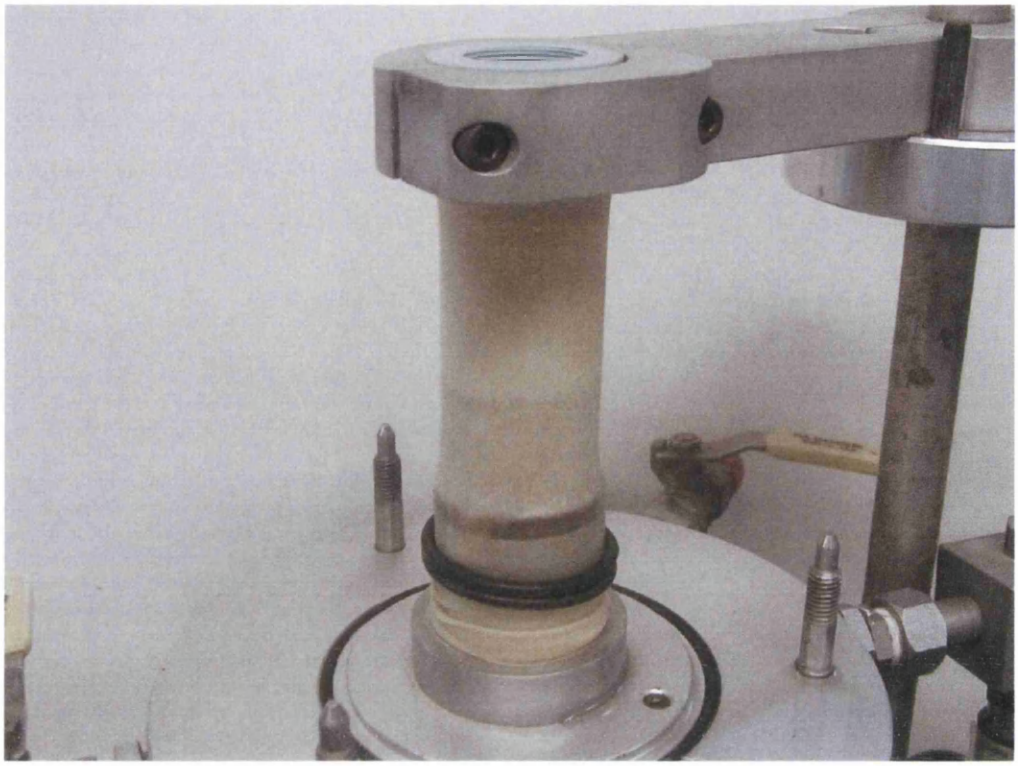

***Figure 3.27** – Infusion of water after 2700 seconds (45 minutes)*

***Figure 3.28** – Infusion of water after 5400 seconds (1½ hours)*

Figure 3.29 *– Infusion of water after 8100 seconds (2¼ hours)*

Figure 3.30 *– Infusion of water after 10800 seconds (3 hours)*

Figure 3.31 *– Specimen in Position with Lock Removed*

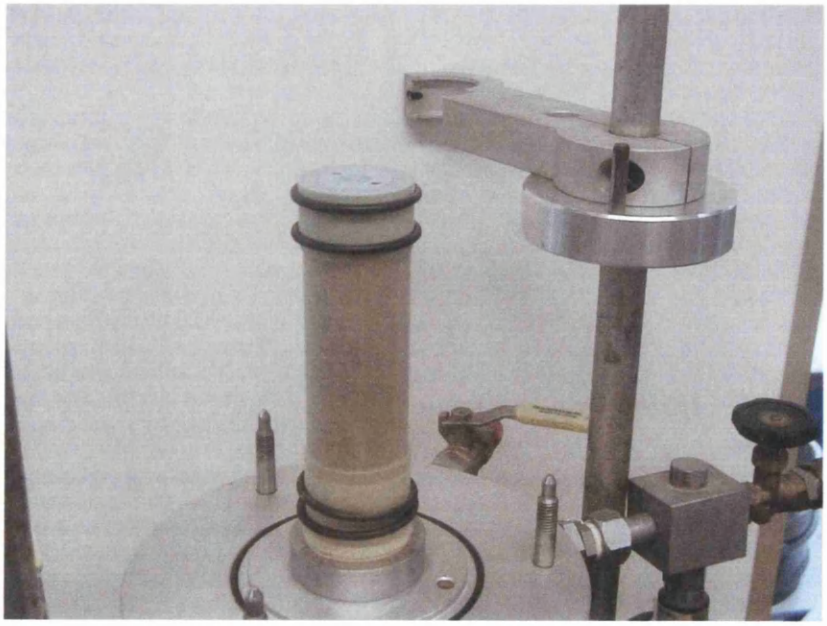

Figure 3.32 *– Specimen in Position with Clamp Swung Away*

3.3.2 The Use Of Zeolite To Produce Partial Saturation

Preparing a sand specimen by the method described above will produce a high degree of saturation, due to two factors. Firstly, de-airing the water is of clear benefit while, secondly, the slow rate of infusion ensures that all parts of the specimen are exposed to the wetting effect. By neglecting small pockets of air maintained by surface tension between the contractile skin and the soil particles, the specimen may be incorrectly deemed to be totally saturated.

However, for the scope of this particular aspect of the experimental phase of the current work, the behaviour of a partially saturated sand specimen was required, in particular the response of the pore-water pressure to cyclic-stress loading. Therefore, it was realised that, if a certain volume of zeolite contained within a sand specimen produced a given degree of saturation, S_r, then applying differing backpressures to similar specimens would produce differing degrees of saturation. In this context, the response of a partially saturated specimen to cyclic loads could be analysed.

Zeolite, as described previously in this Chapter, is a substance in powder form. When the powder is mixed with water, a chemical reaction between the zeolite and the water will produce oxygen. It follows that, if zeolite is distributed evenly within a soil matrix, then the oxygen produced by the reaction between the zeolite powder and the water would remain locked in the matrix by the soil particles. This is a fundamental requirement of any proposal for any liquefaction mitigation method which employs partially saturated sands.

3.3.3 Backpressuring of the Specimen

The theory behind back pressuring has been outlined earlier in this Chapter. In brief, backpressuring is the process by which air bubbles or air pockets (termed 'free air') are absorbed by the pore water from a soil specimen or sample by the application of an internal pressure. This is the theoretical basis of Henry's Law, and is the cornerstone upon which the success of testing those specimens deemed to be fully saturated, due to physical application of a backpressure, is based.

Through the absorption of air (oxygen) contained within the soil matrix, it should be clear that backpressuring is a process that significantly alters the degree of saturation within a soil specimen. In particular, the application of a pore-water pressure above atmospheric forces air into solution, thereby increasing the degree of

saturation. If the pore-water pressure is less than atmospheric, then air will be drawn progressively out of solution. This phenomenon is known as 'cavitation'.

It was initially necessary to establish the pressure required to completely saturate a specimen which had an initial degree of saturation, S_r, less than 1.00. An arbitrary time of 1 hour (3600 seconds) was chosen as the period over which the backpressuring was to take place for this and subsequent tests. It was deemed that this period would be sufficient for equilibrium to be reached in the specimen once full saturation had been achieved.

The specimen had first been mixed with zeolite, the volume of which was 2% of the total specimen volume. Care was taken to ensure that the zeolite was in its correct aggregate-free form, by first grinding the powder, and then by mixing vigorously with the sand prior to placement into the modified triaxial mould. Preliminary investigations by the author had clearly indicated that aggregations of the zeolite powder produced much larger gas occlusions on reaction with the water, an effect which subsequently had serious consequences for the physical stability of the specimen. This can be seen in Section 3.2.

At the outset, the value of the degree of saturation, S_r, was not known. Therefore, Skempton's B-parameter (1954) was used to approximate the degree of saturation in the specimen. The B-parameter is defined as:

$$B = \frac{\Delta u}{\Delta \sigma} \qquad [3.8]$$

where Δu is the change in the pore-water pressure induced by a change in the ambient confining pressure, $\Delta \sigma$. Here, the change in ambient pressure will be a change in the confining pressure inside the triaxial cell. Values of B can range between 0.00 for a completely dry soil, to 1.00 for a completely saturated soil, although it should be noted that, despite this similarity, the relationship between the B-parameter and S_r is non-linear.

From Equation [3.8], it can be seen that a specimen may only be considered fully saturated when B = 1.00. For any values of B less than 1.00, it can be deduced that the discrepancy between Δu and $\Delta \sigma$ can only be attributed to some mechanism which is preventing the pore-water pressure from rising further. The compressibility

of air is this mechanism in a partially saturated soil. Therefore, any value of B other than 1.00 indicates the presence of air in the specimen.

The test procedure was as follows:

- The data logger was activated so that values of cell (ambient) pressure and pore-water pressure (backpressure) may be recorded.
- Under drained conditions, both the cell pressure and the pore-water pressure (backpressure) were manually increased by equal increments of 20 kPa, whilst it was ensured that the cell pressure remained greater than the pore-water pressure by between 3 and 5 kPa. Keeping this small discrepancy constant ensures that the effective stress on the specimen, $(\sigma_3 - u_w)$ remains constant.
- After each increment of cell pressure and pore-water pressure had been slowly applied, a period of 5 minutes was allowed for internal pressure equilibrium to take effect. This is necessary since the pore water flows through the bottom of the specimen, and the pore-water pressure is not applied at all points in the specimen at the same time.
- Increments continued to be applied until the required value of backpressure was reached. At this point, the cell pressure should remain between 3 and 5 kPa above the value of the backpressure.
- The system was then left with no further increments of pressure for 1 hour, the required backpressure having been reached. After this period, and referring to Figure 3.16, the 'T'-valve F was closed.
- The cell pressure was manually increased by 160 kPa, again in increments of 20 kPa followed by an interval of 5 minutes to allow for internal pressure equilibrium to be reached. These increments were applied under undrained conditions, since valve F was now closed.
- The rise in internal pore-water pressure at the end of each increment, plus 5-minute interval, was recorded.
- The value of B according to equation [3.8] was re-estimated.
- Once equilibrium had been established after the concluding 20 kPa rise, the final values of Δu and $\Delta\sigma$ were recorded.

The full results of the initial investigation into the value of backpressure required to completely saturate a Hostun sand specimen, prepared by the method described earlier in this Chapter, are presented in Table 3.1 below.

Test No.	Backpress.	$\Delta\sigma$ (kPa)	Δu (kPa)	B
BP-2	100	160	114	0.71
BP-3	150	161	127	0.79
BP-4	200	161	135	0.84
BP-6	250	160	144	0.89 - 0.90
BP-8	300	160	155	0.97
BP-9	350	160	160	0.99 - 1.00

***Table 3.1** – Determination of Saturation Backpressure Value*

Notes:

- Test BP-1 was aborted before backpressuring commenced.
- The effective confining pressures in tests BP-3 and BP-4 were unintentionally set at 161 kPa
- Test BP-5 failed due to investigator error.
- Test BP-7 was aborted due to a fault in pressure regulator *PR1* while backpressuring was taking place (see Figure 3.18).
- Final results were averaged over three individual tests, with conditions reproduced as far as was possible.
- Values of Δu remained steady during each of the 5-minute intervals during which internal pressure equilibrium was reached, indicating the stability of the air pockets and oxygen inclusions formed by the chemical reaction between the zeolite powder and the pore water. This was confirmed on visual inspection of the exterior of the specimen, where air bubbles and pockets could be continually observed through the rubber membrane.

Conclusions:

- The value of backpressure, applied for 1 hour, required to effect full saturation in a Hostun sand-zeolite matrix lies somewhere between 300 and 350 kPa. Thus, a backpressure of 350 kPa would be applied to all future triaxial tests where full saturation would be required.
- Without the zeolite, the backpressure required for full saturation would be greatly reduced, due to the presence of de-aired of water, the slow rate of infusion of water into the specimen, and no larger oxygen pockets. Whatever the rate of infusion into a specimen containing zeolite, the reactions will still occur and the oxygen pockets will still be produced.

It will be seen later that a B-parameter value of 0.71 (see Table 3.1, test BP-2) corresponds to an approximate initial degree of saturation of 0.92. Taking the volumetric solubility of water, h, as 0.01868, and the absolute initial air pressure, u_{ao} as 101.3 kPa, then the increase of pore-air pressure required to produce full saturation may be estimated by means of Equation [3.7]:

$$\Delta u_a = \frac{(1-S_{r0})(1-h)}{h} u_{a0}$$

$$\therefore \Delta u_a = \frac{(1-0.93)(1-0.01868)}{0.01868}(101.3)$$

$$\therefore \Delta u_a = \frac{(0.07)(0.98132)}{0.01868}(101.3) = \frac{0.06869}{0.01868}(101.3) = 372.5$$

Therefore, the backpressure required to completely saturate a Hostun sand specimen is 372.5 kPa, which is satisfactorily close to the data given in the preliminary test programme for these results to be deemed reliable.

It is worth noting at this early stage that the advocation of the use of zeolite as a method of liquefaction mitigation is not the primary purpose of this work. However, the effect of using zeolite, namely the generation and subsequent behaviour of partially saturated sand in an otherwise saturated matrix, is of immediate interest. Zeolite is a chemical whose reaction with the elements and compounds which exist in natural subsurface layers is not fully understood at the time of writing and, as such, it would not be appropriate to propose the widespread use of zeolite until more relevant information is collated.

3.3.4 Specific Gravity, Moisture Content, & Void Ratio

In order to calculate the densities and various unit weights associated with the partially saturated specimens being generated for the purposes of this research, it was necessary to establish three of the primary phase parameters, namely the specific gravity, G_s, the moisture content, w, and the initial void ratio, e_0. From these quantities, it is possible to establish the initial degree of saturation, S_{r0} for each test,

and therefore to form a graphical relationship between S_{r0} and Skempton's *B*-parameter.

Specific Gravity, G_s

The specific gravity of the Hostun sand was established by the procedure as detailed in British Standards (BS1377). Three tests were conducted, each given the 'SG' prefix. The results are given in Table 3.2 below.

Test No.	G_s
SG-1	2.56
SG-2	2.56
SG-3	2.56

***Table 3.2** – Determination of Specific Gravity for Hostun Sand*

From these data, the specific gravity, G_s, of Hostun sand was taken as 2.56.

Moisture Content, w

As with the specific gravity, the moisture content was also established by the procedure outlined in BS1377. Each *untested* specimen from which the moisture content was to be taken was first backpressured to full saturation as described earlier. The moisture content for a specimen in an undrained triaxial test does not change. Five tests were used to determine the moisture content of the Hostun sand specimens. The results of these tests are outlined in Table 3.3 below.

Test No.	w
MC-1	0.3724
MC-2	0.3833
MC-3	0.3743
MC-4	0.3807
MC-5	0.3834

***Table 3.3** – Determination of Moisture Content for Hostun Sand Specimens*

Averaging the values obtained for the moisture content, *w*, and rounding to 2 decimal places, it is established that the moisture content for fully saturated Hostun sand specimens prepared by the modified apparatus is 0.38.

Initial Void Ratio, e_0

For the purposes of this work, the void ratio, e, was not measured directly. Instead, the phase relationship:

$$G_s w = S_{r0} e_0 \qquad [3.9]$$

was used for this purpose. While the void ratio and degree of saturation may change throughout a given test, the product of these two quantities will always be constant.

Having established the specific gravity, G_s, of the soil, and also the moisture content, w, of the saturated specimen, it is a trivial matter to determine the initial void ratio when the initial degree of saturation, S_{r0}, is equal to 1.00, as is the case with a Hostun sand specimen that has been backpressured to 350 kPa for 1 hour. From Equation [3.9], with $S_{r0} = 1.00$, we have:

$$e_0 = G_s w = (2.56)(0.38) = 0.9728 = 0.97 \quad \text{(to 2 decimal places)}$$

Values of the initial void ratio for sands various sands are given in Table 3.4 below. Note that, although Hostun sand is not listed here, it can be seen that an initial void ratio of 0.97 would certainly classify the Hostun sand specimens, as prepared by the modified apparatus, as being in a loose to very loose state.

The success of the method is more explicitly confirmed by Flavigny et. al. (1990), who state that the maximum void ratio, e_{max}, for Hostun sand is 1.041, while the minimum void ratio, e_{min}, is 0.648.

Sand/Soil Type	**e_{max} (very loose)**	**e_{min} (dense)**
Uniform Spheres	0.92	0.35
Standard Ottawa Sand	0.80	0.50
Clean Uniform Sand	1.00	0.40
Uniform Inorganic Silt	1.10	0.40
Silty Sand	0.90	0.30
Fine to Coarse Sand	0.95	0.20
Micaceous Sand	1.20	0.40
Silty Sand and Gravel	0.88	0.14

***Table 3.4** – Comparison of Void Ratios for Various Sands (from Hough, 1957)*

3.4 THE RELIABILITY OF THE MODIFIED APPARATUS

3.4.1 Introduction

Having completed the preliminary investigations into those aspects of Hostun sand that would be required to provide a full description into its nature, such as backpressure values and phase properties, the focus of the work now turns to the triaxial testing programme itself. The next Chapter provides a comprehensive account of the research work that was undertaken using the modified triaxial apparatus in order to establish the success (or otherwise) of employing partial saturation as a possible means of liquefaction mitigation in the field, once the merits of using the modified upper platen had been established. These merits are covered in this Section.

3.4.2 Available Methods of Measurement

In devising the strategy which underpinned the triaxial test programme, it was first deemed necessary to outline exactly what properties of the specimen were being investigated, and which properties might be safely disregarded without compromising the objectives of the work.

As already outlined at length in Chapter 2, the change in excess pore-water pressure, Δu, is the most visible criterion used to establish the susceptibility to liquefaction of a given soil deposit. In the triaxial apparatus, measurement of pore-water pressure is, given certain precautions being observed by the investigator, straight-forward to achieve. The recording of pore-water pressure is relatively quick and accurate when measured using a manometer but, for the recording of hundreds of values, electronic logging is more practical. Therefore, the automatic recording of excess pore-water pressure assumed a high priority in this testing programme.

It was not considered necessary to measure the pore-air pressure during the testing programme. The generation of air (oxygen) bubbles and pockets within the sand specimen had already been achieved by using zeolite, and initial degrees of saturation, with a knowledge of the specific gravity, moisture content, and initial void ratio, could be established. This testing programme was designed to determine the response of a partially saturated soil specimen to those applied loads which, when simulated using the triaxial apparatus, are known to produce increased susceptibility

to liquefaction. It was not the purpose of this programme to directly measure the response of the pore air to these applied loads.

Also, the measurement of pore-air pressure was not desirable as this required an outlet leading from the sample and through the upper platen which, for the purposes of this work, has already been modified. The author considered it more important to test the modified platen in its current form, before any further complications were introduced.

The volume change for a saturated specimen, in the undrained condition, is always assumed to be zero. In a partially saturated specimen, also in the undrained condition, volume change will occur due to compressibility of the pore-air, and the solubility of air into the pore-water. The volume change apparatus available to the author was of the automated type, rather than the traditional method of burettes, etc. However, the volume change apparatus, when connected, gave results that were inconclusive. Therefore, attention turned not to measuring volume change, but to measuring axial displacements during each test. These measurements could be normalised and re-termed 'axial strain'.

The axial displacement and the axial (applied) load were recorded by transducers connected to the data logger. Both of these transducers were in place on the original triaxial apparatus, and were retained in the modified design. As described earlier, a proving ring was used for all tests undertaken in the current research. Not only did the proving ring give a reliable estimation of the load being applied to the test specimens, but the readings obtained were also continuous. The data logger used for this research, as with most other electronic recording devices of a similar type, gave readings that were not continuous, but which were re-displayed after an interval of one second. This was clearly undesirable when one-way cycles of equal magnitude were to be applied to test specimens and so, while the logger recorded all results over the period of a single test, continuous monitoring of the proving ring was used to regulate the stress cycles. The data logger's results were corrected in order to remove any discrepancy between these figures and the author's notes. This resulted in a very slight smoothing of the values of the applied stress near the point where the direction of the stress application was necessarily changed to effect cycling.

In the original triaxial apparatus, the cell (ambient) pressure was monitored by a single dial gauge. This is perfectly satisfactory in tests where the effective stress on the specimen is not significant, such as a drained test on clay but, in a test programme

in which the recording of pore-water pressures is crucial, effective and continuous monitoring of the cell pressure is essential. With the pressure regulators in place in the modified system, the cell pressure was more properly maintained than with the original water bottle, but monitoring still had to be undertaken for the purpose of troubleshooting when required. For example, the failure of test BP-7 in the backpressure evaluation outlined in the previous Section was attributed to a fault in pressure regulator *PR1* (see Figure 3.16), which reduced the cell pressure, thus reducing the effective stress on the specimen. Thus, the cell pressure, axial strain, axial load, and pore-water pressure were all monitored automatically. Cell pressure and pore-water pressure were monitored to the nearest kPa, axial strain was monitored to the nearest one hundredth of a millimetre, while the axial load was monitored to the nearest whole newton. These values may appear somewhat restrictive but, as will be seen, the results produced proved satisfactory in the context of the overall response of a partially saturated soil to an applied load.

3.4.3 Reliability of the Specimen Preparation Technique

It was necessary to determine the reliability of preparing a loose sand specimen using the modifications described earlier. If the method were not reliable, and produced markedly different results for specimens seemingly produced in the same way, the method would have to have been deemed unworkable, which would have had serious implications for the remainder of the research in this area. Therefore, it was decided that a set of consolidated drained and undrained tests be conducted on the loose specimens of Hostun sand produced by the procedure described earlier, in order to confirm their assumed homogeneous and isotropic nature.

Consolidated-Undrained [CU] and Consolidated-Drained [CD] Triaxial Tests

In the consolidated-undrained [CU] test, the specimen, after preparation, was backpressured to 350 kPa for 1 hour, thereby ensuring complete saturation (see Section 3.3). The cell pressure was then increased in 20 kPa increments until the *effective* stress on the specimen reached 100 kPa. During this period, the pore-water pressure remained at the backpressure value of 350 kPa (i.e. 0 kPa excess pore-water pressure), as the T-valve *F*, as shown in Figure 3.16 was kept open. Thus, the specimen was isotropically consolidated at a pressure of 100 kPa.

After a period of 5 minutes, during which the sample was deemed to have reached internal pressure equilibrium, the valve *F* was closed, and monotonic axial compression began. At this stage, the cell pressure, pore-water pressure, axial load, and axial strain, were all being recorded simultaneously by the data logger at 60-second intervals. The rate of feed of the loading ram on the triaxial apparatus was set at 0.3 mm per minute. The consolidated-undrained [CU] tests took between 19 and 21 minutes to reach the point where no further increases in axial load were observed i.e. the critical state.

The consolidated-drained test followed exactly the same procedure as the consolidated-undrained, except that the valve *F* remained open, to allow any drainage of excess pore-water pressure back to the datum value of the original backpressure level. The consolidated-drained [CD] tests took between 24 and 26 minutes to reach the critical state.

In both the [CU] and [CD] cases, the failure criterion is taken to be evidence of a constant axial load being applied to the specimen. It is noted that peaks should not appear on the graphs since, in a loose sand specimen, there is no interlocking of particles to be overcome. At the point of constant load application, the specimen is assumed to have reached the critical state, and a constant force is all that is required to produce relative movement of the sand particles across any given failure plane. This force, which may be expressed as $(\sigma_1-\sigma_3)_{max}$, was reached in all of the tests whose results are illustrated in Figure 3.33 and Figure 3.34. The structure of the testing programme for both the [CU] and [CD] tests is given below in Tables 3.5 and 3.6.

Test No.	Specimen Type	$(\sigma_1 - \sigma_3)_{max}$ (kPa)	Axial Strain (%)
CU-2	Loose Hostun Sand	152	7.50
CU-3	Loose Hostun Sand	157	8.29
CU-4	Loose Hostun Sand	158	7.50
CU-6	Loose Hostun Sand	146	7.89

***Table 3.5** – Consolidated-Undrained [CU] Tests*

Test No.	Specimen Type	$(\sigma_1 - \sigma_3)_{max}$ (kPa)	Axial Strain (%)
CD-2	Loose Hostun Sand	275	10.26
CD-3	Loose Hostun Sand	256	9.87
CD-4	Loose Hostun Sand	248	9.87
CD-5	Loose Hostun Sand	266	9.47

***Table 3.6** – Consolidated-Drained [CD] Tests*

While the results of the [CU] tests and [CD] tests are not shown on the same axes, they have been plotted on similar scales, for ease of reference.

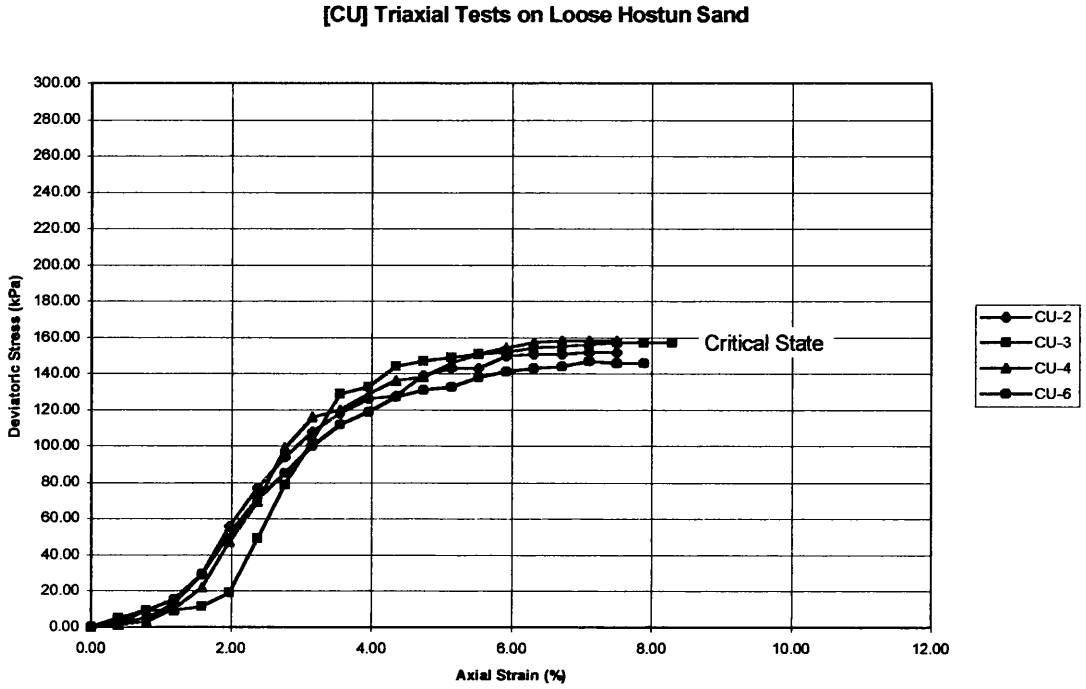

Figure 3.33 – *Consolidated-Undrained [CU] Test Results* (S_{r0} = 1.00)

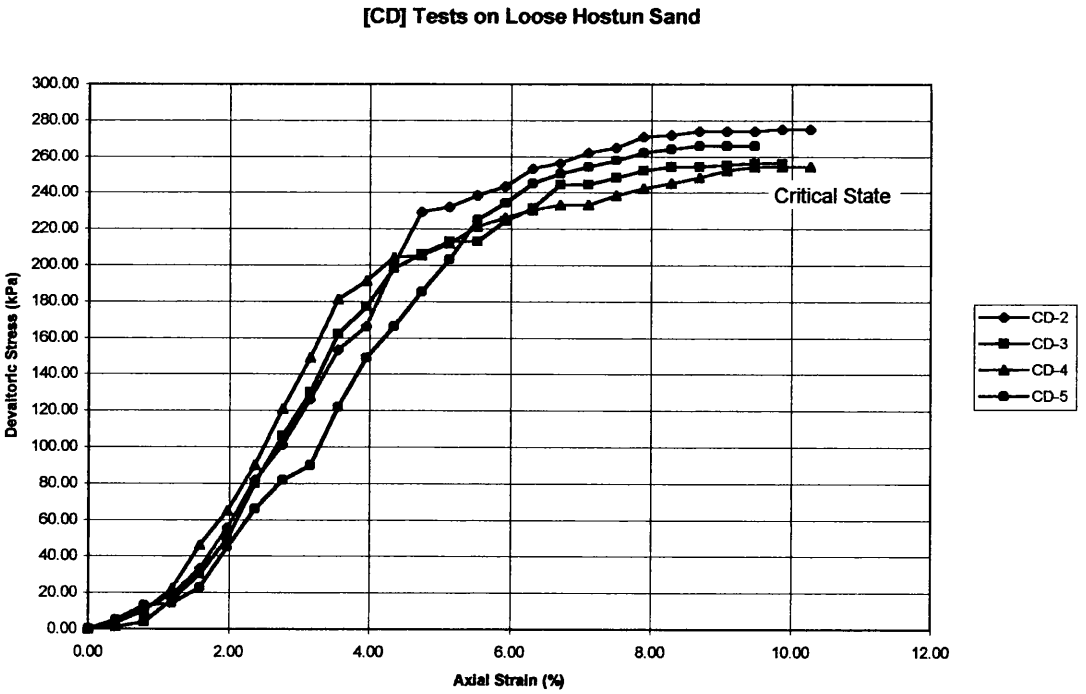

Figure 3.34 – *Consolidated-Drained [CD] Test Results* (S_{r0} = 1.00)

In the undrained [CU] tests, the effective angle of internal friction, ϕ', was estimated by means of elementary Mohr circle constructions to be approximately 31°. In these tests, measurements of pore-water pressure were also recorded. These are shown in Figure 3.35 below. As would be expected, stability in the mechanical behaviour of the [CU] tests results in pore-water pressure values that are consistent throughout the four tests.

Healy (1963) stated that, for a loose saturated sand, the peak pore pressure would be reached at approximately 8% strain, a value slightly higher than those reported for the purposes of the current work.

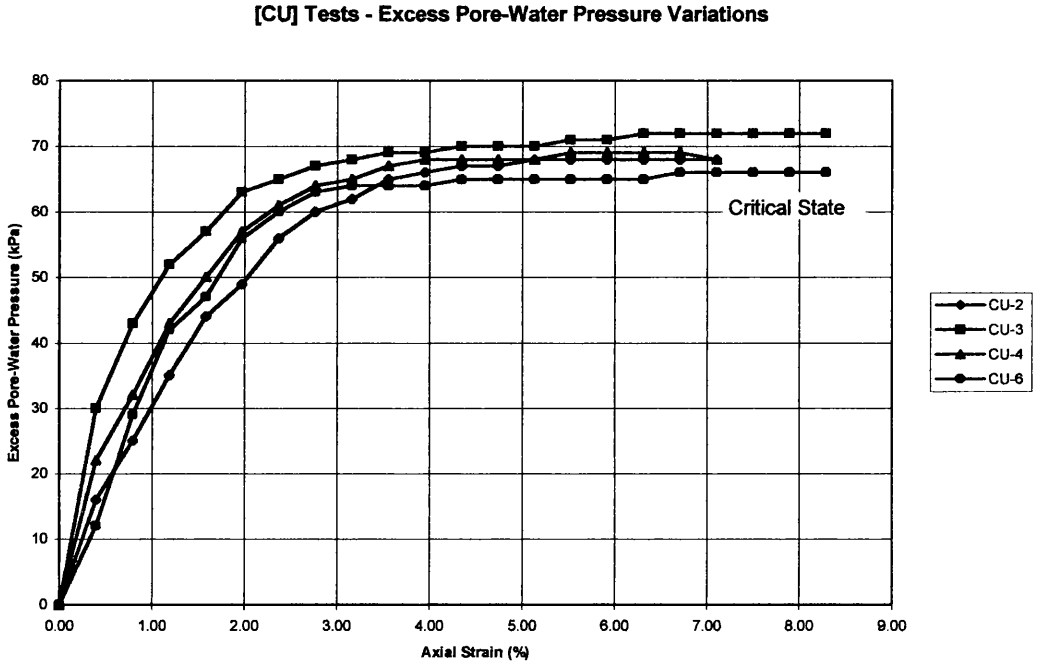

***Figure 3.35** – Excess Pore-Water Pressure Variations*

Notes:

- Tests CU-1 and CD-1 were 'dummy' tests, in which the procedures required for [CU] and [CD] tests respectively were finalised.
- Test CU-5 was aborted due to investigator error.
- Only in test CD-2 was a failure plane observed. All other tests resulted in a 'barrel'-type failure of the specimen.

- The effective stress is initially slow to rise in all tests. This is due to the loose nature of the Hostun sand, which requires more time to bring the particles into contact so that the axial load may be transmitted through the specimen. It is during this period of axial compression that excess pore-water pressure is seen to increase at its fastest rate. In the testing programme outlined in Chapter 4, axial load readings are not included until the excess pore-water pressure had begun to rise.

Conclusions:

- In both the [CU] and [CD] cases, the final residual strengths in kPa differ very little, indicating a strong similarity in the specimen structures in the two cases.
- There is no peak strength visible, indicating that all specimens were prepared in the loose state.
- From the above, it may be concluded that the modified upper platen not only produces loose sand specimens, but specimen structures can be closely reproduced for subsequent tests.

These conclusions suggest that use of the modified upper platen is a viable means of producing loose sand specimens for the purposes of a laboratory test programme. With this now established by means of the test results given above, attention can now be turned to the first programme of practical research to be conducted, namely the investigation into the use of partially saturated sand for the purpose of liquefaction mitigation. All tests in this first programme were completed using Hostun sand, the modified triaxial apparatus, the modified upper platen arrangement, and the chemical zeolite, as described in detail in previous Sections.

3.4.4 Reliability in Respect of Cyclic Triaxial Tests

Having discussed at length the reliability of the modified triaxial apparatus it applies to monotonic testing, it is now necessary to outline the means by which the system can support one-way cyclic tests.

Having applied a compressive stress at a constant rate, it was possible to reverse the direction of application on the triaxial apparatus, while still maintaining

the rate of loading. The apparatus does not require pausing before the change of direction of stress application can take place. This has the advantage of allowing a continuous cyclic triaxial test to be conducted.

However, it should be noted that, while the rate of unloading *on the apparatus* was maintained at the same level as the rate of loading, the rate of unloading *from the specimen* was increased due to irreversible plastic strains produced in the soil due to the previous compressive cycle. Such strains meant that the duration of the unloading cycle was invariably shorter than the loading cycle, a phenomenon which will be clarified by inspection of the results presented in Chapter 4.

Preliminary investigations, which have not been included here, indicated that the results produced when a specimen was subjected to a cyclic test were of the same quality as those outlined in the monotonic tests in the previous Section. The nature of these results, however, will be necessarily different, and it is this nature which permits the investigation into the viability of using partially saturated soil as a means of liquefaction mitigation.

3.5 POST-PROCESSING AND CONCLUSIONS

3.5.1 Introduction

In this Section, a summary of the work outlined in Chapter 3 will be presented, as well as a comprehensive set of conclusions and recommendations. It is important that these details are reiterated in order that the foundation upon which the triaxial test results are based is scientifically sound.

3.5.2 A Summary of the Work

In Section 3.1, a brief account of the physical and mechanical nature of partially saturated soil was presented. In particular, previous endeavours to establish a single-valued effective stress equation for partially saturated soil were highlighted, leading on to efforts, including one by the author, to establish a method of reducing the degree of saturation in a soil in order that an efficient form of liquefaction mitigation might be effected. A short account of the theory of backpressuring was also included, as was a very general description of zeolite, a chemical in powder form which reacts with water to produce oxygen gas. It was crucial that backpressuring and zeolite were introduced at this stage, as both were extensively employed in the triaxial test programme described later in Chapter 4.

Sections 3.2, 3.3, and 3.4, provide the backbone of the Chapter, and also the basis upon which the practical research conducted using the triaxial apparatus was centred. Section 3.2 focused upon necessary modifications to the triaxial set-up that were deemed necessary for this research. These included a newly-designed upper platen within which a plug is incorporated. This plug not only permits the use of the upper platen as a means of stress transmission through a soil specimen, but also as a means of preparing a specimen of Hostun sand in a loose state. Other additions, such as a key for the plug, a clamp to hold the platen in place, and a collar to maintain its vertical position are also outlined. Significant alterations made to the triaxial apparatus itself are also described in detail, including operating instructions for the reference of future researchers.

Section 3.3 focused primarily on the method of specimen preparation for which the upper platen was designed. A full description of the method is included, with accompanying photographs for clarity. For the purposes of the current work, specimen preparation included the use of zeolite in the sand specimens, and also

backpressuring the specimen in order to bring its degree of saturation to the required level. In this context, a test programme in which the backpressure value required to bring the specimen to full saturated was instigated. Finally, the specific gravity, G_s, the moisture content, w, degree of saturation, S_r, and void ratio, e, for specimens prepared with the previously-outlined procedure, were determined.

In Section 3.4, the results of tests used to determine the reliability of all modifications were presented. In addition, the methods by which triaxial test results were to be recorded were outlined.

3.5.3 Conclusions

Considering the full range of work as detailed in Chapter 3, the following conclusions may be safely drawn.

- Despite the fact that a single-valued effective stress state for partially saturated soils has yet to be established, it is permissible, in the context of the current work, to monitor pore-water pressures in isolation as values of pore-air pressure, which are required to completely describe the stress state of the soil, were neither measurable nor available. The focus of this work is on the response of the pore-water pressure in a partially saturated soil to a one-way cyclic stress application; a complete description of the stress state was not required.
- Zeolite is capable of producing pockets of oxygen which are retained within the soil matrix, as shown in Figure 3.3 and, more especially in Figure 3.4. As indicated in the later Figure, aggregations of zeolite, when in contact with water, can have a significant effect on the homogeneity of the specimen.
- In terms of physically preparing a specimen, the upper platen performed its function satisfactorily.
- The value of the backpressure which, according to the results of a test programme specially effected for the current work, completely saturated a given soil specimen was sufficiently in accordance with the theoretical value to be considered reliable. This value was taken as 350 kPa.
- The value of G_s, the specific gravity of the Hostun sand particles, was determined using only slightly modified standard testing procedures, and is

sufficiently in accordance with values for other sands to be considered reliable.

- The procedure employed for determining the moisture content, w, was also based on established methods, and so the value of w, as measured for the purposes of assessing the reliability of the apparatus and also, in retrospect, with values quoted elsewhere in this work, are sufficiently in accordance with each other to be considered reliable.
- The results from monotonic tests, presented in this Chapter, confirm that the proposed method of specimen preparation is capable of producing sand specimens possessing very similar characteristics.
- The method of specimen preparation was demonstrated to be sufficiently uniform to produce a reliable value for the initial void ratio, e_0, inherent in the soil specimen prior to any testing. The initial void ratio was estimated at 0.9728.
- Values of e_0 as quoted from elsewhere in the literature (e.g. Hough, 1957; Flavigny et. al., 1990) indicate that this value of the initial void ratio, as obtained from tests on fully saturated Hostun sand specimens for the purposes of the current research, is typical of that for a loose specimen.
- Knowing G_s, w, and e_0, to be reliable, the values of the initial degree of saturation, S_{r0}, obtained throughout this work could also be deemed reliable.

All of these conclusions will be drawn upon in further validating the performance of the modified triaxial apparatus in the test programme outlined in Chapter 4.

CHAPTER 4

TRIAXIAL TEST RESULTS

4.1 TRIAXIAL TESTS EMPLOYING CYCLES OF 60 kPa

4.1.1 Introduction

This sub-Section outlines the results of eight one-way cyclic triaxial tests (60 kPa cycles) performed on specimens of loose Hostun sand. The specimens were prepared as outlined in Section 3.3. The degree of partial saturation was varied by means of mixing the Hostun sand with zeolite. The zeolite comprised 2% of the total volume of each of the eight triaxial specimens, and had previously been ground to remove unwanted aggregations.

All tests were conducted under undrained conditions, a necessary requirement of pore-water pressure measurement, and all specimens were consolidated to a confining pressure of 100 kPa before the first stage of axial compression began.

The initial degree of saturation, S_{r0}, was varied by means of backpressuring the specimen to differing levels prior to testing. The reader is referred to Section 3.3 for an account of the viability of this procedure. The test conditions are outlined in Table 4.1 below. Test CA-1 was used merely as a 'dummy' run to the main test programme, and the results obtained from this test are not incorporated here.

Test No.	Backpressure (kPa) / duration (min.)	Cycles
CA-2	350 kPa / 60 minutes	10
CA-3	300 kPa / 60 minutes	10
CA-4	250 kPa / 60 minutes	10
CA-5	200 kPa / 60 minutes	10
CA-6	150 kPa / 60 minutes	10
CA-7	100 kPa / 60 minutes	10
CA-8	50 kPa / 60 minutes	10
CA-9	0 kPa / 0 minutes	10

***Table 4.1** – Details of Test Programme for 60 kPa Cycles*

The results are reported in the form of five graphs, and a table indicating the more vital quantities pertaining to the specimen. The graphs plot:

- the effective stress path (q' against p', both kPa).
- cyclic (deviatoric) stress (kPa) against time (s);
- excess pore-water pressure (kPa) against time (s);
- cyclic (deviatoric) stress (kPa) against axial strain (%)
- excess pore-water pressure (kPa) against axial strain (%)

The data outlined within these graphs provides valuable information with regard to the success (or otherwise) of employing partially saturated soil as a means of mitigation of liquefaction phenomena. The most important criterion for this will be the change in excess pore-water pressure as the stress cycles are applied.

Each specimen was backpressured to the required level, before being consolidated under an all round pressure of 100 kPa. Prior to the consolidation phase, Skempton's *B*-parameter was measured by closing valve the 'T'-valve *F* (reference Figure 3.18) as the confining pressure was applied. Once the corresponding rise in the pore-water pressure had been measured, dissipation was permitted to take place by opening valve *F* by only $^1/_{16}$ of a complete turn. The specimen was then consolidated to the confining pressure of 100 kPa, and *F* was once again closed.

During all process of consolidation, the volume of the soil or, in this case, the specimen, will always be reduced. However, it is possible to reduce the effect of the volume change by allowing the water to dissipate as slowly as possible, with the intention of preventing excessive disturbance of the sand particles. Such a slow rate of dissipation, in the context of this work, should ensure that the initial void ratio, e_0, remains constant up to the point of the commencement of the stress cycles. This is particularly important in sand specimens, where the lack of cohesion between particles allows for a greater freedom of movement of the particles than in, for example, a clay sample. This is the reason for opening the 'T'-valve *F* by $^1/_{16}$ of a complete turn. Note that, in an effort to preserve continuity, this was also the degree that the 'T'-valve *F* was opened when distilled, de-aired water was initially infused into the specimen.

The effective stress path is also plotted, using the coordinates:

$$q' = \sigma_1 - \sigma_3 = q \qquad [4.1a]$$

$$p' = \frac{1}{3}(\sigma_1 + 2\sigma_3) - u \qquad [4.1b]$$

where q (= q') is simply the applied axial stress (kPa), σ_1' is the major principal stress, σ_3' is the minor principal stress, and u is the pore water pressure. The drained stress path, which has a slope 3 to 1, is also included in the graphs for reference.

Finally, the critical state line (CSL) is included for reference. The critical state line has a gradient, m, given by:

$$m = \frac{6\sin\phi'}{3-\sin\phi'} \qquad [4.2]$$

where ϕ' is the effective angle of internal friction ($\approx 31°$ for fully saturated Hostun sand, leading to $m \approx 1.24$). The gradient of the critical stress line will increase as the initial degree of saturation, S_{r0}, decreases. As $S_{r0} \rightarrow 0.9$, $\phi' \rightarrow 34°$, and $m \rightarrow 1.4$).

A table of specimen parameters, which precedes the presentation of the graphs for each test, contains the following quantities:

- backpressure value (from preparation procedure);
- *B*-parameter (from pre-consolidation application of confining pressure);
- moisture content; (from untested specimens);
- initial degree of saturation (from phase relations);
- bulk density (as above);
- unit weight (as above).

The initial degree of saturation is quoted to 4 decimal places in order to increase accuracy when investigating its relationship with Skempton's *B*-parameter. Normally, the initial degree of saturation would be quoted to 2 decimal places only. Note that the buoyant weight is not included in this list, as this quantity applies only to a saturated soil. Following each table, a brief set of notes is supplied, indicating regions of interest on the graphs.

Measurement of moisture content was established by preparing specimens purely for this purpose. After required backpressuring, the untested specimens were removed from the triaxial apparatus, and the procedure for establishing the moisture content was conducted according to BS1377. The value of the moisture content recorded for each test is the average of the moisture contents of three independent samples taken from different specimens. Additional specimens were prepared if the results of the previous three samples differed significantly.

The axial stress is merely the applied load (N) divided by the cross-sectional area of the specimen at its centre. Relations have been derived to incorporate the

small changes to the cross-sectional area due to compression, but these have been neglected for the purposes of this work.

Having established the moisture content, it was possible to derive the initial degree of saturation, S_{r0}, from the phase relation:

$$G_s w = S_{r0} e_0 \qquad [4.3]$$

With G_s constant, and the initial void ratio, e_0, also assumed constant, the initial degree of saturation, S_{r0}, may be determined, provided the rate of consolidation of the specimen is sufficiently slow. Knowledge of G_s, w, and e_0 permitted both the bulk density, ρ, and the unit weight, γ, to be calculated. The unit weight is merely the bulk density multiplied by g, the acceleration due to gravity (i.e. 9.81 m/s^2).

Graphs of both the deviatoric stress and excess pore-pressure time histories are included for clarity. It is on these graphs that the application of the stress cycles and the corresponding pore-pressure response can be visualised. The rate of feed of the loading ram was set at 0.1 mm/minute, with simultaneous readings of cell pressure, axial stress, axial strain and pore-water pressure being logged every 10 seconds. This slow feed permitted the author to conduct manual reversing of the applied axial load, with reference to the proving ring, when required.

4.1.2 Test No. CA-2

Quantity	Value
Test Number / Type	CA-2 / Stress-controlled
Backpressure value	350 kPa, applied for 1 hour
B-parameter	Some variation between 0.99 and 1.00
Moisture Content, w	0.3797
Initial Degree of Saturation, S_{r0}	0.9992
Bulk Density, ρ	1793 kg/m^3
Unit Weight, γ	17.592 kN/m^3

***Table 4.2** – Details of Test CA-2 Specimen Parameters*

Notes:

- Max. excess pore-water pressure after 10 cycles = 51 kPa (i.e. $r_{0,10} = 0.51$)
- Axial strain at the end of 10 cycles = 0.51 %
- Cycles produce axial strains between 0.34 % and 0.57 %
- Test ended after 1090 seconds.

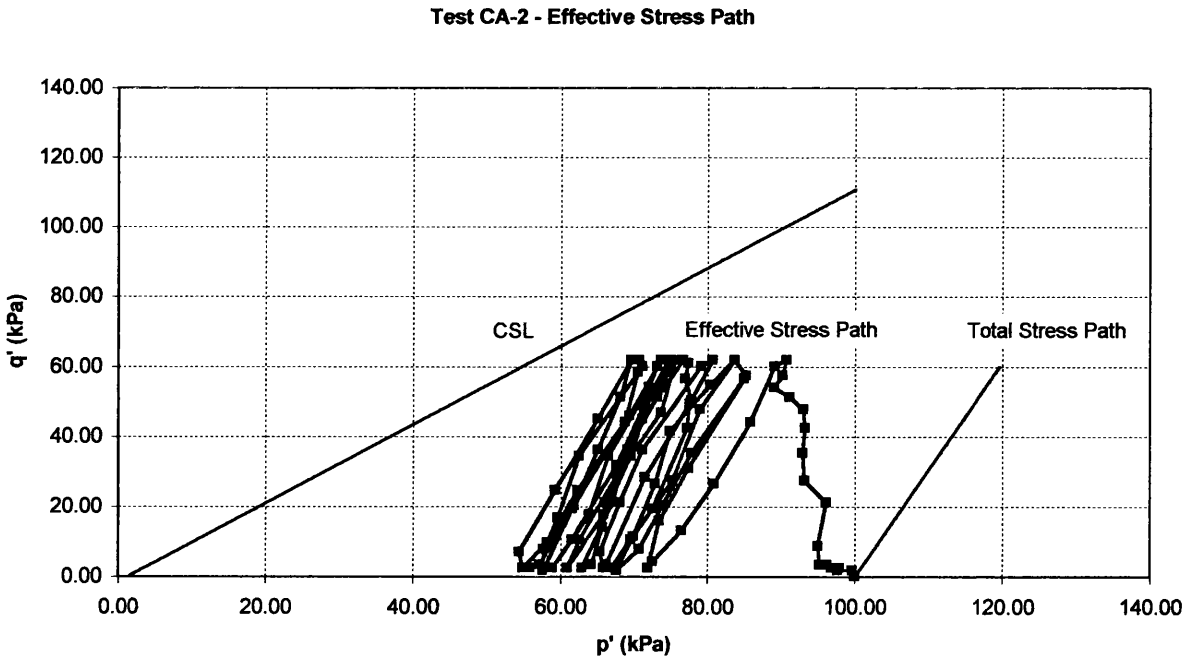

***Figure 4.1** - Effective Stress Path [Test CA-2]*

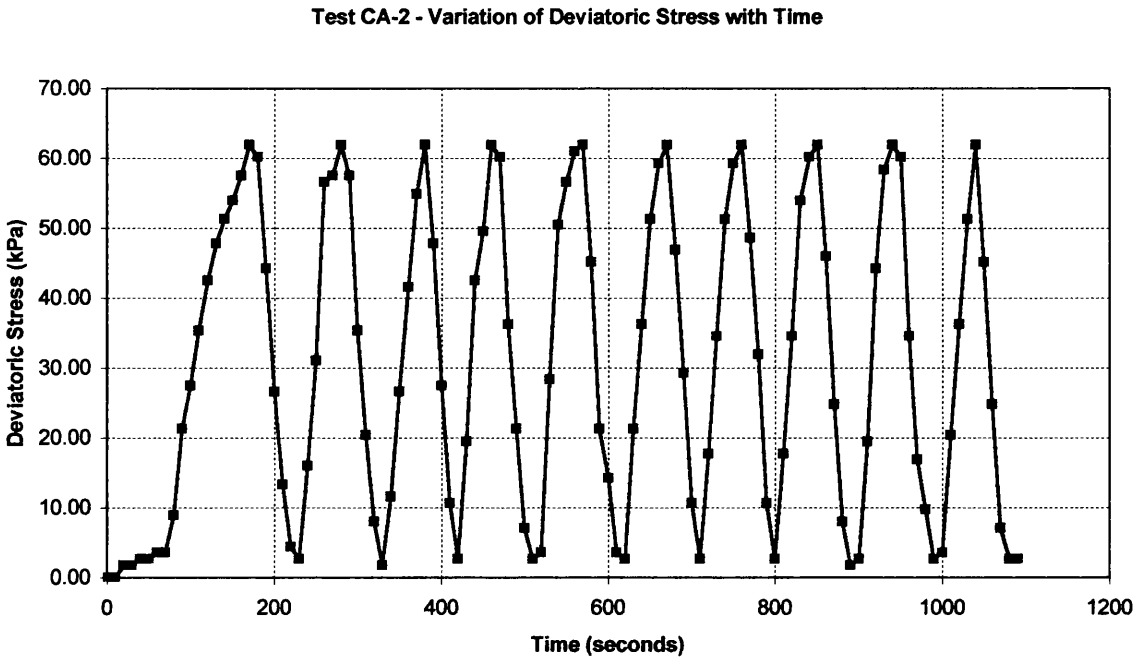

Figure 4.2 *– Variation of Deviatoric Stress with Time [Test CA-2]*

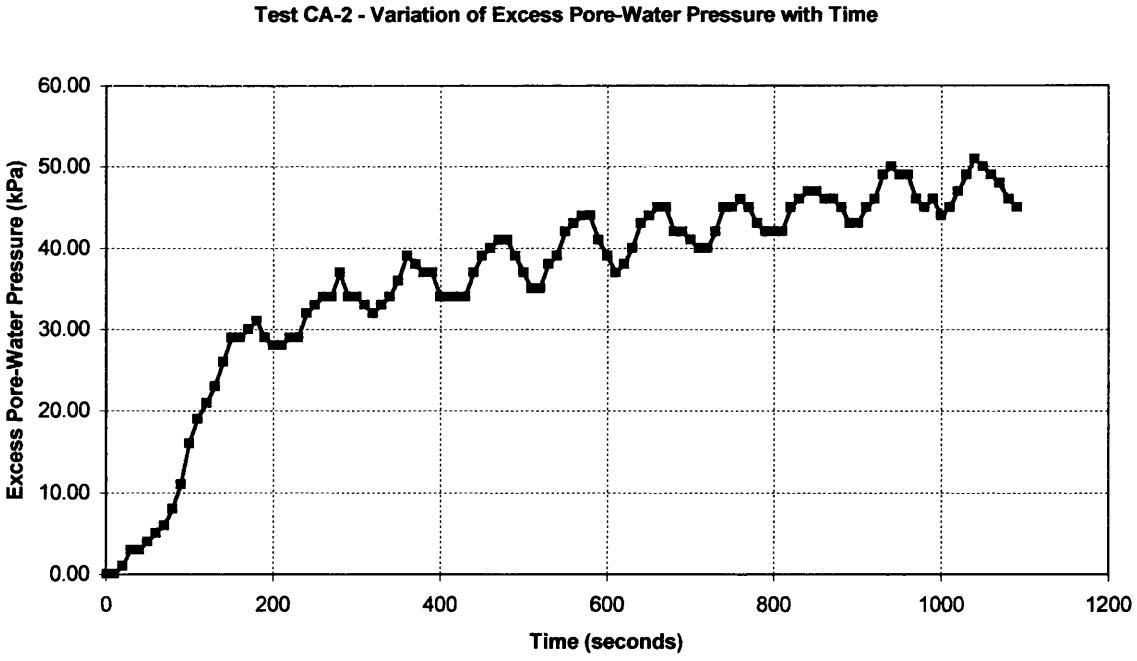

Figure 4.3 *– Variation of Excess Pore-Water Pressure with Time [Test CA-2]*

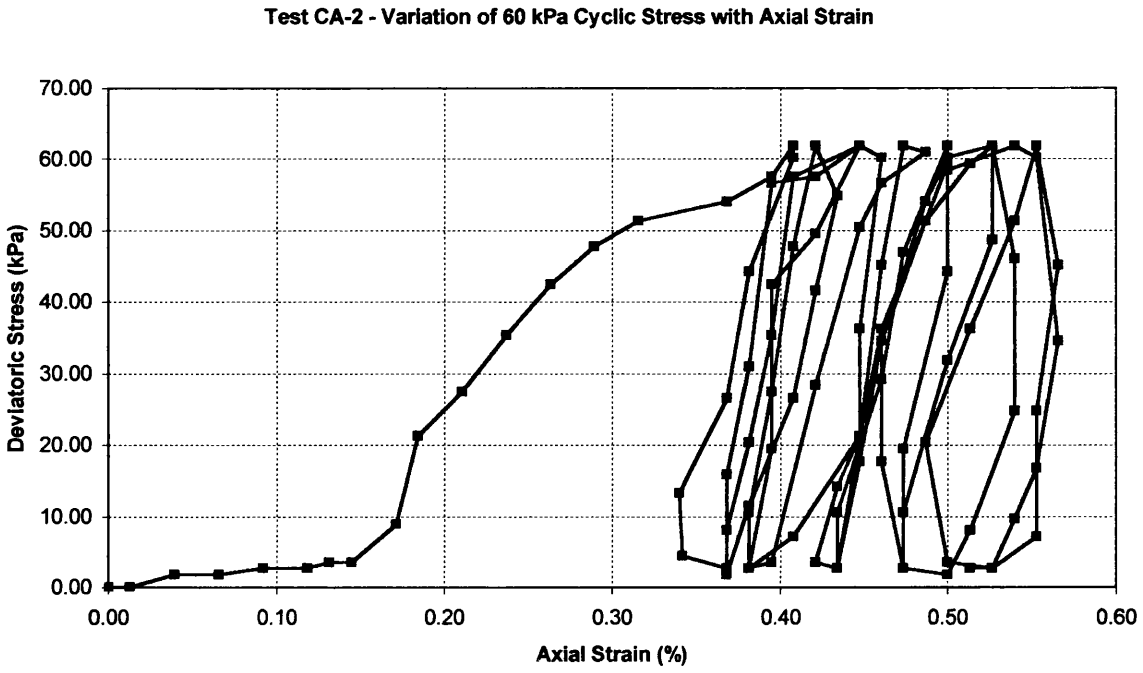

Figure 4.4 *– Variation of Deviatoric Stress with Axial Strain [Test CA-2]*

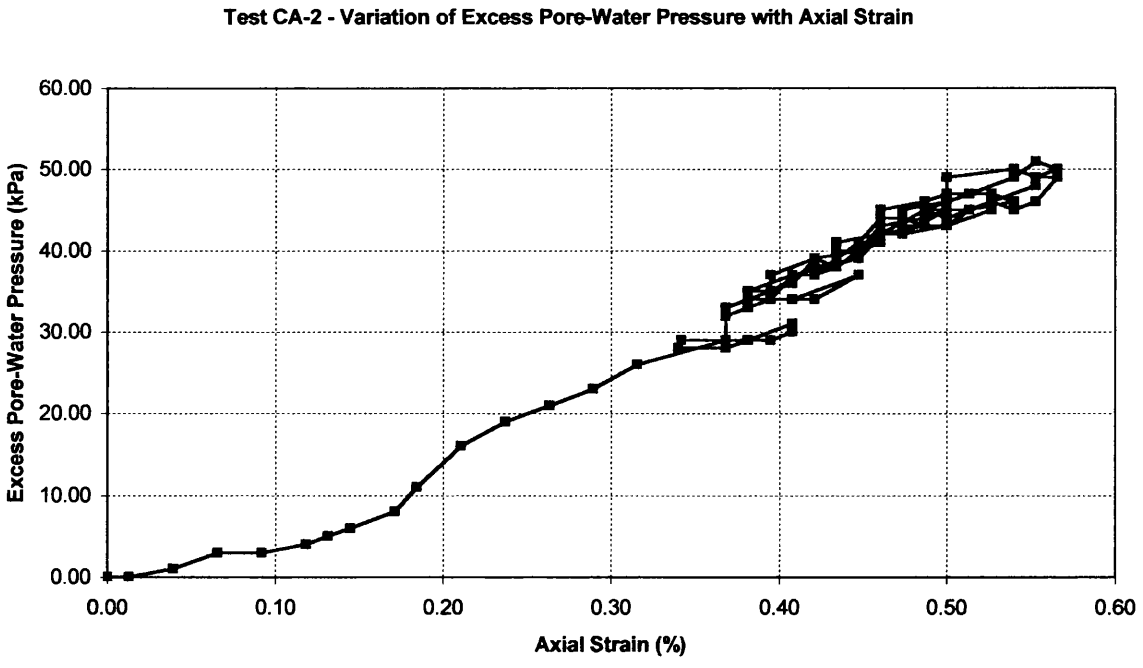

Figure 4.5 *– Variation of Excess Pore-Water with Axial Strain [Test CA-2]*

4.1.3 Test No. CA-3

Quantity	Value
Test Number / Type	CA-3 / Stress-controlled
Backpressure value	300 kPa, applied for 1 hour
B-parameter	0.95
Moisture Content, w	0.3746
Initial Degree of Saturation, S_{r0}	0.9858
Bulk Density, ρ	1786 kg/m^3
Unit Weight, γ	17.521 kN/m^3

Table 4.3 *– Details of Test CA-3 Specimen Parameters*

Notes:

- Max. excess pore-water pressure after 10 cycles = 16 kPa (i.e. $r_{0,10} = 0.16$)
- Axial Strain at the end of 10 cycles = 0.21 %
- Cycles produce axial strains between 0.12 % and 0.28 %
- Test ended after 1660 seconds.

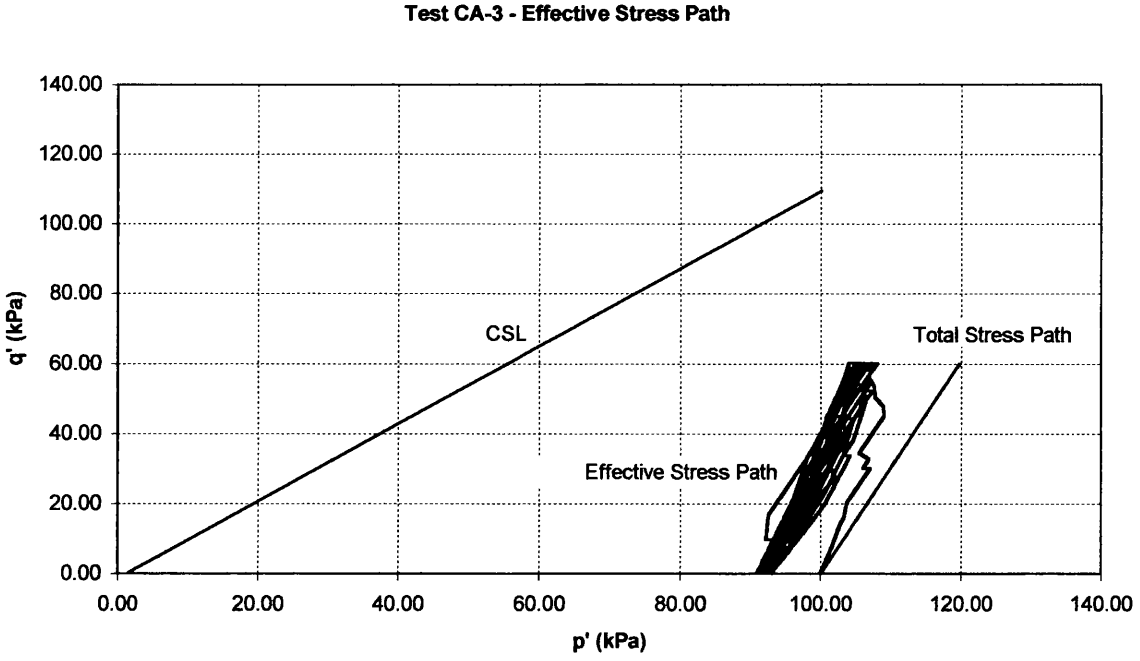

Figure 4.6 *– Effective Stress Path [Test CA-3]*

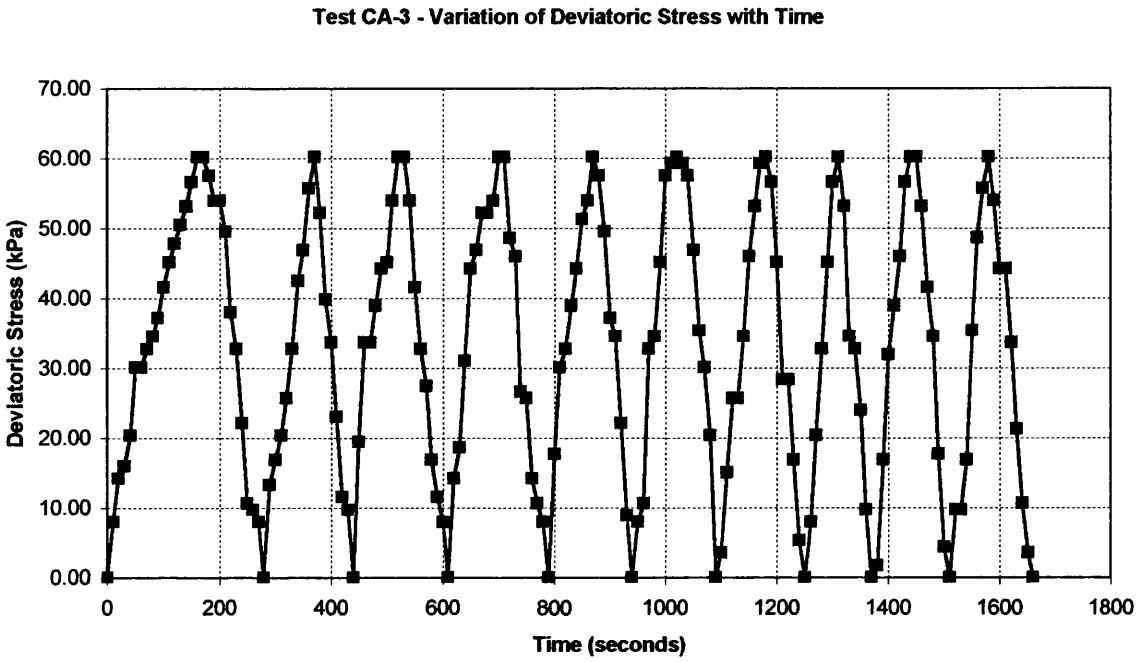

Figure 4.7 – Variation of Deviatoric Stress with Time [Test CA-3]

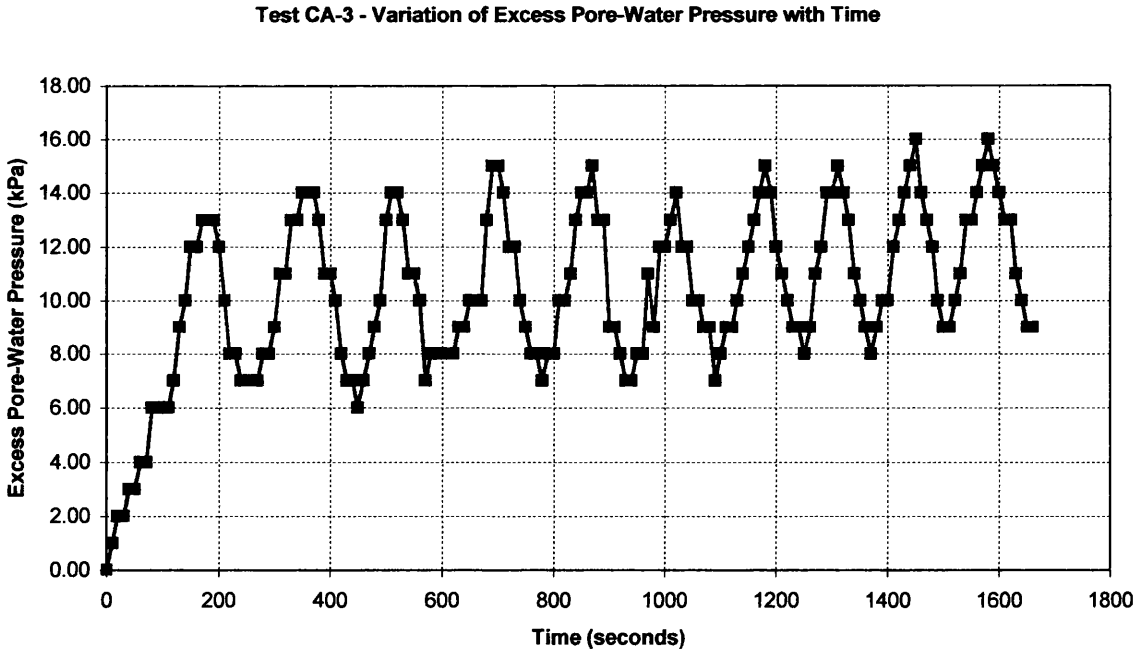

Figure 4.8 – Variation of Excess Pore-Water Pressure with Time [Test CA-3]

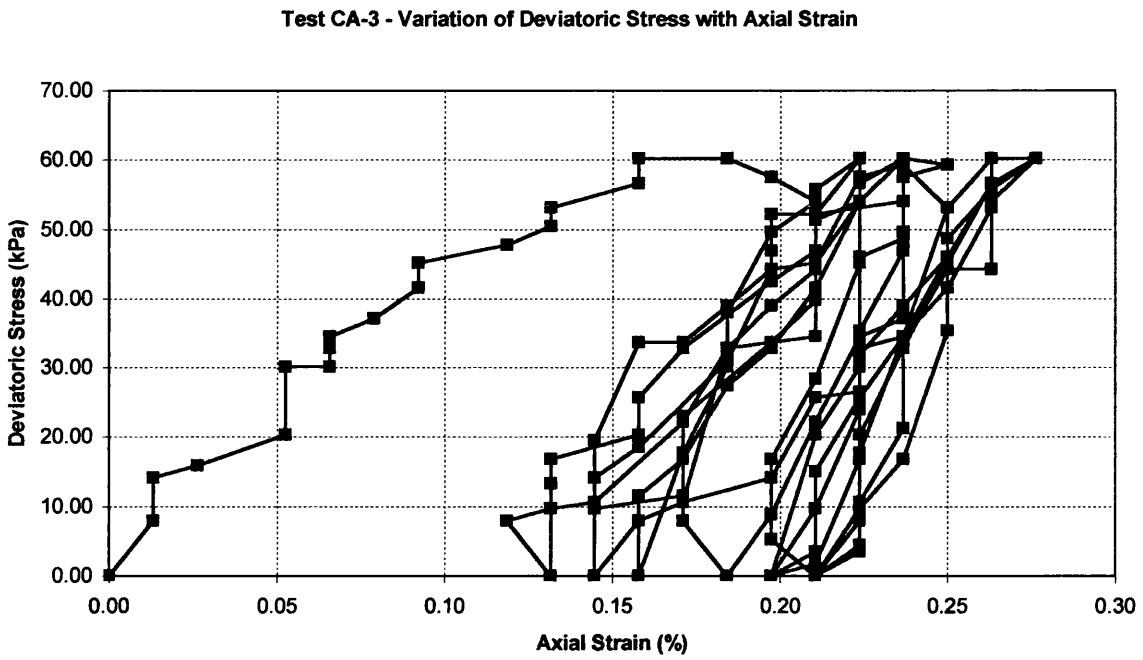

Figure 4.9 *– Variation of Deviatoric Stress with Axial Strain [Test CA-3]*

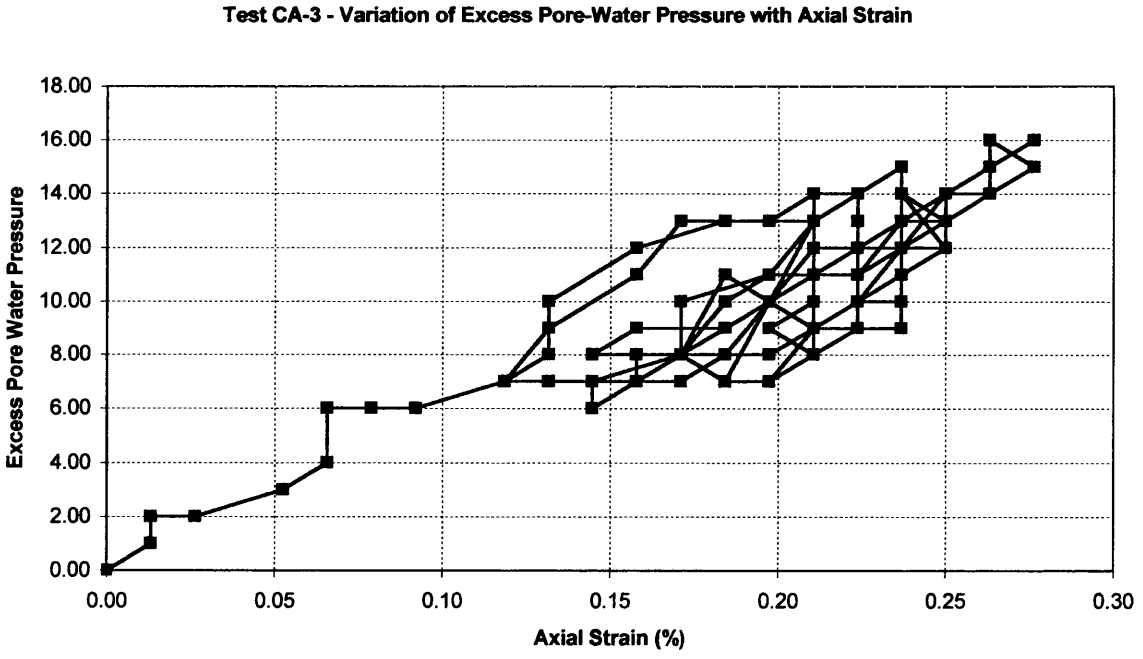

Figure 4.10 *– Variation of Excess Pore-Pressure with Axial Strain [Test CA-3]*

4.1.4 Test No. CA-4

Quantity	Value
Test Number / Type	CA-4 / Stress-controlled
Backpressure value	250 kPa, applied for 1 hour
B-parameter	Some variation between 0.91 and 0.92
Moisture Content, w	0.3671
Initial Degree of Saturation, S_{r0}	0.9661
Bulk Density, ρ	1777 kg/m^3
Unit Weight, γ	17.432 kN/m^3

Table 4.4 *– Details of Test CA-4 Specimen Parameters*

Notes:

- Max. excess pore-water pressure after 10 cycles = 16 kPa (i.e. $r_{0,10} = 0.16$)
- Axial Strain at the end of 10 cycles = 0.24 %
- Cycles produce axial strains between 0.13 % and 0.32 %
- Test ended after 2000 seconds.

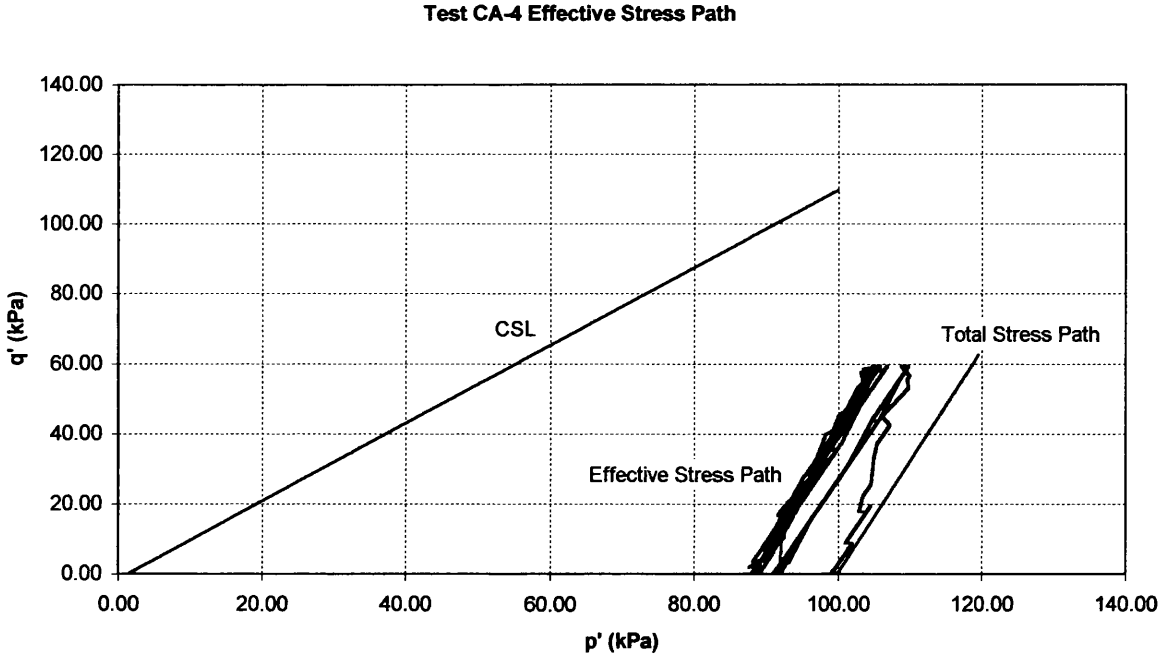

Figure 4.11 *– Effective Stress Path [Test CA-4]*

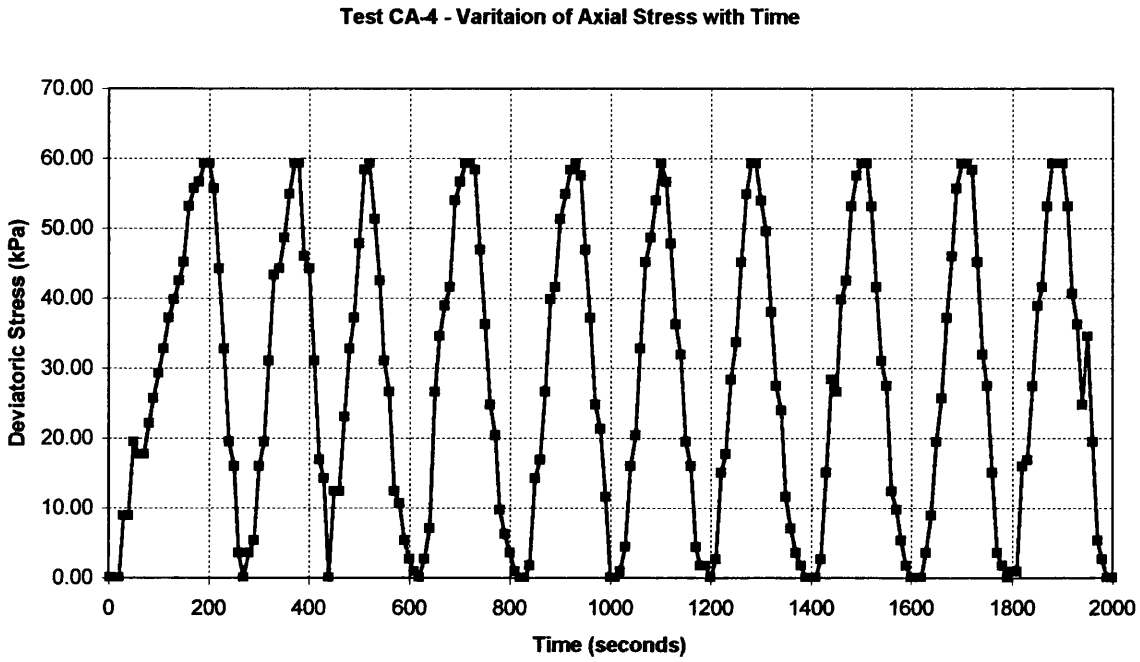

Figure 4.12 *– Variation of Deviatoric Stress with Time [Test CA-4]*

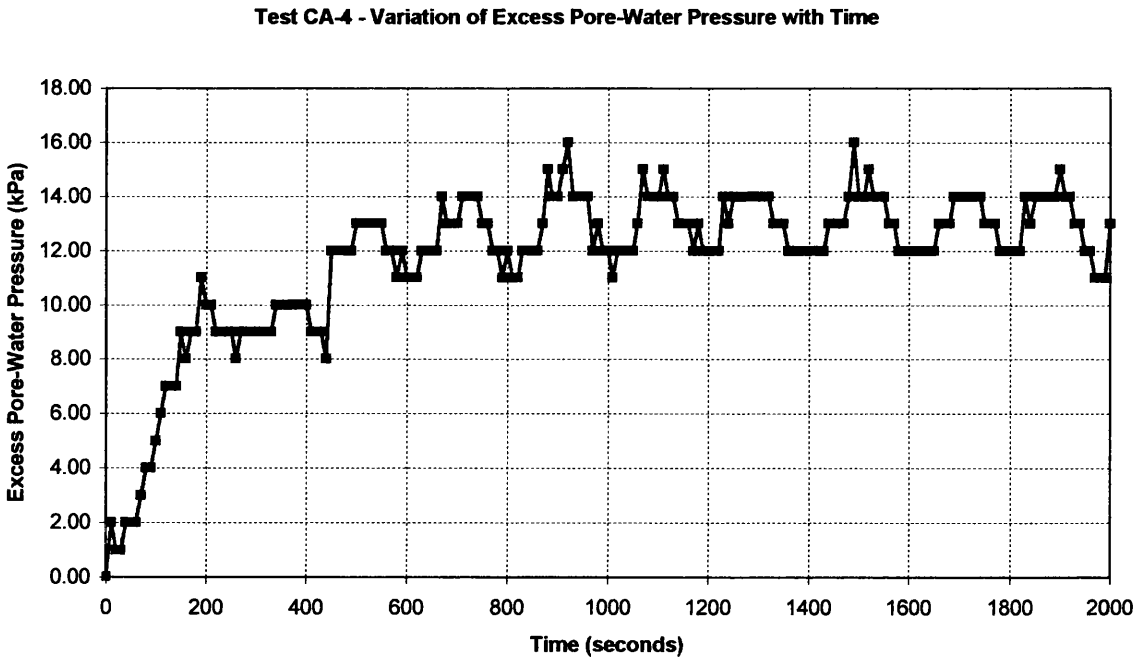

Figure 4.13 *– Variation of Excess Pore-Water Pressure with Time [Test CA-4]*

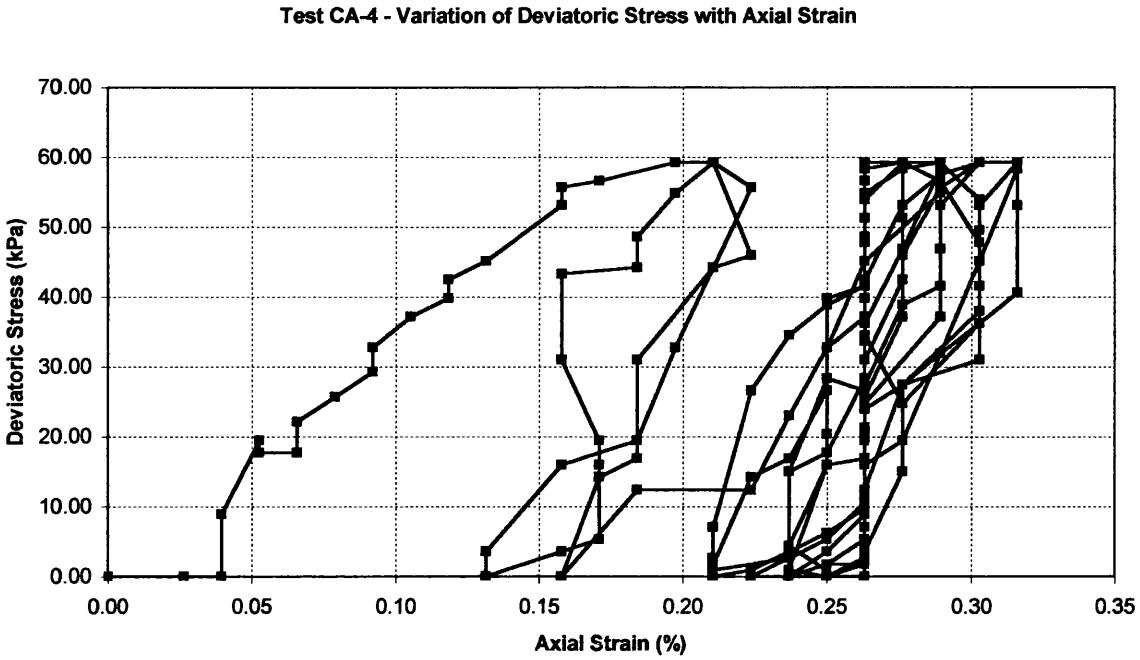

Figure 4.14 *– Variation of Deviatoric Stress with Axial Strain [Test CA-4]*

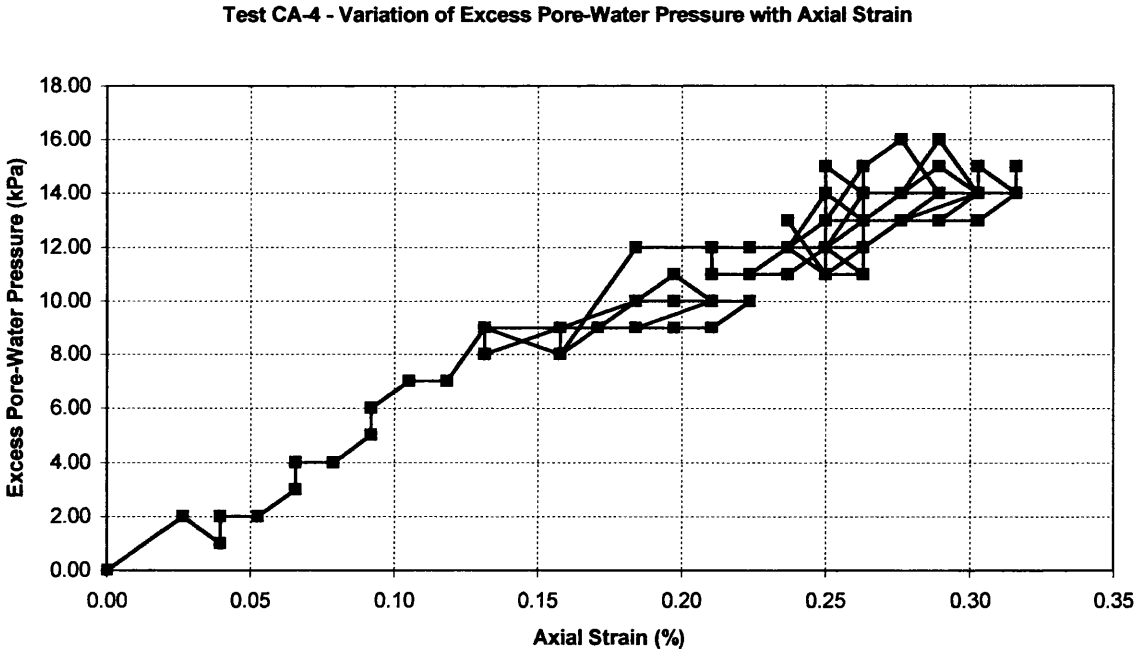

Figure 4.15 *– Variation of Excess Pore-Water Pressure with Axial Strain [Test CA-4]*

4.1.5 Test No. CA-5

Quantity	Value
Test Number / Type	CA-5 / Stress-controlled
Backpressure value	200 kPa, applied for 1 hour
B-parameter	0.89
Moisture Content, w	0.3626
Initial Degree of Saturation, S_{r0}	0.9542
Bulk Density, ρ	1773 kg/m^3
Unit Weight, γ	17.393 kN/m^3

***Table 4.5** – Details of Test CA-5 Specimen Parameters*

Notes:

- Max. excess pore-water pressure after 10 cycles = 11 kPa (i.e. $r_{0,10} = 0.11$)
- Axial Strain at the end of 10 cycles = 0.24 %
- Cycles produce axial strains between 0.14 % and 0.32 %
- Test ended after 1910 seconds.

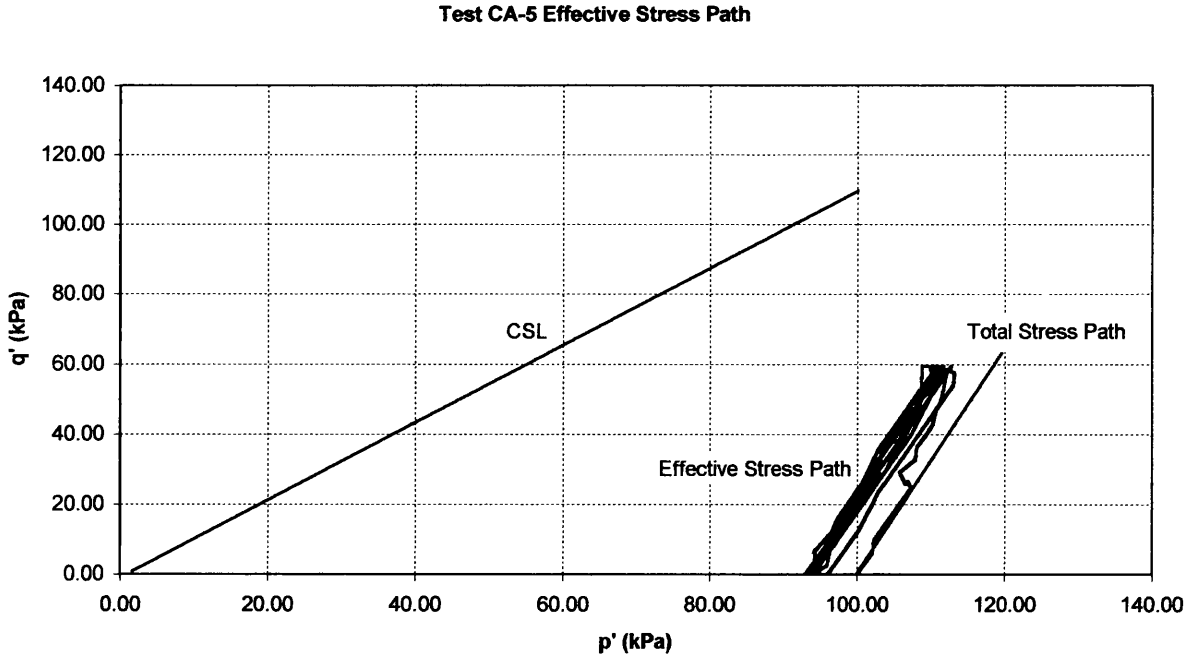

***Figure 4.16** – Effective Stress Path [Test CA-5]*

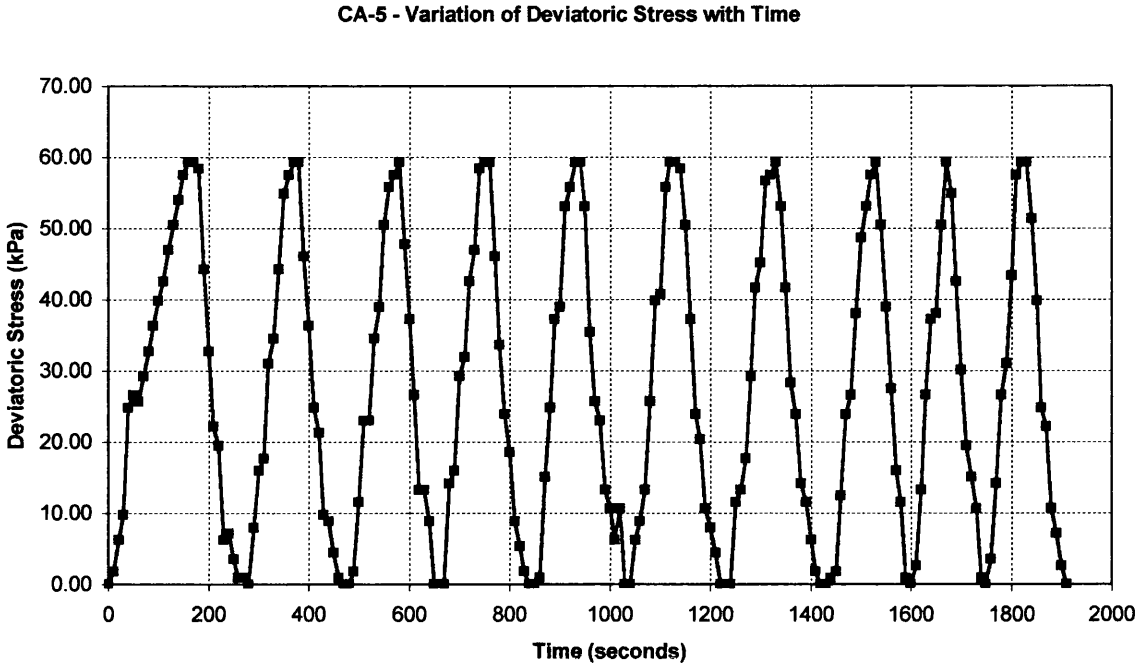

Figure 4.17 – Variation of Deviatoric Stress with Time [Test CA-5]

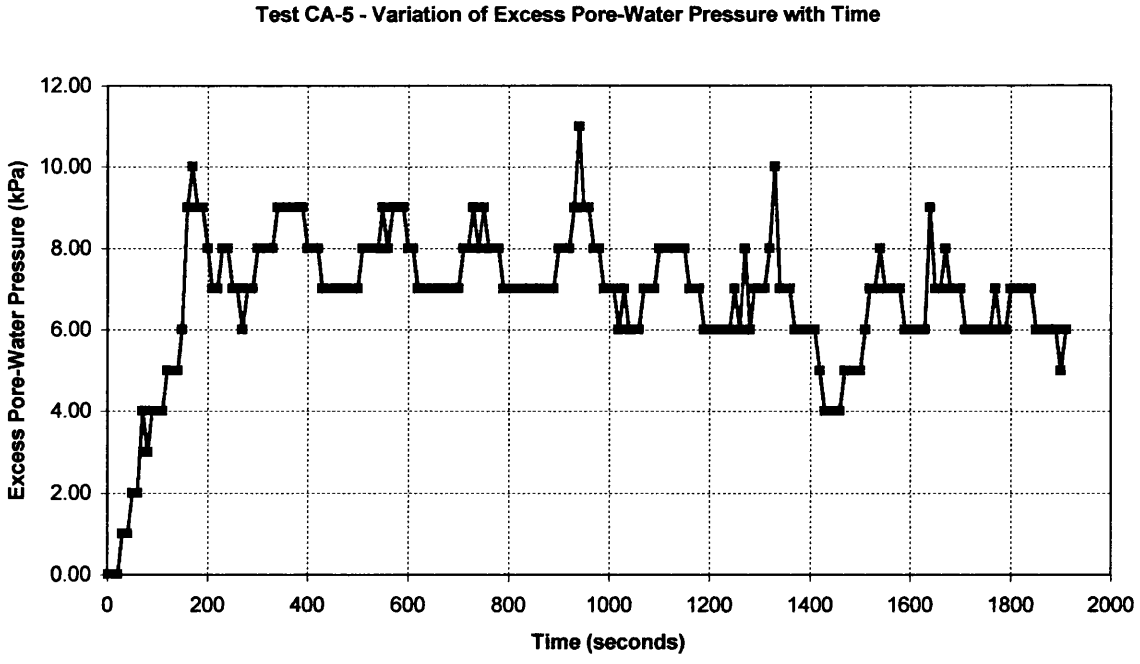

Figure 4.18 – Variation of Excess Pore-Water Pressure with Time [Test CA-5]

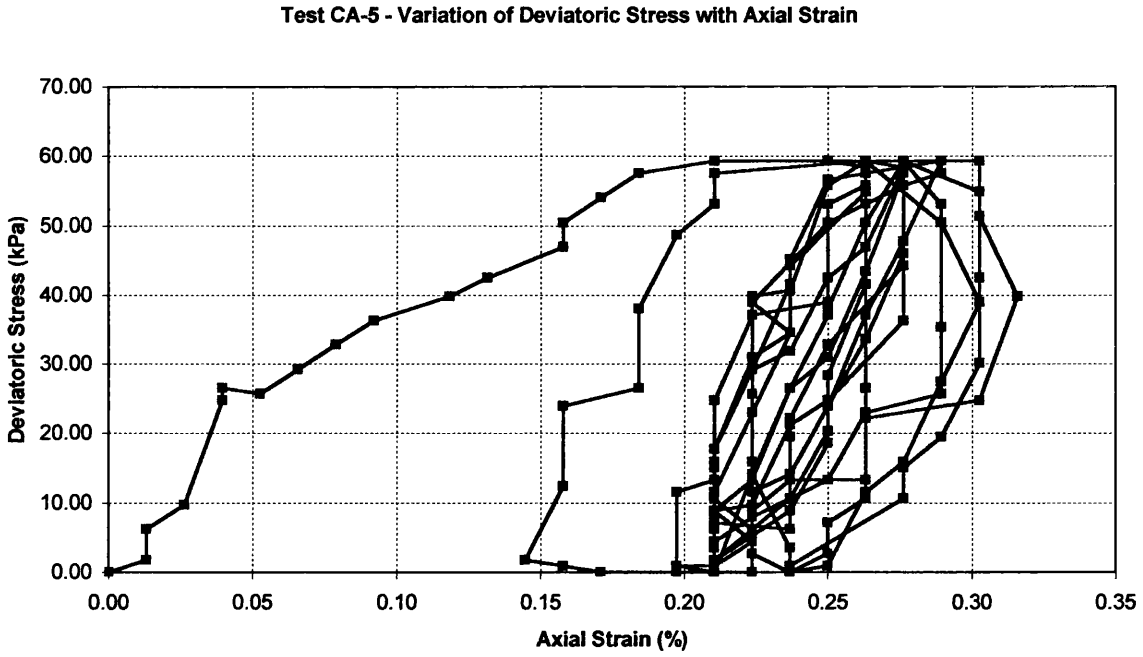

Figure 4.19 *– Variation of Deviatoric Stress with Axial Strain [Test CA-5]*

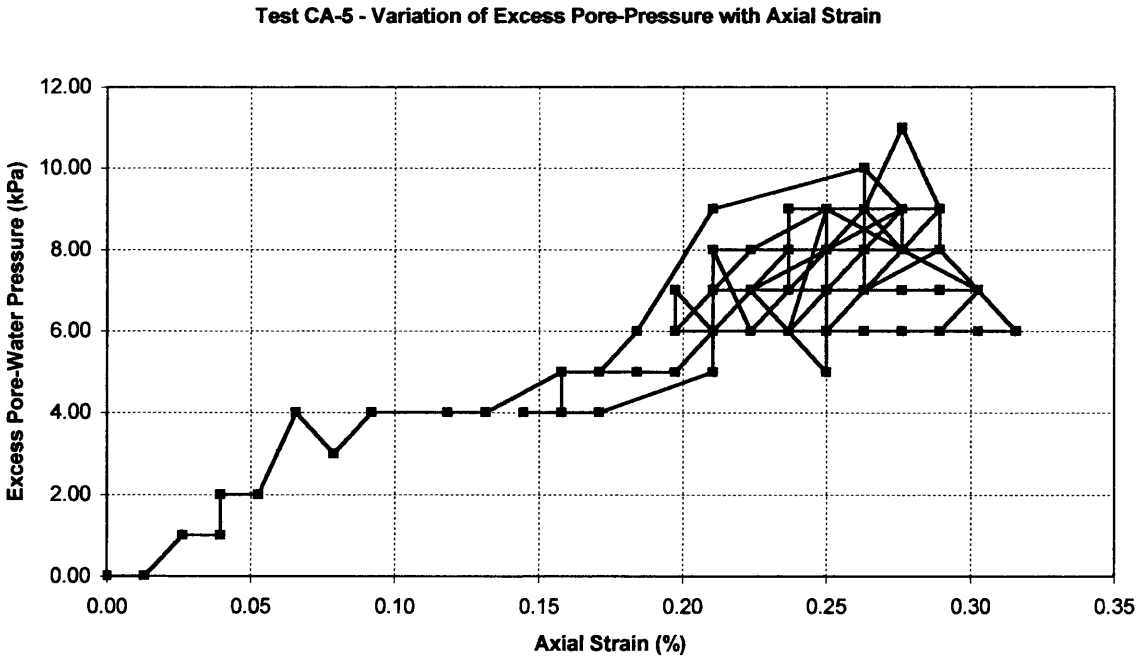

Figure 4.20 *– Variation of Excess Pore-Water Pressure with Axial Strain [Test CA-5]*

4.1.6 Test No. CA-6

Quantity	Value
Test Number / Type	CA-6 / Stress-controlled
Backpressure value	150 kPa, applied for 1 hour
B-parameter	0.85
Moisture Content, w	0.3581
Initial Degree of Saturation, S_{r0}	0.9424
Bulk Density, ρ	1765 kg/m^3
Unit Weight, γ	17.315 kN/m^3

Table 4.6 *– Details of Test CA-6 Specimen Parameters*

Notes:

- Max. excess pore-water pressure after 10 cycles = 6 kPa (i.e. $r_{0,10} = 0.06$)
- Axial Strain at the end of 10 cycles = 0.14 %
- Cycles produce axial strains between 0.08 % and 0.21 %
- Test ended after 1740 seconds.

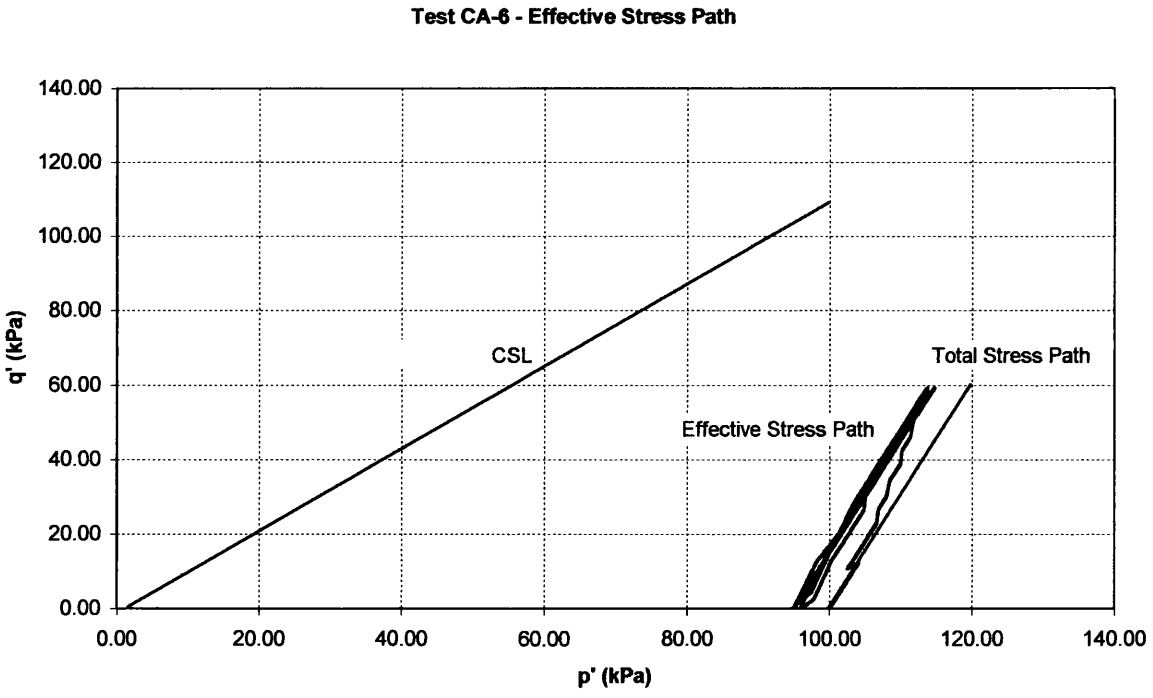

Figure 4.21 *– Effective Stress Path [Test CA-6]*

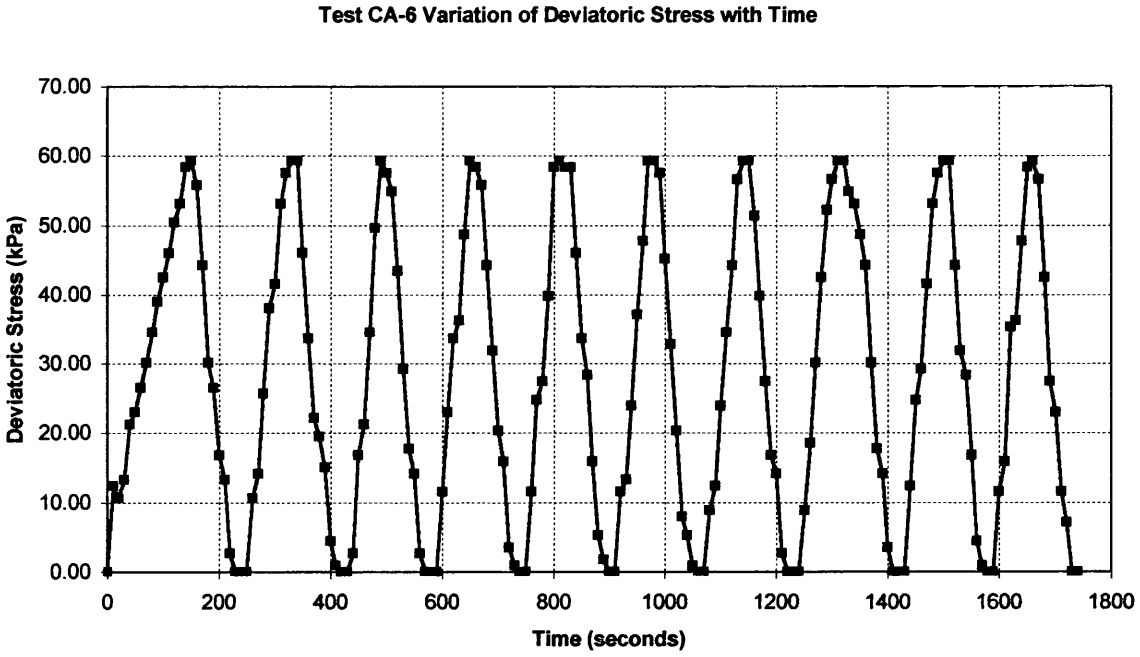

Figure 4.22 – Variation of Deviatoric Stress with Time [Test CA-6]

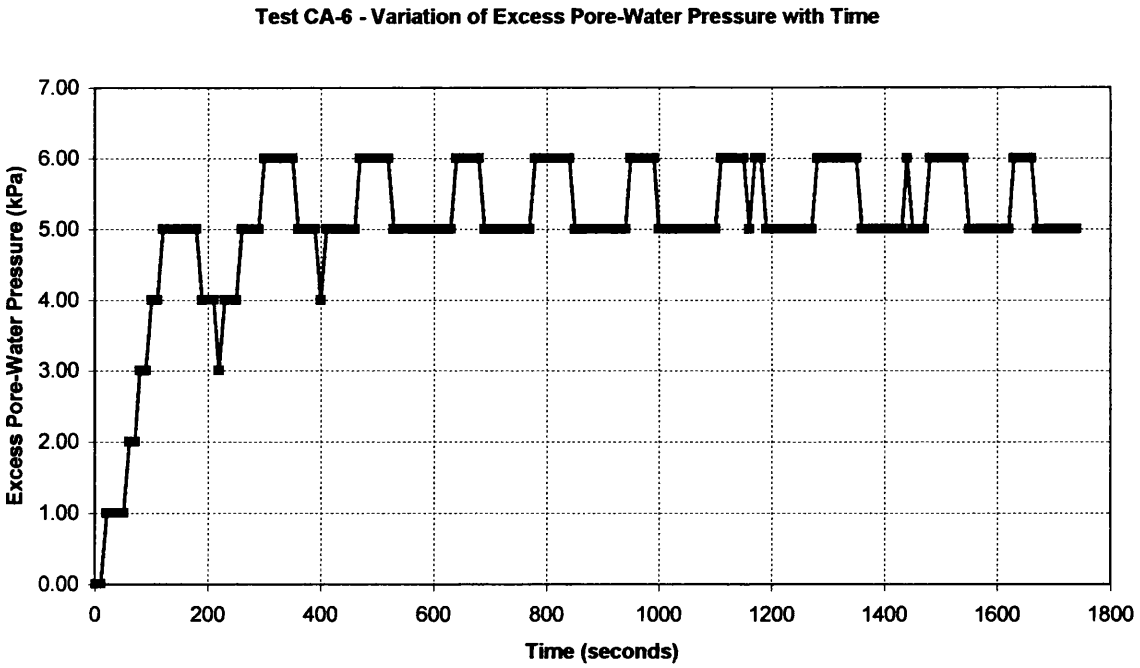

Figure 4.23 – Variation of Excess Pore-Water Pressure with Time [Test CA-6]

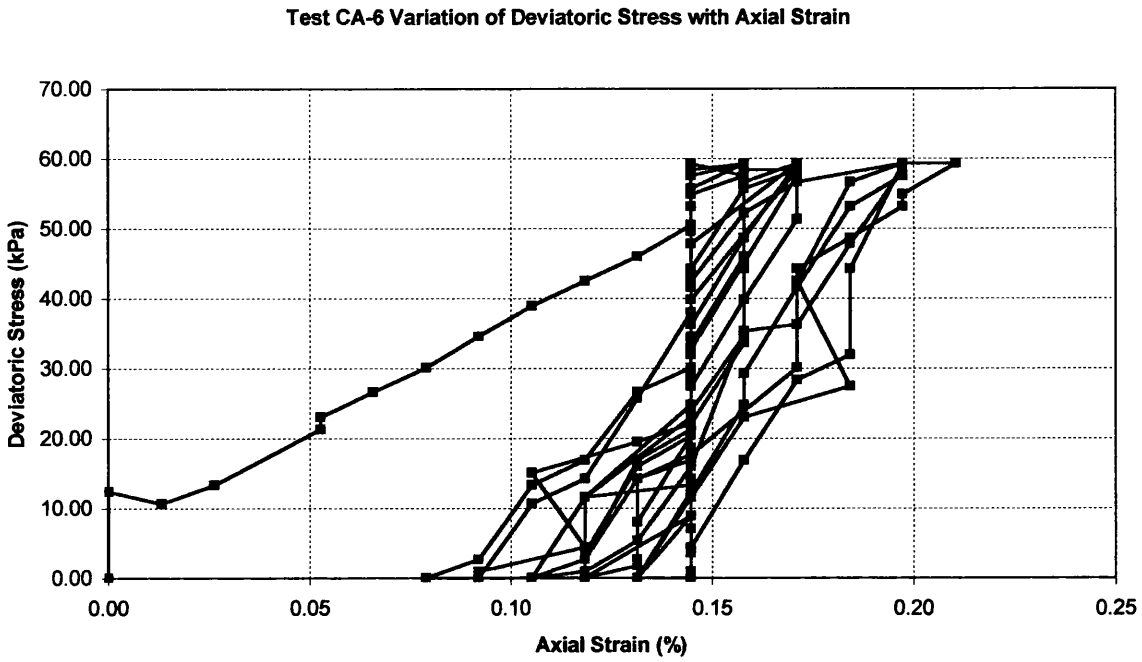

Figure 4.24 *– Variation of Deviatoric Stress with Axial Strain [Test CA-6]*

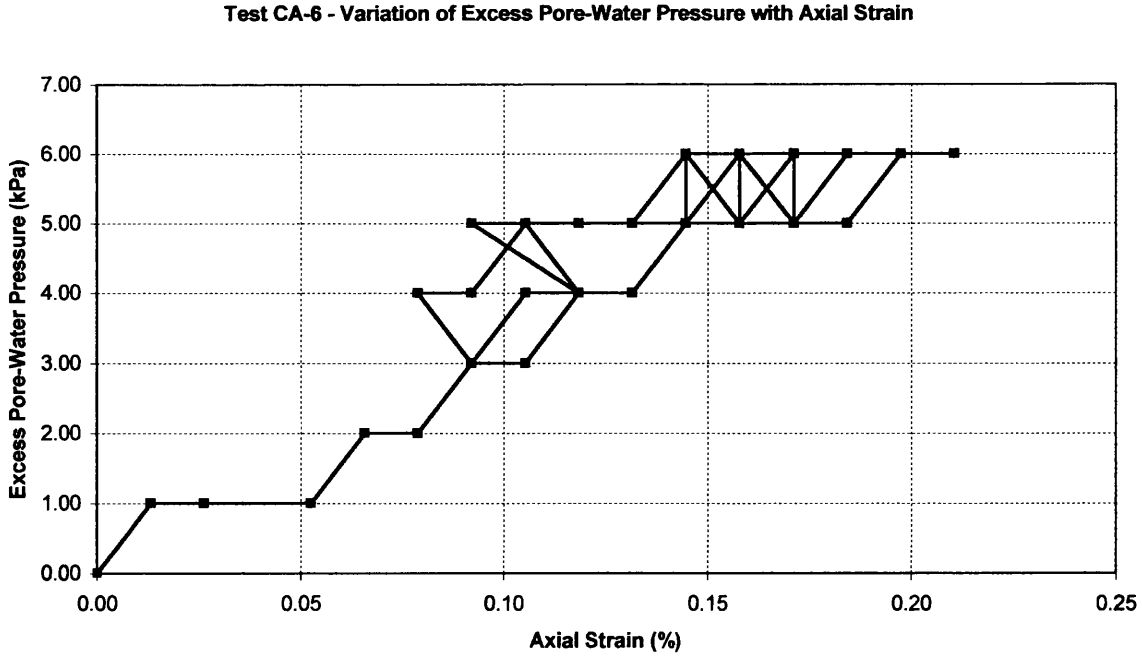

Figure 4.25 *– Variation of Excess Pore-Water Pressure with Axial Strain [Test CA-6]*

4.1.7 Test No. CA-7

Quantity	Value
Test Number / Type	CA-7 / Stress-controlled
Backpressure value	100 kPa, applied for 1 hour
B-parameter	0.79
Moisture Content, w	0.3559
Initial Degree of Saturation, S_{r0}	0.9366
Bulk Density, ρ	1756 kg/m^3
Unit Weight, γ	17.226 kN/m^3

***Table 4.7** – Details of Test CA-7 Specimen Parameters*

Notes:

- Max. excess pore-water pressure after 10 cycles = 9 kPa (i.e. $r_{0,10} = 0.09$)
- Axial Strain at the end of 10 cycles = 0.22 %
- Cycles produce axial strains between 0.17 % and 0.34 %
- Test ended after 2130 seconds.

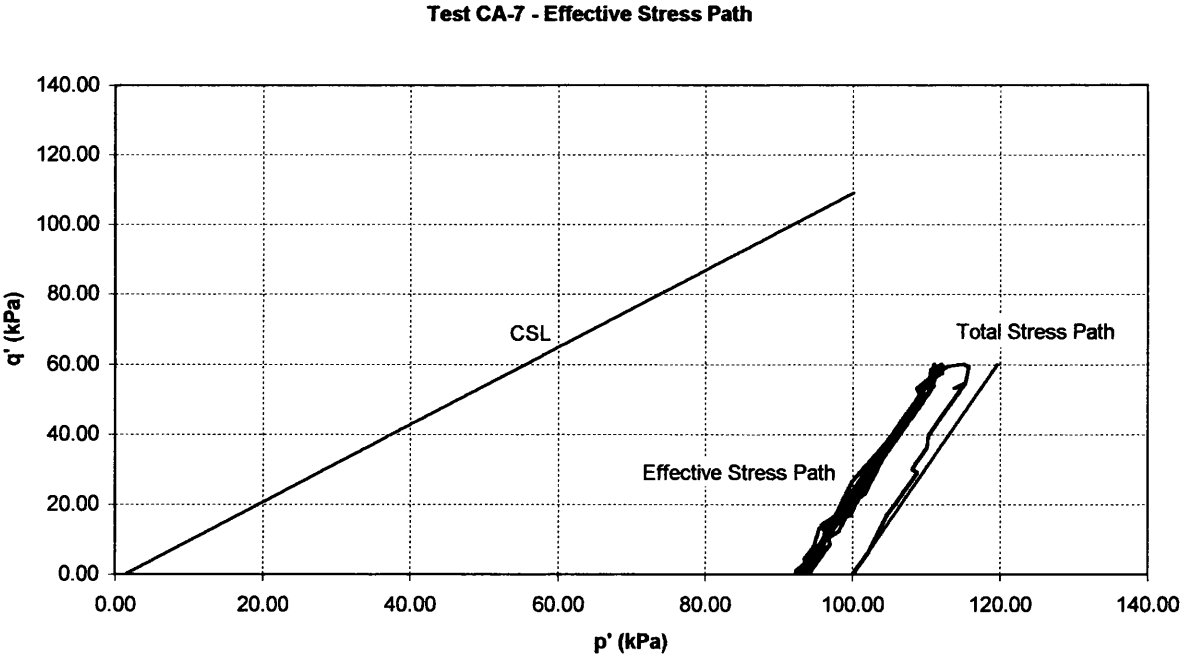

***Figure 4.26** – Effective Stress Path [Test CA-7]*

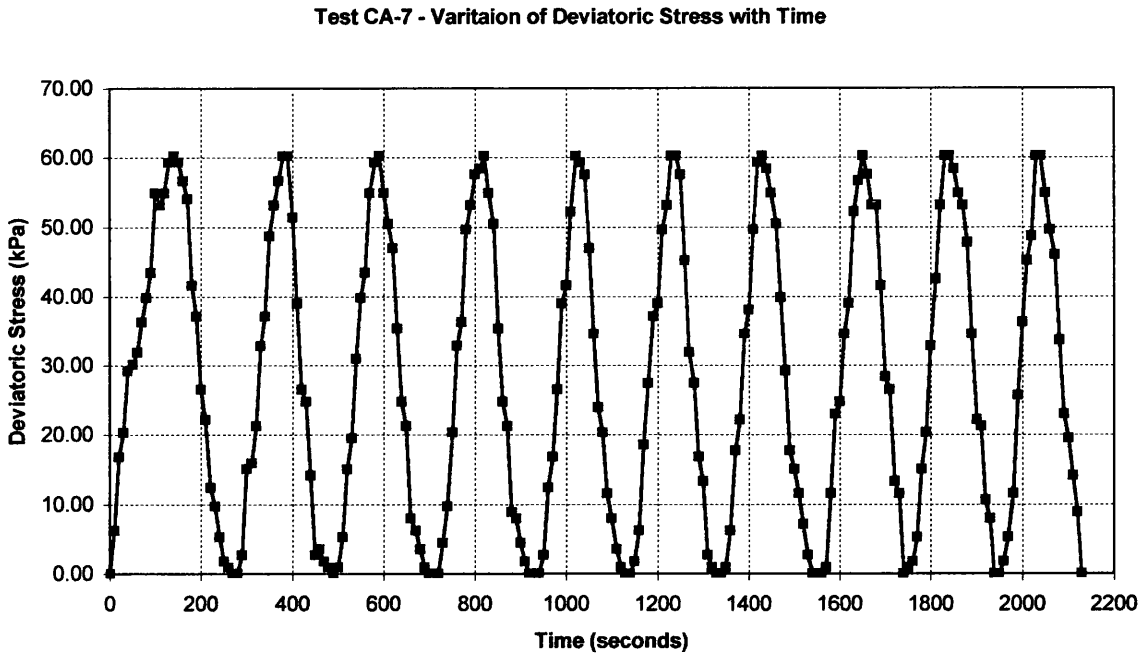

Figure 4.27 *– Variation of Deviatoric Stress with Time [Test CA-7]*

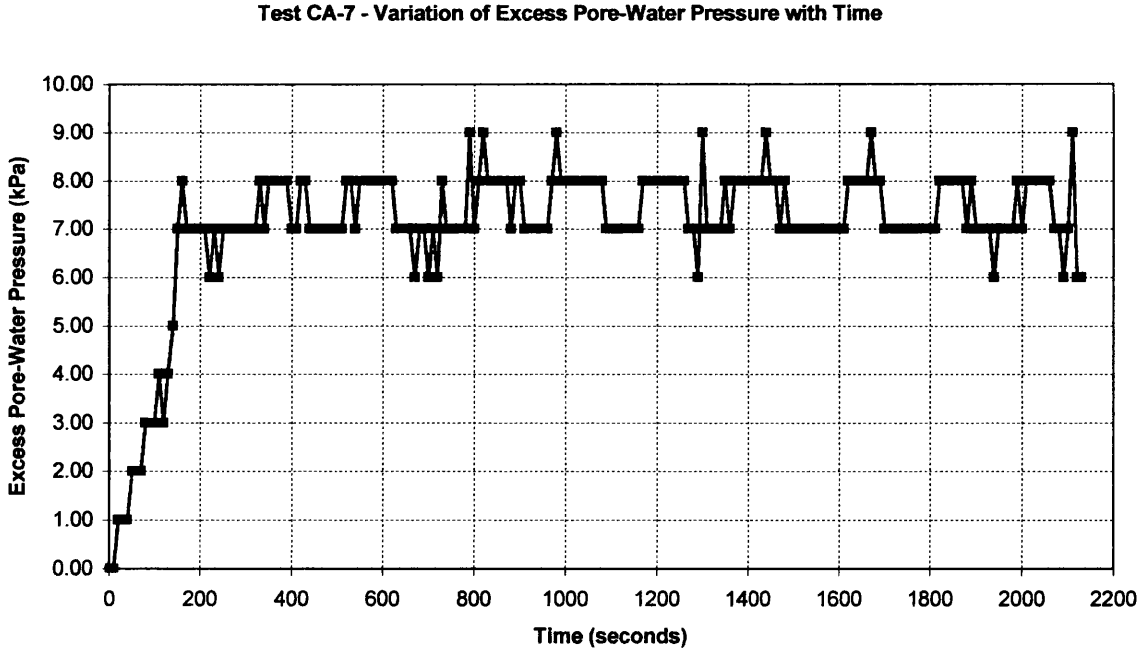

Figure 4.28 *– Variation of Excess Pore-Water Pressure with Time [Test CA-7]*

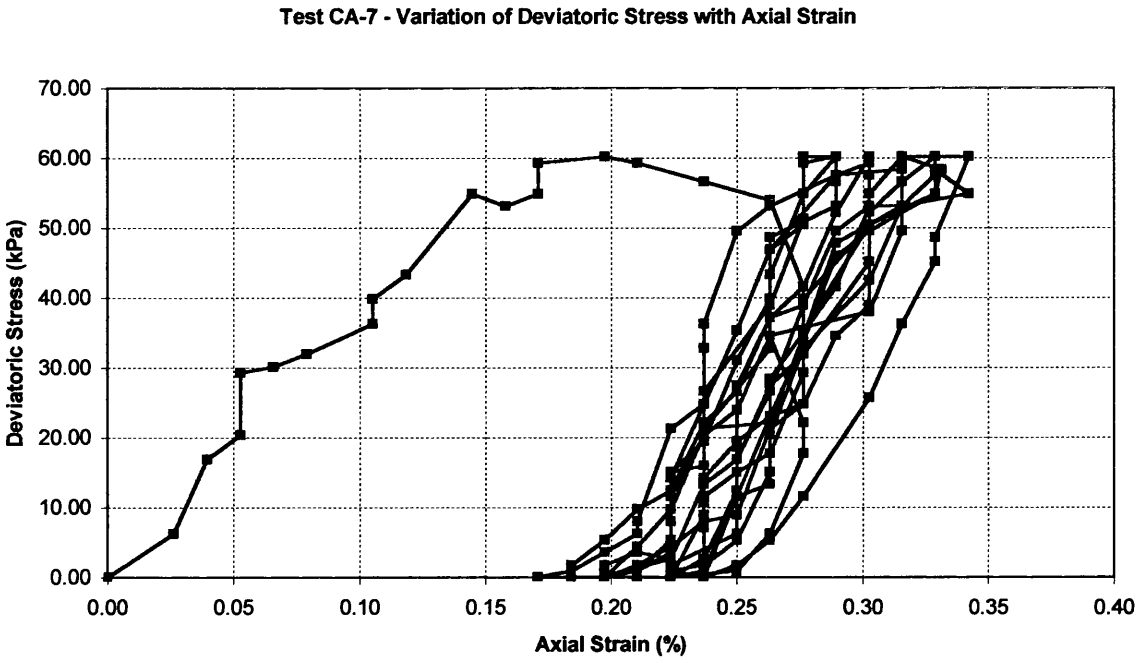

Figure 4.29 *– Variation of Deviatoric Stress with Axial Strain [Test CA-7]*

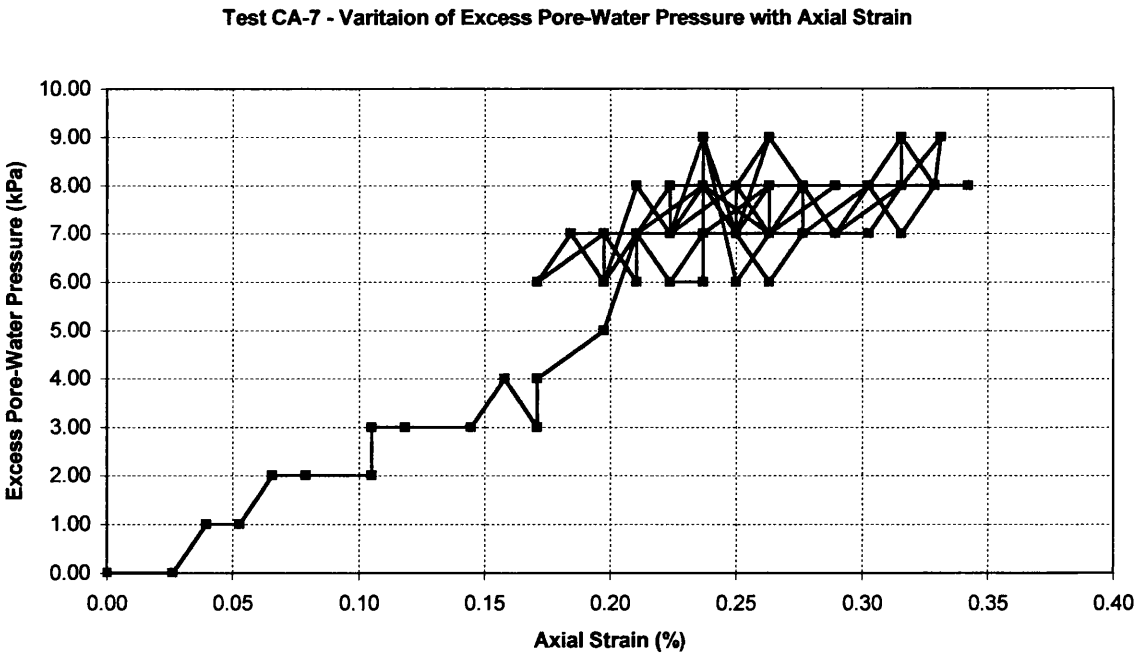

Figure 4.30 *– Variation of Excess Pore-Water Pressure with Axial Strain [Test CA-7]*

4.1.8 Test No. CA-8

Quantity	Value
Test Number / Type	CA-8 / Stress-controlled
Backpressure value	50 kPa, applied for 1 hour
B-parameter	0.73
Moisture Content, w	0.3503
Initial Degree of Saturation, S_{r0}	0.9218
Bulk Density, ρ	1755 kg/m^3
Unit Weight, γ	17.217 kN/m^3

Table 4.8 *– Details of Test CA-8 Specimen Parameters*

Notes:

- Max. excess pore-water pressure after 10 cycles = 5 kPa (i.e. $r_{0,10} = 0.05$)
- Axial Strain at the end of 10 cycles = 0.16 %
- Cycles produce axial strains between 0.12 % and 0.23 %
- Test ended after 1670 seconds

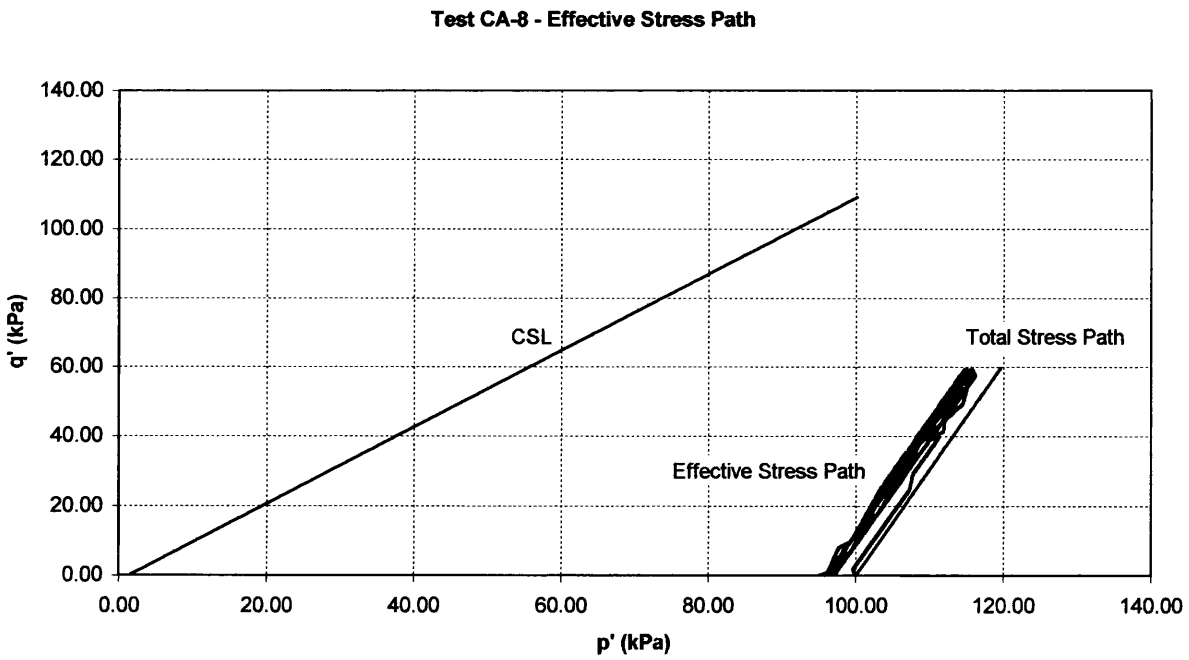

Figure 4.31 *– Effective Stress Path [Test CA-8]*

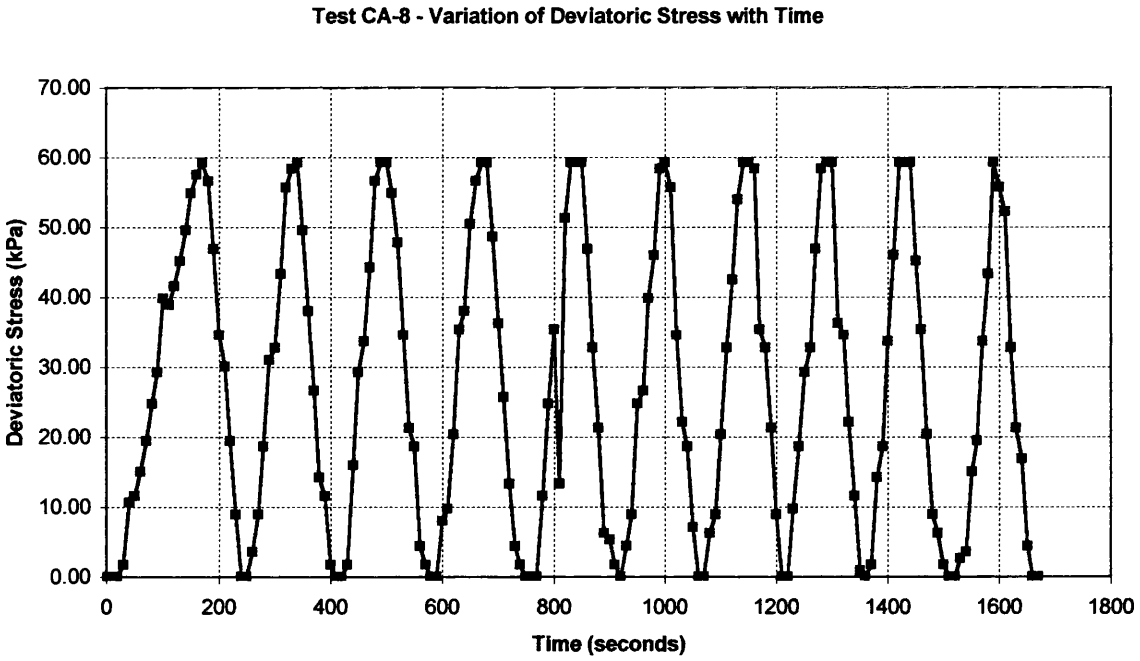

Figure 4.32 *– Variation of Deviatoric Stress with Time [Test CA-8]*

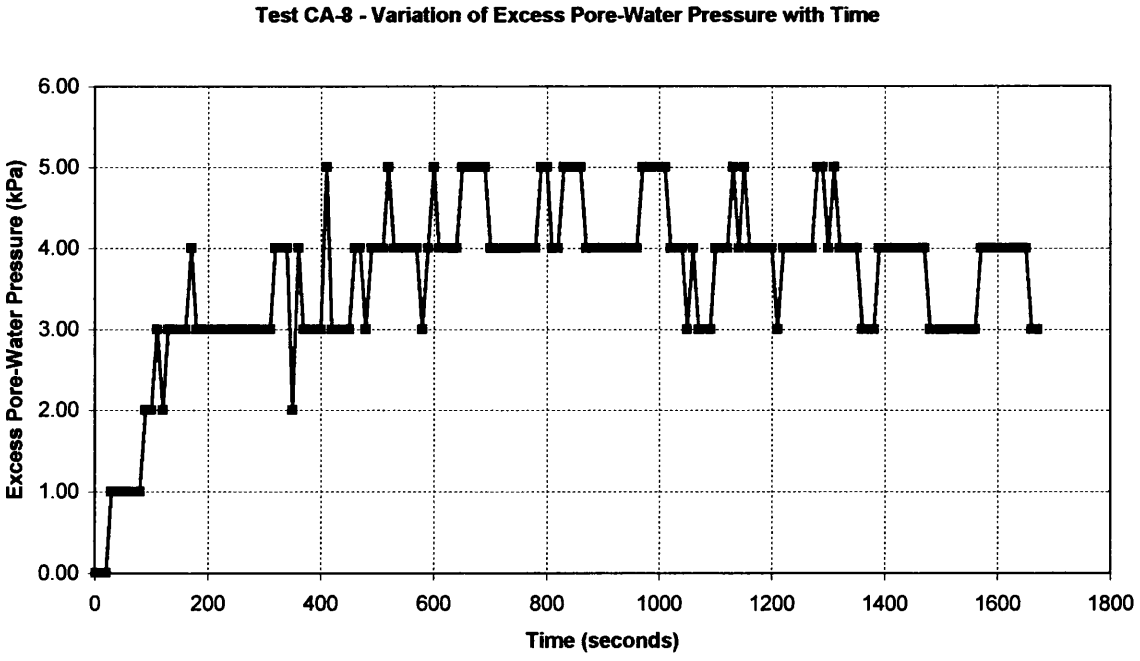

Figure 4.33 *– Variation of Excess Pore-Water Pressure with Time [Test CA-8]*

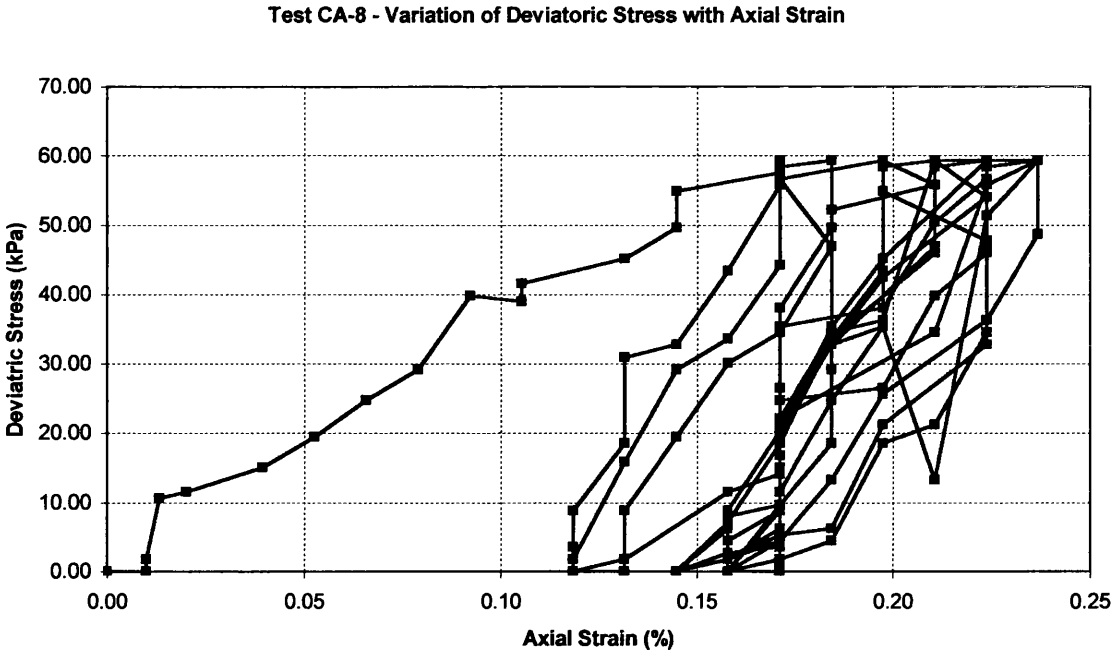

Figure 4.34 – Variation of Deviatoric Stress with Axial Strain [Test CA-8]

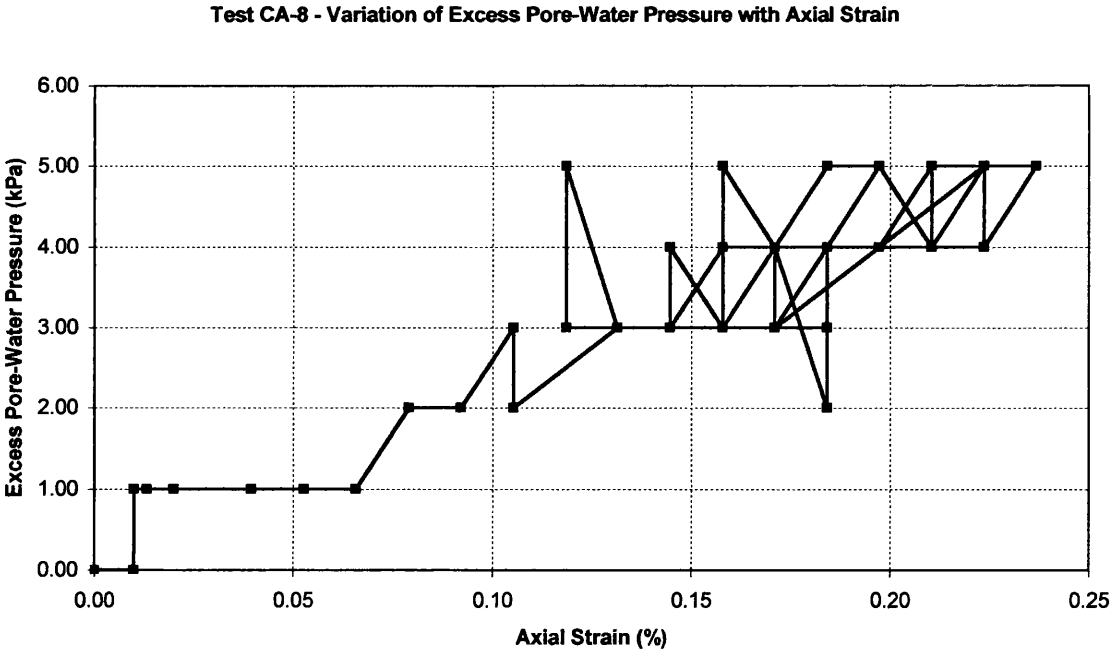

Figure 4.35 – Variation of Excess Pore-Water Pressure with Axial Strain [Test CA-8]

4.1.9 Test No. CA-9

Quantity	Value
Test Number / Type	CA-9 / Stress-controlled
Backpressure value	0 kPa
B-parameter	Some variation between 0.60 and 0.61
Moisture Content, w	0.3468
Initial Degree of Saturation, S_{r0}	0.9126
Bulk Density, ρ	1750 kg/m^3
Unit Weight, γ	17.166 kN/m^3

Table 4.9 *– Details of Test CA-9 Specimen Parameters*

Notes:

- Max. excess pore-water pressure after 10 cycles = 5 kPa (i.e. $r_{0,10} = 0.05$)
- Axial Strain at the end of 10 cycles = 0.16 %
- Cycles produce axial strains between 0.08 % and 0.22 %
- Test ended after 1640 seconds

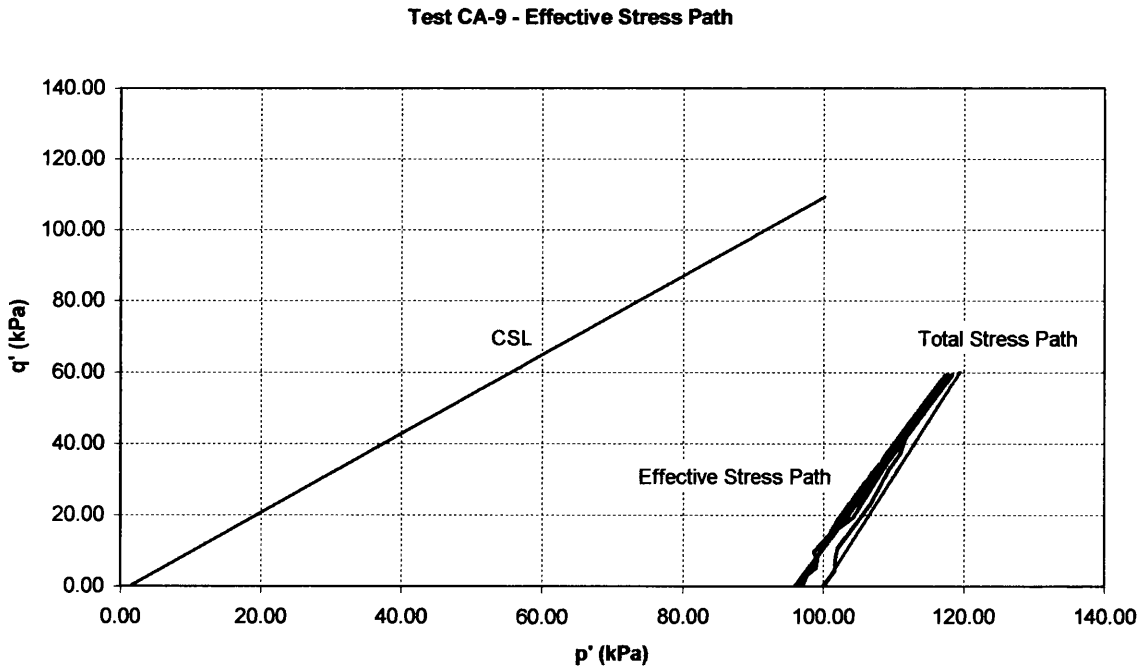

Figure 4.36 *– Effective Stress Path [Test CA-9]*

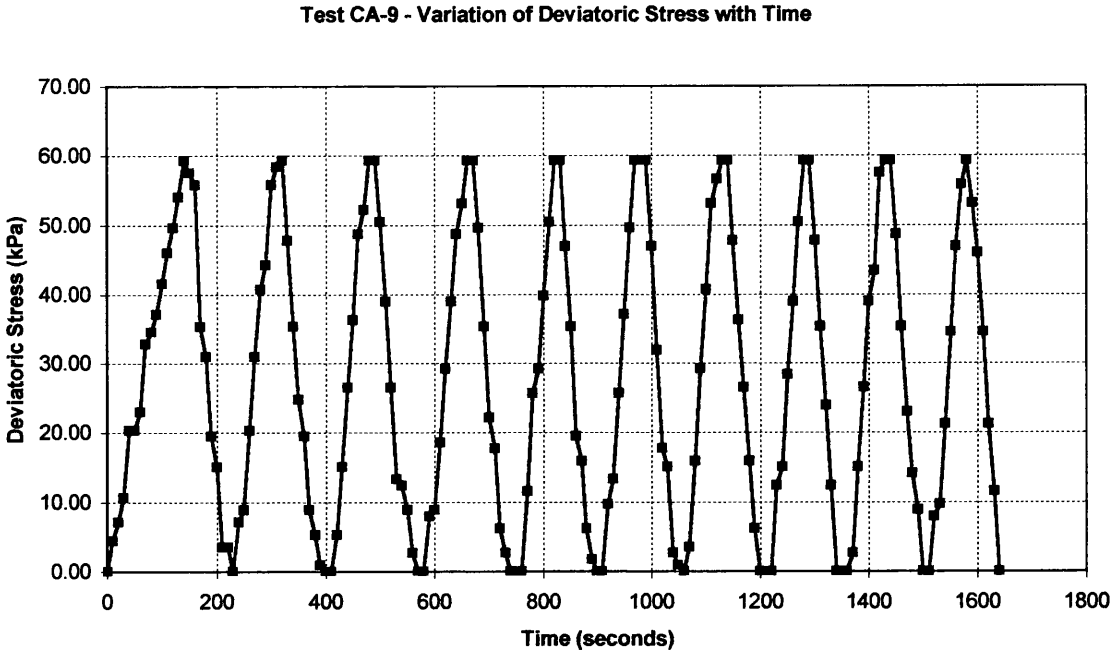

Figure 4.37 – Variation of Deviatoric Stress with Time [Test CA-9]

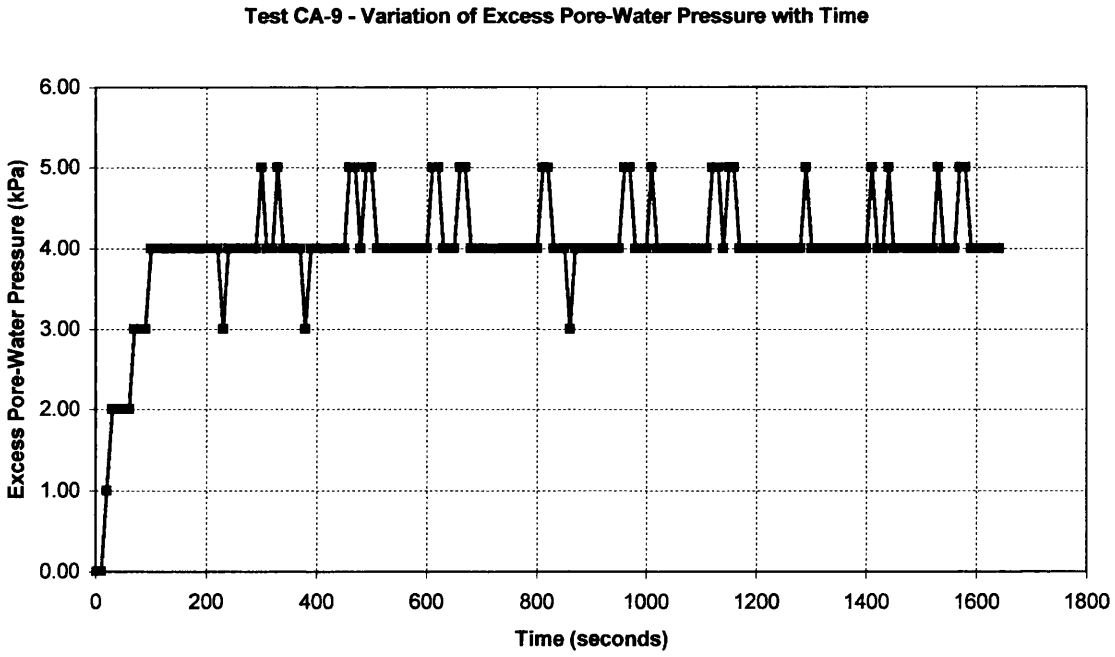

Figure 4.38 – Variation of Excess Pore-Water Pressure with Time [Test CA-9]

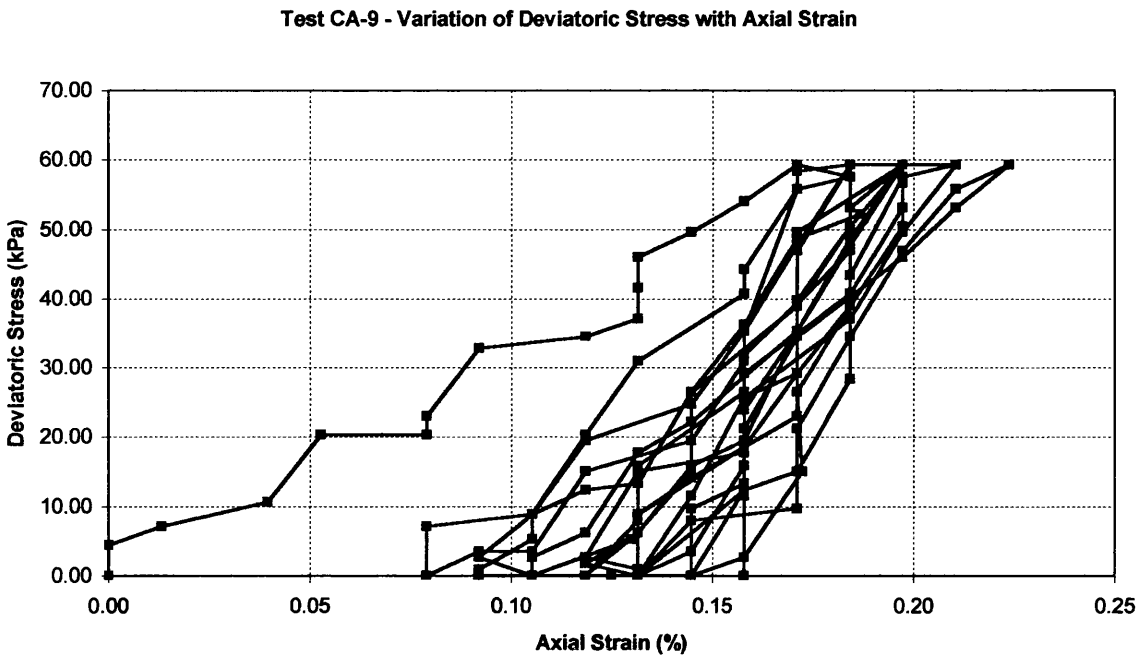

Figure 4.39 – Variation of Deviatoric Stress with Axial Strain [Test CA-9]

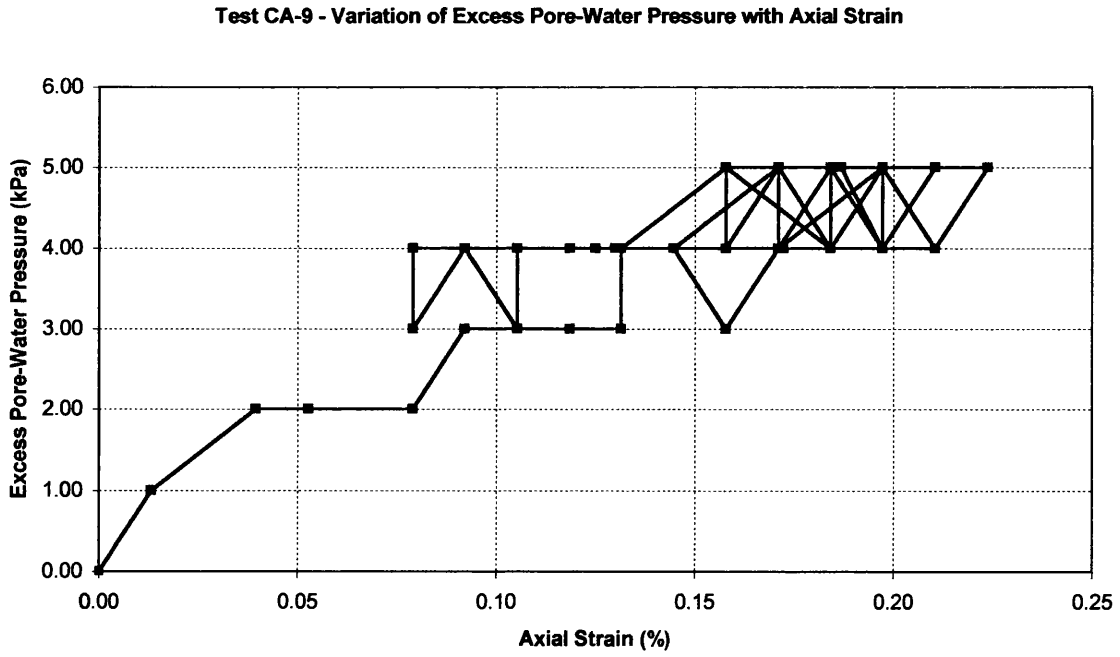

Figure 4.40 – Variation of Excess Pore-Water Pressure with Axial Strain [Test CA-9]

4.2 TRIAXIAL TESTS EMPLOYING CYCLES OF 80 kPa

4.2.1 Introduction

This Section reports the results from cyclic triaxial tests (80 kPa cycles) conducted on loose Hostun sand. The experimental procedure has been discussed previously in Chapter 3, and will not be repeated here. The manner in which the results are reported is outlined in Section 4.1, immediately prior to the results of the 60 kPa-cycle tests being presented.

Eight tests were conducted using 80 kPa cycles. The test conditions are tabulated below. Note that Test CB-5 was aborted due to temporary mechanical failure of pressure regulator *PR1* (reference Figure 3.18). Test CB-1 was used as a 'dummy' run for the main test programme.

Test No.	Backpressure (kPa) / duration (min.)	Cycles
CB-2	350 kPa / 60 minutes	10
CB-3	300 kPa / 60 minutes	10
CB-4	250 kPa / 60 minutes	10
CB-6	200 kPa / 60 minutes	10
CB-7	150 kPa / 60 minutes	10
CB-8	100 kPa / 60 minutes	10
CB-9	50 kPa / 60 minutes	10
CB-10	0 kPa / 0 minutes	10

***Table 4.10** – Details of Test Programme for 80 kPa Cycles*

In order to maintain continuity and facilitate the understanding of the principles presented, the results in this Section are reported in an identical manner to those in Section 4.1.

4.2.2 Test No. CB-2

Quantity	Value
Test Number / Type	CB-2 / Stress-controlled
Backpressure value	350 kPa, applied for 1 hour
B-parameter	Some variation between 0.99 and 1.00
Moisture Content, w	0.3782
Initial Degree of Saturation, S_{r0}	0.9953
Bulk Density, ρ	1791 kg/m^3
Unit Weight, γ	17.570 kN/m^3

Table 4.11 *– Details of Test CB-2 Specimen Parameters*

Notes:

- Max. excess pore-water pressure after 10 cycles = 58 kPa (i.e. $r_{0,10} = 0.58$)
- Axial strain at the end of 10 cycles = 1.43 %
- Cycles produce axial strains between 0.44 % and 1.54 %
- Test ended after 1850 seconds.

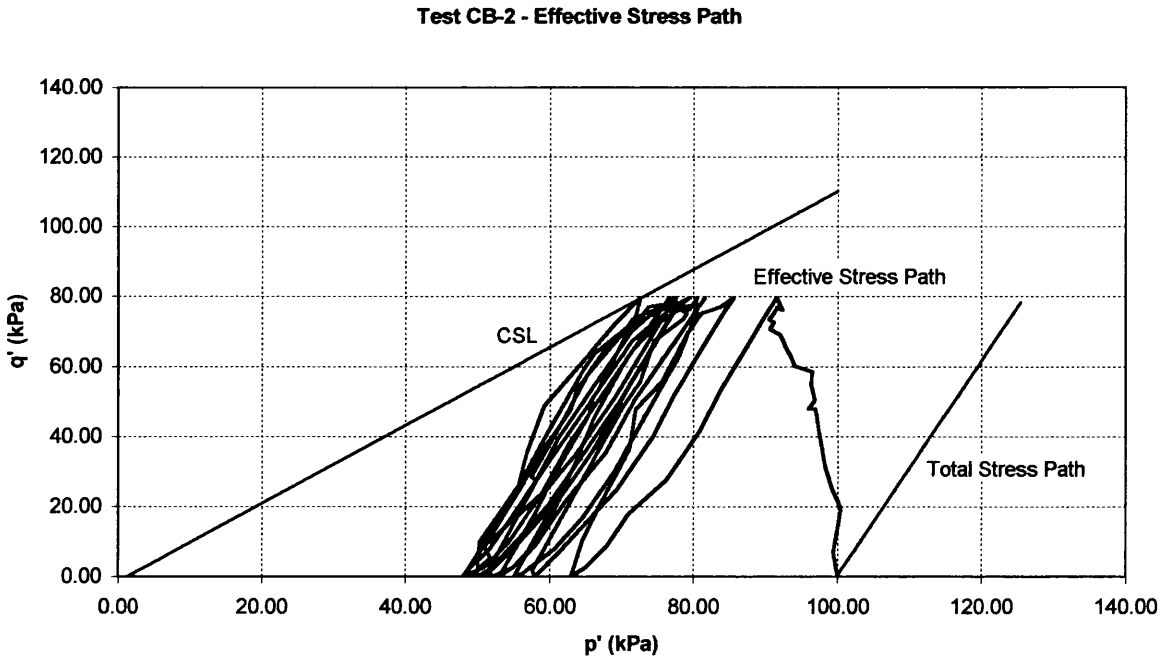

Figure 4.41 *– Effective Stress Path [Test CB-2]*

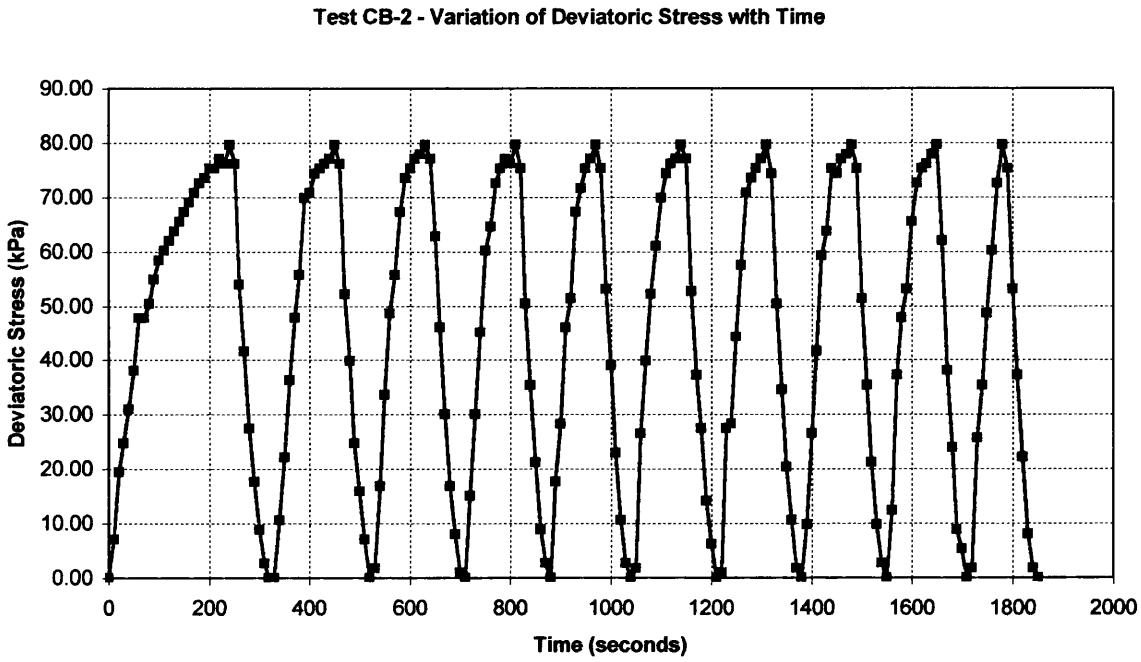

Figure 4.42 – Variation of Deviatoric Stress with Time [Test CB-2]

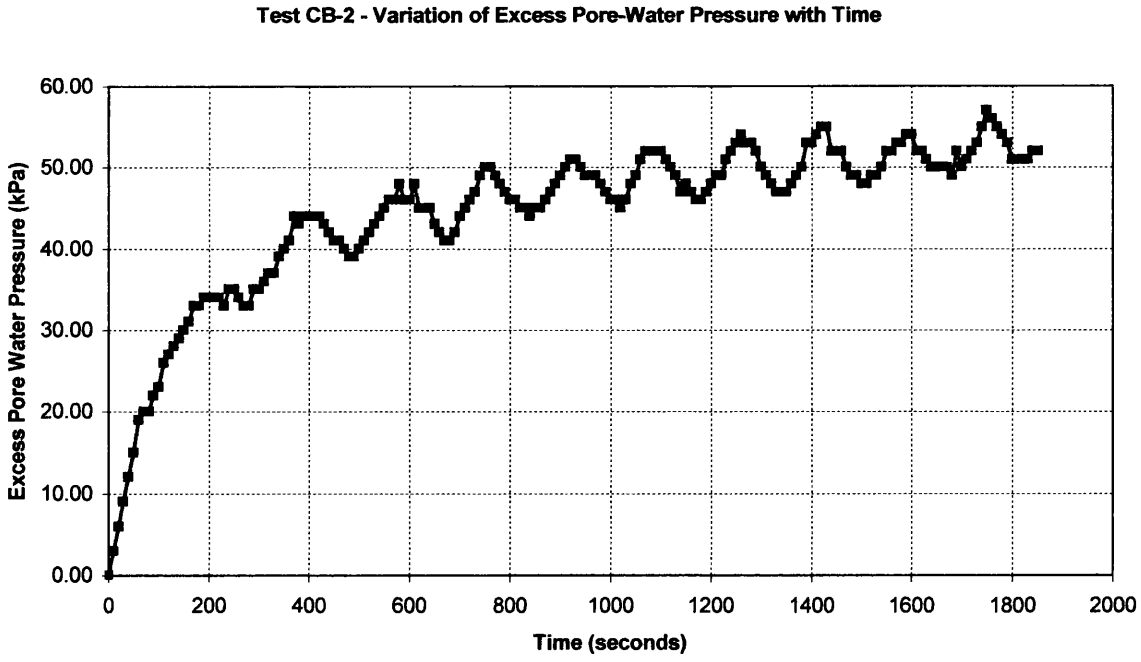

Figure 4.43 – Variation of Excess Pore-Water Pressure with Time [Test CB-2]

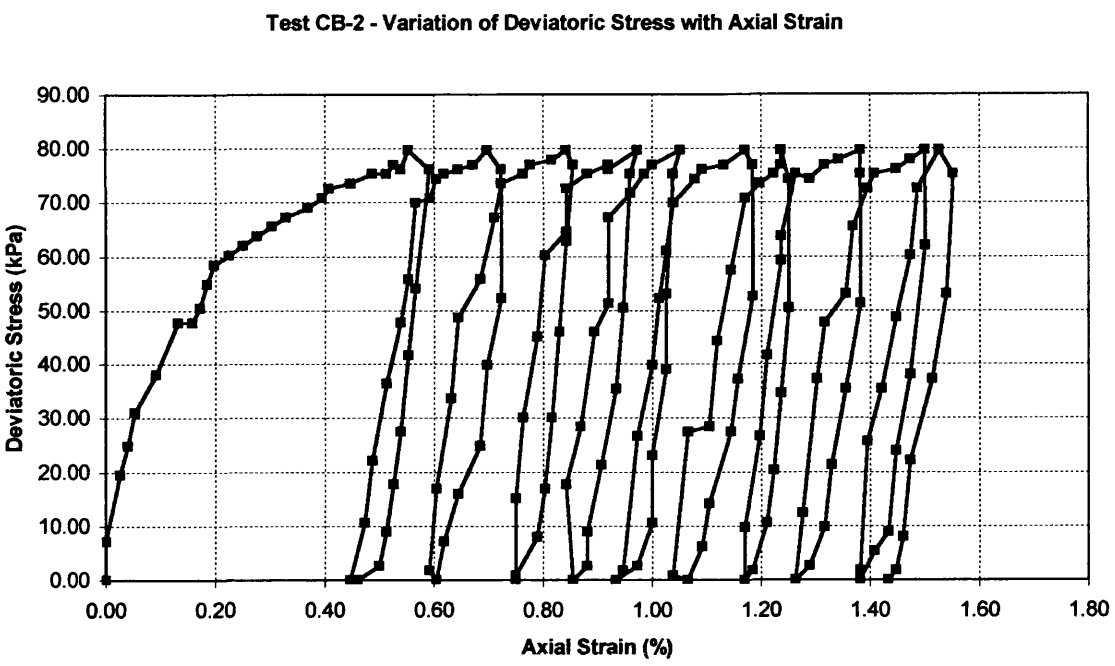

Figure 4.44 – Variation of Deviatoric Stress with Axial Strain [Test CB-2]

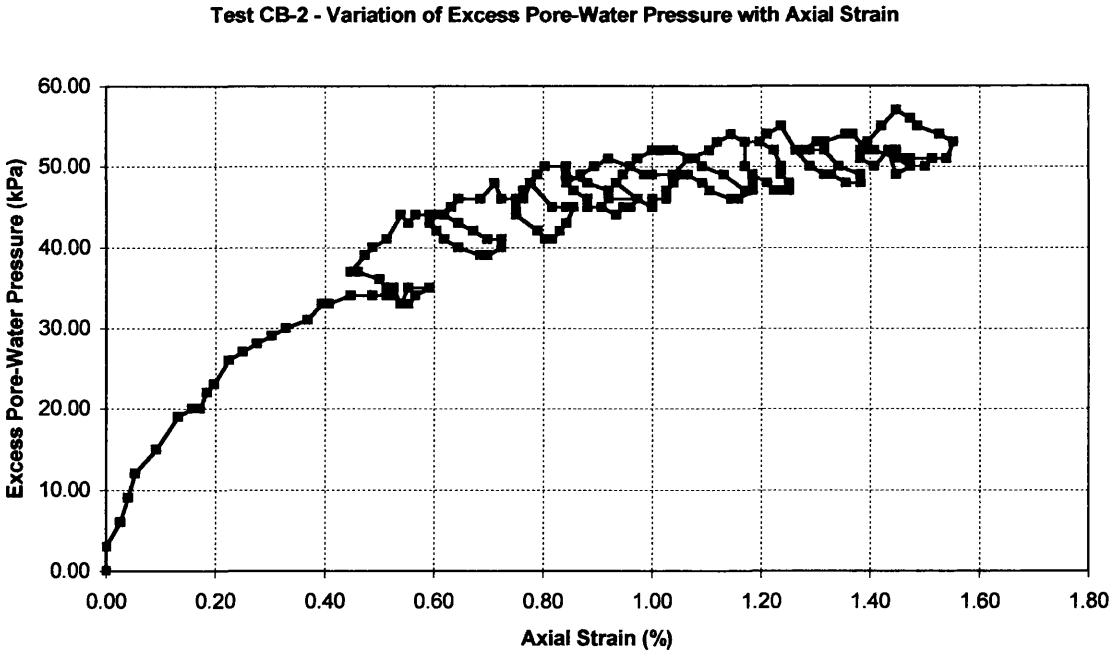

Figure 4.45 – Variation of Excess Pore-Water Pressure with Axial Strain [Test CB-2]

4.2.3 Test No. CB-3

Quantity	Value
Test Number / Type	CB-3 / Stress-controlled
Backpressure value	300 kPa, applied for 1 hour
B-parameter	0.93 - 0.94
Moisture Content, w	0.3700
Initial Degree of Saturation, S_{r0}	0.9737
Bulk Density, ρ	1780 kg/m^3
Unit Weight, γ	17.462 kN/m^3

Table 4.12 *– Details of Test CB-3 Specimen Parameters*

Notes:

- Max. excess pore-water pressure after 10 cycles = 24 kPa (i.e. $r_{0,10} = 0.24$)
- Axial strain at the end of 10 cycles = 0.25 %
- Cycles produce axial strains between 0.16 % and 0.33 %
- Test ended after 2070 seconds.

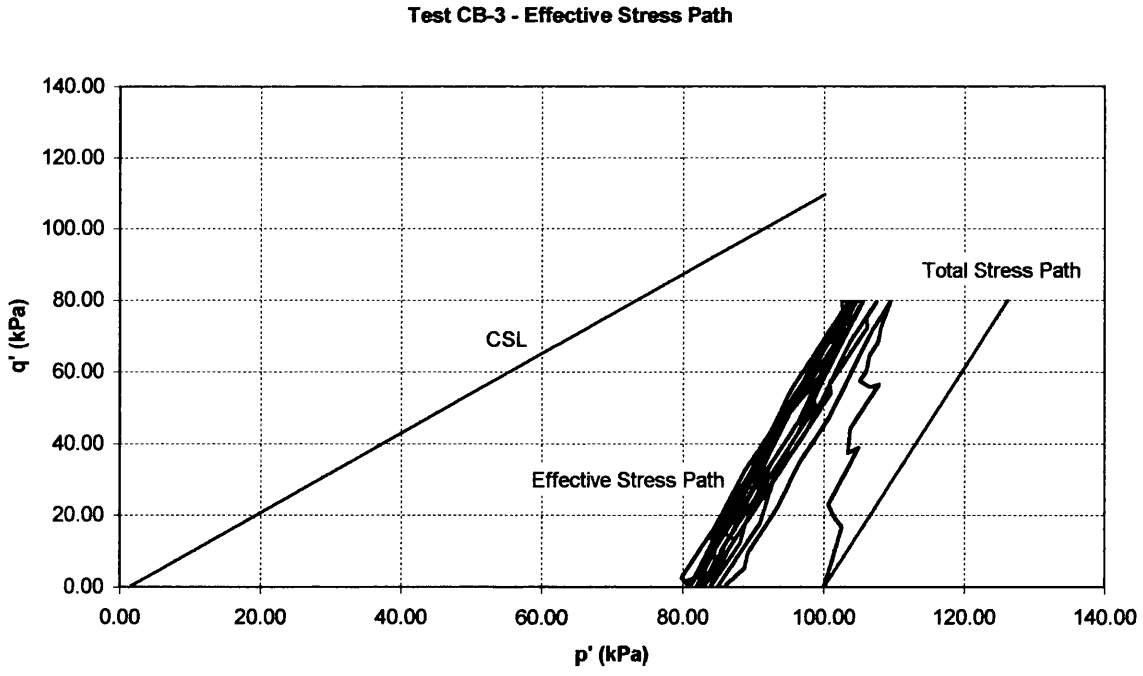

Figure 4.46 *– Effective Stress Path [Test CB-3]*

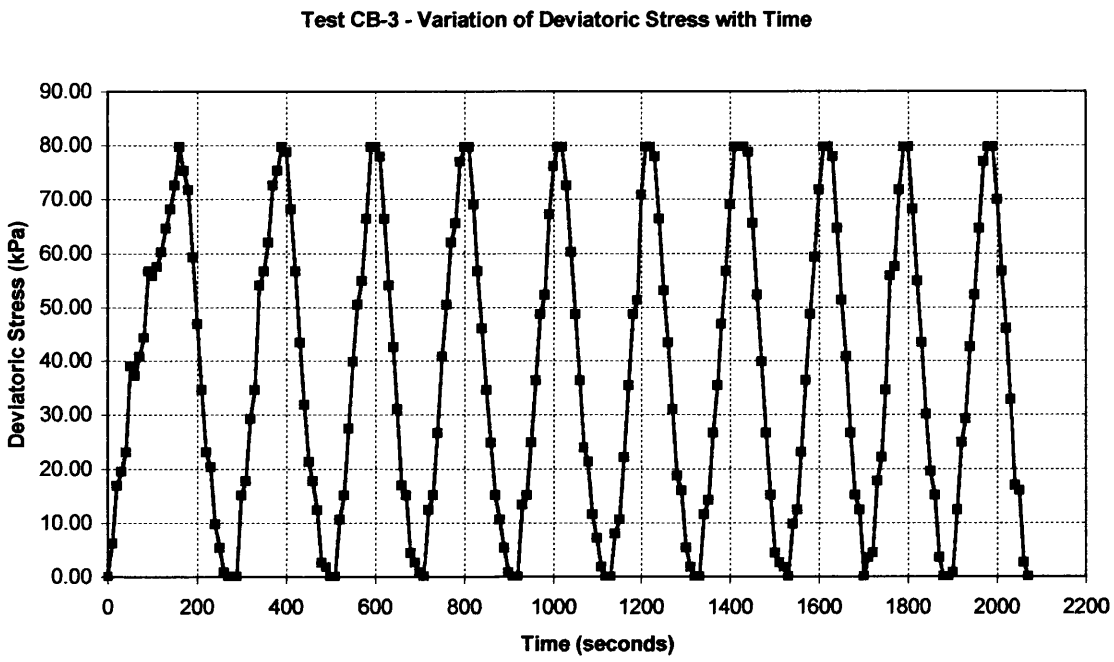

Figure 4.47 – Variation of Deviatoric Stress with Time [Test CB-3]

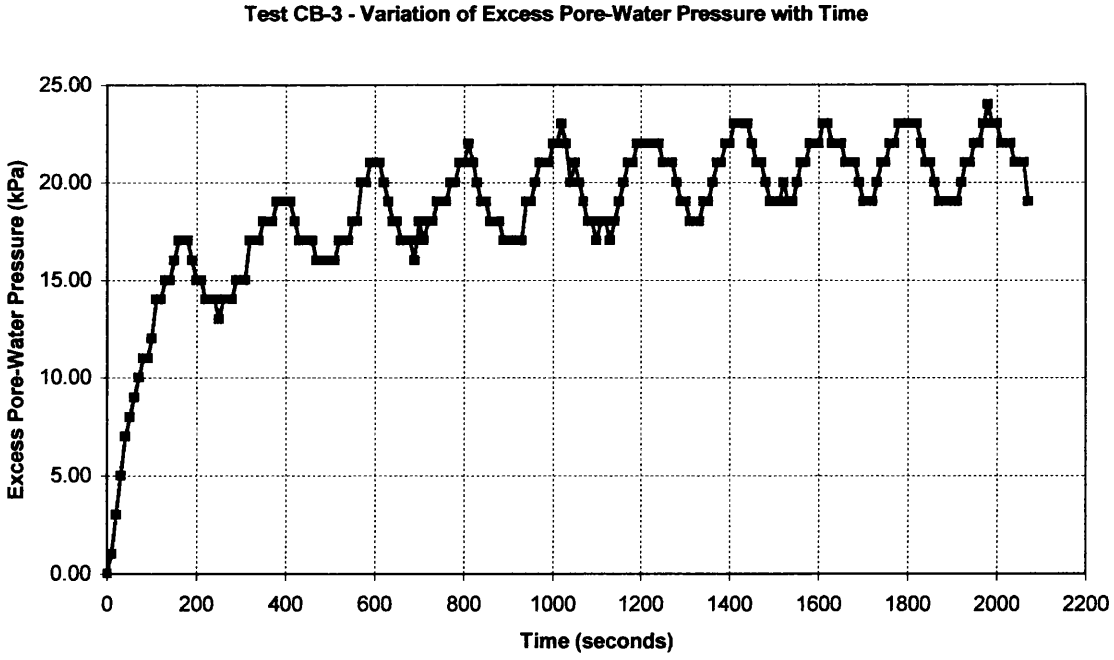

Figure 4.48 – Variation of Excess Pore-Water Pressure with Time [Test CB-3]

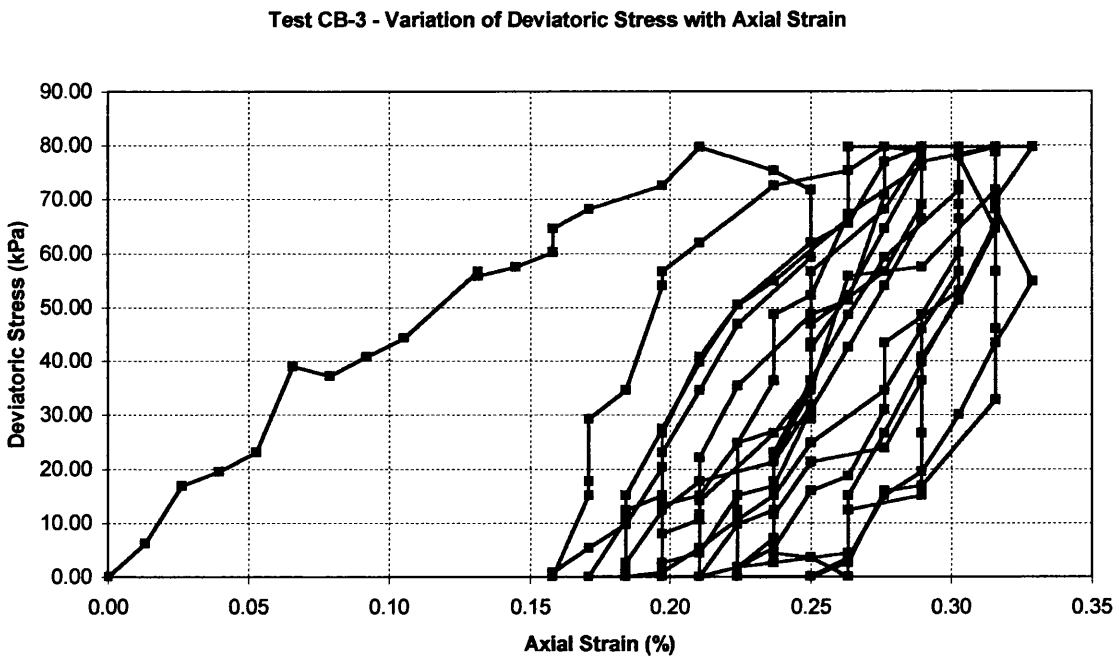

Figure 4.49 *– Variation of Deviatoric Stress with Axial Strain [Test CB-3]*

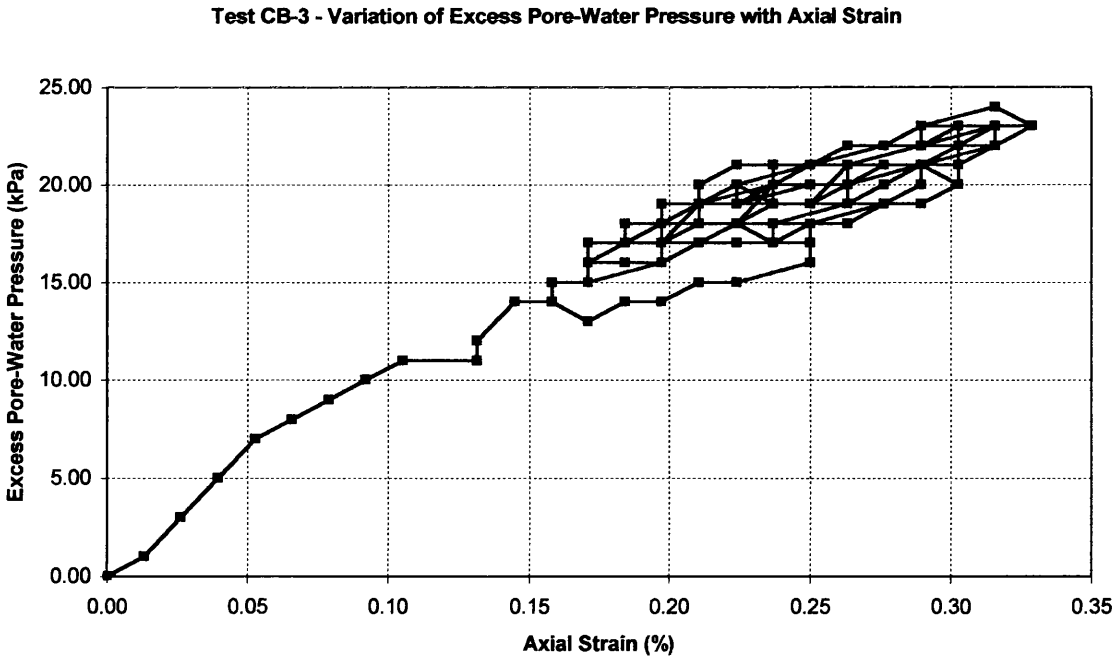

Figure 4.50 *– Variation of Excess Pore-Water Pressure with Axial Strain [Test CB-3]*

4.2.4 Test No. CB-4

Quantity	Value
Test Number / Type	CB-4 / Stress-controlled
Backpressure value	250 kPa, applied for 1 hour
B-parameter	0.90
Moisture Content, w	0.3674
Initial Degree of Saturation, S_{r0}	0.9668
Bulk Density, ρ	1777 kg/m^3
Unit Weight, γ	17.432 kN/m^3

Table 4.13 *– Details of Test CB-4 Specimen Parameters*

Notes:

- Max. excess pore-water pressure after 10 cycles = 20 kPa (i.e. $r_{0,10} = 0.20$)
- Axial strain at the end of 10 cycles = 0.26 %
- Cycles produce axial strains between 0.11 % and 0.36 %
- Test ended after 2250 seconds.

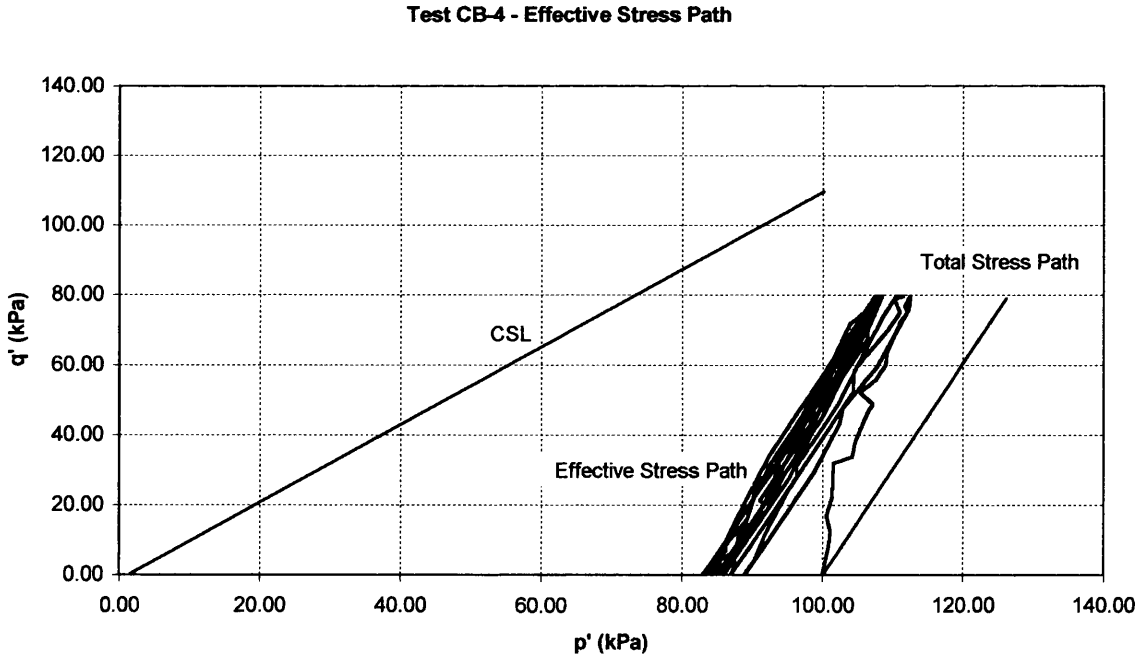

Figure 4.51 *– Effective Stress Path [Test CB-4]*

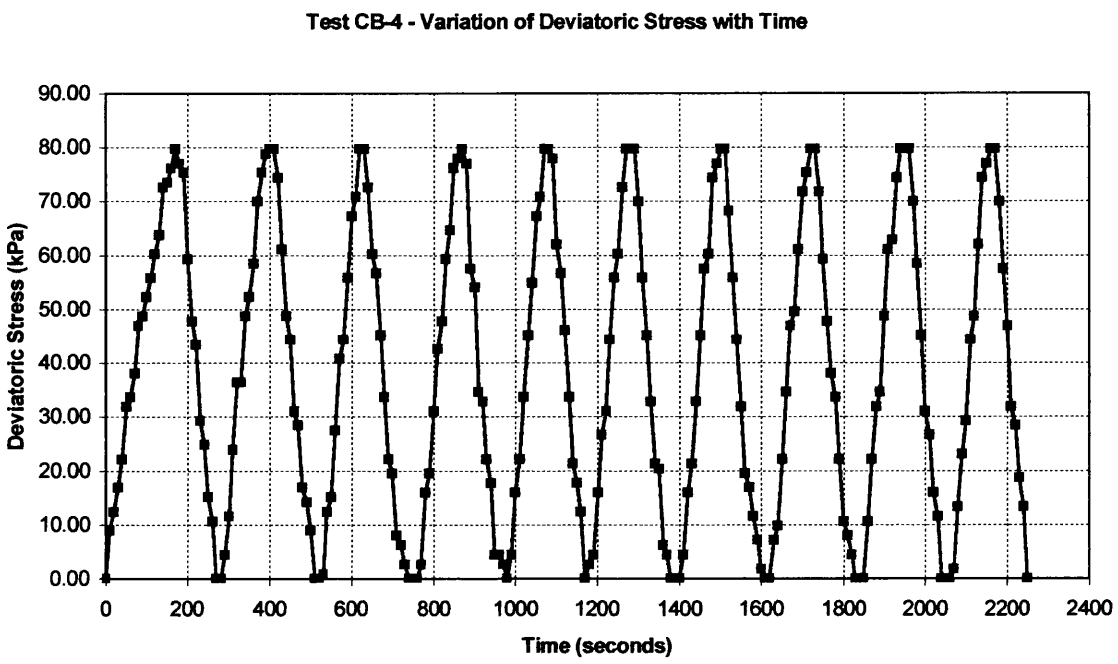

Figure 4.52 *– Variation of Deviatoric Stress with Time [Test CB-4]*

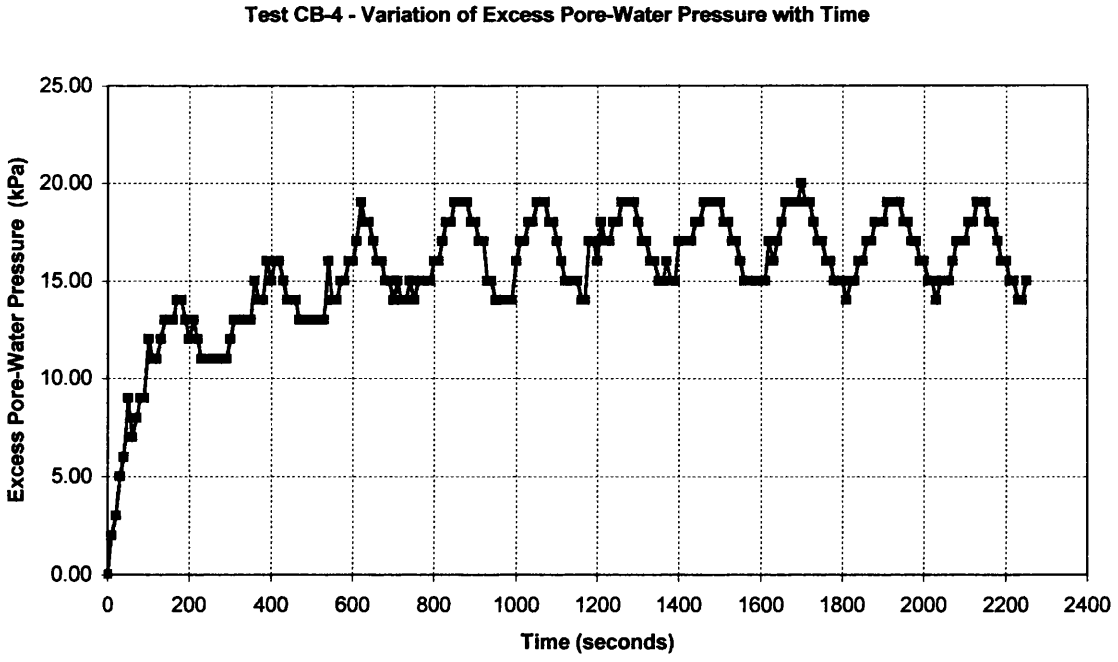

Figure 4.53 *– Variation of Excess Pore-Water Pressure with Time [Test CB-4]*

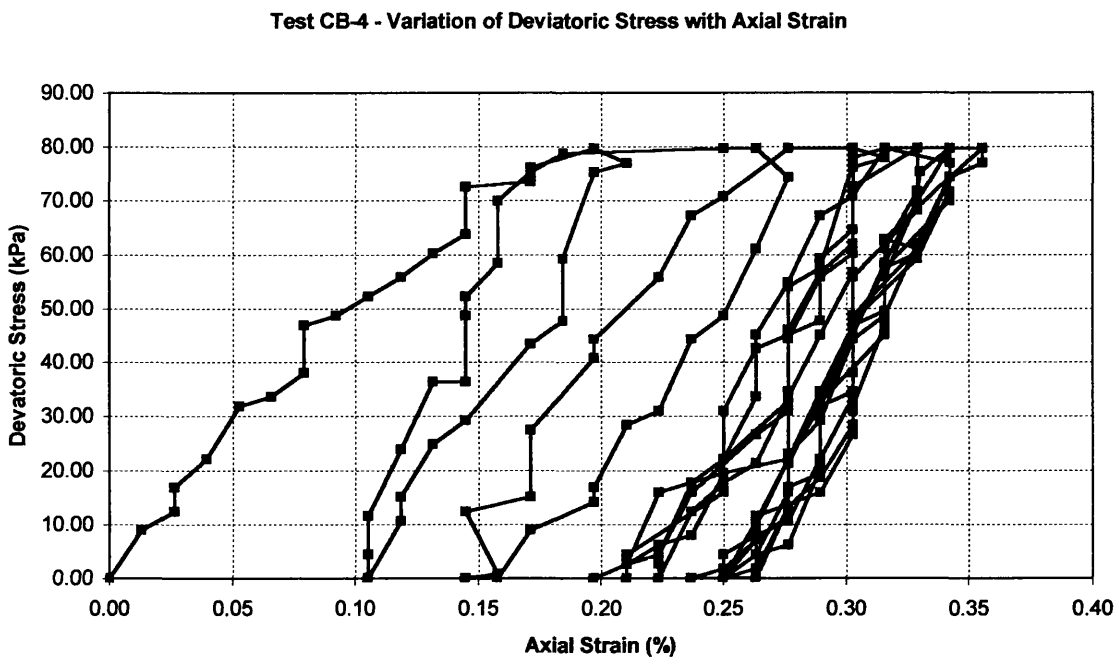

Figure 4.54 *– Variation of Deviatoric Stress with Axial Strain [Test CB-4]*

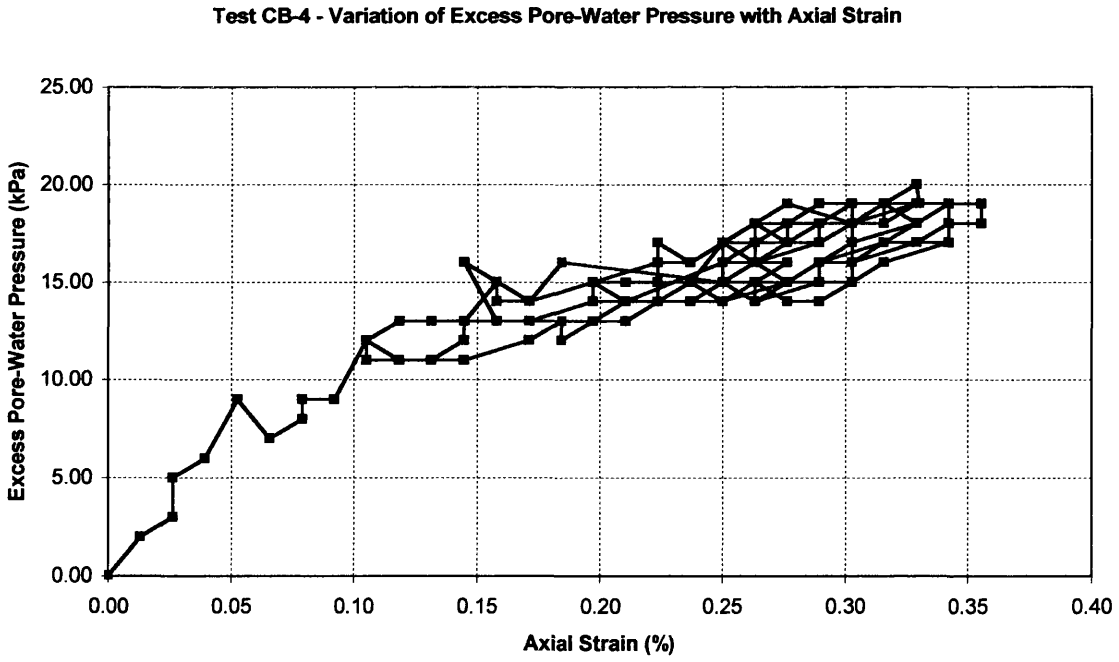

Figure 4.55 *– Variation of Excess Pore-Water Pressure with Axial Strain [Test CB-4]*

4.2.5 Test No. CB-6

Quantity	Value
Test Number / Type	CB-6 / Stress-controlled
Backpressure value	200 kPa, applied for 1 hour
B-parameter	0.86
Moisture Content, w	0.3652
Initial Degree of Saturation, S_{r0}	0.9611
Bulk Density, ρ	1774 kg/m^3
Unit Weight, γ	17.403 kN/m^3

Table 4.14 *– Details of Test CB-6 Specimen Parameters*

Notes:

- Max. excess pore-water pressure after 10 cycles = 19 kPa (i.e. $r_{0,10} = 0.19$)
- Axial strain at the end of 10 cycles = 0.41 %
- Cycles produce axial strains between 0.24 % and 0.49 %
- Test ended after 2390 seconds.

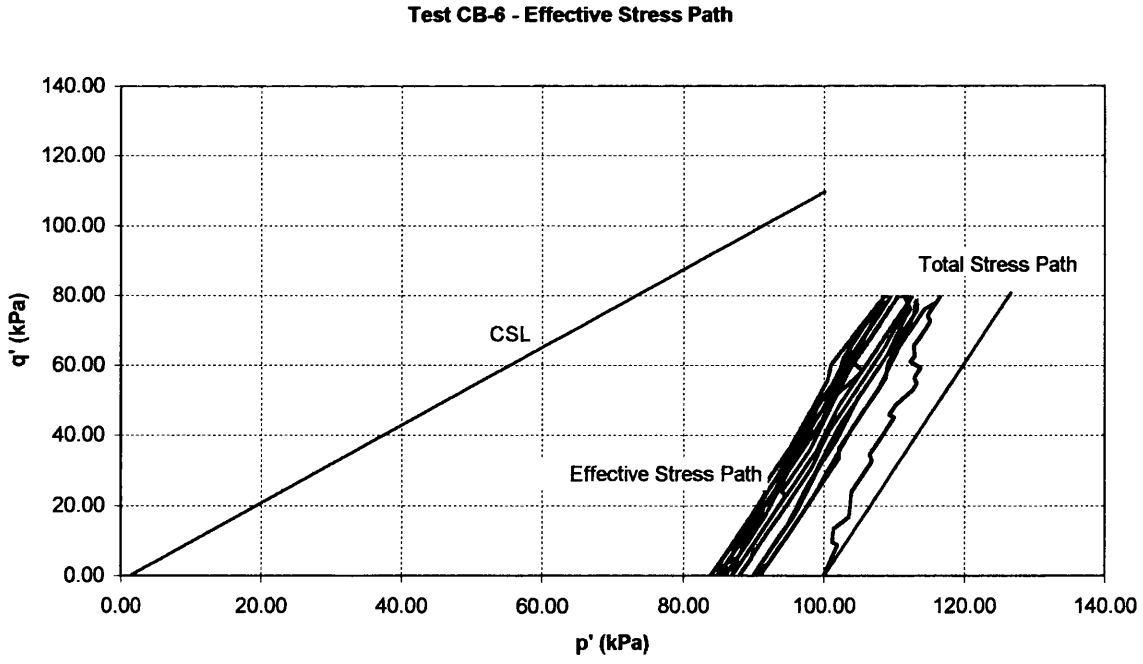

Figure 4.56 *– Effective Stress Path [Test CB-6]*

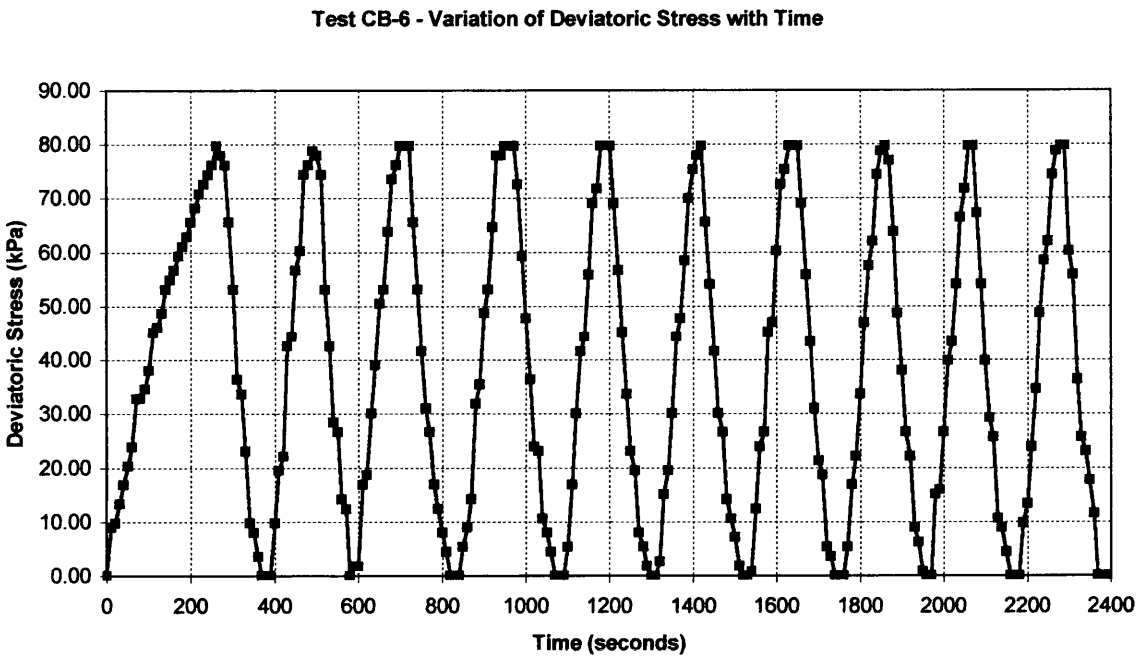

Figure 4.57 – Variation of Deviatoric Stress with Time [Test CB-6]

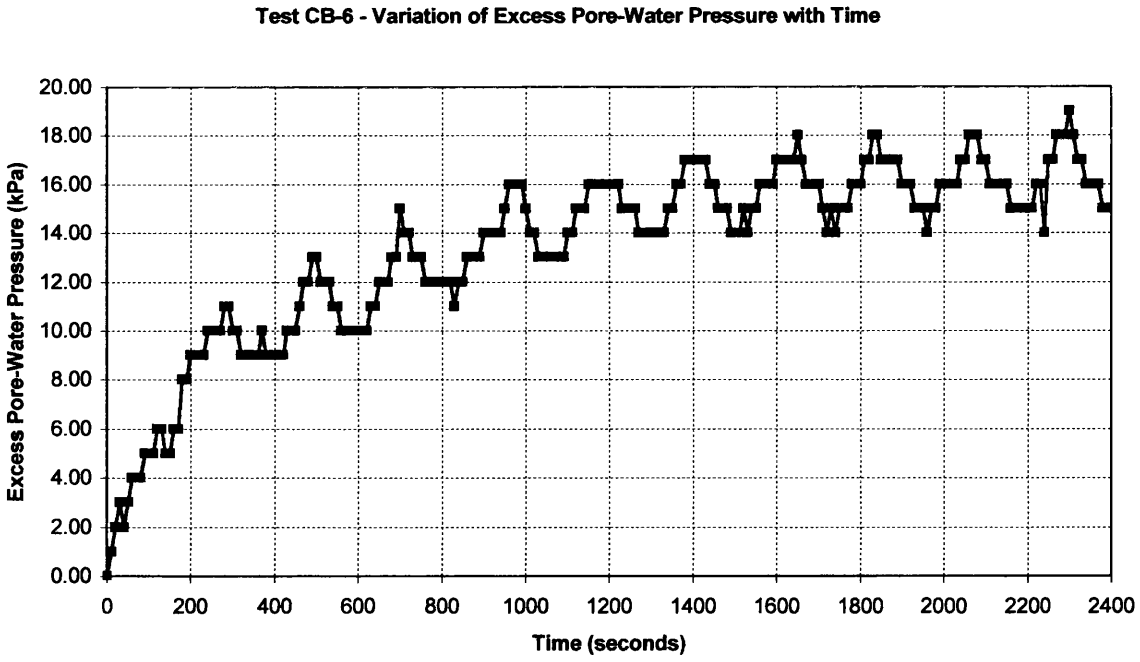

Figure 4.58 – Variation of Excess Pore-Water Pressure with Time [Test CB-6]

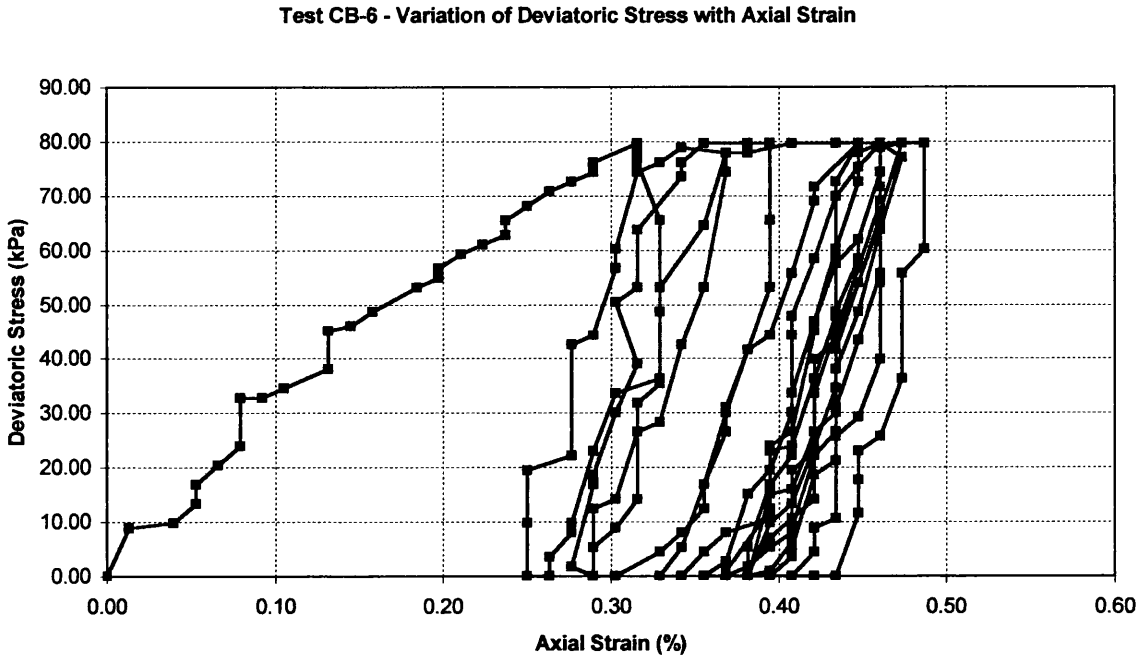

Figure 4.59 *– Variation of Deviatoric Stress with Axial Strain [Test CB-6]*

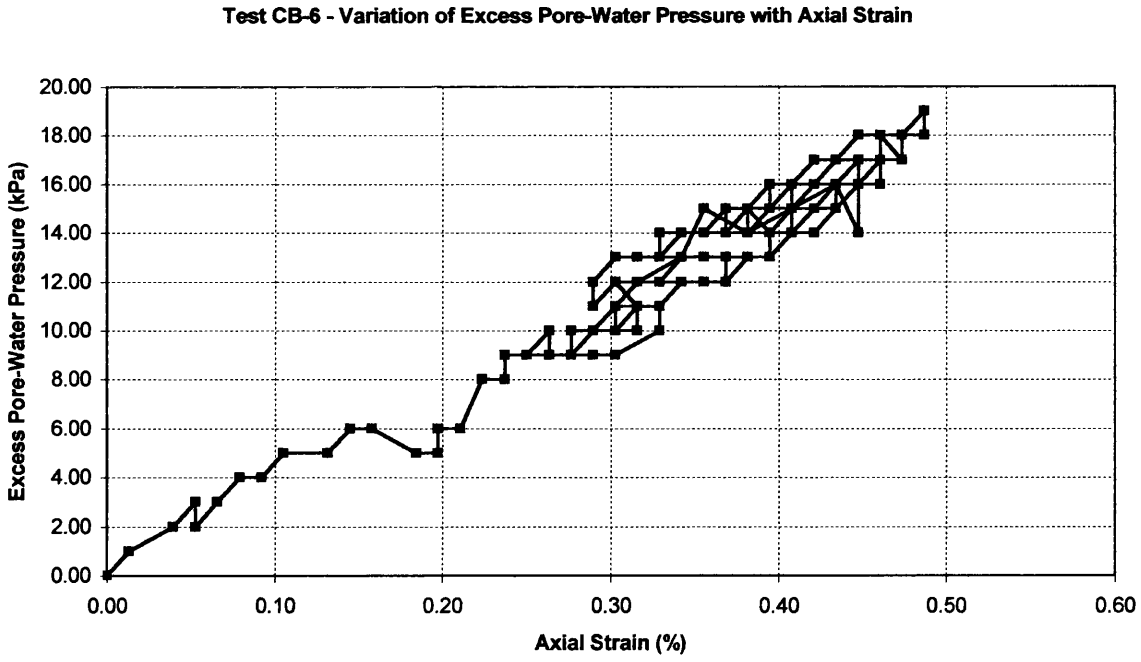

Figure 4.60 *– Variation of Excess Pore-Water Pressure with Axial Strain [Test CB-6]*

4.2.6 Test No. CB-7

Quantity	Value
Test Number / Type	CB-7 / Stress-controlled
Backpressure value	150 kPa, applied for 1 hour
B-parameter	Some variation between 0.81 and 0.82
Moisture Content, w	0.3623
Initial Degree of Saturation, S_{r0}	0.9534
Bulk Density, ρ	1770 kg/m^3
Unit Weight, γ	17.364 kN/m^3

Table 4.15 *– Details of Test CB-7 Specimen Parameters*

Notes:

- Max. excess pore-water pressure after 10 cycles = 15 kPa (i.e. $r_{0,10} = 0.15$)
- Axial strain at the end of 10 cycles = 0.46 %
- Cycles produce axial strains between 0.35 % and 0.46 %
- Test ended after 2540 seconds.

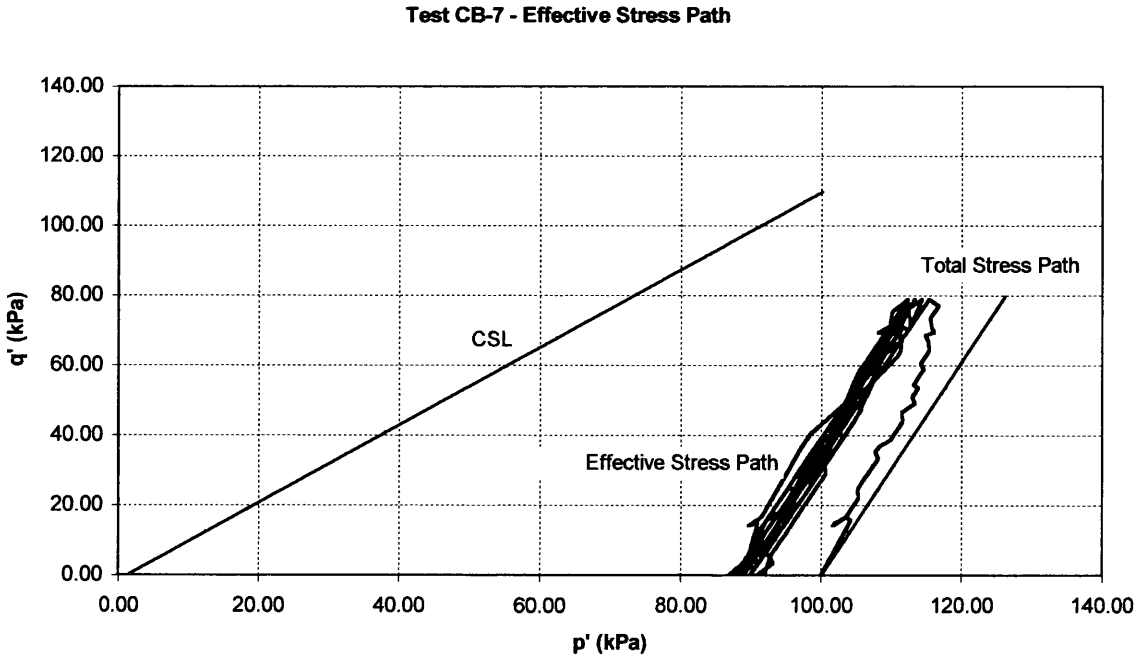

Figure 4.61 *– Effective Stress Path [Test CB-7]*

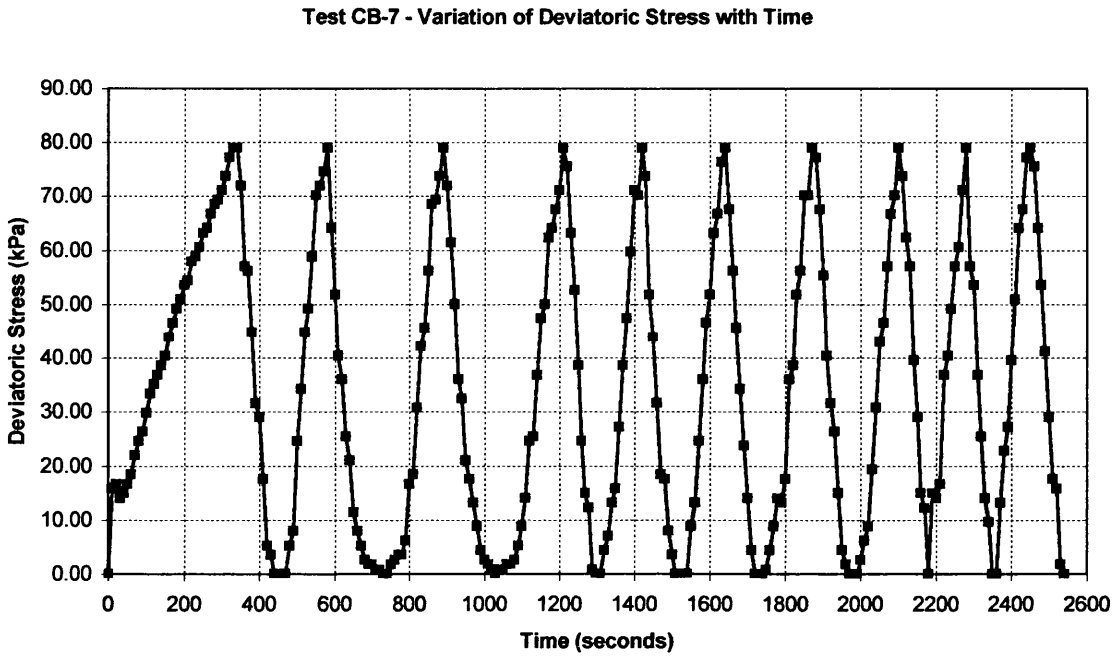

Figure 4.62 – Variation of Deviatoric Stress with Time [Test CB-7]

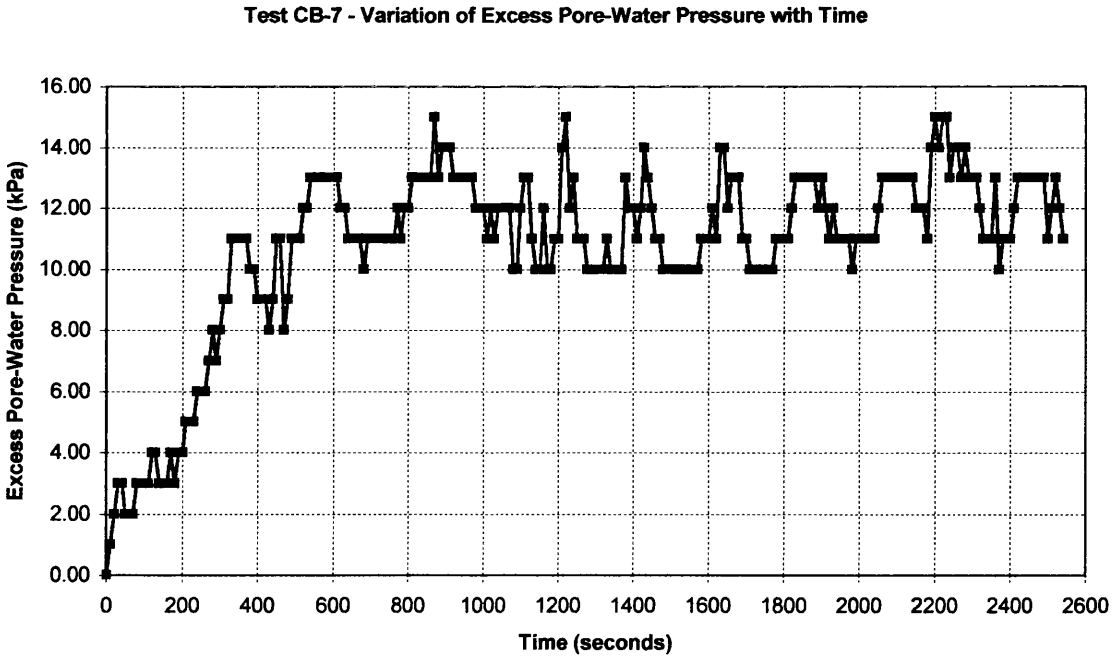

Figure 4.63 – Variation of Excess Pore-Water Pressure with Time [Test CB-7]

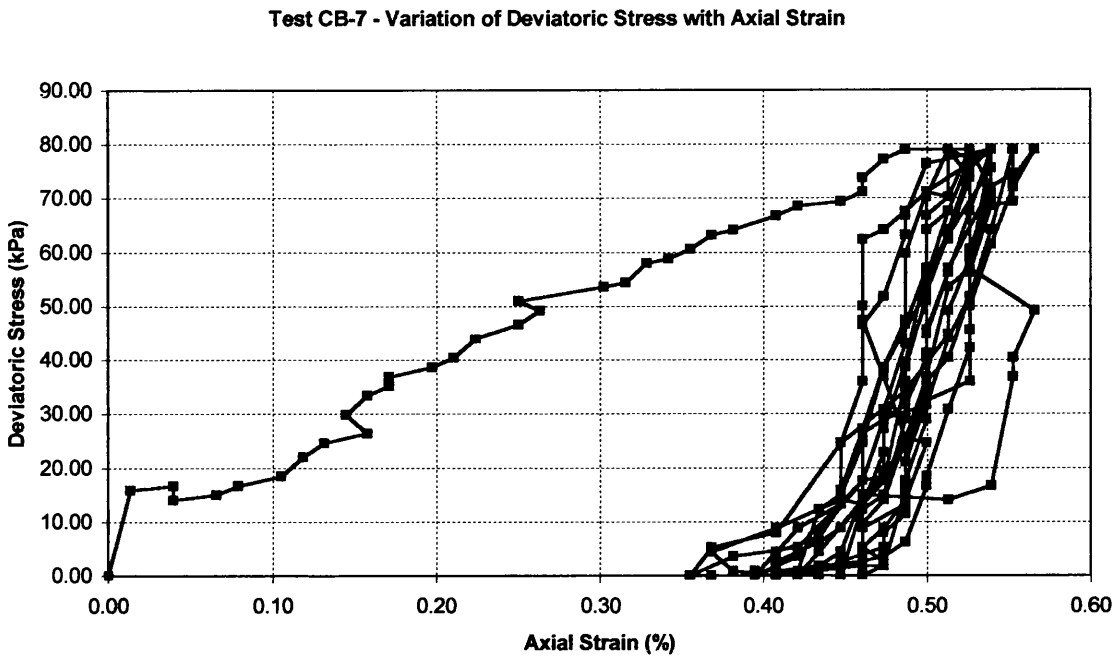

Figure 4.64 – Variation of Deviatoric Stress with Axial Strain [Test CB-7]

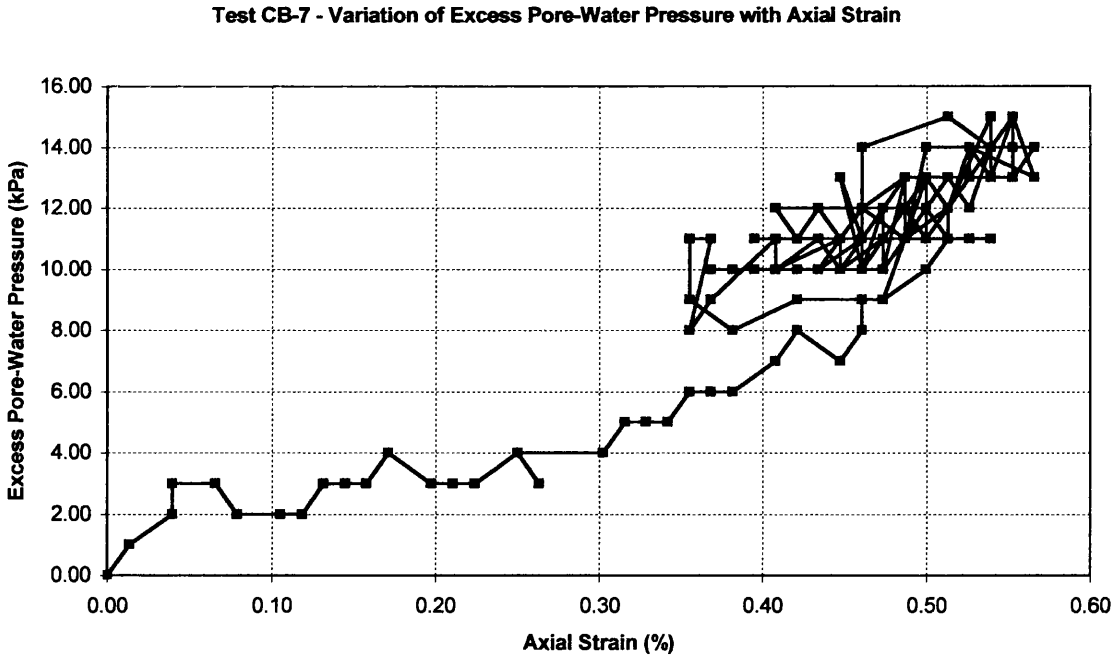

Figure 4.65 – Variation of Excess Pore-Water Pressure with Axial Strain [Test CB-7]

4.2.7 Test No. CB-8

Quantity	Value
Test Number / Type	CB-8 / Stress-controlled
Backpressure value	100 kPa, applied for 1 hour
B-parameter	0.77
Moisture Content, w	0.3544
Initial Degree of Saturation, S_{r0}	0.9326
Bulk Density, ρ	1760 kg/m^3
Unit Weight, γ	17.266 kN/m^3

Table 4.16 *– Details of Test CB-8 Specimen Parameters*

Notes:

- Max. excess pore-water pressure after 10 cycles = 9 kPa (i.e. $r_{0,10} = 0.09$)
- Axial strain at the end of 10 cycles = 0.36 %
- Cycles produce axial strains between 0.27 % and 0.43 %
- Test ended after 2160 seconds.

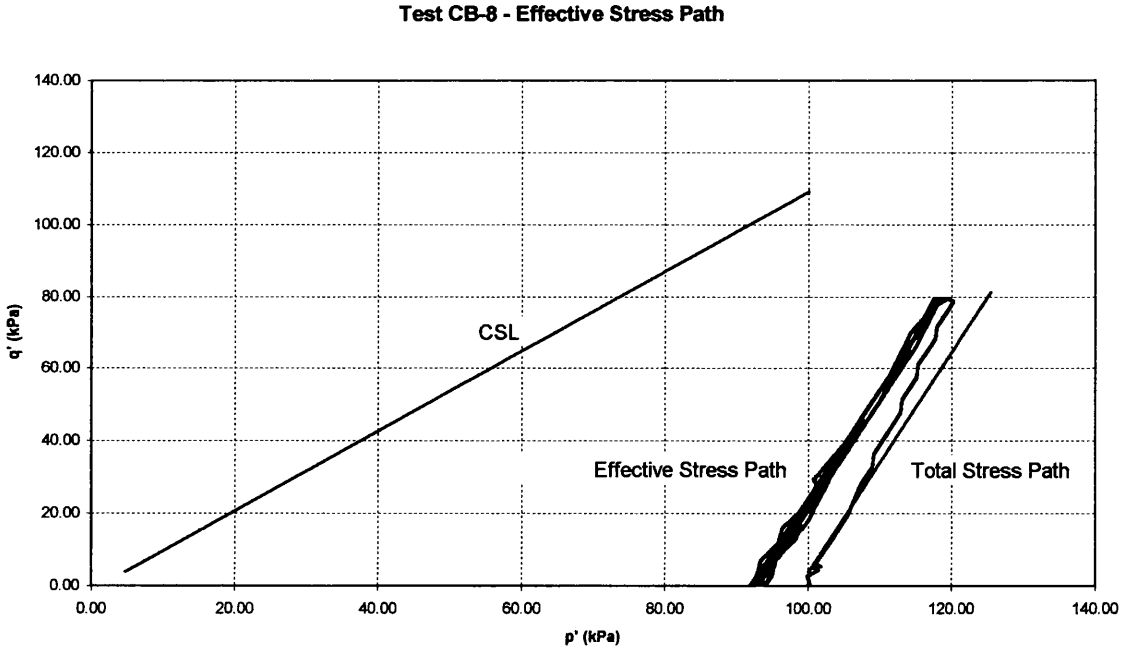

Figure 4.66 *– Effective Stress Path [Test CB-8]*

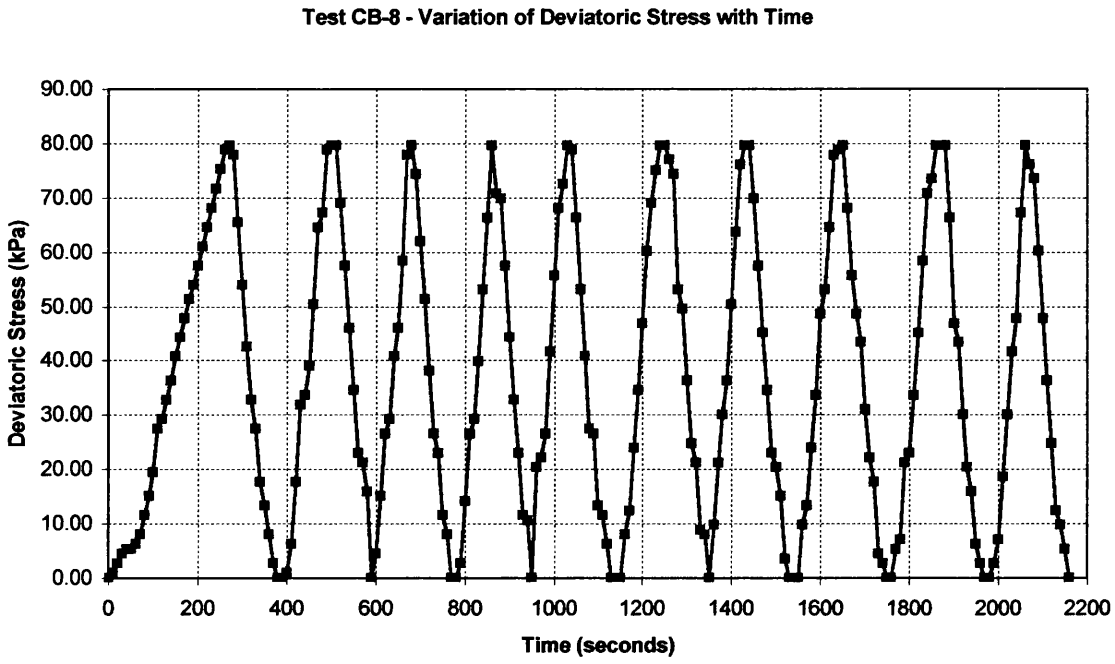

Figure 4.67 *– Variation of Deviatoric Stress with Time [Test CB-8]*

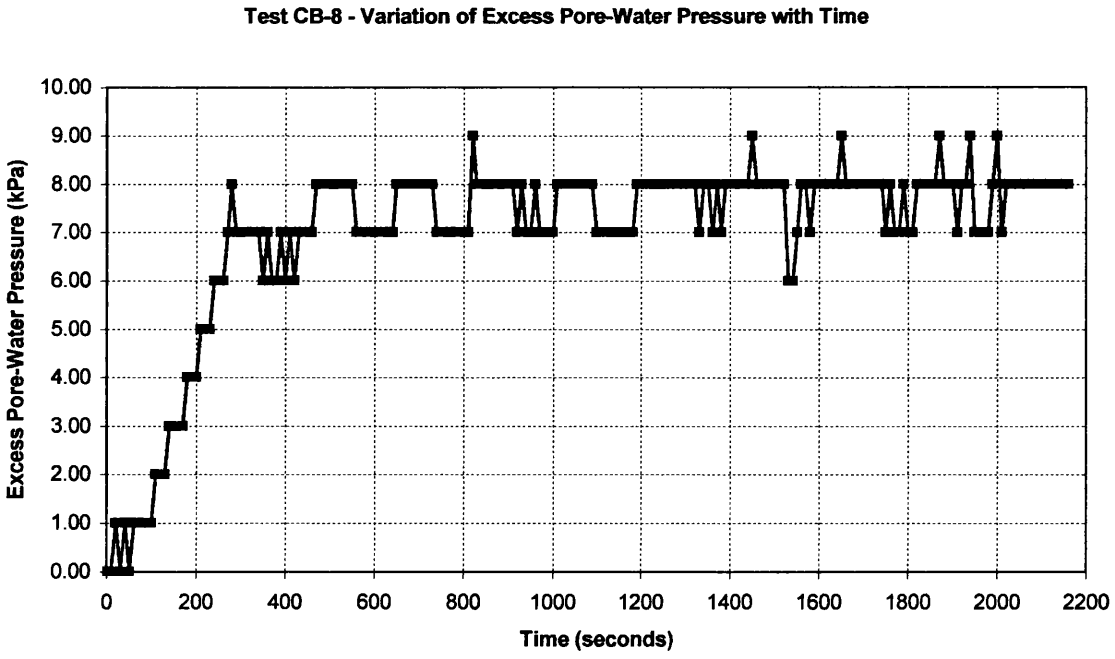

Figure 4.68 *– Variation of Excess Pore-Water Pressure with Time [Test CB-8]*

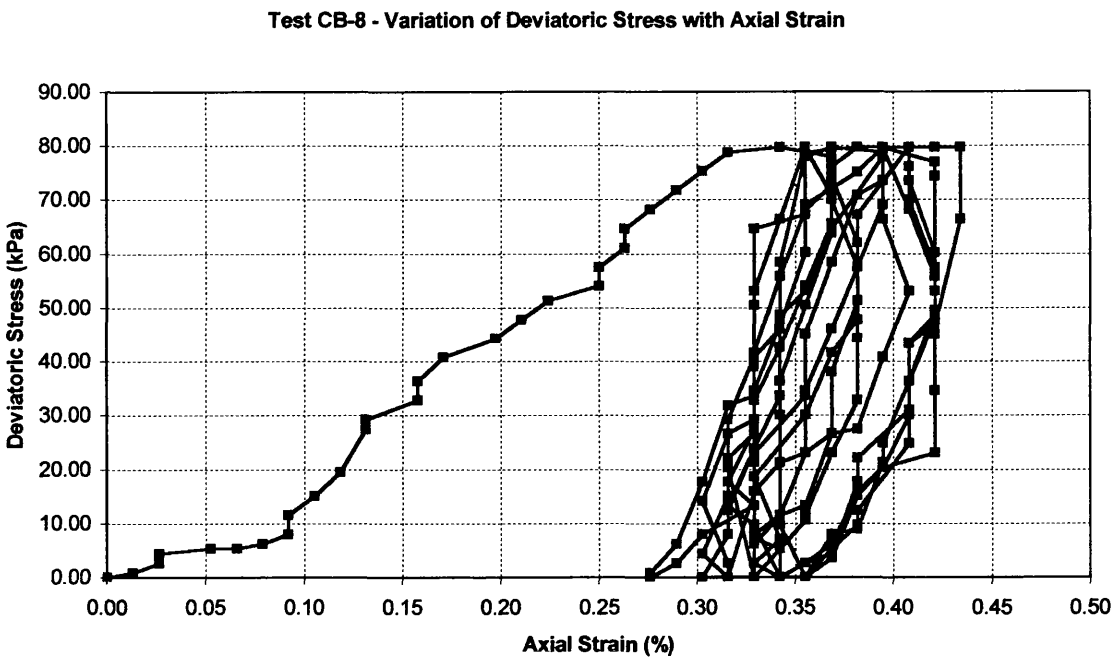

Figure 4.69 – Variation of Deviatoric Stress with Axial Strain [Test CB-8]

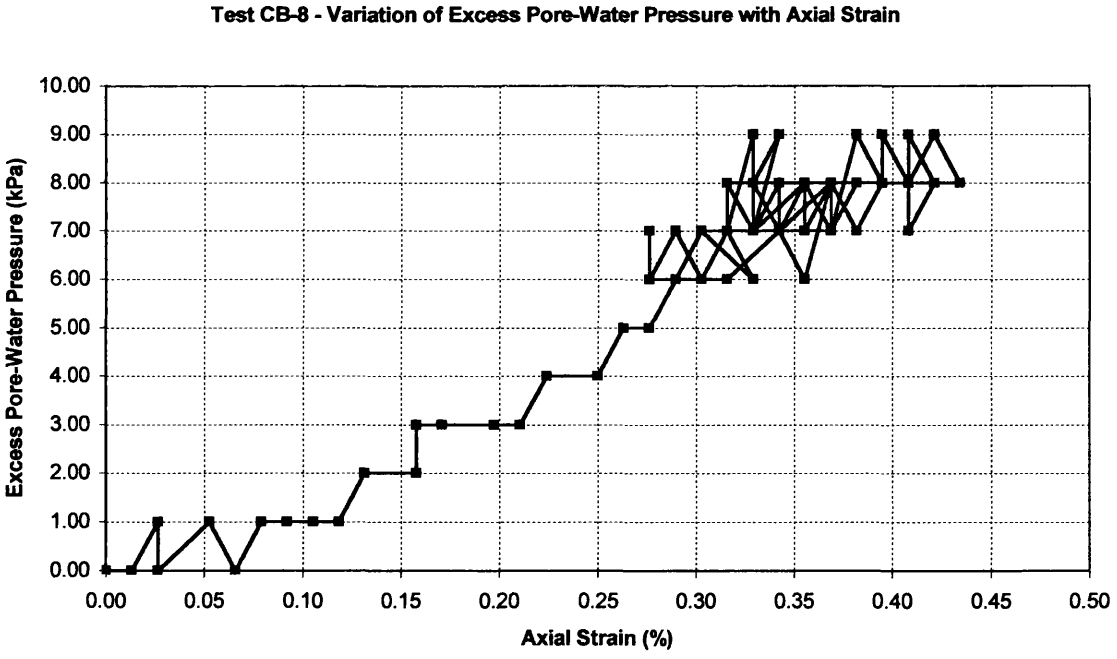

Figure 4.70 – Variation of Excess Pore-Water Pressure with Axial Strain [Test CB-8]

4.2.8 Test No. CB-9

Quantity	Value
Test Number / Type	CB-9 / Stress-controlled
Backpressure value	50 kPa, applied for 1 hour
B-parameter	Some variation between 0.72 and 0.73
Moisture Content, w	0.3481
Initial Degree of Saturation, S_{r0}	0.9161
Bulk Density, ρ	1752 kg/m^3
Unit Weight, γ	17.187 kN/m^3

Table 4.17 *– Details of Test CB-9 Specimen Parameters*

Notes:

- Max. excess pore-water pressure after 10 cycles = 7 kPa (i.e. $r_{0,10} = 0.07$)
- Axial strain at the end of 10 cycles = 0.29 %
- Cycles produce axial strains between 0.22 % and 0.39 %
- Test ended after 2310 seconds.

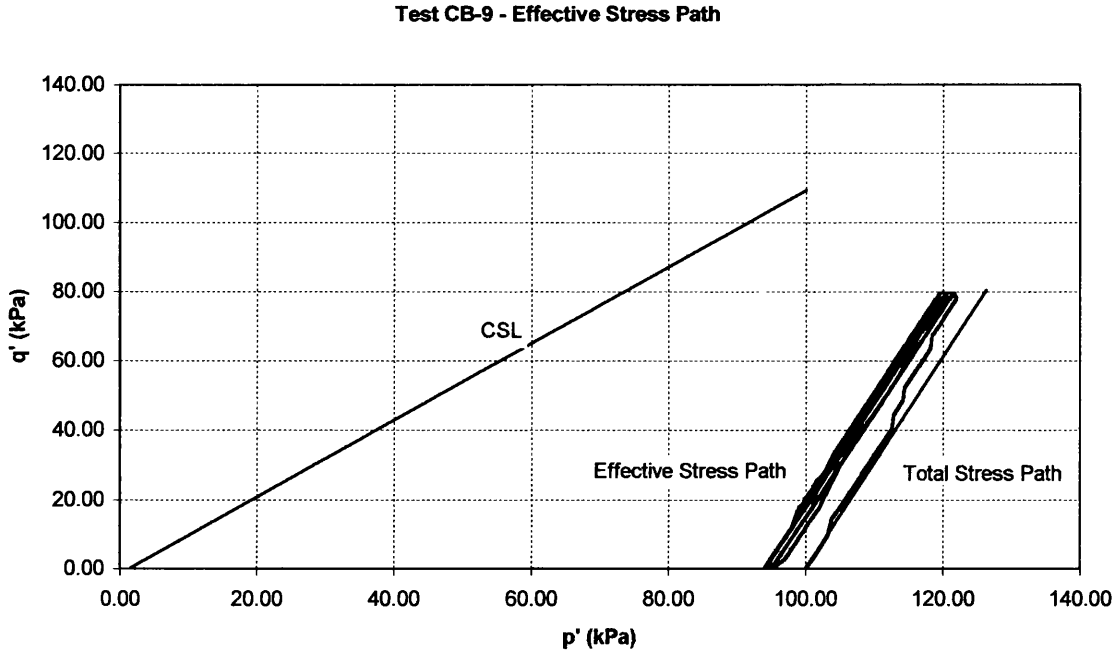

Figure 4.71 *– Effective Stress Path [Test CB-9]*

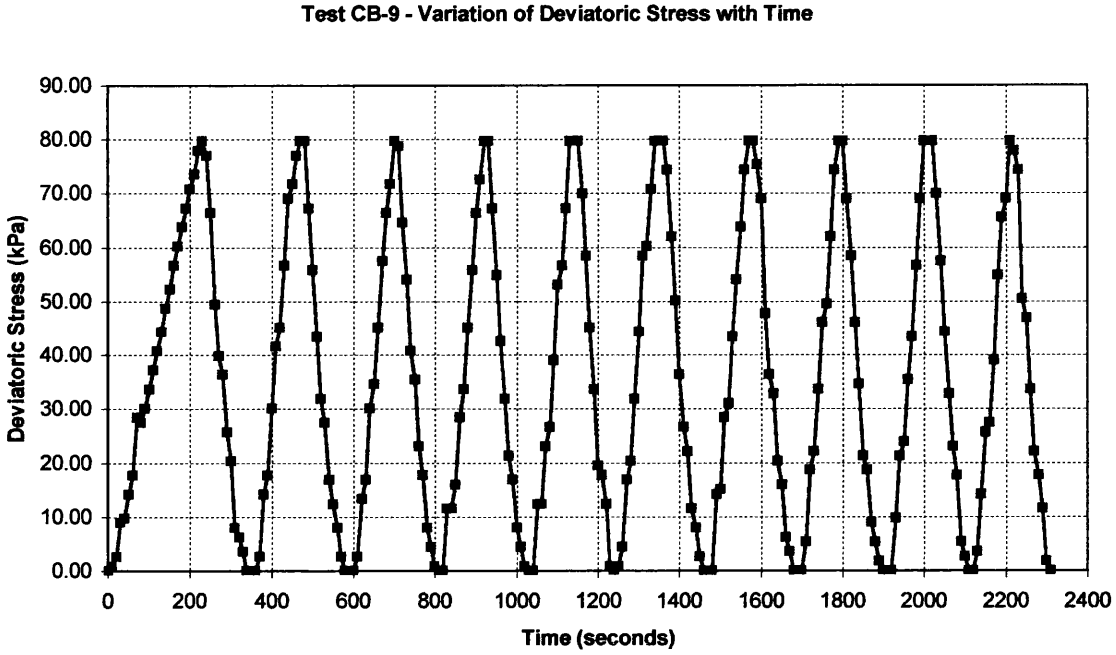

Figure 4.72 *– Variation of Deviatoric Stress with Time [Test CB-9]*

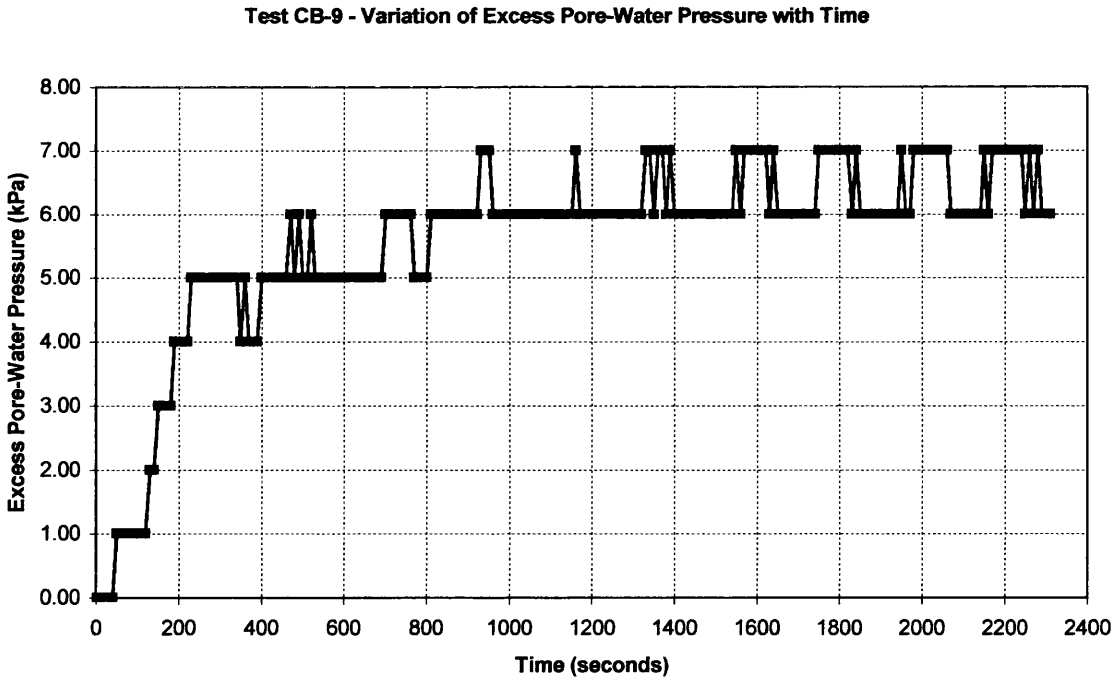

Figure 4.73 *– Variation of Excess Pore-Water Pressure with Time [Test CB-9]*

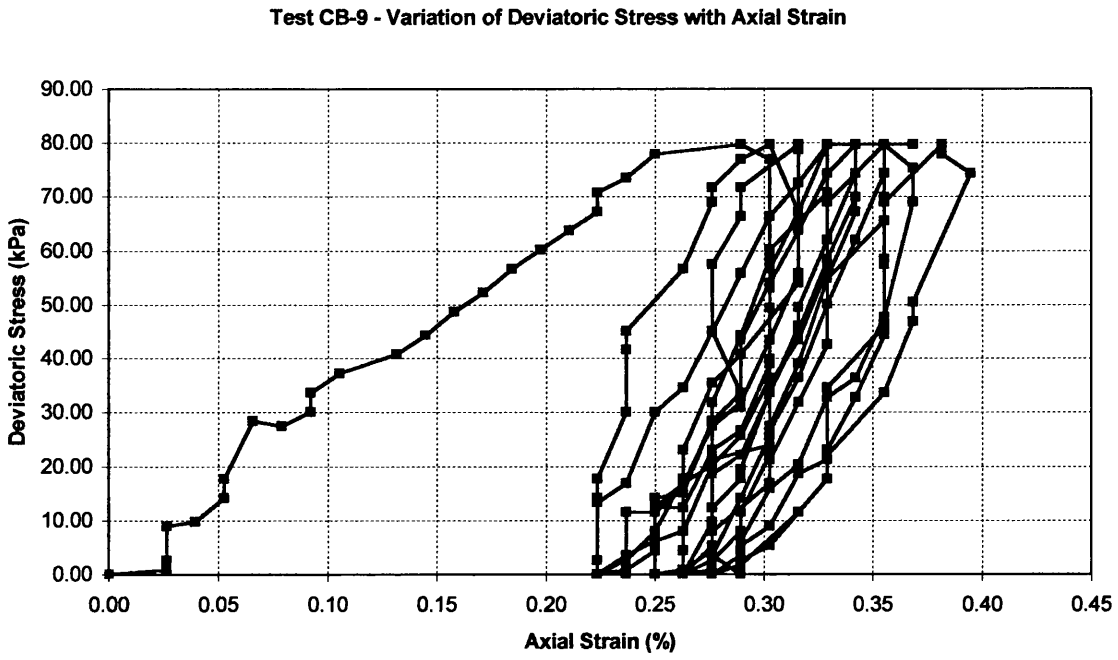

Figure 4.74 – Variation of Deviatoric Stress with Axial Strain [Test CB-9]

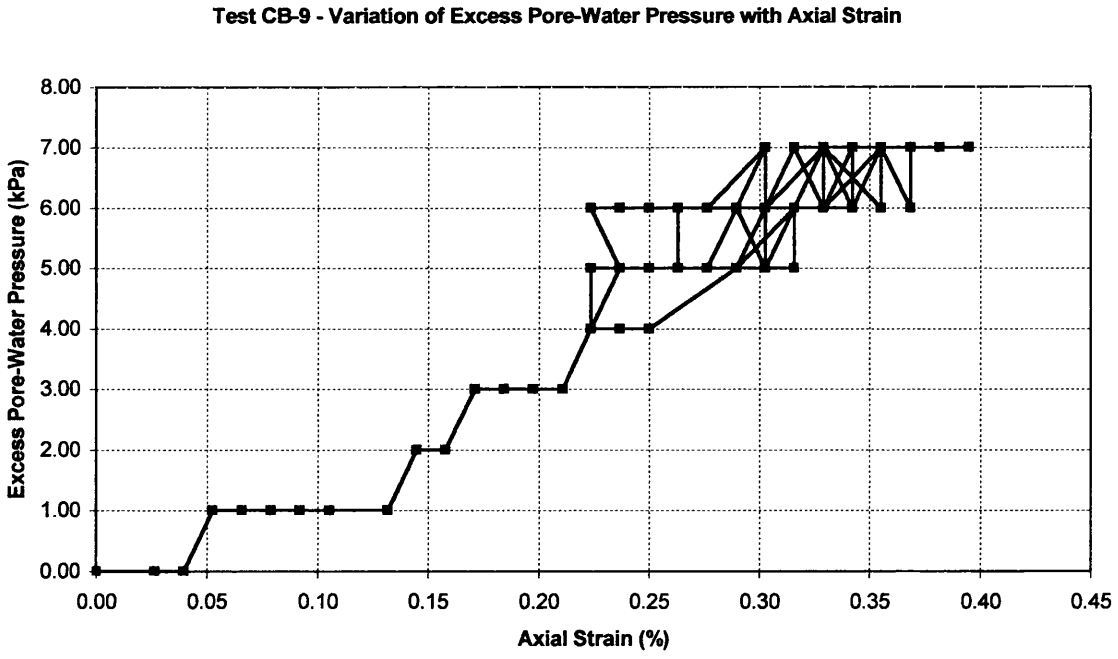

Figure 4.75 – Variation of Excess Pore-Water Pressure with Axial Strain [Test CB-9]

4.2.9 Test No. CB-10

Quantity	Value
Test Number / Type	CB-10 / Stress-controlled
Backpressure value	0 kPa
B-parameter	0.62
Moisture Content, w	0.3452
Initial Degree of Saturation, S_{r0}	0.9084
Bulk Density, ρ	1748 kg/m^3
Unit Weight, γ	17.148 kN/m^3

Table 4.18 *– Details of Test CB-9 Specimen Parameters*

Notes:

- Max. excess pore-water pressure after 10 cycles = 7 kPa (i.e. $r_{0,10} = 0.07$)
- Axial strain at the end of 10 cycles = 0.22 %
- Cycles produce axial strains between 0.16 % and 0.36 %
- Test ended after 2470 seconds.

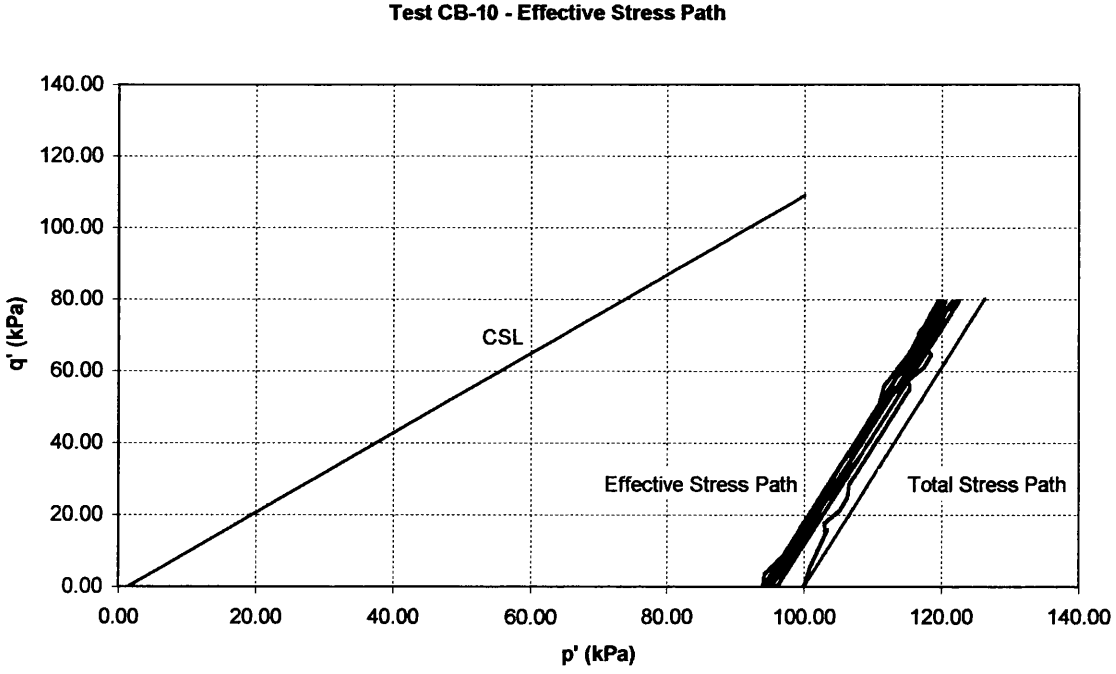

Figure 4.76 *– Effective Stress Path [Test CB-10]*

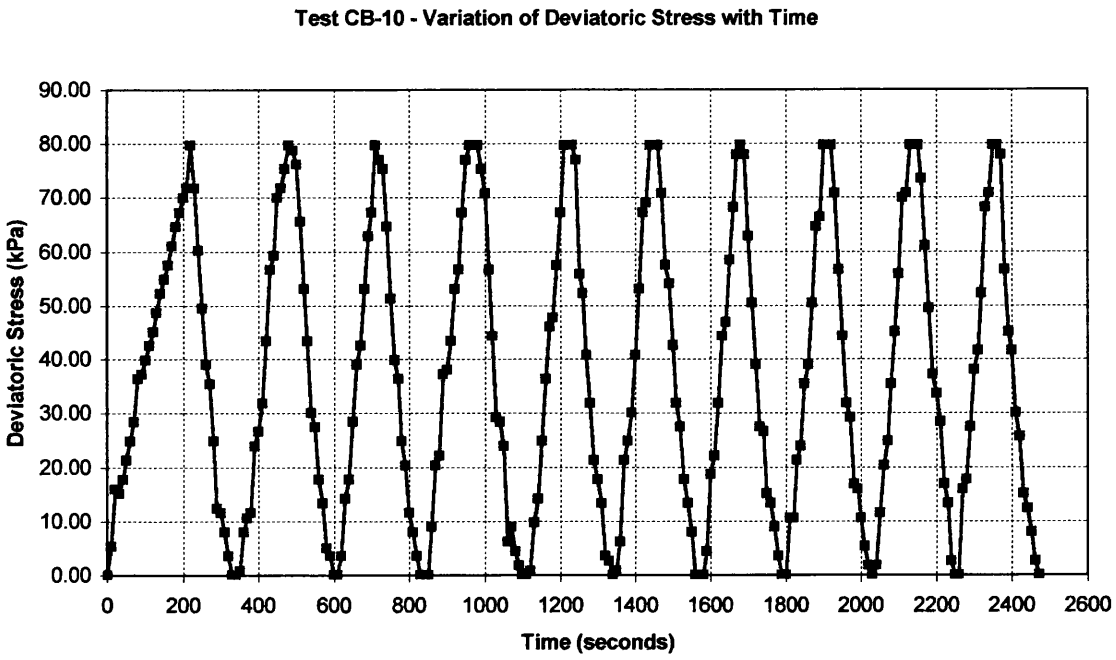

Figure 4.77 – Variation of Deviatoric Stress with Time [Test CB-10]

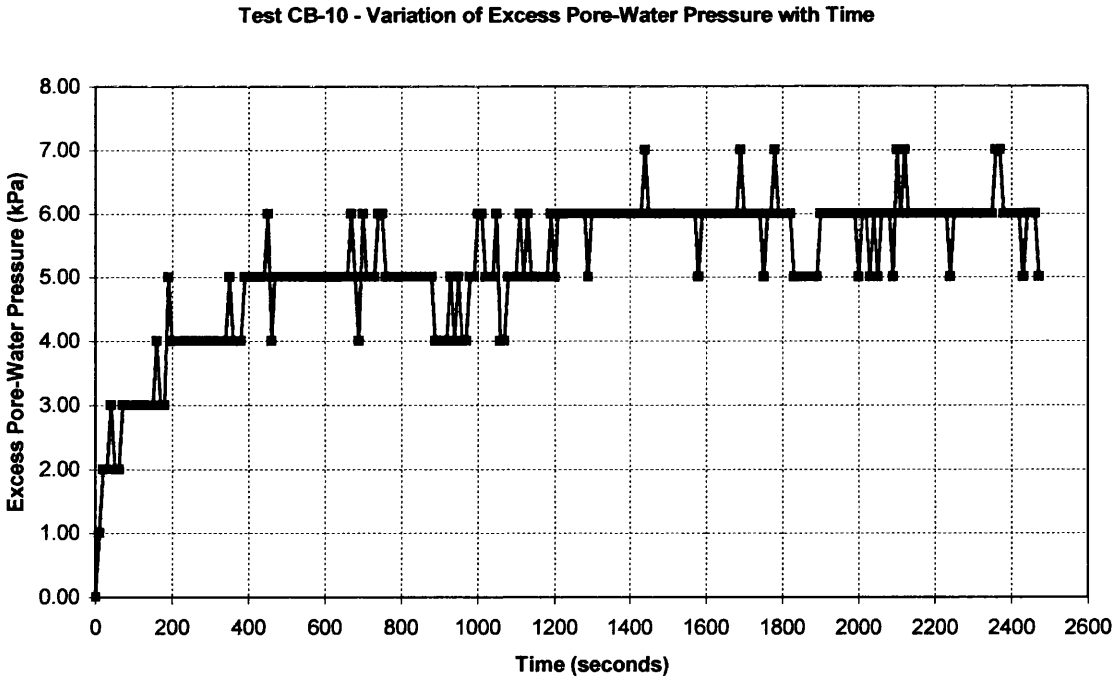

Figure 4.78 – Variation of Excess Pore-Water Pressure with Time [Test CB-10]

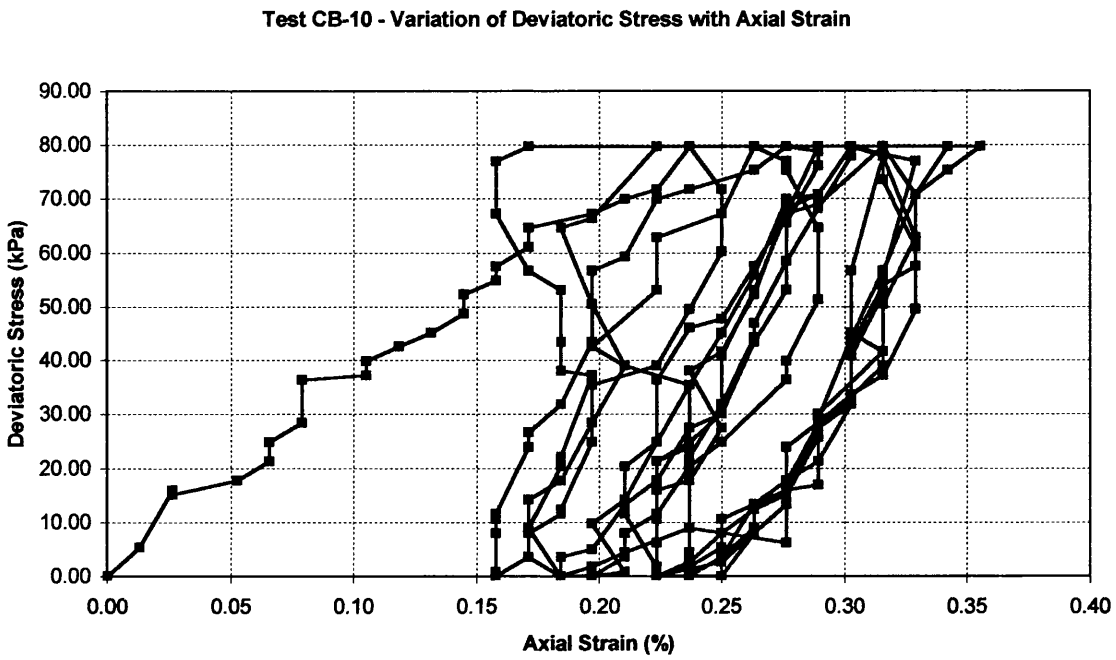

Figure 4.79 *– Variation of Deviatoric Stress with Axial Strain [Test CB-10]*

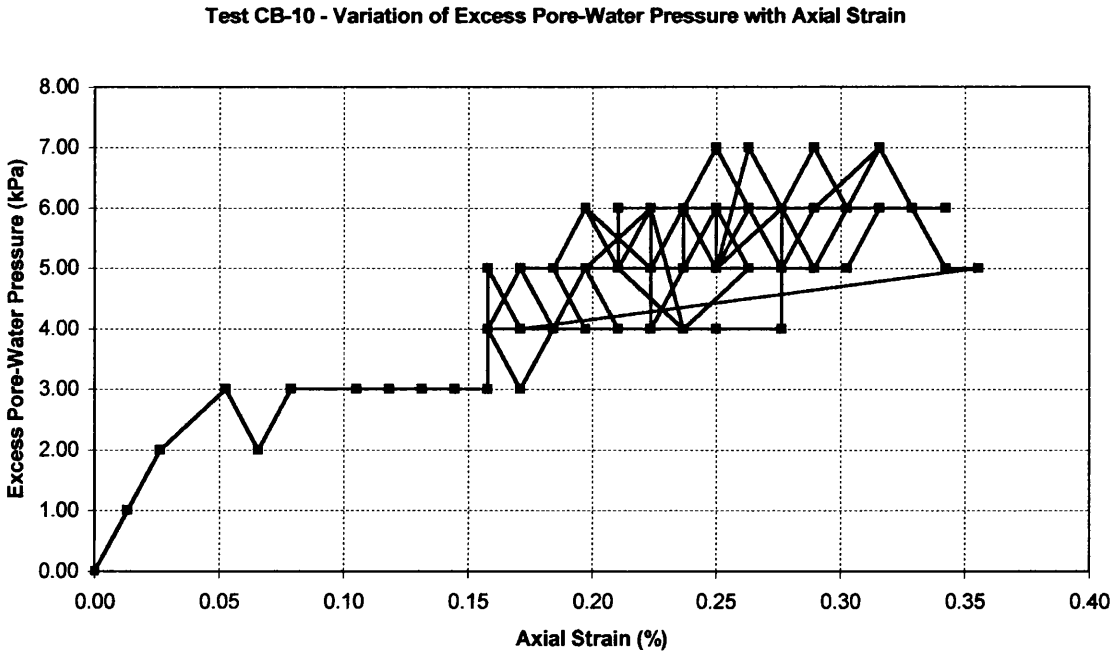

Figure 4.80 *– Variation of Excess Pore-Water Pressure with Axial Strain [Test CB-10]*

4.3 TRIAXIAL TESTS EMPLOYING CYCLES OF 100 kPa

4.3.1 Introduction

This Section reports the results from cyclic triaxial tests (100 kPa cycles) conducted on loose Hostun sand. The experimental procedure has been outlined previously in this Chapter, and will not be repeated here. The manner in which the results are reported is outlined in Section 4.1, prior to the results of the 60 kPa-cycle tests being presented.

Eight tests were conducted using 100 kPa cycles. The test conditions are tabulated below. Note that Test CB-6 was aborted due to investigator error. Test CC-1 was used as a 'dummy' run for the main test programme.

Test No.	Backpressure (kPa) / duration (min.)	Cycles
CC-2	350 kPa / 60 minutes	10
CC-3	300 kPa / 60 minutes	10
CC-4	250 kPa / 60 minutes	10
CC-5	200 kPa / 60 minutes	10
CC-7	150 kPa / 60 minutes	10
CC-8	100 kPa / 60 minutes	10
CC-9	50 kPa / 60 minutes	10
CC-10	0 kPa / 0 minutes	10

Table 4.19 *– Details of Test Programme for 100 kPa Cycles*

In order to maintain continuity and facilitate the understanding of the principles presented, the results in this Section are reported in an identical manner to those in both Section 4.1 and Section 4.2.

4.3.2 Test No. CC-2

Quantity	Value
Test Number / Type	CC-2 / Stress-controlled
Backpressure value	350 kPa, applied for 1 hour
B-parameter	Some variation between 0.99 and 1.00
Moisture Content, w	0.3794
Initial Degree of Saturation, S_{r0}	0.9984
Bulk Density, ρ	1793 kg/m^3
Unit Weight, γ	17.589 kN/m^3

Table 4.20 *– Details of Test CC-2 Specimen Parameters*

Notes:

- Max. excess pore-water pressure after 10 cycles = 50 kPa (i.e. $r_{0,10} = 0.50$)
- Axial strain at the end of 10 cycles = 2.33 %
- Cycles produce axial strains between 1.10 % and 2.40 %
- Test ended after 2370 seconds.

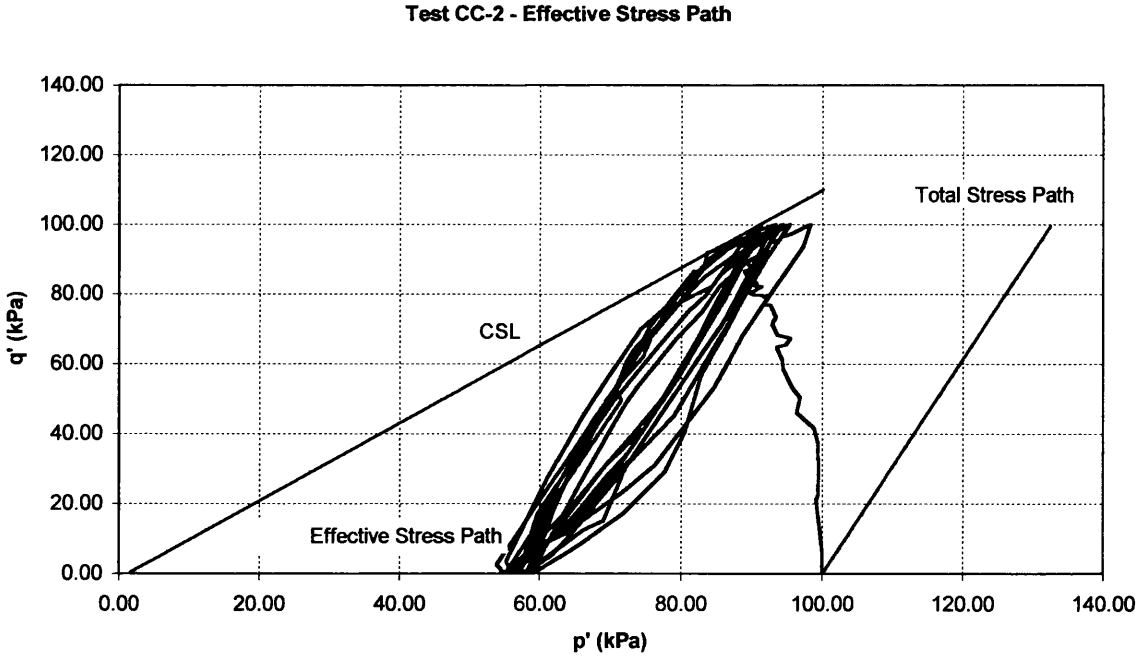

Figure 4.81 *– Effective Stress Path [Test CC-2]*

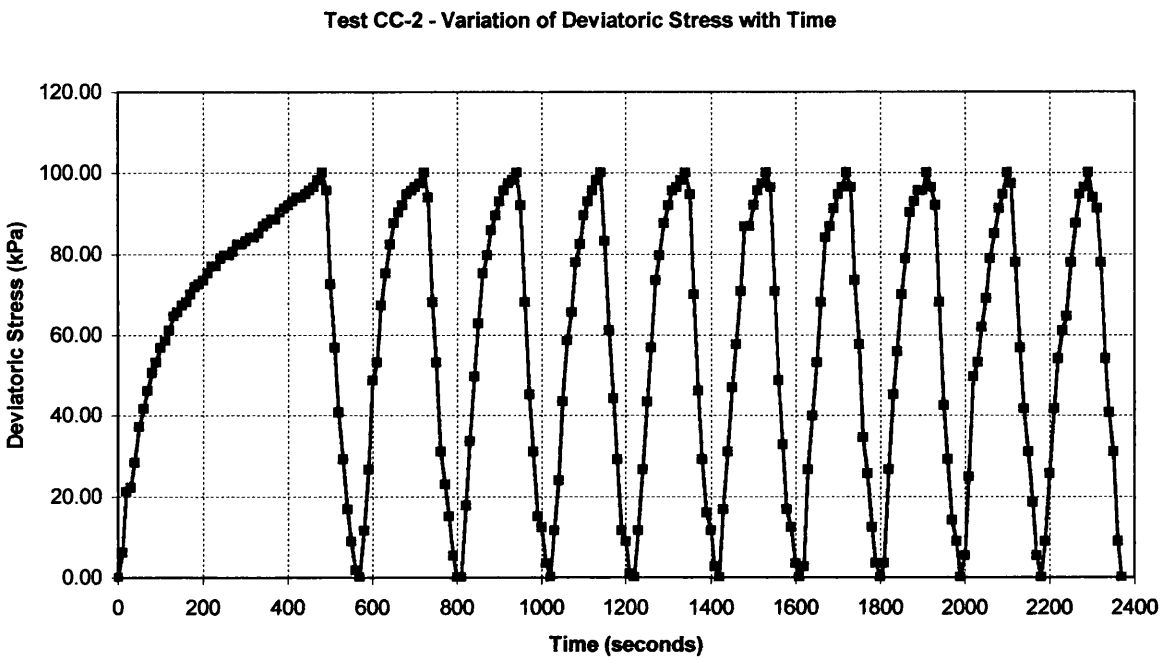

Figure 4.82 *– Variation of Deviatoric Stress with Time [Test CC-2]*

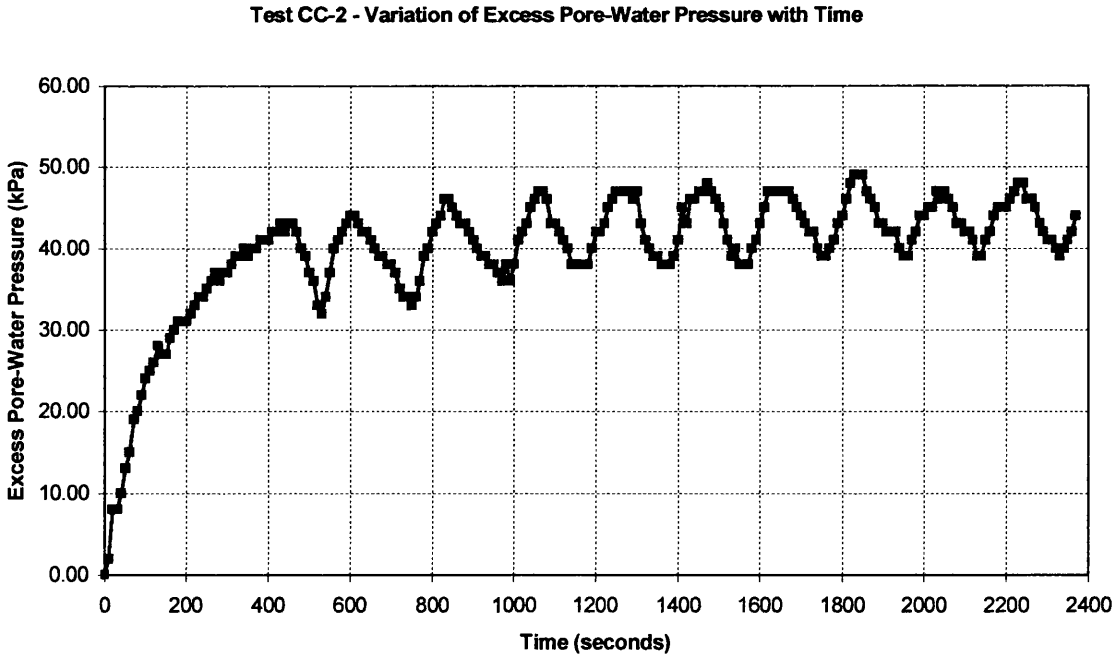

Figure 4.83 *– Variation of Excess Pore-Water Pressure with Time [Test CC-2]*

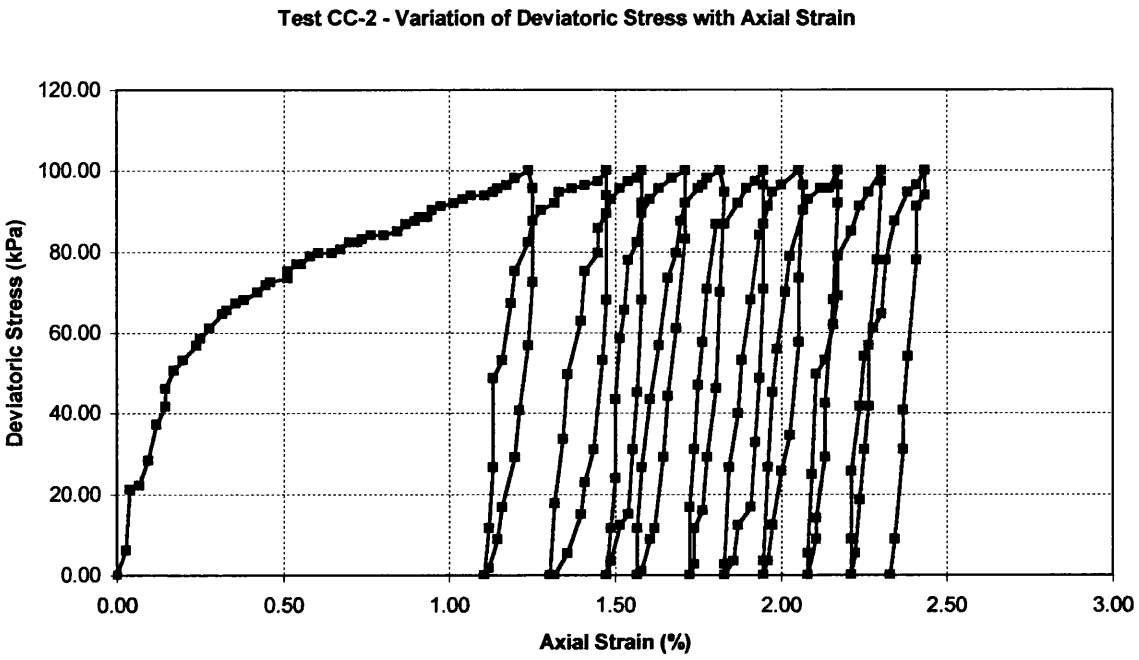

Figure 4.84 *– Variation of Deviatoric Stress with Axial Strain [Test CC-2]*

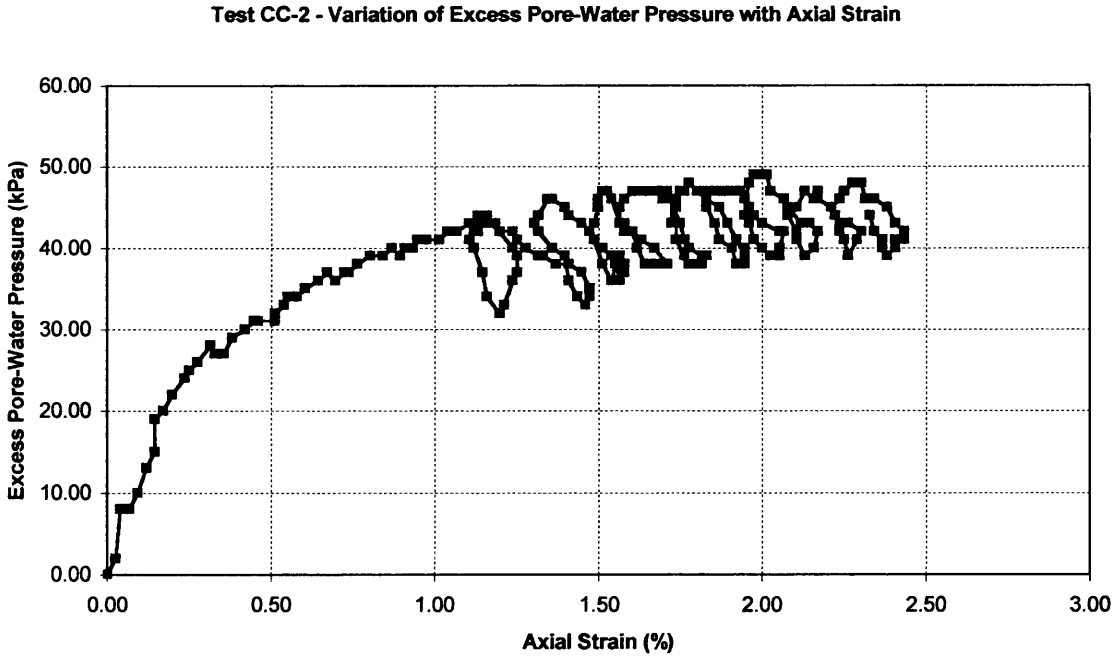

Figure 4.85 *– Variation of Excess Pore-Water Pressure with Axial Strain [Test CC-2]*

4.3.3 Test No. CC-3

Quantity	Value
Test Number / Type	CC-3 / Stress-controlled
Backpressure value	300 kPa, applied for 1 hour
B-parameter	0.95
Moisture Content, w	0.3709
Initial Degree of Saturation, S_{r0}	0.9761
Bulk Density, ρ	1781 kg/m^3
Unit Weight, γ	17.472 kN/m^3

Table 4.21 *– Details of Test CC-3 Specimen Parameters*

Notes:

- Max. excess pore-water pressure after 10 cycles = 28 kPa (i.e. $r_{0,10} = 0.28$)
- Axial strain at the end of 10 cycles = 0.62 %
- Cycles produce axial strains between 0.39 % and 0.71 %
- Test ended after 3130 seconds.

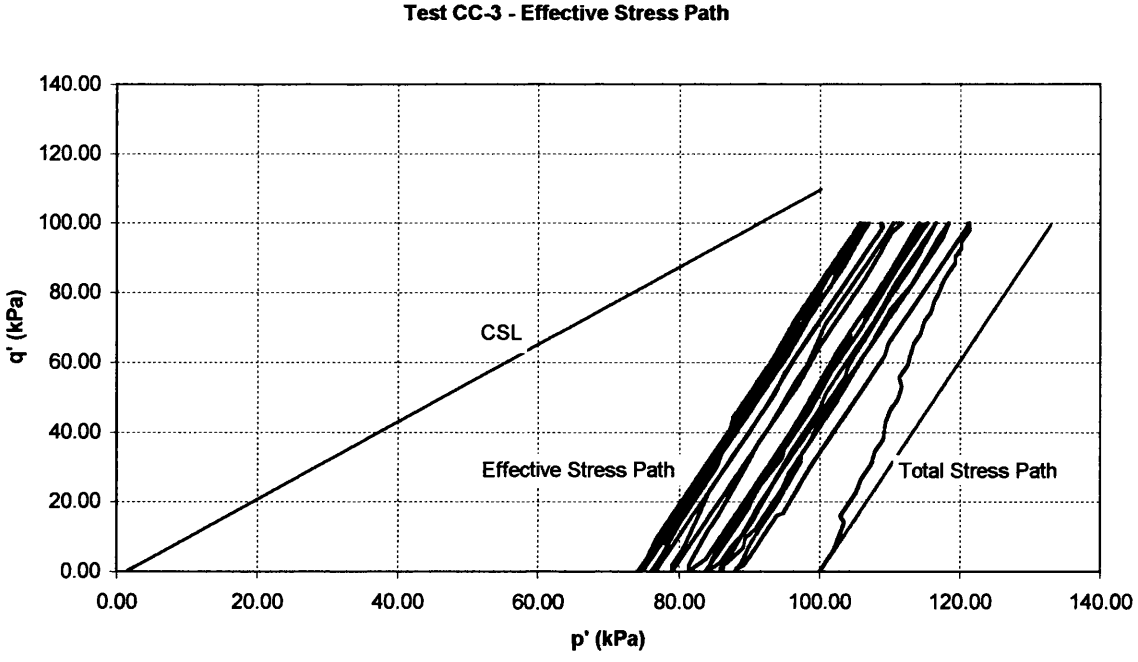

Figure 4.86 *– Effective Stress Path [Test CC-3]*

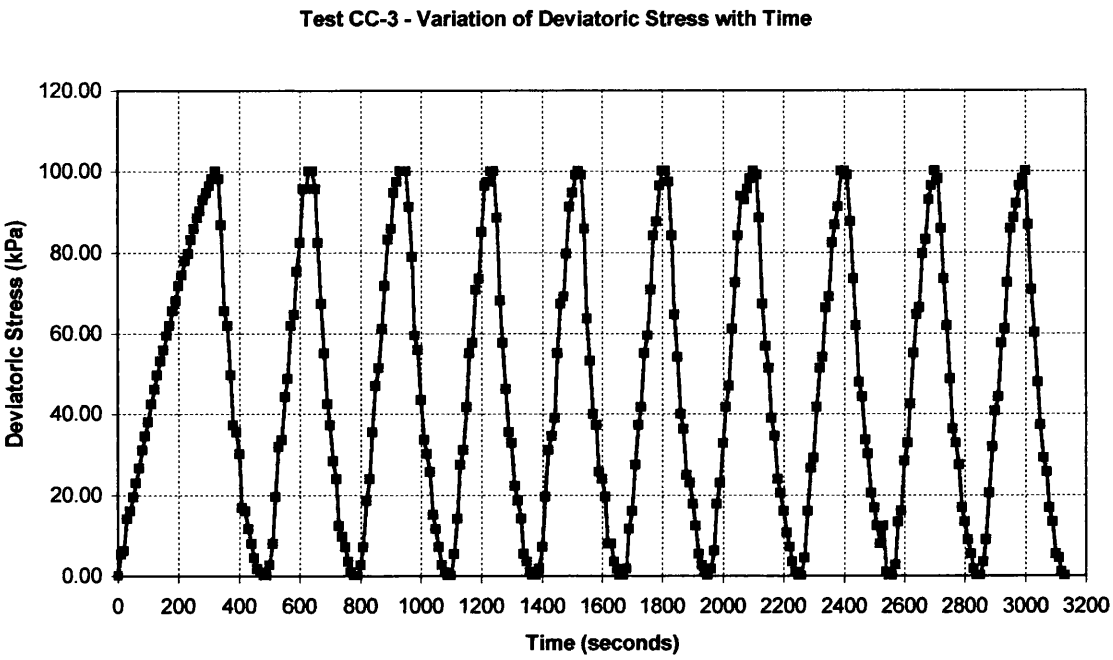

Figure 4.87 – Variation of Deviatoric Stress with Time [Test CC-3]

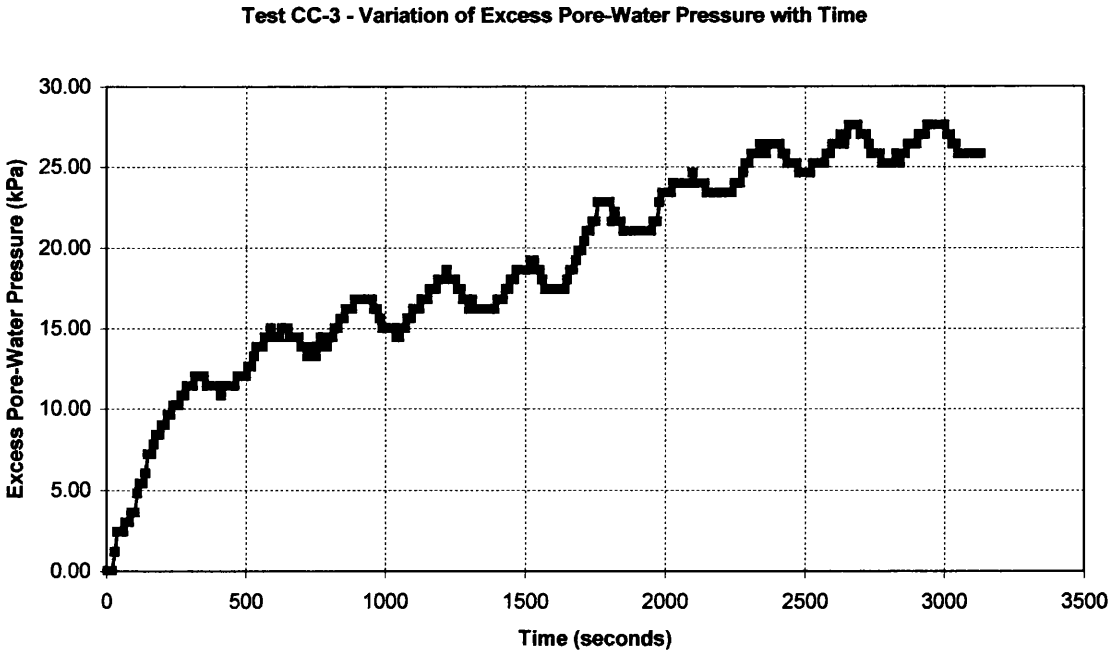

Figure 4.88 – Variation of Excess Pore-Water Pressure with Time [Test CC-3]

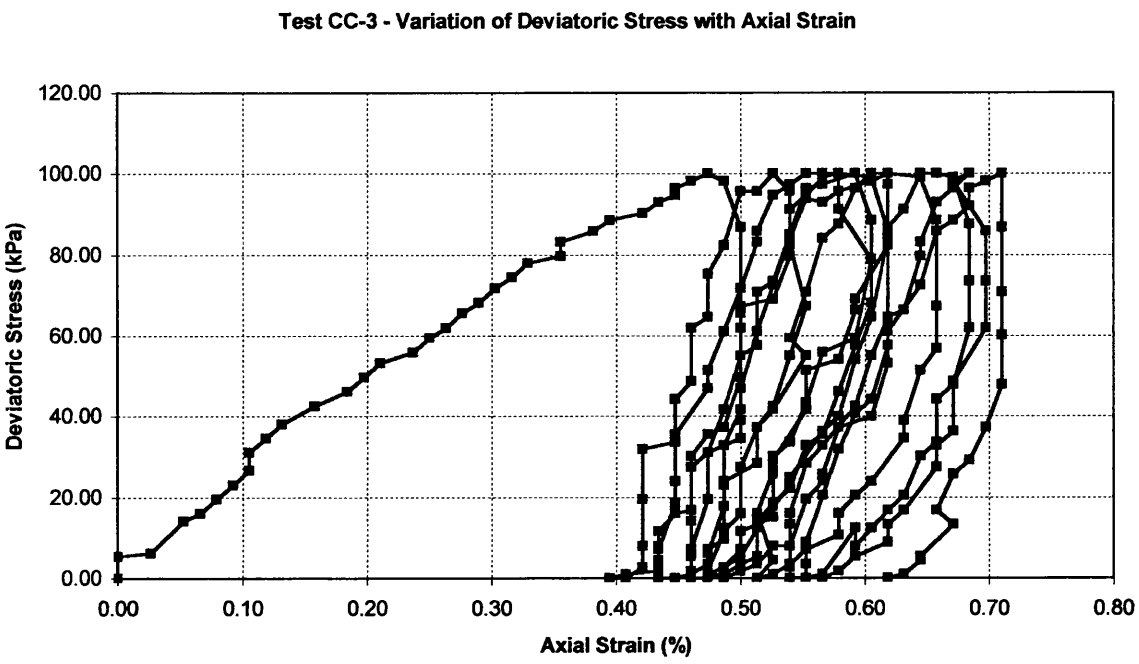

Figure 4.89 *– Variation of Deviatoric Stress with Axial Strain [CC-3]*

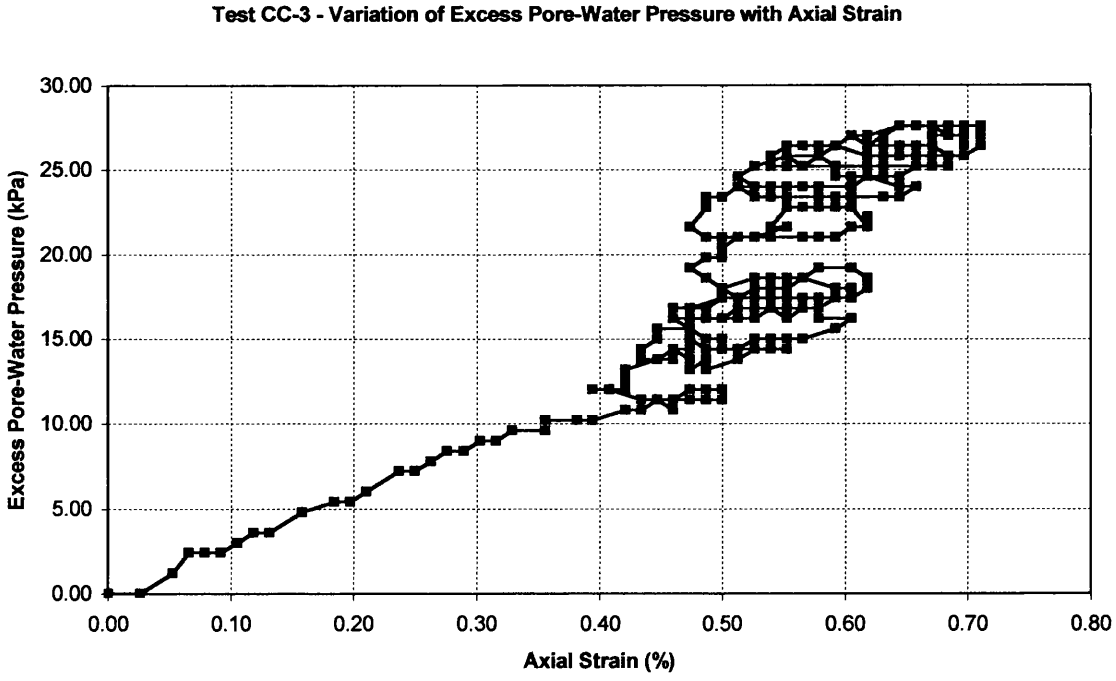

Figure 4.90 *– Variation of Excess Pore-Water Pressure with Axial Strain [CC-3]*

4.3.4 Test No. CC-4

Quantity	Value
Test Number / Type	CC-4 / Stress-controlled
Backpressure value	250 kPa, applied for 1 hour
B-parameter	0.90
Moisture Content, w	0.3666
Initial Degree of Saturation, S_{r0}	0.9647
Bulk Density, ρ	1776 kg/m^3
Unit Weight, γ	17.423 kN/m^3

***Table 4.22** – Details of Test CC-4 Specimen Parameters*

Notes:

- Max. excess pore-water pressure after 10 cycles = 23 kPa (i.e. $r_{0,10} = 0.23$)
- Axial strain at the end of 10 cycles = 0.51 %
- Cycles produce axial strains between 0.39 % and 0.61 %
- Test ended after 2710 seconds.

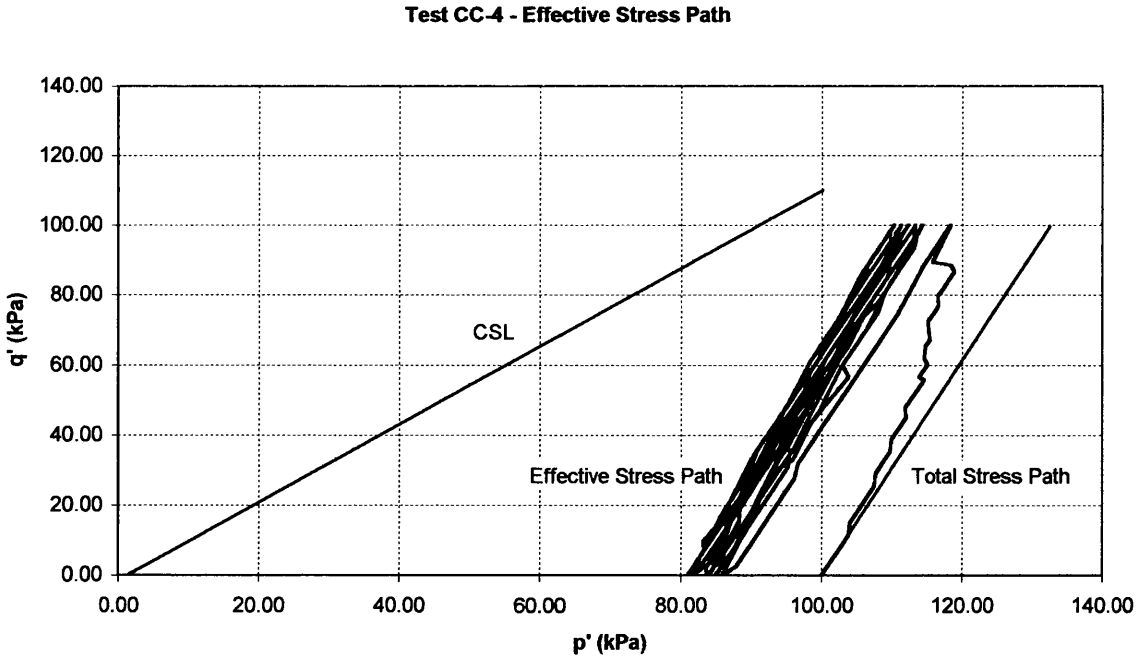

***Figure 4.91** – Effective Stress Path [Test CC-4]*

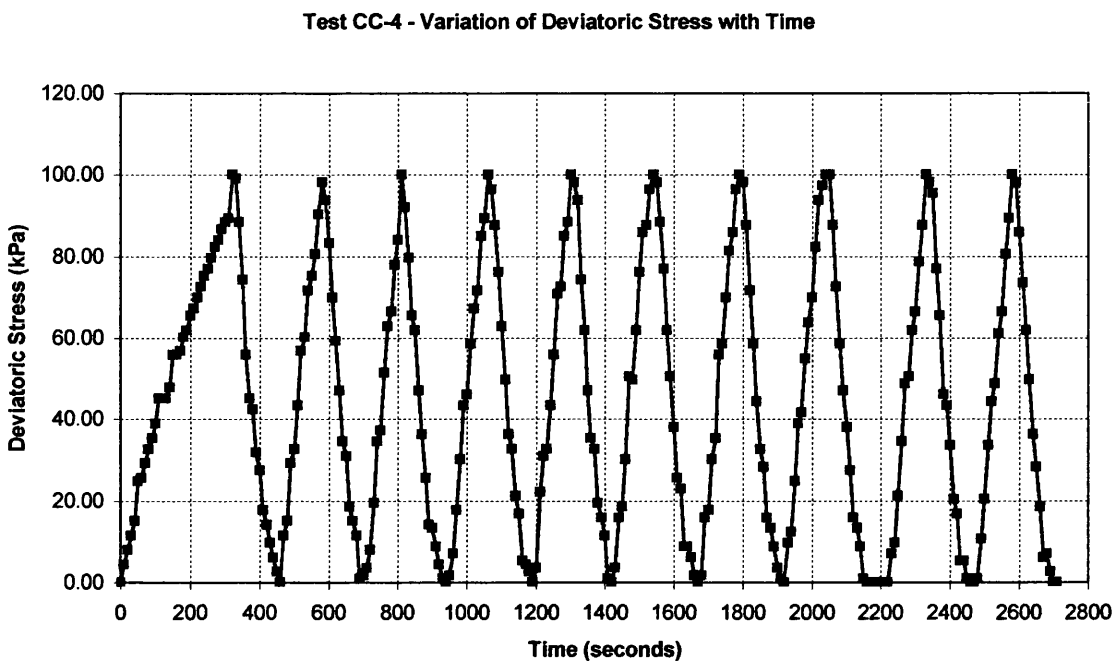

Figure 4.92 *– Variation of Deviatoric Stress with Time [Test CC-4]*

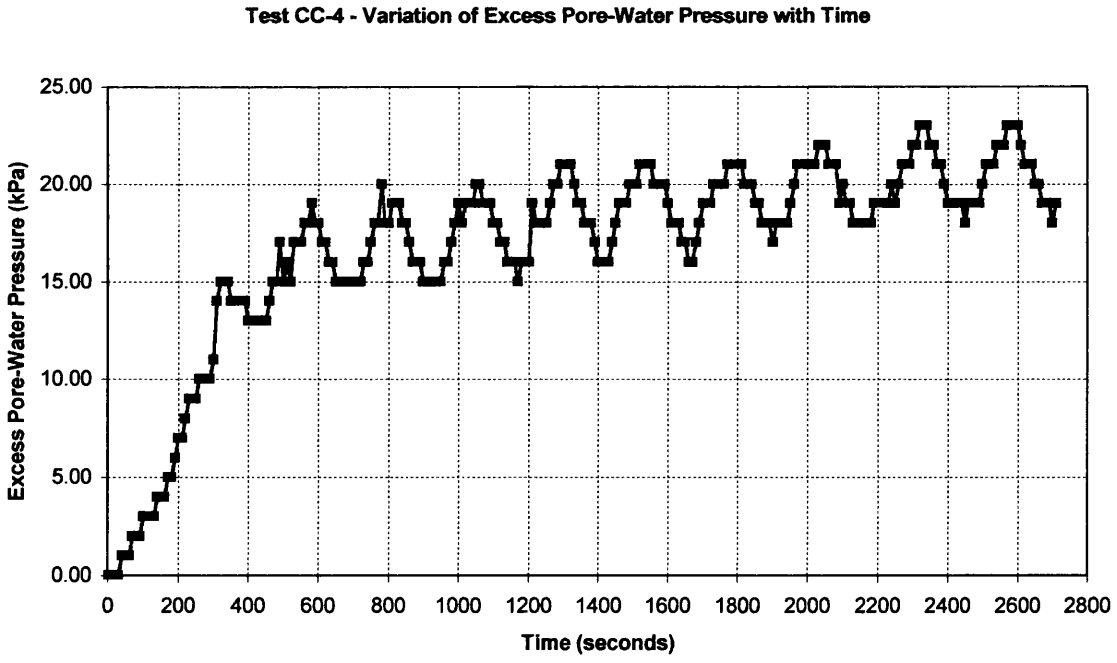

Figure 4.93 *– Variation of Excess Pore-Water Pressure with Time [Test CC-4]*

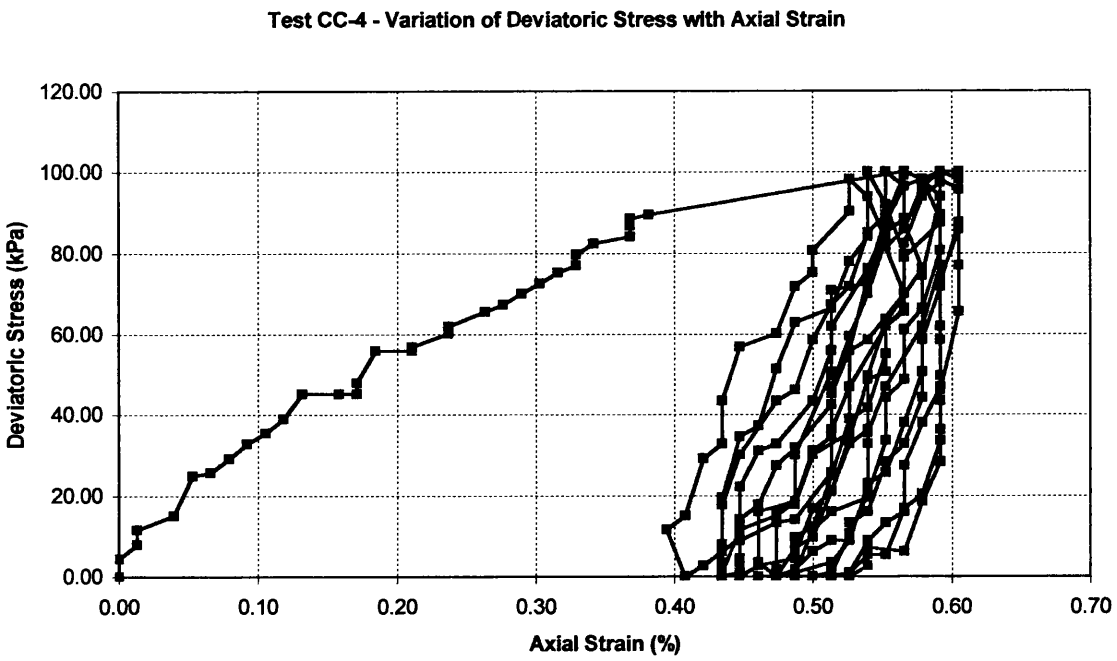

Figure 4.94 *– Variation of Deviatoric Stress with Axial Strain [Test CC-4]*

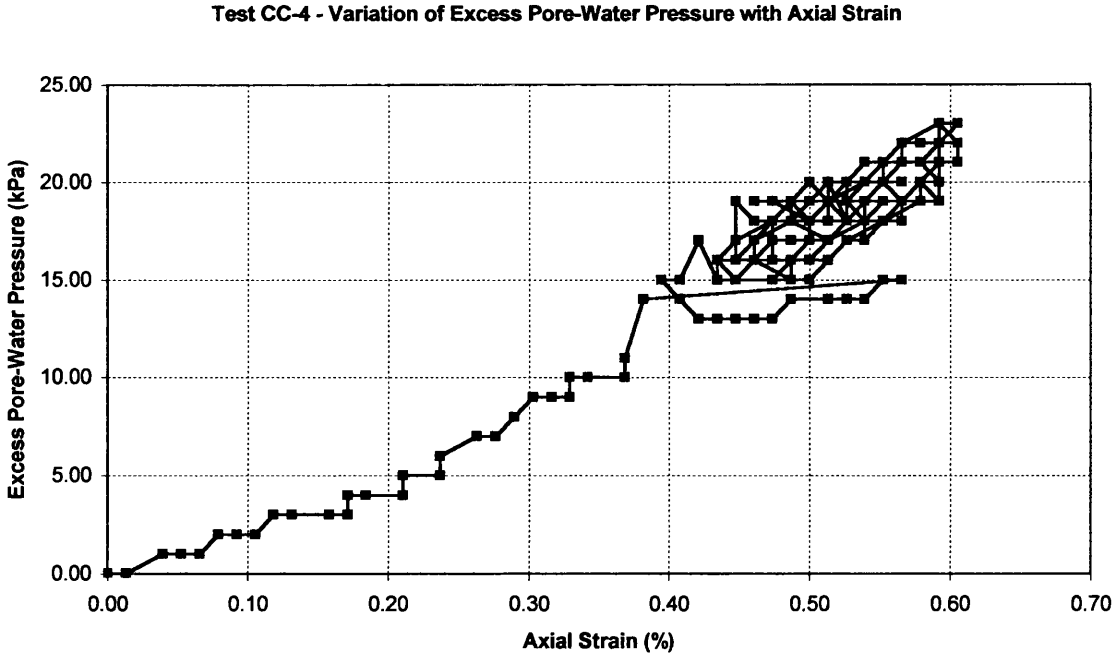

Figure 4.95 *– Variation of Excess Pore-Water Pressure with Axial Strain [Test CC-4]*

4.3.5 Test No. CC-5

Quantity	Value
Test Number / Type	CC-5 / Stress-controlled
Backpressure value	200 kPa, applied for 1 hour
B-parameter	Some variation between 0.86 and 0.87
Moisture Content, w	0.3637
Initial Degree of Saturation, S_{r0}	0.9571
Bulk Density, ρ	1776 kg/m^3
Unit Weight, γ	17.423 kN/m^3

Table 4.23 *– Details of Test CC-5 Specimen Parameters*

Notes:

- Max. excess pore-water pressure after 10 cycles = 16 kPa (i.e. $r_{0,10} = 0.16$)
- Axial strain at the end of 10 cycles = 0.30 %
- Cycles produce axial strains between 0.23 % and 0.41 %
- Test ended after 2520 seconds.

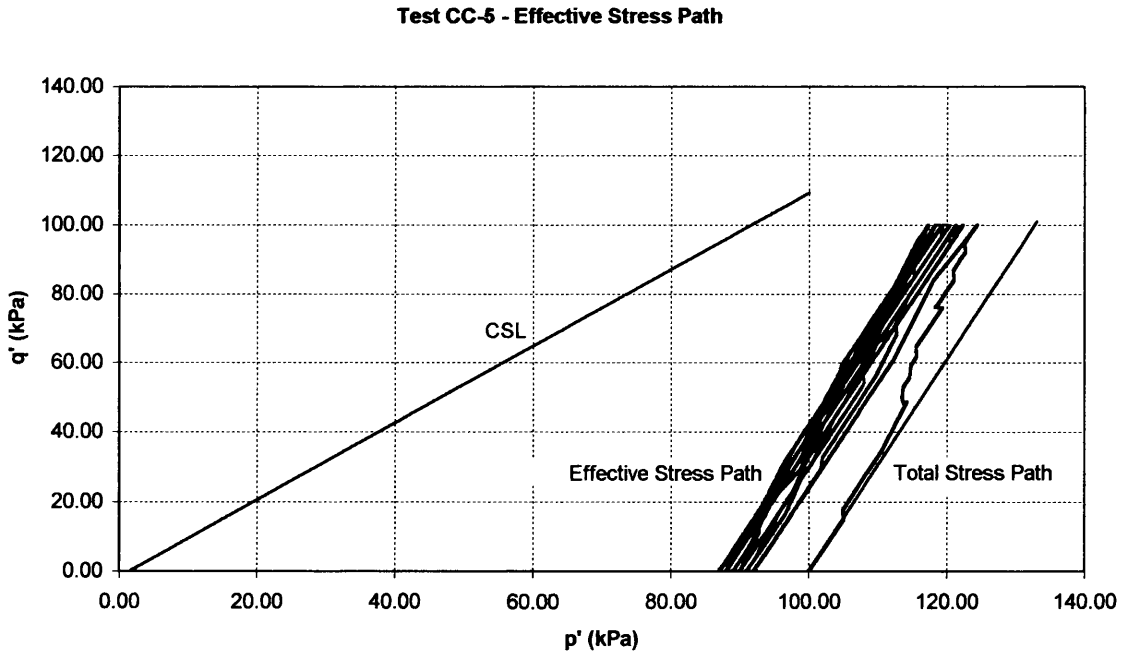

Figure 4.96 *– Effective Stress Path [Test CC-5]*

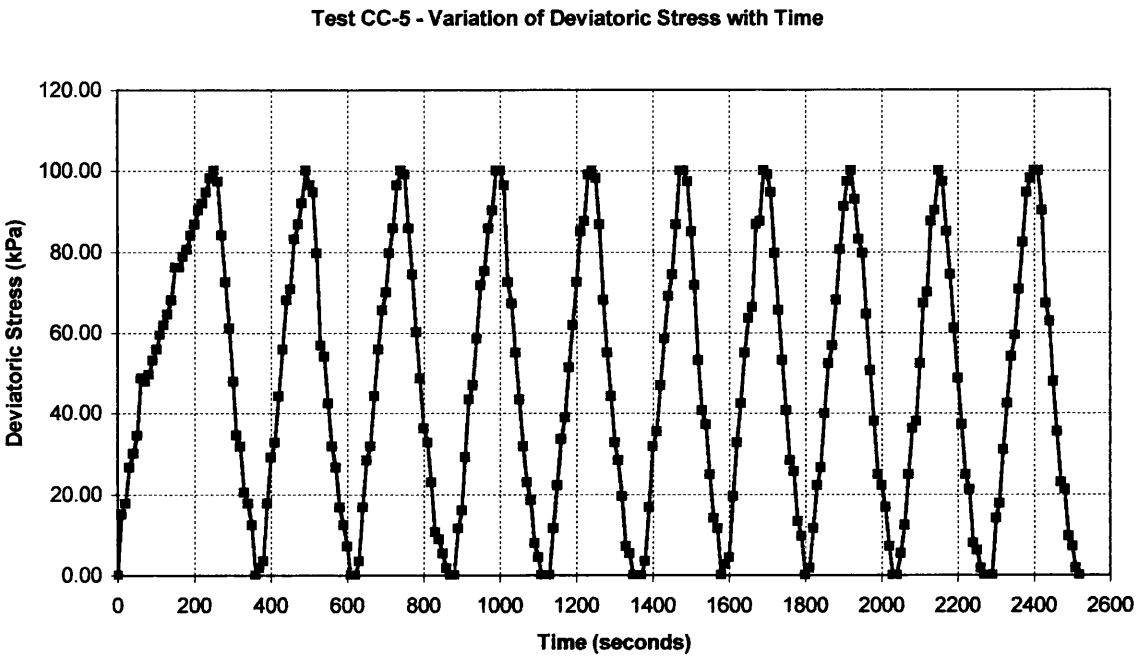

Figure 4.97 – Variation of Deviatoric Stress with Time [Test CC-5]

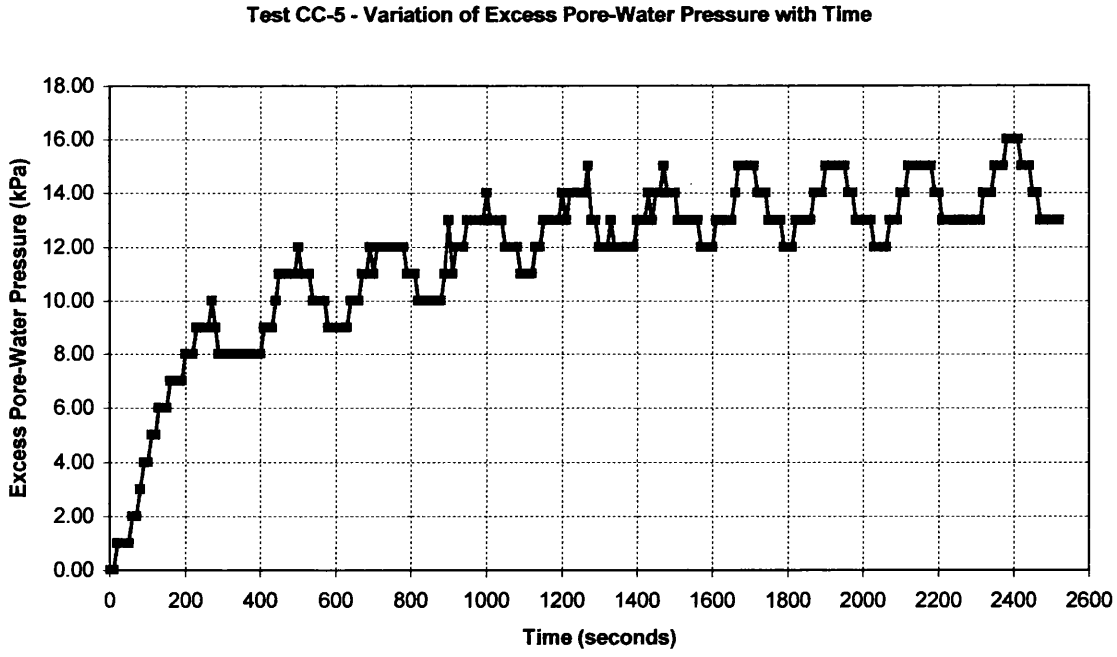

Figure 4.98 – Variation of Excess Pore-Water Pressure with Time [Test CC-5]

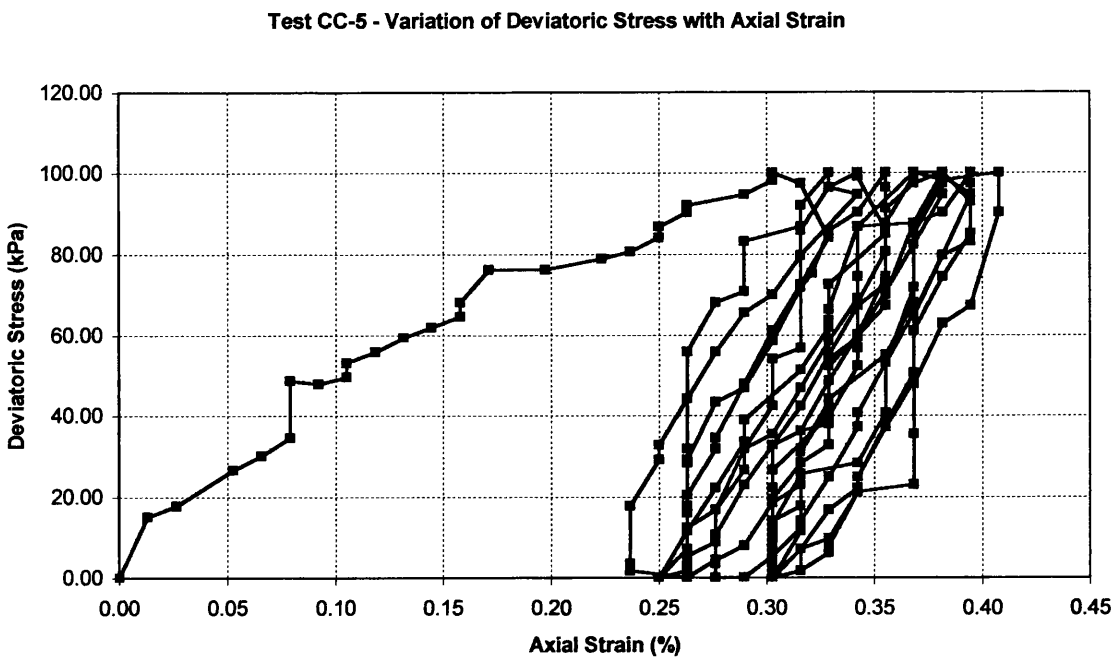

Figure 4.99 *– Variation of Deviatoric Stress with Axial Strain [Test CC-5]*

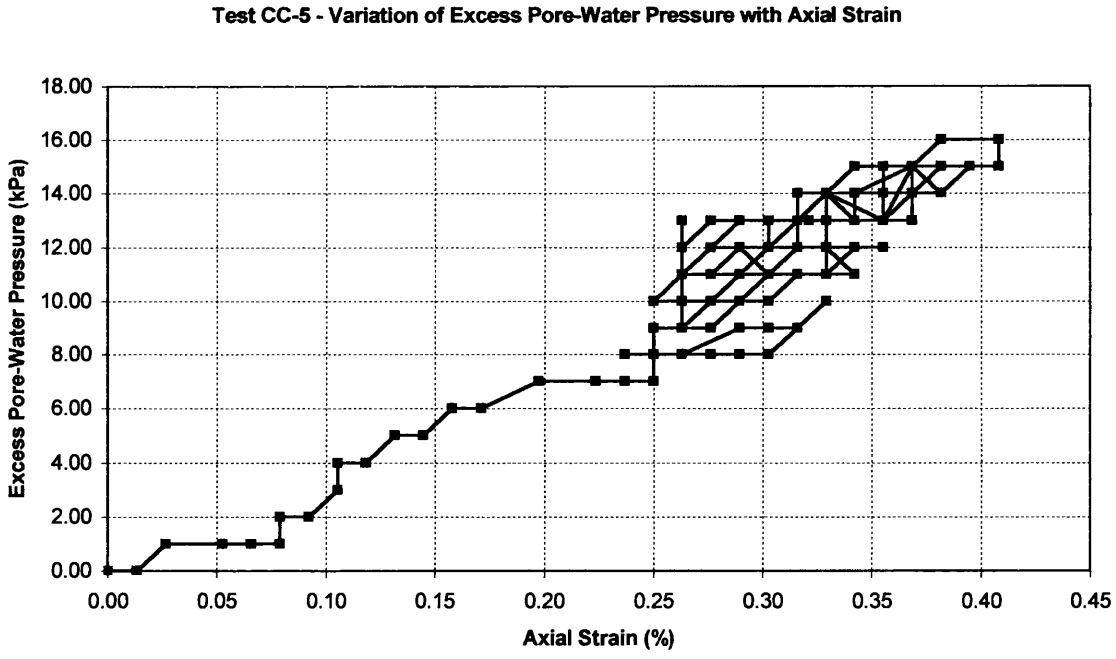

Figure 4.100 *– Variation of Excess Pore-Water Pressure with Axial Strain [Test CC-5]*

4.3.6 Test No. CC-7

Quantity	Value
Test Number / Type	CC-7 / Stress-controlled
Backpressure value	150 kPa, applied for 1 hour
B-parameter	Some variation between 0.83 and 0.84
Moisture Content, w	0.3598
Initial Degree of Saturation, S_{r0}	0.9468
Bulk Density, ρ	1767 kg/m^3
Unit Weight, γ	17.334 kN/m^3

Table 4.24 *– Details of Test CC-7 Specimen Parameters*

Notes:

- Max. excess pore-water pressure after 10 cycles = 14 kPa (i.e. $r_{0,10} = 0.14$)
- Axial strain at the end of 10 cycles = 0.38 %
- Cycles produce axial strains between 0.29 % and 0.50 %
- Test ended after 2560 seconds.

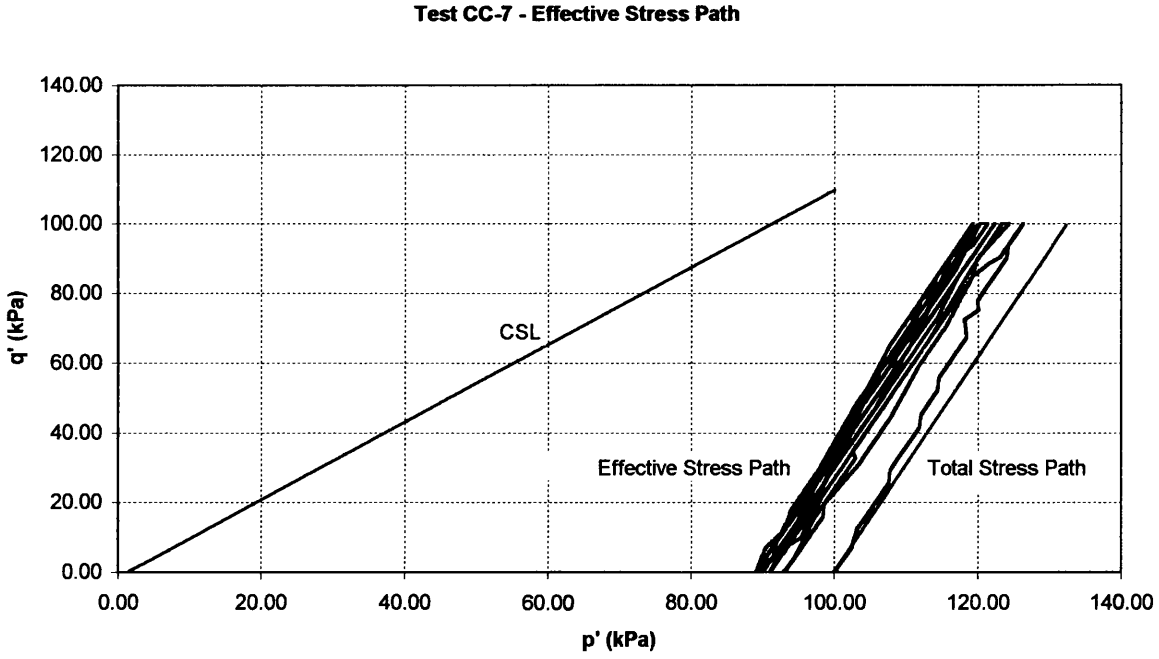

Figure 4.101 *– Effective Stress Path [Test CC-7]*

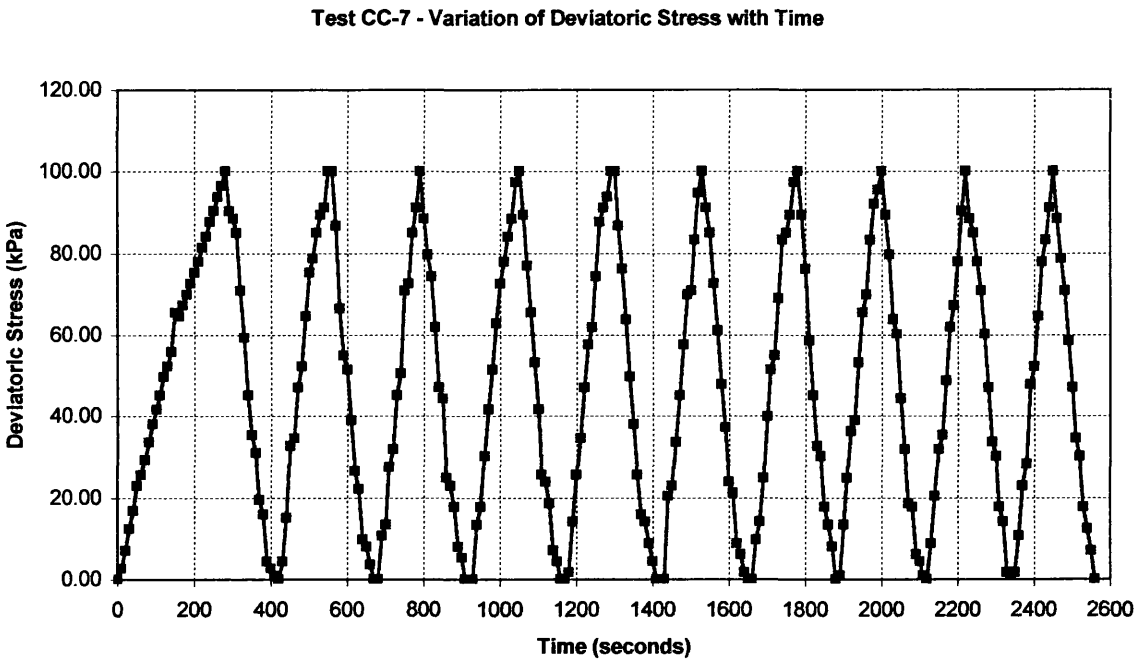

Figure 4.102 *– Variation of Deviatoric Stress with Time [Test CC-7]*

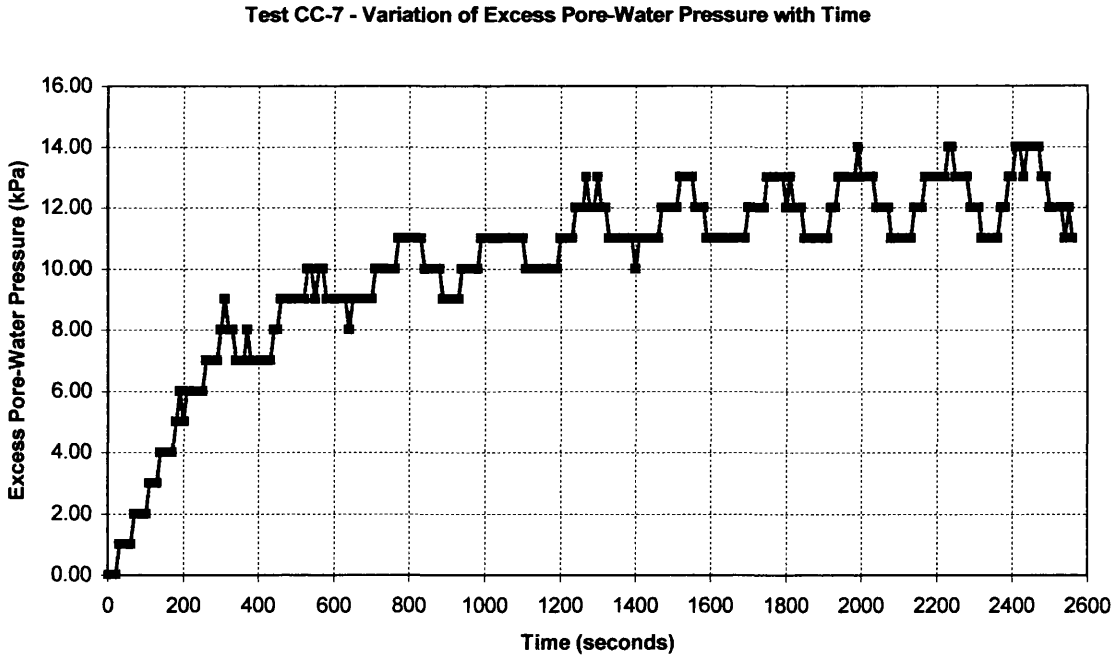

Figure 4.103 *– Variation of Excess Pore-Water Pressure with Time [Test CC-7]*

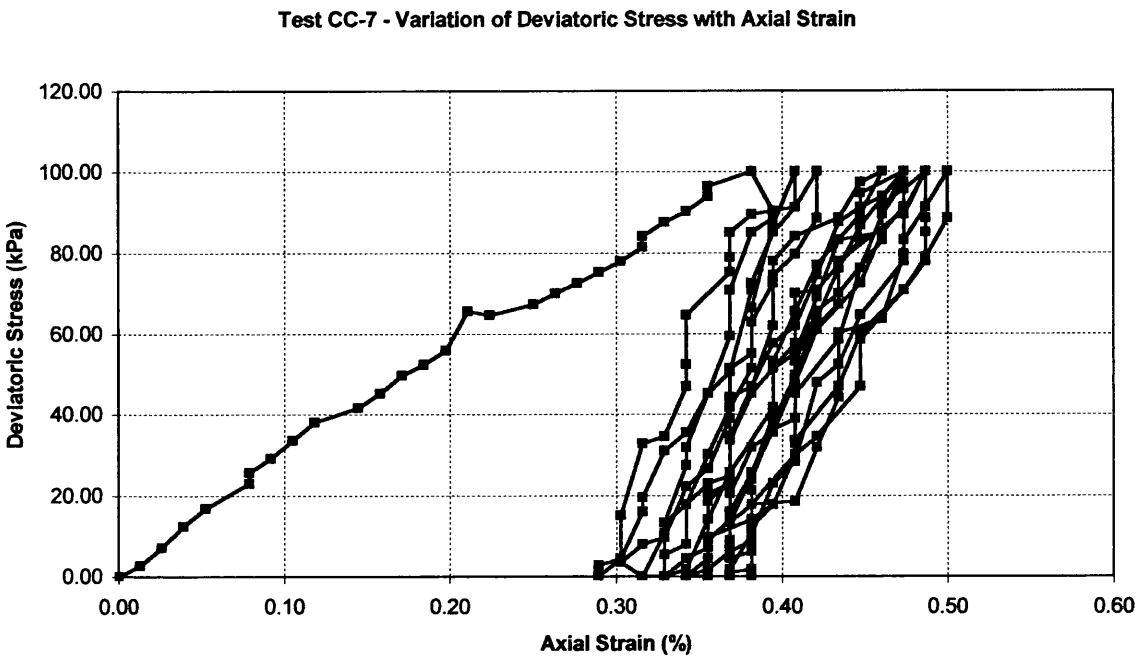

Figure 4.104 – Variation of Deviatoric Stress with Axial Strain [Test CC-7]

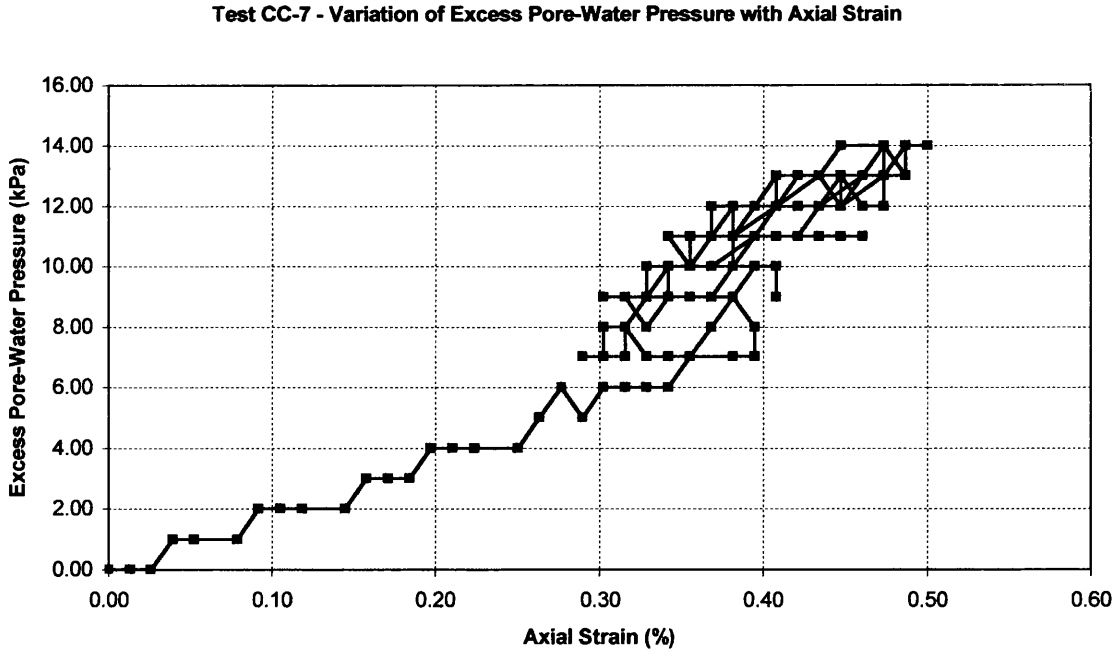

Figure 4.105 – Variation of Excess Pore-Water Pressure with Axial Strain [Test CC-7]

4.3.7 Test No. CC-8

Quantity	Value
Test Number / Test	CC-8 / Stress-controlled
Backpressure value	100 kPa, applied for 1 hour
B-parameter	0.77
Moisture Content, w	0.3573
Initial Degree of Saturation, S_{r0}	0.9403
Bulk Density, ρ	1764 kg/m^3
Unit Weight, γ	17.305 kN/m^3

Table 4.25 *– Details of Test CC-8 Specimen Parameters*

Notes:

- Max. excess pore-water pressure after 10 cycles = 9 kPa (i.e. $r_{0,10} = 0.09$)
- Axial strain at the end of 10 cycles = 0.42 %
- Cycles produce axial strains between 0.22 % and 0.55 %
- Test ended after 3360 seconds.

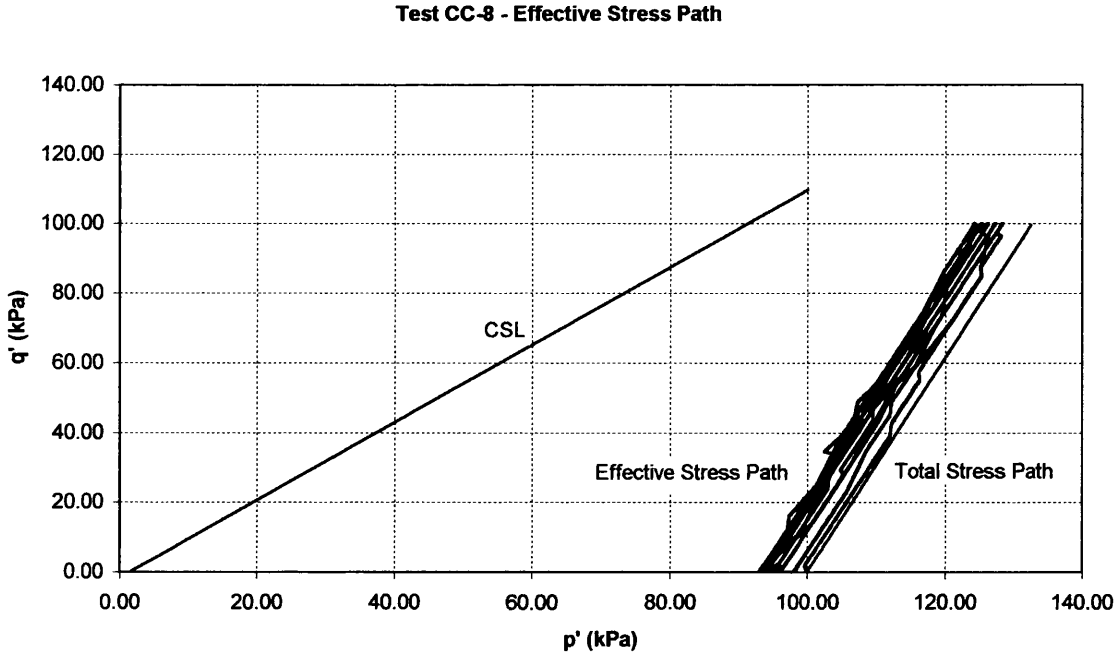

Figure 4.106 *– Effective Stress Path [Test CC-8]*

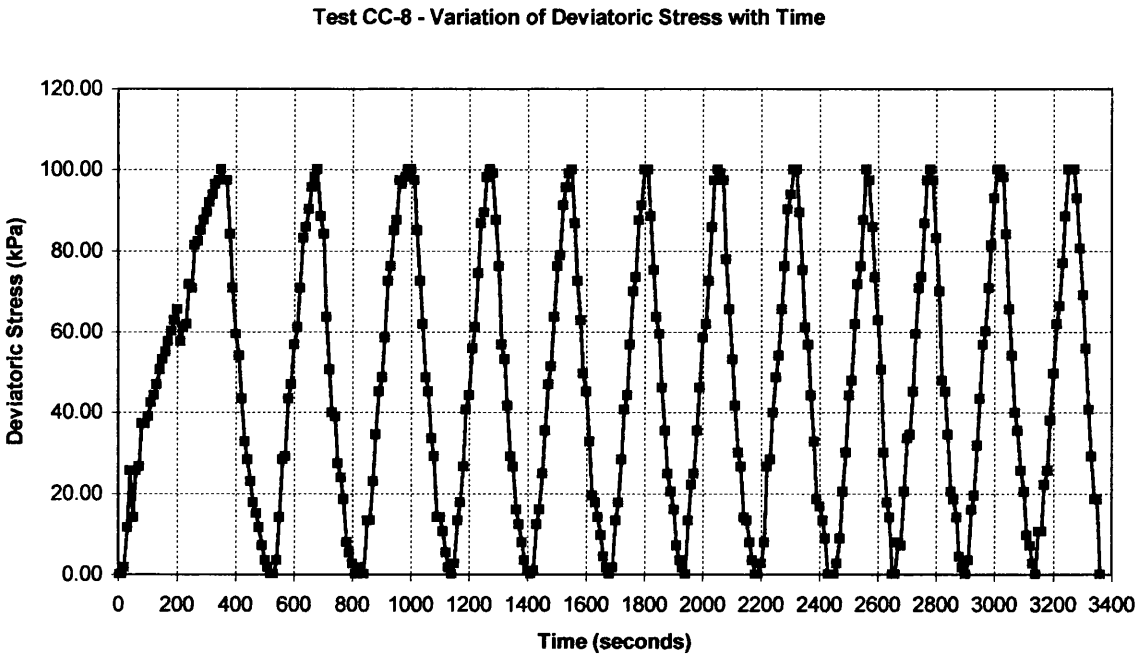

Figure 4.107 *– Variation of Deviatoric Stress with Time [Test CC-8]*

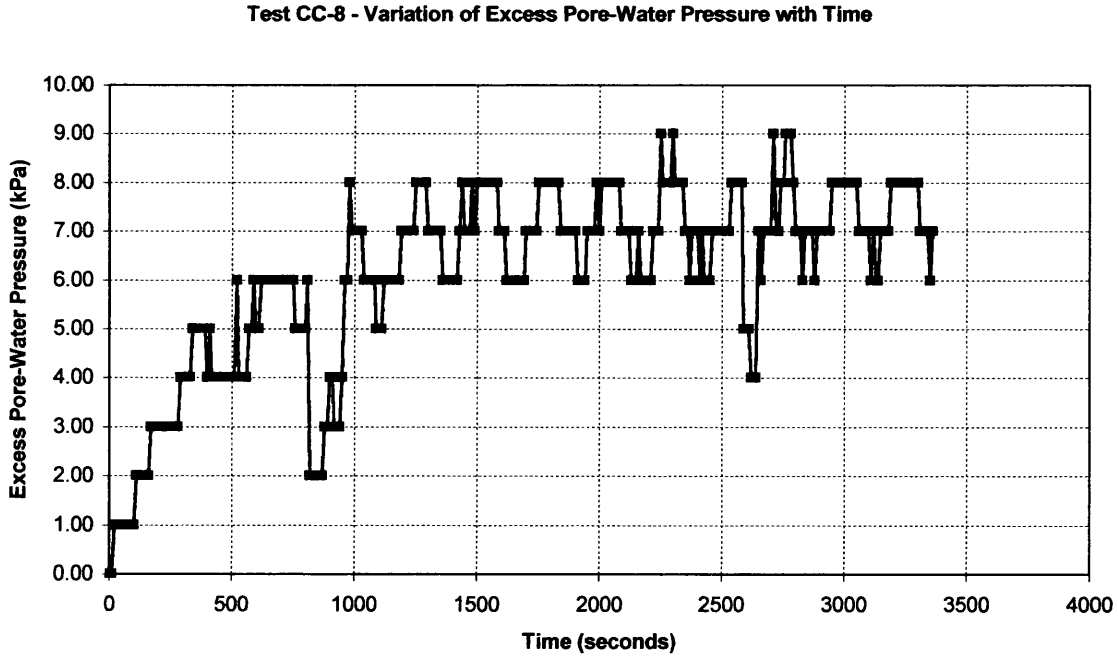

Figure 4.108 *– Variation of Excess Pore-Pressure with Time [Test CC-8]*

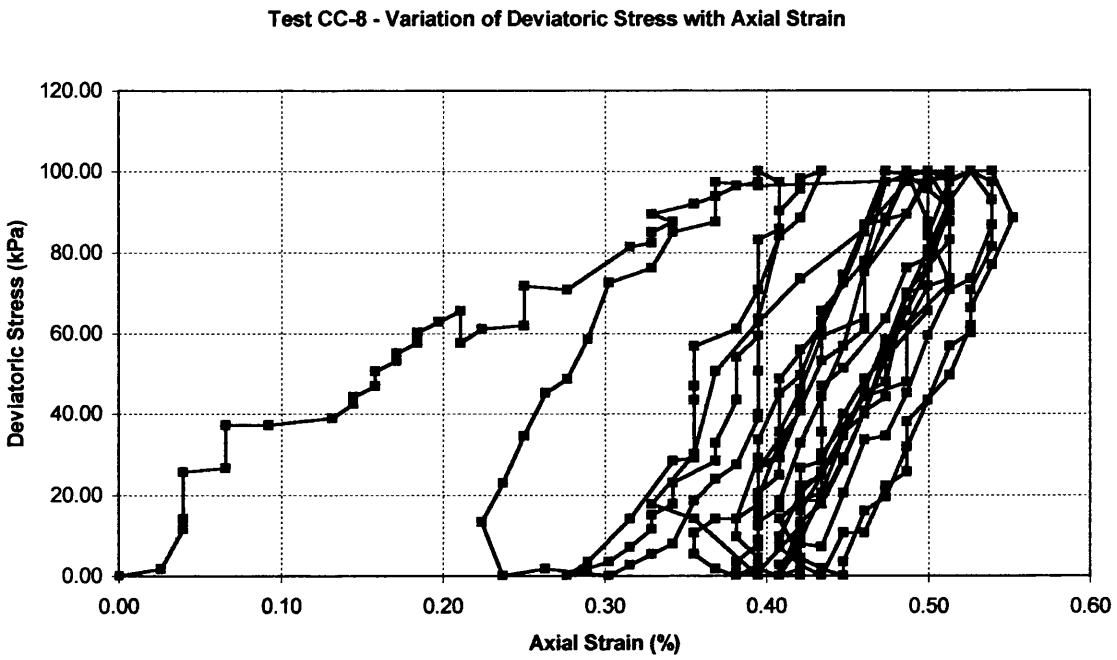

Figure 4.109 *– Variation of Deviatoric Stress with Axial Strain [Test CC-8]*

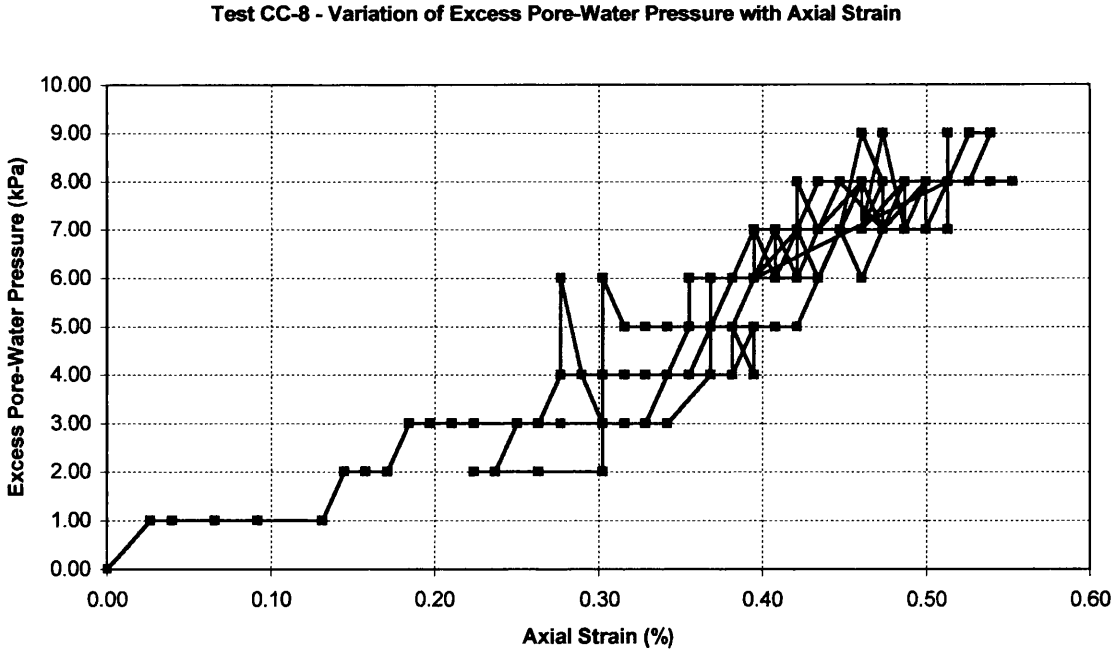

Figure 4.110 *– Variation in Exc. Pore-Water Pressure with Axial Strain [Test CC-8]*

4.3.8 Test No. CC-9

Quantity	Value
Test Number / Type	CC-9 / Stress-controlled
Backpressure value	50 kPa, applied for 1 hour
B-parameter	0.72
Moisture Content, w	0.3470
Initial Degree of Saturation, S_{r0}	0.9132
Bulk Density, ρ	1750 kg/m^3
Unit Weight, γ	17.168 kN/m^3

Table 4.26 *– Details of Test CC-9 Specimen Parameters*

Notes:

- Max. excess pore-water pressure after 10 cycles = 8 kPa (i.e. $r_{0,10} = 0.08$)
- Axial strain at the end of 10 cycles = 0.37 %
- Cycles produce axial strains between 0.29 % and 0.49 %
- Test ended after 2390 seconds.

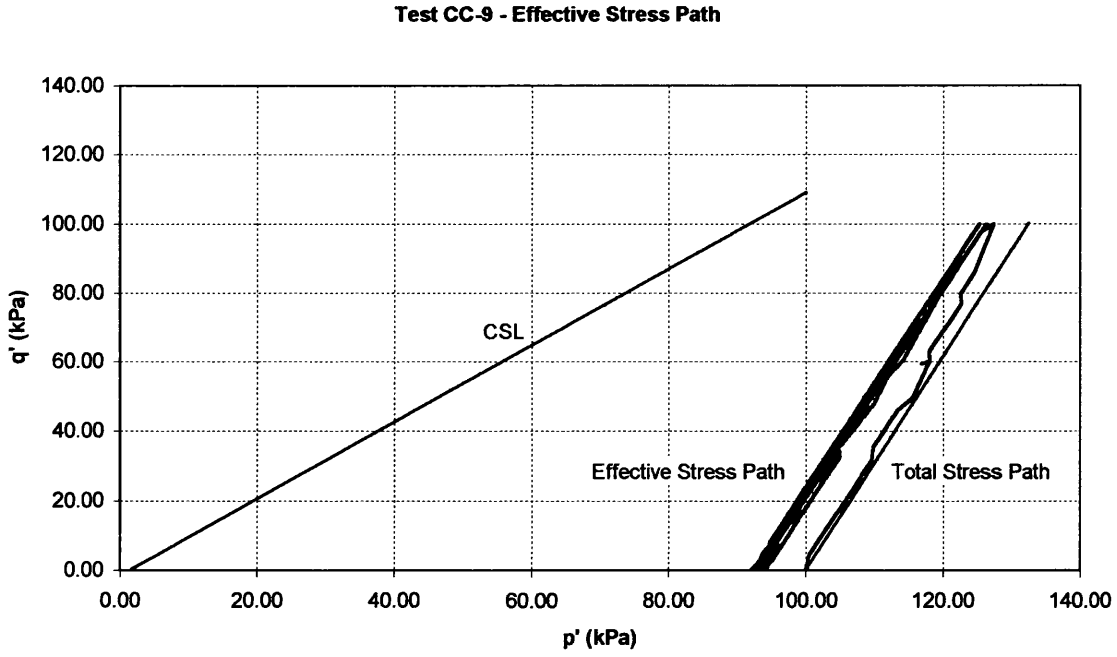

Figure 4.111 *– Effective Stress Path [Test CC-9]*

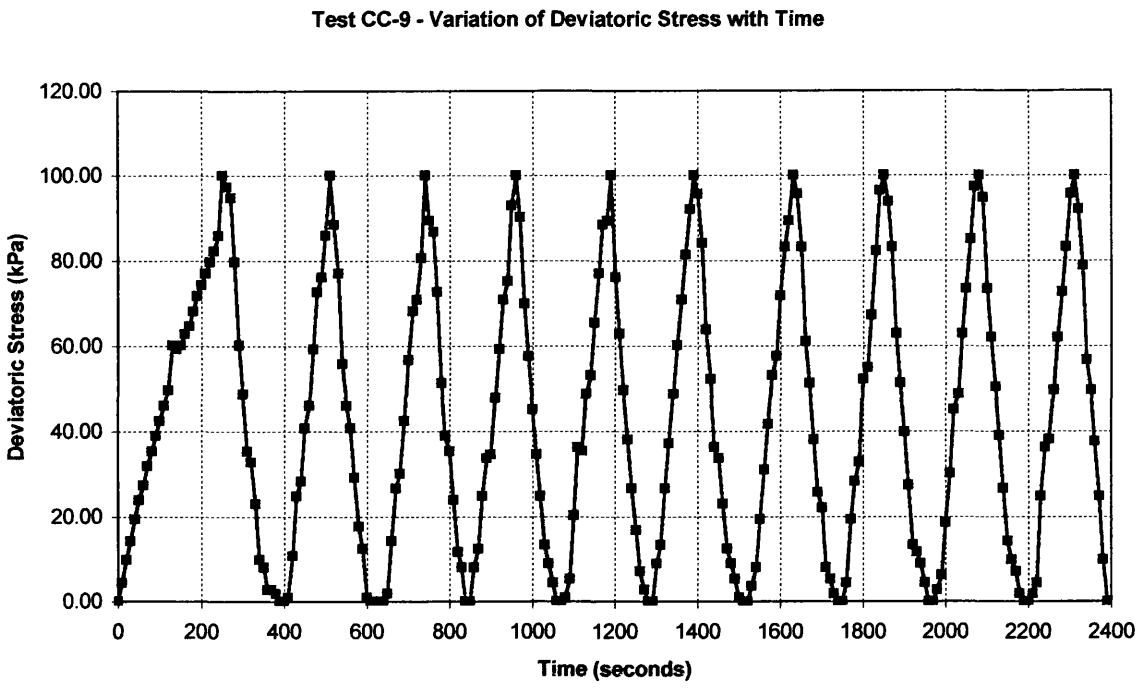

Figure 4.112 – Variation of Deviatoric Stress with Time [Test CC-9]

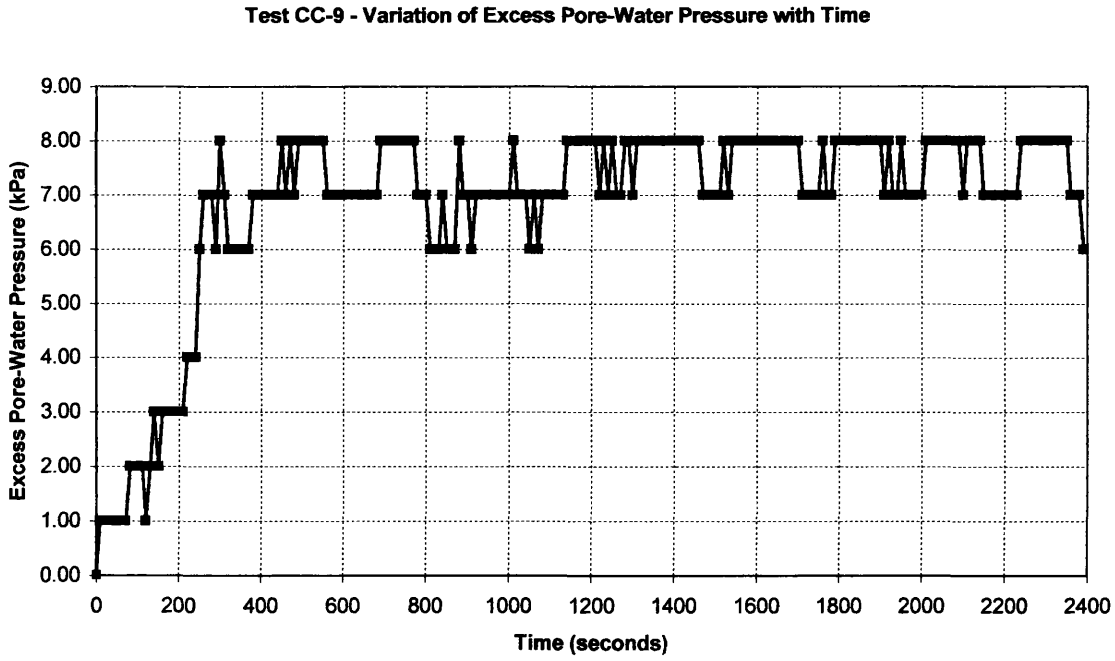

Figure 4.113 – Variation of Excess Pore-Water Pressure with Time [Test CC-9]

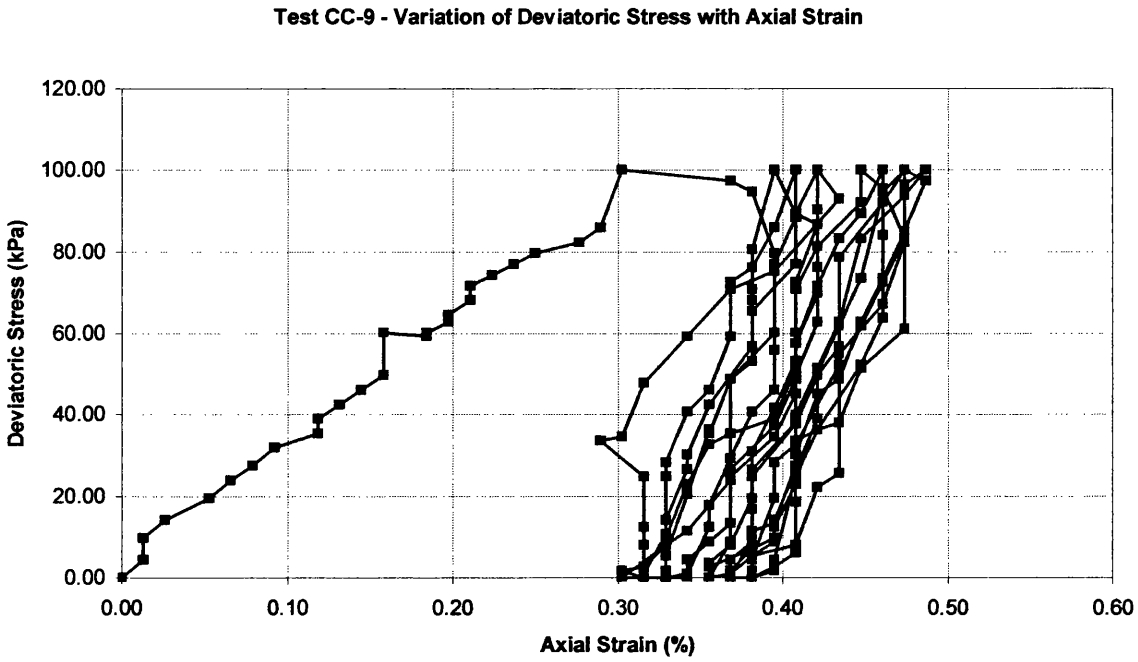

Figure 4.114 – Variation of Deviatoric Stress with Axial Strain [Test CC-9]

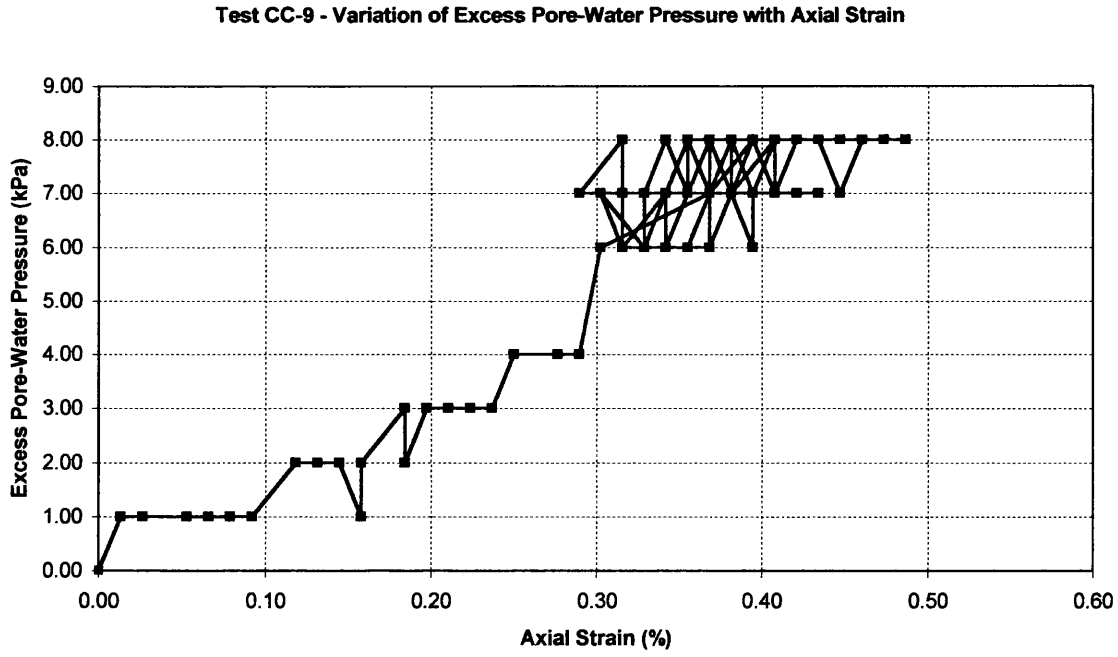

Figure 4.115 – Variation of Excess Pore-Water Pressure with Axial Strain [Test CC-9]

4.3.9 Test No. CC-10

Quantity	Value
Test Number / Type	CC-10 / Stress-controlled
Backpressure value	0 kPa
B-parameter	0.60
Moisture Content, w	0.3466
Initial Degree of Saturation, S_{r0}	0.9121
Bulk Density, ρ	1747 kg/m^3
Unit Weight, γ	17.138 kN/m^3

***Table 4.27** – Details of Test CC-10 Specimen Parameters*

Notes:

- Max. excess pore-water pressure after 10 cycles = 7 kPa (i.e. $r_{0,10} = 0.07$)
- Axial strain at the end of 10 cycles = 0.39 %
- Cycles produce axial strains between 0.32 % and 0.46 %
- Test ended after 2610 seconds.

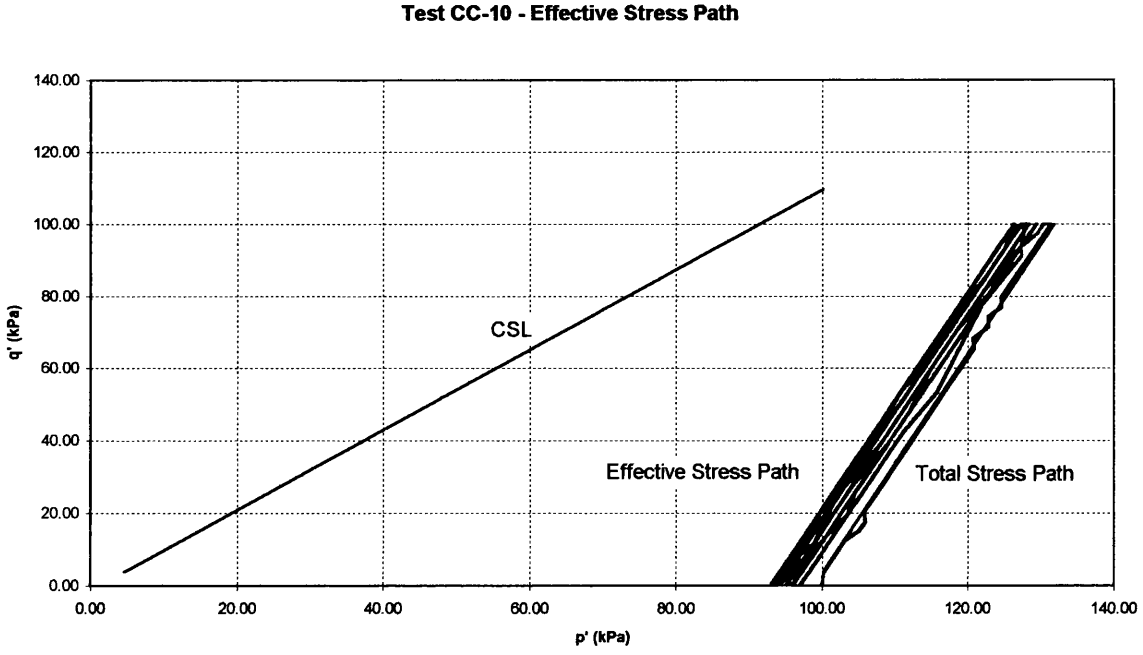

***Figure 4.116** – Effective Stress Path [Test CC-10]*

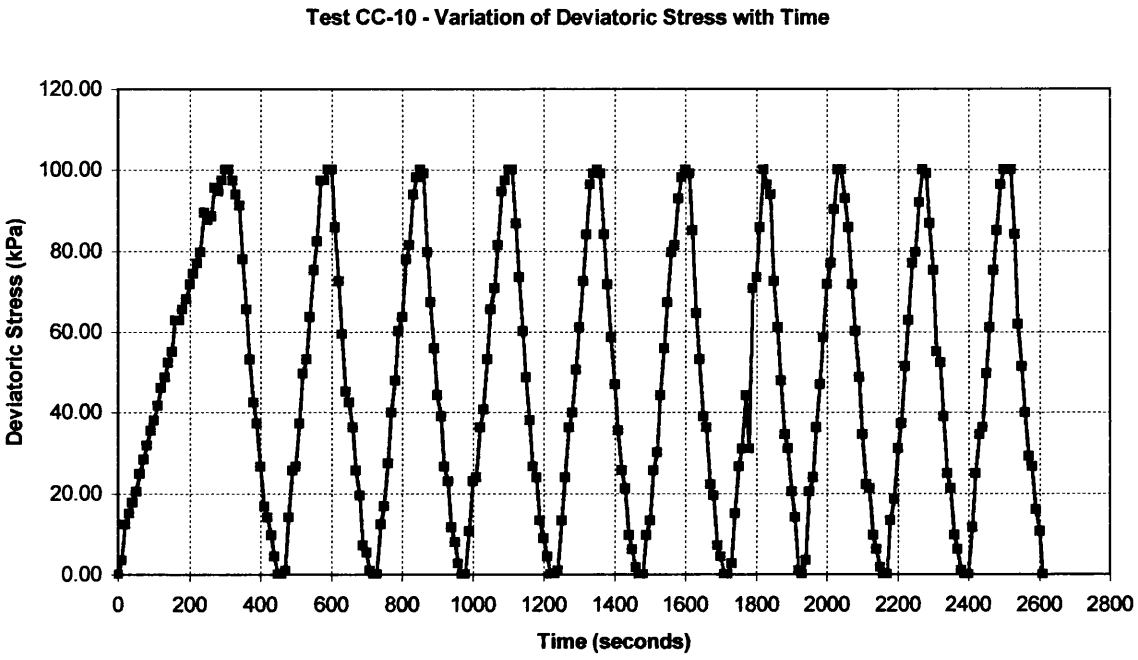

Figure 4.117 – Variation of Deviatoric Stress with Time [CC-10]

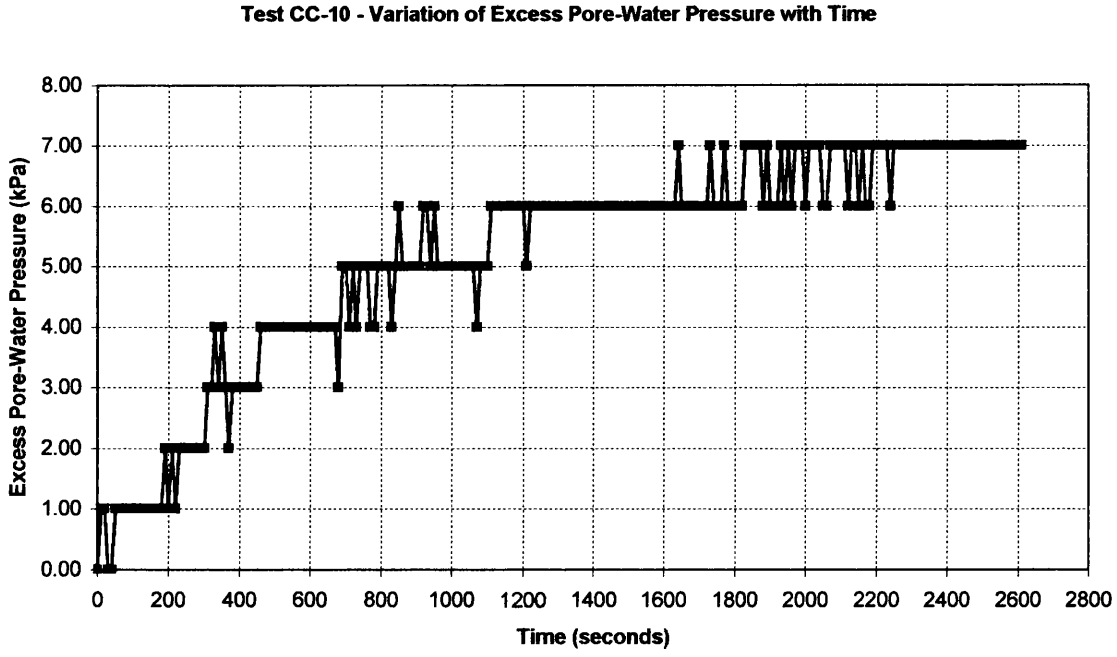

Figure 4.118 – Variation of Excess Pore-Water Pressure with Time [Test CC-10]

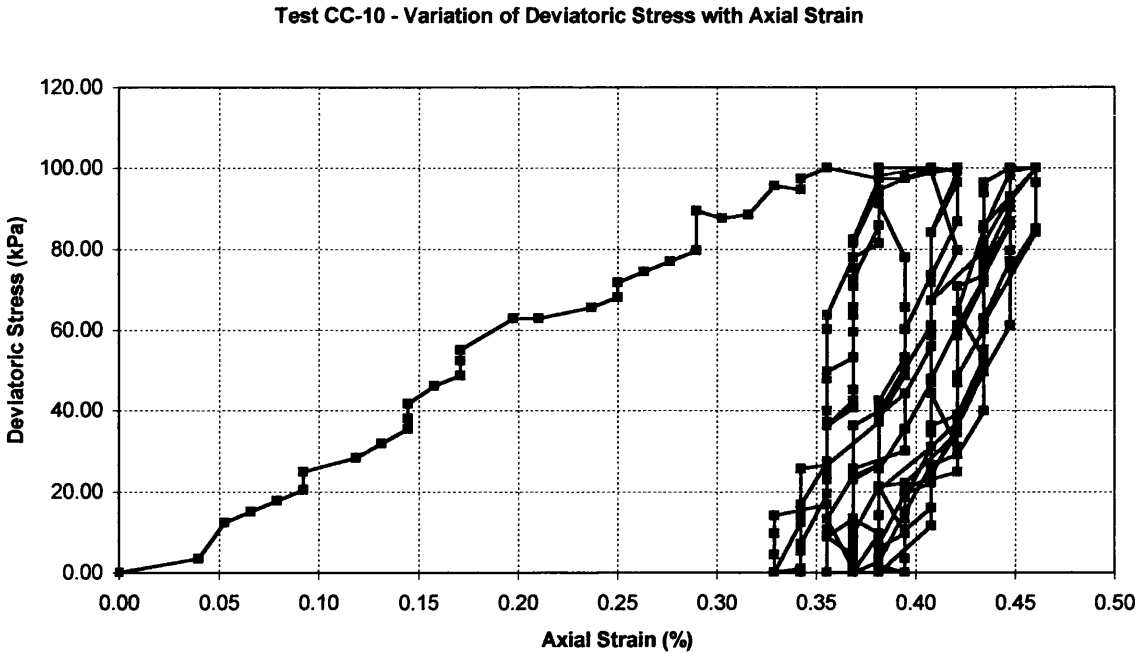

Figure 4.119 *– Variation of Deviatoric Stress with Axial Strain [Test CC-10]*

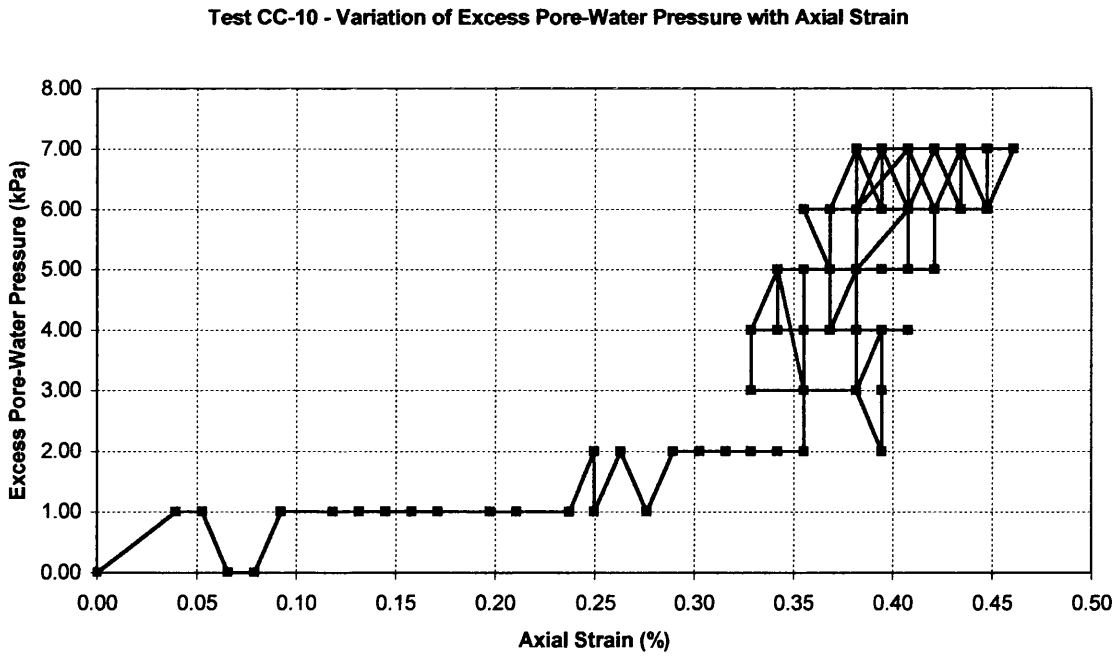

Figure 4.120 *– Variation of Excess Pore-Water Pressure with Axial Strain [Test CC-10]*

4.4 POST-PROCESSING AND CONCLUSIONS

4.4.1 Introduction

Previously in this Chapter, the results of cyclic triaxial tests on loose Hostun sand specimens have been presented. These tests were stress-controlled, employing one-way cycles of 60 kPa, 80 kPa, and 100 kPa.

Here, the results from these tests will be rigorously analysed, in order to determine the viability of the use of partially saturated soil as a possible method of liquefaction mitigation.

4.4.2 Summary of the Results

A summary of the results of all tests previously presented, is given in Tables 4.28 to 4.33 below.

Test No.	σ_3	Cycle (kPa)	B	S_{r0}	w
CA-2	100	60	0.99 - 1.00	0.9992	0.3797
CA-3	100	60	0.95	0.9858	0.3746
CA-4	101	60	0.91 - 0.92	0.9661	0.3671
CA-5	101	60	0.89	0.9542	0.3626
CA-6	100	60	0.85	0.9424	0.3581
CA-7	100	60	0.79	0.9366	0.3559
CA-8	100	60	0.73	0.9218	0.3503
CA-9	100	60	0.60 – 0.61	0.9126	0.3468

***Table 4.28** – Test Results CA-2 to CA-9 [Block 1]*

Test No.	$r_{0,10}$	ε_{min}	ε_{max}	ρ (kg/m^3)	γ (kN/m^3)
CA-2	0.51	0.34	0.57	1793	17.592
CA-3	0.16	0.12	0.28	1786	17.521
CA-4	0.16	0.13	0.32	1777	17.432
CA-5	0.11	0.14	0.32	1773	17.393
CA-6	0.06	0.08	0.21	1765	17.315
CA-7	0.09	0.17	0.34	1756	17.226
CA-8	0.05	0.12	0.23	1755	17.217
CA-9	0.05	0.08	0.22	1750	17.166

***Table 4.29** – Test Results CA-2 to CA-9 [Block 2]*

Test No.	σ_3	Cycle (kPa)	B	S_{r0}	w
CB-2	100	80	0.99 - 1.00	0.9953	0.3782
CB-3	99	80	0.93 - 0.94	0.9737	0.3700
CB-4	100	80	0.90	0.9668	0.3674
CB-6	100	80	0.86	0.9611	0.3652
CB-7	100	80	0.81 - 0.82	0.9534	0.3623
CB-8	100	80	0.77	0.9326	0.3544
CB-9	99	80	0.72 – 0.73	0.9161	0.3481
CB-10	101	80	0.62	0.9084	0.3452

***Table 4.30** – Test Results CB-2 to CA-10 [Block 1]*

Test No.	$r_{0,10}$	ε_{min}	ε_{max}	ρ (kg/m^3)	γ (kN/m^3)
CB-2	0.58	0.44	1.54	1791	17.570
CB-3	0.24	0.16	0.33	1780	17.462
CB-4	0.20	0.11	0.36	1777	17.432
CB-6	0.19	0.24	0.49	1774	17.403
CB-7	0.15	0.35	0.46	1770	17.364
CB-8	0.09	0.27	0.43	1760	17.266
CB-9	0.07	0.22	0.39	1752	17.187
CB-10	0.07	0.16	0.36	1748	17.148

***Table 4.31** – Test Results CB-2 to CB-10 [Block 2]*

Test No.	σ_3	Cycle (kPa)	B	S_{r0}	w
CC-2	101	100	0.99 - 1.00	0.9984	0.3794
CC-3	100	100	0.95	0.9761	0.3709
CC-4	100	100	0.90	0.9647	0.3666
CC-5	101	100	0.86 - 0.87	0.9571	0.3637
CC-7	99	100	0.83 – 0.84	0.9468	0.3598
CC-8	100	100	0.77	0.9403	0.3573
CC-9	100	100	0.72	0.9132	0.3470
CC-10	100	100	0.60	0.9121	0.3466

***Table 4.32** – Test Results CC-2 to CC-10 [Block 1]*

Test No.	$r_{0,10}$	ε_{min}	ε_{max}	ρ (kg/m^3)	γ (kN/m^3)
CC-2	0.50	1.10	2.40	1793	17.589
CC-3	0.28	0.39	0.71	1781	17.472
CC-4	0.23	0.39	0.61	1776	17.423
CC-5	0.16	0.23	0.41	1776	17.423
CC-7	0.14	0.29	0.50	1767	17.334
CC-8	0.09	0.22	0.55	1764	17.305
CC-9	0.08	0.29	0.49	1750	17.168
CC-10	0.07	0.32	0.46	1747	17.138

***Table 4.33** – Test Results CC-2 to CC-10 [Block 2]*

Measurement of σ_3 (kPa)

The measurement of σ_3, the confining (cell) pressure, was achieved by bringing it to the required value, via the pressure regulator (Figure 3.16), by referencing it to the reading on the data logger. Once the required value was reached, no further adjustment to the pressure regulator setting was made.

Control of the Cycle Amplitude (N)

The cycle amplitude was controlled by continued reference to the data logger and the proving ring, which had been calibrated against known load values in newtons (N). Reversing the direction of the applied loading was achieved by means of the gear switch on the front of the triaxial apparatus.

Skempton's B-parameter (dimensionless)

Established by measuring the increment of the confining pressure, and the resulting rise in the excess pore-water pressure under undrained conditions. The *B*-parameter may be calculated from:

$$B = \frac{\Delta u}{\Delta \sigma_3} \qquad [4.4]$$

In certain tests, $\Delta\sigma_3$ was not set at 100 kPa, which was established by the author to be the requirement for these tests. *B* could still be reliably measured, however, by dividing by the value of Δu according to Equation [4.1]. Tables 4.28 to 4.33 indicate for which tests $\Delta\sigma_3$ was not set at 100 kPa.

Initial Degree of Saturation, S_{r0} (dimensionless)

Established from the phase relation:

$$S_{r0} = \frac{G_s w}{e_0} \qquad [4.5]$$

where G_s is the specific gravity of the soil particles (established in Chapter 3 as 2.56), w is the moisture content (varying for each specimen), and e_0 is the void ratio (assumed for all tests to be 0.97).

Moisture Content, w (dimensionless)

Specimens affected by zeolite (i.e. partially saturated) were weighed intact within the membrane, and then allowed to dry in air. This ensured that the oxygen pockets remained within the soil matrix during drying.

The Excess Pore-Water Pressure Ratio after 10 Cycles, $r_{0,10}$ (dimensionless)

This normalising variable is the maximum value of the excess pore-water pressure reached, Δu, divided by the confining pressure, σ_3.

$$r_{0,10} = \frac{\Delta u}{\sigma_3} \qquad [4.6]$$

The Minimum Shear Strain Level, γ_{min} (%)

The maximum or minimum level of axial strain reached during the application of the cyclic loading. These values are obtained from the graphs of deviatoric stress versus axial strain, and excess pore-water pressure versus axial strain. For a given load increment, a specimen exhibiting lower strain levels will have a greater stiffness than those exhibiting higher strain levels. This is significant in terms of the processes which result in rises in excess pore-water pressures, as outlined in Chapter 2. Strains are calculated from:

$$\varepsilon = \frac{\xi_{axial}}{76} \cdot 100$$

where ξ_{axial} is the axial displacement in millimetres, '76' is the original length of the specimen (76 mm), while '100' converts this ratio into a percentage.

Bulk Density, ρ (kg/m^3)

This is the value of the total density of the soil specimen, prior to application of the cyclic loading. The bulk density of the soil mass is given by:

$$\rho = \frac{G_s(1+w)}{(1+e_0)}\rho_w \qquad [4.7]$$

where ρ_w is the density of water, taken as 1000 kg/m^3.

Unit Weight, γ (kN/m^3)

The unit weight is merely the bulk density, ρ, multiplied by g, the acceleration due to gravity (9.81 m/s^2). Therefore, the unit weight is given by:

$$\gamma = \frac{G_s(1+w)}{(1+e_0)}\gamma_w \qquad [4.8]$$

where γ_w is the unit weight of water, taken as 1000 kN/m^3.

All of the above quantities are described earlier in this work, and elsewhere in the literature. They are listed in brief here for completeness, and as a reference when considering the results from those triaxial tests presented in Chapter 4.

4.4.3 Relationship Between *B* and S_{r0}

In most geotechnical engineering application, values of the initial degree of saturation, S_{r0}, tend to be of greater significance than those of B. While S_{r0} explicitly states the initial degree of saturation within a given specimen or sample, B is more frequently used as a check for full saturation (i.e. $S_{r0} = 1.00$) only.

The relationship between B and S_{r0} is not linear (Skempton, 1954), which justifies the use of two extra decimal places when quoting S_{r0} in this current work. This accuracy permits a more accurate plot of S_{r0} against B, particularly when it has

already been stated that σ_3 and Δu could only be measured to the nearest integer, thereby slightly reducing the certainty in the value of B. As Δu decreases in magnitude, the value of the error rises to approximately 1% of the true value of B while, for values of Δu closer to σ_3, the error becomes negligible. These restrictions are considered by the author to be within acceptable limits for the present work.

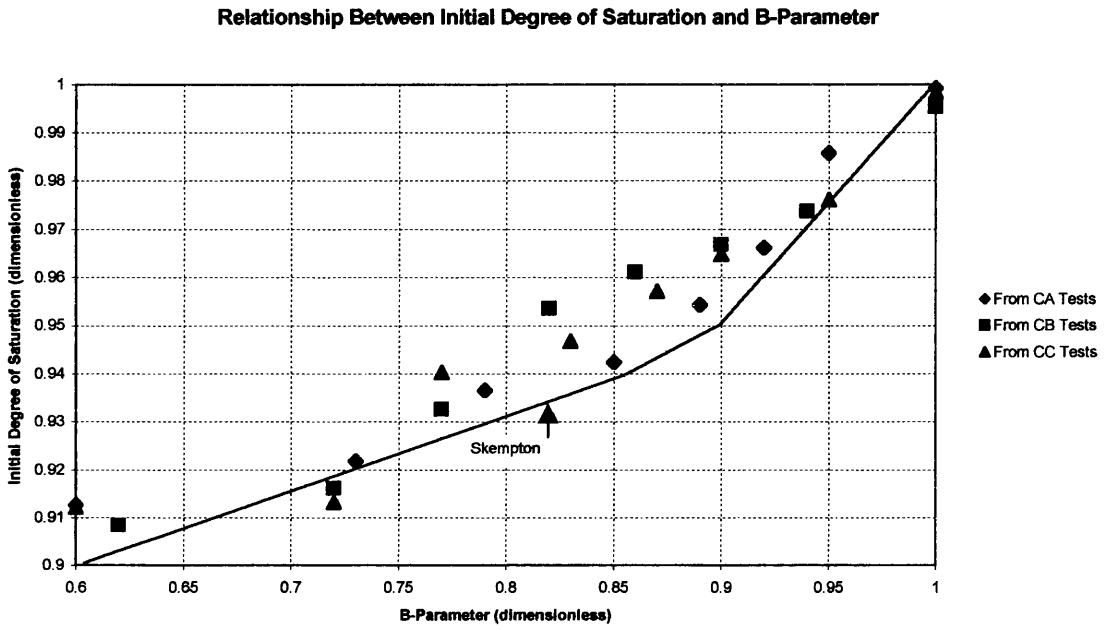

***Figure 4.121** – Relationship Between S_r and B-Parameter From Triaxial Test Programme*

Figure 4.121 above shows the relationship between the initial degree of saturation, S_{r0}, and Skempton's B-parameter, as obtained from the test programme presented earlier in this work. The Figure also shows the empirical relationship between S_{r0} and B, for a typical sand, as reported in Skempton's own work (1954). As can be seen, the similarity between the two relationships is clear, which further confirms the reliability of the triaxial testing modifications as outlined in Chapter 3.

4.4.4 Relationship Between $r_{0,10}$ and S_{r0}

As stated throughout this thesis, the rise in excess pore-water pressure is a vital factor in any liquefaction analysis. Here, attention is focused upon changes in excess pore-water pressures when cyclic stresses are applied to specimens having different initial degrees of saturation. The excess pore-water pressure is expressed here in terms of the normalising variable $r_{0,10}$, which is the change in this pressure, Δu, divided by the confining pressure, σ_3.

Figures 4.122 to 4.124 show this relationship for cyclic stresses of 60 kPa, 80 kPa, and 100 kPa, as presented earlier in this Chapter.

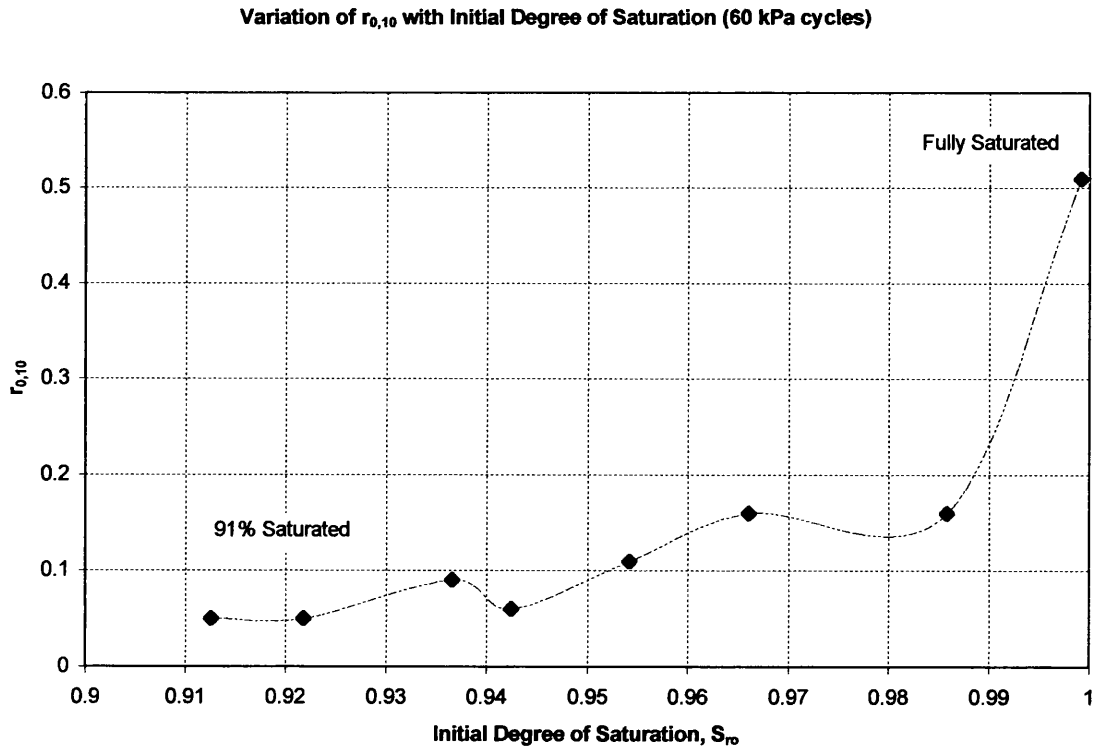

***Figure 4.122** – Variation of $r_{0,10}$ and S_{r0} for 60 kPa Stress Cycles*

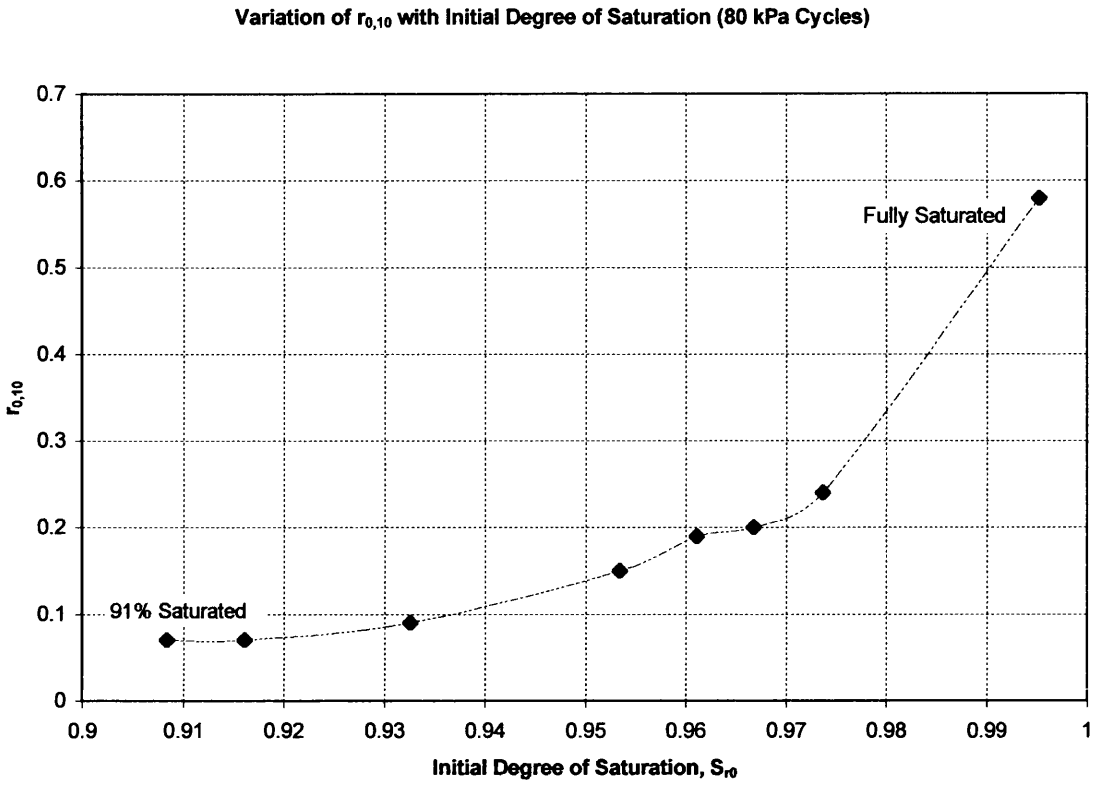

Figure 4.123 – Variation of $r_{0,10}$ and S_{r0} for 80 kPa Stress Cycles

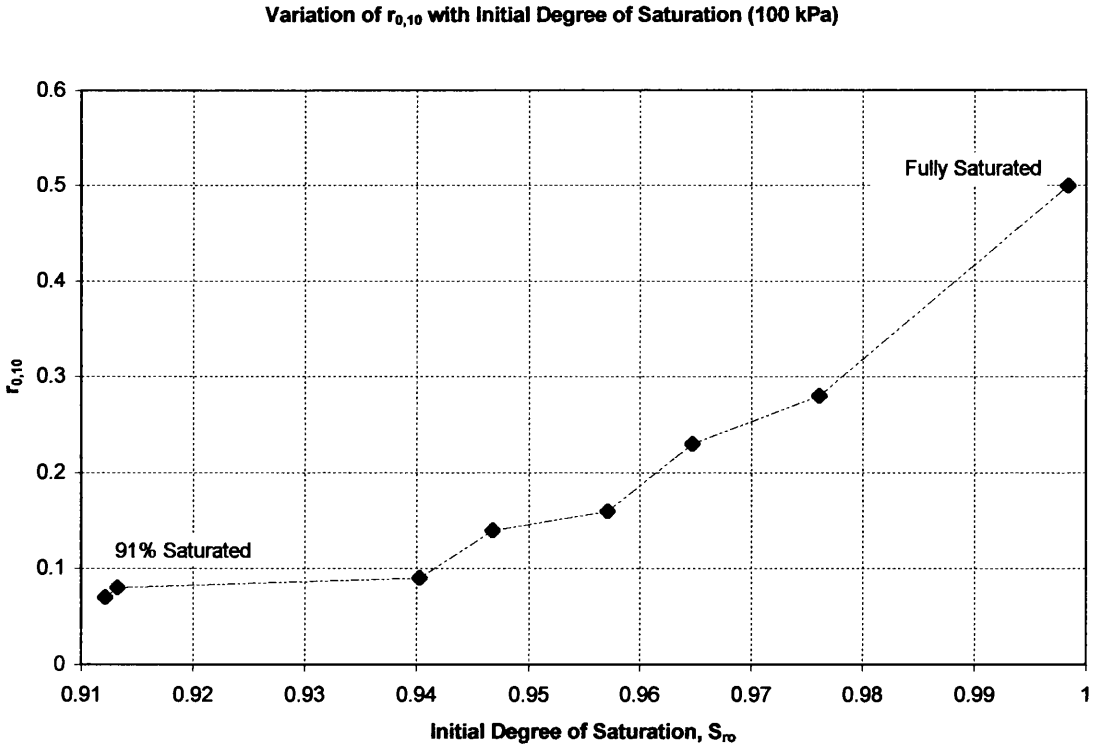

Figure 4.124 – Variation of $r_{0,10}$ and S_{r0} for 100 kPa Stress Cycles

In each of the three cases covered by Figures 4.122 to 4.124, the maximum excess pore-pressure in 10 one-way cycles is seen to reach its maximum value when the initial degree of saturation in the specimen is also at a maximum. As the initial degree of saturation decreases, the maximum excess pore-water pressure also decreases.

However, it can be seen that the fall in excess pore-water pressure appears to have the highest gradient for the lowest stress cycle amplitude. The explanation for this can be discussed in terms of the plastic strains that are on the point of being set up in the specimen, primarily toward the end of the first stage of compression. Referring to Figure 3.30 (Section 3.4), the elastic limit for specimens tested under undrained conditions appears to lie somewhere between 80 and 100 kPa. From Figure 4.83 (Section 4.3), in which the relationship between the excess pore-water pressure and time is presented, it can be seen that the rate of pore-water pressure increase begins to decrease in this region, indicating the onset of dilative behaviour.

The semi-permanent strains induced in the specimen are, by definition, not readily recovered during unloading, resulting in a reduced capacity for the excess pore-water pressures, generated during the loading stage, to be dissipated throughout the specimen during the unloading stage. This accounts for the shallower, more uniform gradient observed in Figure 4.124, compared to those in Figures 4.123 and 4.122. Note also that $r_{0,10}$ tends to have higher values for higher stress cycle amplitudes, for similar degrees of saturation. This is further evidence of the plastic straining in the specimen preventing the dissipation of excess pore-water pressures.

The reduction of excess pore-water pressure with decreasing degree of saturation is better exemplified by the effective stress paths, presented throughout Sections 4.1, 4.2 and 4.3. Here, it can be seen that, as the degree of saturation decreases, so the tendency for the effective stress path to approach the critical state line (CSL) is also reduced. In this connection, it can be seen that partial saturation prevents the specimen from experiencing those states of stress which are most likely to produce liquefaction, and the effect is more prominent as the initial degree of saturation is decreased.

Therefore, it should be clear that the primary consequence of reducing the initial degree of saturation in a given specimen which is to be subjected to cyclic stress applications, is to significantly reduce the potential for liquefaction in that specimen.

4.4.5 Stress Paths

In the previous sub-Section, the importance of the stress paths in attempting to understand the behaviour of the specimens tested for the purposes of the current research was discussed. A more detailed explanation of the role of the stress path will now be presented, along with a further insight of how the results from these stress paths contribute toward any conclusions drawn from the present work.

The stress path is the locus of points which represents the states of stress in a given soil specimen or sample, as increments of stress are applied. The stress path is normally represented in two dimensions, the coordinates for an undrained specimen being:

$$q' = \sigma_1 - \sigma_3 = q \qquad [4.9]$$

$$p' = \frac{1}{3}(\sigma_1 + 2\sigma_3) - u \qquad [4.10]$$

where the definitions of each of these quantities have previously been given in Section 4.1.

In a drained test, the instantaneous value of the excess pore-water pressure, u, is always zero. Then, Equations [4.9] and [4.10] need no longer to be expressed in terms of the effective stress, and they reduce to:

$$q = \sigma_1 - \sigma_3 \qquad [4.11]$$

$$p = \frac{1}{3}(\sigma_1 + 2\sigma_3) \qquad [4.12]$$

Thus, for a given rise in σ_1, within which the axial stress will be incorporated, the rise in q will always be three times the corresponding rise in p. For a drained test, therefore, the stress path will always have a slope of three to one, and will originate at the point where $q = 0$ and $p = \sigma_3$. The drained stress path is often called the total stress path, and is labelled as such in all stress path diagrams presented earlier in Sections 4.1, 4.2, and 4.3. As can be seen from these diagrams, the difference between the drained and undrained stress paths is the excess pore-water pressure induced during undrained compression. When excess pore-water pressures are above gauge or

atmospheric pressure, the undrained stress path will always lie to the left of the drained stress path.

The gradient of the critical state line (CSL), as expressed in terms of the effective angle of internal friction, ϕ', was given in Section 4.1, while qualitative definition was given in Chapter 2. It should be understood that, as the tendency for the effective stress path to approach the CSL decreases, so the deformations that would be required to produce liquefaction in the sand specimen are also reduced. From the diagrams of the effective stress paths given in this Chapter, it can be seen that as the initial degree of saturation, S_{r0}, decreases, so this tendency also decreases, resulting in a reduced risk of liquefaction phenomena occurring.

It is clear from the above discussion that the undrained stress path will, in the majority of cases, be constrained between the drained stress path and the critical state line. These two references, therefore, provide information not only of the undrained behaviour of the specimen, but also of that specimen's tendency to liquefy. From the effective stress paths presented in Sections 4.1, 4.2, and 4.3, two observations can be made, namely that:

- the undrained stress path will move further from the critical state line as the initial degree of saturation is decreased, and;
- the undrained stress path begins to assume a ratio of three to one, as with the drained path, again as the degree of saturation is reduced. The only difference between the undrained and drained paths is a small increment of excess pore-water pressure, generated during the first compressive stage of the test.

From these observations, the following two conclusions may be safely drawn.

- As the initial degree of saturation, S_{r0}, is decreased, so the tendency for the specimen to liquefy is also decreased. It is only when the specimen is fully saturated (i.e. S_{r0} = 1.00) that the stress states necessary to produce liquefaction (as defined by the low liquefaction surface) are approached.
- As S_{r0} is decreased, so the specimen will exhibit behaviour exclusively attributed to a drained specimen (as indicated by the 3 to 1 ratio of its stress path), even though undrained conditions are prevailing. Therefore, it may be stated that, due to the compressibility of the air phase, the excess pore-water pressure is dissipating or 'draining' through expenditure of energy in the pore-water phase when compressing the air. This effect becomes more pronounced

as the initial degree of saturation is reduced, and the air phase increases in volume. Here, then, drained behaviour is being imposed upon undrained conditions.

During an earthquake in the field, the saturated ground is assumed to behave as an undrained medium, even though the excess pore-water pressure is free to dissipate. This is because the rapid loading experienced during earthquake shaking produces instantaneous rises in pore-water pressures. This pore-water pressures do eventually dissipate and reach equilibrium, but not before the conditions required for the occurrence of liquefaction may have already been reached in this relatively short time interval.

It has already been seen from the preceding discussion that the introduction of partial saturation not only significantly reduces the scope for deleterious rises in excess pore-water pressures, but that this is due to the superimposition of 'drained' characteristics on an undrained specimen. This superimposition can be attributed to the introduction of an initial degree of saturation of less than 1.00. Both of these considerations would be of considerable value when assessing the use of partial saturation as a viable method of liquefaction mitigation in engineering practice.

4.4.6 Strain Considerations

While the stress path is of undoubted value in the current work, the stress path coordinates do not permit the inclusion of strain increments. Therefore, the effects of partial saturation on the straining of the tested specimens needs to be considered separately.

In Chapter 2, the relevance of the application of shear strain on a given element was discussed. It was stated there that straining of a saturated soil element produces excess pore-water pressures, where the magnitude of straining is directly related to the change in excess pore-water pressure. The higher the shear strength of the soil, the smaller will be the increment of strain for a given stress application and, consequently, the scope for significant change in excess pore-water pressure will be reduced.

In each of the tests presented in Sections 4.1, 4.2, and 4.3, the maximum and minimum strain levels, during each application of 10 one-way stress cycles, were estimated. During the stress cycles, the specimen experienced strains that lay

somewhere between these two levels. It is clear that examination of these figures would provide a crucial insight into the response of a partially saturated soil to a cyclic stress application.

During the tests outlined in Sections 4.1, 4.2, and 4.3, readings of axial displacement, deviatoric stress, confining pressure, and excess pore-water pressure, began to be logged when:

- the deviatoric stress was seen to rise, and;
- the excess pore-water pressure was seen to rise.

These should happen together and close to the start of the test. However, due to the very loose nature of the loose Hostun sand specimens, stress increments tend to be small until there are sufficient interparticle sand-grain contacts to transmit the load through the specimen. Until this time, readings remained unlogged. This accounts for the slight difference in shape between the plots presented earlier in this Chapter, and those presented in Section 3.4.

The relationships between maximum and minimum strain levels are presented in Figures 4.125, 4.126, and 4.127 below.

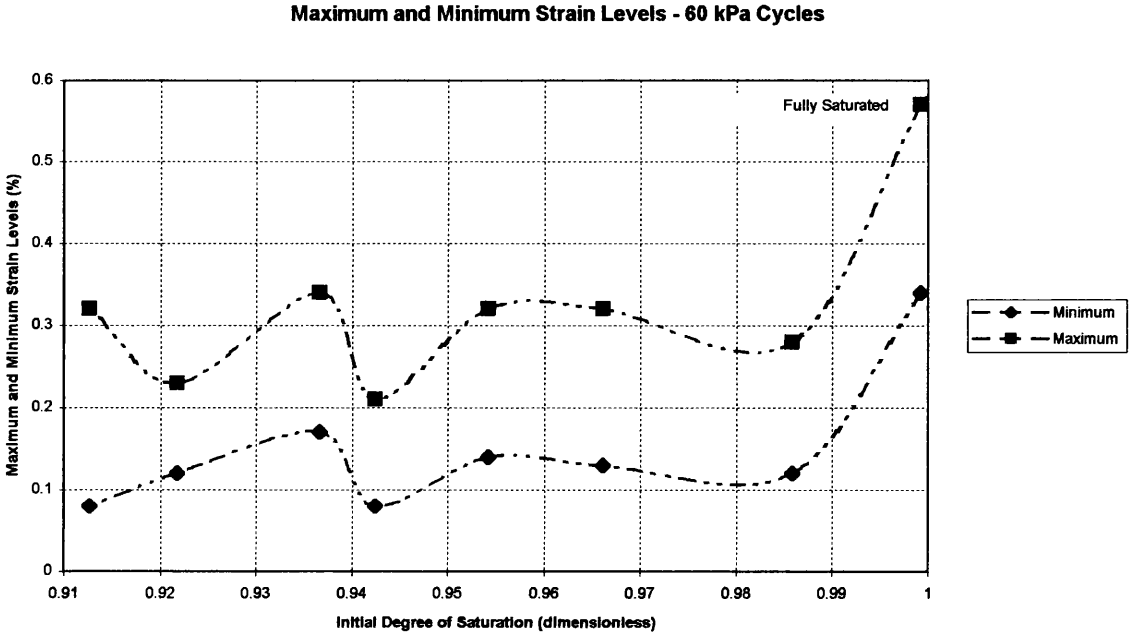

Figure 4.125 – Maximum and Minimum Strain Levels [60 kPa Cycles]

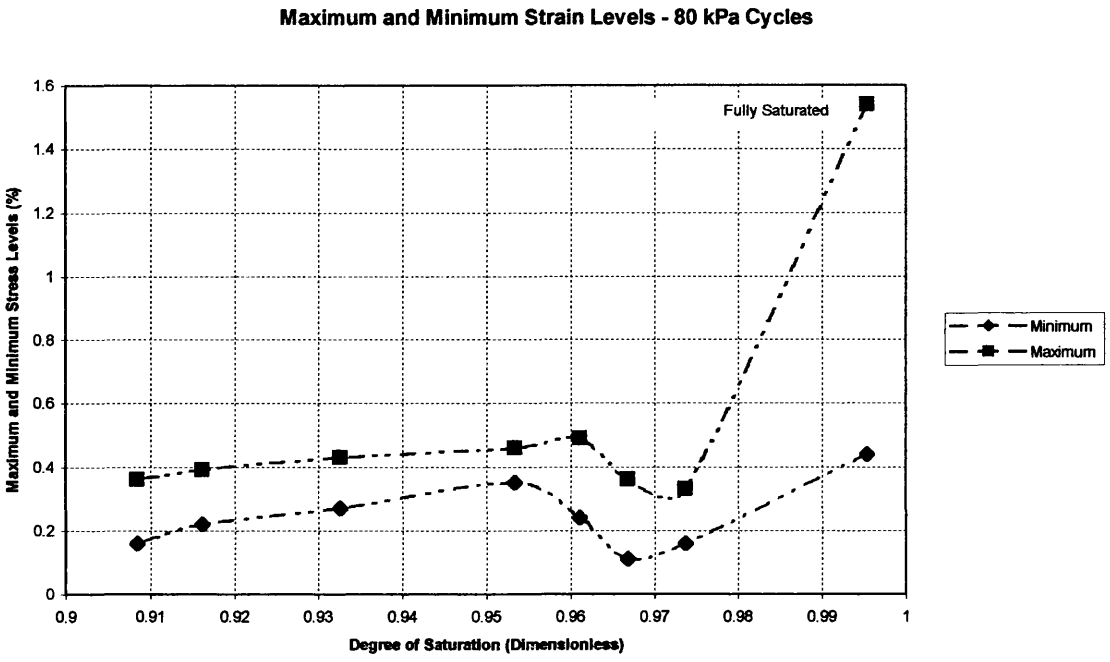

Figure 4.126 – Maximum and Minimum Strain Levels [80 kPa Cycles]

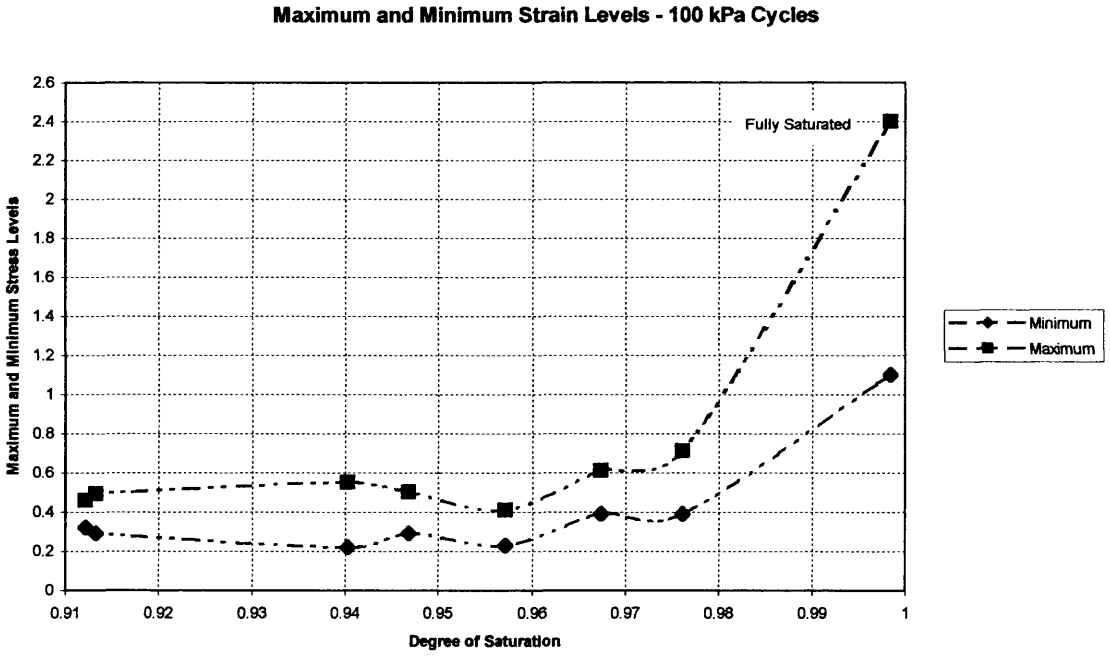

Figure 4.127 – Maximum and Minimum Strain Levels [100 kPa Cycles]

It can be seen clearly from the preceding Figures that, for unsaturated specimens, the maximum and minimum axial strain levels will be approximately constant, and then increase sharply as full saturation is approached. Although not strictly equal to the shear strain which, as described in Chapter 2, is responsible for excess pore-water pressure increases, an increment of *volumetric* strain is directly proportional to the increase in excess pore-water pressure, and so the relationship will be very similar.

The reduction in maximum and minimum strain levels below full saturation is due to the presence of matric suction, generated when air (and, therefore, pore-air pressure) is present within the specimen. The matric suction increases the shear strength of a given soil specimen by generating a tensile force within the soil matrix. Thus, for a given increment of applied stress, the observed strain level will be lower for a soil with matric suction present ($S_{r0} < 1.00$) than would be expected for a soil without matric suction ($S_{r0} = 1.00$).

It may therefore be safely reiterated that, due to the reduced capacity of a partially saturated soil to undergo shear straining, a partially saturated soil may be used as a means of liquefaction mitigation, based upon the results presented in this Chapter.

4.4.7 Bulk Densities and Unit Weights

Although not integral to the work already presented in this Section, the bulk densities and unit weights are important quantities which will be used later in this thesis when further investigation into liquefaction susceptibility are presented. This later work was conducted using the *ProShake* computer program, used for seismic ground response analysis.

As expected, bulk densities and unit weights decrease as the degree of saturation decreases, since decreases in the bulk density of the specimen are produced by decreasing its moisture content, and the unit weight is simply the bulk density multiplied by the acceleration due to gravity, g. It has been shown that, for specimens containing 2% by volume of zeolite, the unit weight is approximately 2.5% less than for saturated specimens. The equations for bulk density and unit weight in terms of the phase properties of the specific gravity (G_s), the moisture content (w), and the initial void ratio (e_0), are given at the start of this Section.

4.4.8 Conclusions

A summary of the more important conclusions relating to the use of partially saturated soil in the triaxial test programme as outlined in this Chapter, and the reliability of the modified triaxial apparatus designed and employed for this purpose, will now be presented.

- The relationship between Skempton's dimensionless *B*-parameter and the initial degree of saturation, S_{r0}, derived here for the purpose of providing the link between *B* and the phase relations, follows closely the results of Skempton's own empirical work on 'typical' sand (1954). It may therefore be stated that the method of specimen preparation using the modified upper platen and plug is capable of producing sand specimens possessing very similar initial void ratios.
- The relationship between $r_{0,10}$, the excess pore-water pressure ratio during 10 stress cycle applications, and the initial degree of saturation, S_{r0}, indicates that the excess pore-water pressure decreases when the initial degree of saturation is reduced. Moreover, this decrease is more pronounced when S_{r0} is reduced slightly from the full saturation level (S_{r0} = 1.00). Therefore, the liquefaction susceptibility of the specimen is gradually reduced when S_{r0} tends away from its maximum value of 1.00.
- From the effective stress paths presented in Sections 4.1, 4.2, and 4.3, it can be seen that, as the excess pore-water pressure reduces, so the states of stress within the specimen become more removed from those that are most likely to cause liquefaction. These deleterious stress states are represented by the critical state line. Therefore, since excess pore-water pressures are reduced by a reduction in the initial degree of saturation, the stress states plotted for each tested specimen, and their proximity to the critical state line, provide further evidence of the viability of the use of partial saturation as a means of liquefaction mitigation.
- As the effective stress path of the specimen moves further from the critical state line, so the slope of the effective stress path approaches the 3-to-1 ratio more commonly associated with the drained or total stress path. Thus, it may be deduced that, as the initial degree of saturation is decreased, producing a decrease in the maximum excess pore-water pressure produced, so the

specimen will display drained characteristics. This is despite the fact that the specimen is being tested under undrained conditions. In the field, pore-water pressures during seismic motions are assumed to take place under undrained conditions, while the current research would appear to indicate that the introduction of partial saturation into the subsurface soil would impose drained characteristics on the susceptible stratum. This would greatly reduce the scope for catastrophic rises in excess pore-water pressures, and provides a further insight into the positive role that partial saturation may be able to play in liquefaction mitigation.

- Strain levels in the tested specimens reduce significantly when the initial degree of saturation is reduced. This is due to the presence of matric suction, a tensile force, which is generated when pores in the soil matrix contain both air and water. The matric suction increases the overall shear strength of the specimen, resulting in smaller strains for a given stress application. As outlined earlier in Chapter 2, shear strains produce rises in excess pore-water pressures, and so it follows that reduced levels of shear strain will produce lower excess pore-water pressures. Since the generation of excess pore-water pressures is the primary criterion for the development of liquefaction, once again the evidence presented indicates that the use of partial saturation is a practical means of liquefaction mitigation.

All of these points lead to the overall conclusion that by reducing the initial degree of saturation in a soil, or by employing some mechanism by which the soil cannot reach full saturation when water is subsequently infused into it, the liquefaction susceptibility of that soil will be reduced.

It should be reiterated here that, in the current work, the mechanism which prevented full saturation in the soil matrix was the zeolite chemical. This purpose of this work is not to determine the viability of zeolite for use in field situations. Instead, the by-product of the reaction between zeolite and water, namely oxygen gas molecules, is of primary interest, as it is the accumulations of these molecules which:

- reduce the degree of saturation in the soil specimen; and
- increase the matric suction.

CHAPTER 5

THE OSCILLATING BOX

5.1 THE OSCILLATING BOX

5.1.1 Introduction

In Chapter 2, the basic concepts relating to the phenomenon of liquefaction were introduced. These were successfully employed in Chapter 3, where the author detailed the necessary changes to the triaxial apparatus which was made available for the current work. These modifications enabled the author to prepare partially saturated, loose Hostun sand specimens for subsequent testing. This work was based on the author's proposal that partial saturation could be used as a means of liquefaction mitigation. The results from this triaxial test programme, which was conducted solely for the purposes of this research, were presented in Chapter 4. There, the empirical data from a series of stress-controlled, one-way cyclic undrained tests were presented. The results from this programme clearly indicated that the generation of excess pore-water pressures, the common feature of all liquefaction phenomena, could be successfully inhibited by reducing the initial degree of saturation, S_{r0}, in a granular soil matrix.

This work was subsequently taken a stage further. The principles behind this existing research were applied to a physical system which more closely resembled the sub-surface conditions that would be expected in a field situation. The author designed an 'oscillating box' for this purpose. This simple rigid box, the specifications of which are detailed in the next sub-Section, is a single-degree-of-freedom system, within which a soil stratum may be subjected to cyclic loading. This loading was provided by an attached motor and speed controller, which provided forced, undamped oscillations of constant frequency.

The soil stratum was prepared in the oscillating box in a similar manner to the triaxial specimens described in earlier Chapters. However, not all of the soil stratum was affected by partial saturation in the current research programme. The soil within the oscillating box was discretised into five 'sub-layers'. Each of these sub-layers would be subjected in turn to partial saturation, and the excess pore-water pressure response within this sub-layer, as well as in the remainder of the oscillating box, would be assessed.

A more rigorous description of the test programme will be presented later in this Chapter. This Section will focus primarily on the specifications of the oscillating box, and the method used to assess the excess pore-water pressures.

5.1.2 The Oscillating Box

In its simplest terms, the oscillating box is a single degree-of-freedom system (SDOF) within which a soil 'stratum' specimen may be prepared. The box is then subjected to a cyclic motion, the constant frequency of which is set by the investigator. The mechanical and physical response of the soil may then be measured in a manner which is applicable to the line of research being followed. For the purposes of this work, only the excess pore-water pressures generated when such a specimen is subjected to cyclic motion were to be investigated. The test programme is therefore somewhat more qualitative than that previously presented for the triaxial apparatus.

As stated in the previous sub-Section, the motion of the oscillating box was both forced and undamped. A mathematical treatment of such a system is summarised by Kramer (1996) for the reference of investigators wishing to study a more comprehensive description of the motion of the oscillating box. However, it will be seen that the fundamental equations of simple harmonic (circular) motion will be sufficient for the investigations described in this Chapter.

The oscillating box used for the purposes of the current work is shown in Figure 5.1 below, and schematically in Figure 5.1 overleaf. The box was manufactured from transparent perspex, thereby permitting some visual confirmation of the physical response of the specimen.

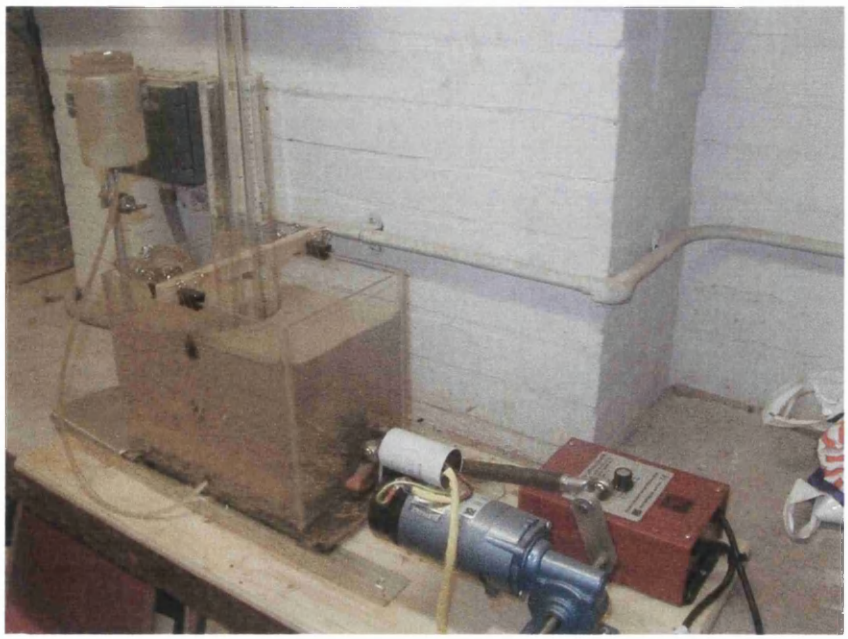

***Figure 5.1** – The Oscillating Box*

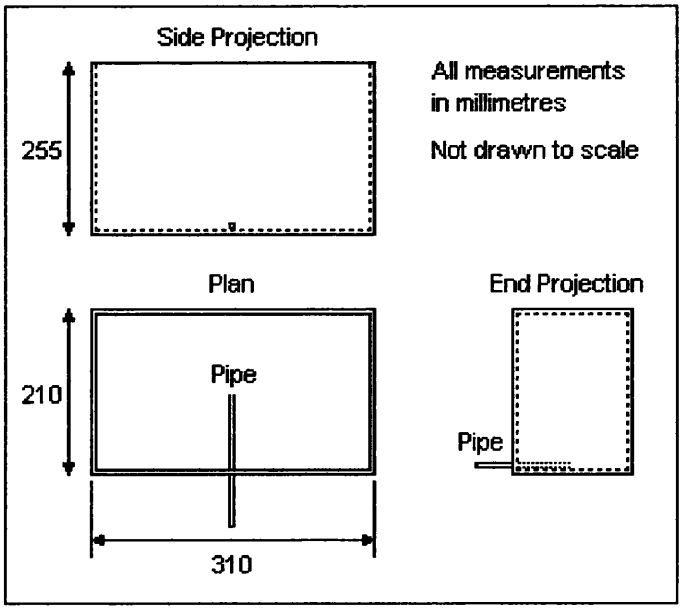

***Figure 5.2** – Exterior Dimensions of the Oscillating Box*

Figure 5.2 also shows the rigid water inlet pipe, from which saturation of the soil specimen was effected. The pipe, which was made of aluminium and had an internal diameter of 2mm, passed through the side wall of the box as shown, and was fixed to the lower surface of the box. There was no significant gap between the pipe and the side wall, although silicon grease was used as a precaution against any unwanted movement of the pipe and subsequent loss of pore water from the soil matrix. The pipe can be clearly seen Figure 5.1, and in the plan and side elevation of Figure 5.2.

The box itself had exterior dimensions of length 310 mm, width 210 mm, and height 255 mm. The perspex, which formed the rigid walls of the box, was of 5mm thickness, so the dimensions of the soil specimen used would be 300 mm (length) by 200 mm (width). The height may be set to a value suiting the research being followed. For the current work, the height of the specimen was set at 200 mm. The top of the box was open to the atmosphere, so that hydrostatic conditions provided the initial boundary condition within the soil, prior to the forced oscillation of the box.

The cyclic load was applied by means of a direct current (d.c.) motor (see Figure 5.1). The constant frequency of the motion was set by means of a speed controller installed on the exterior of the motor. The controller was graduated in integer values, which were included for the reference of the investigator and which related directly to the applied frequency of the motion.

The motion of the oscillating box was generated by means of a rod attached to the motor. The rod was made of rigid steel, thereby removing the possibility of a secondary motion superimposed on the box due to compressional or tensional variations in the rod itself. The whole system, therefore, behaved in the familiar manner of a mechanical piston, thus simplifying any mathematical treatment of the motion. As stated earlier in this Section, the reader is directed to Kramer (1996) for a rigorous résumé of the theory of forced, undamped motions.

One-dimensional movement of the box was prevented by means of a steel base, which had guides on either side within which the box is constrained to move. These guides can be seen in Figure 5.1. The base moved along oiled bearings, which provided smooth and continuous movement with the full range of frequencies available from the motor. The whole apparatus was mounted on a hardwood base of thickness 25mm. This base served an important function, as it prevented any lateral movement of the apparatus due to the applied vibrations. It was found that, even with the highest possible frequency of oscillation applied to the box, no lateral movement of the apparatus was observed.

5.1.3 Pore-Water Pressure Response

As outlined previously in this Section, the only criterion by which the mechanical response of the soil specimen was estimated was the change in excess pore-water pressure when the box was subjected to oscillatory motion.

For the fully saturated soil specimen used in the triaxial test programme, the highest excess pore-water pressure, u_c, which could be generated in the pore spaces was governed by the confining pressure, σ_3. For partially saturated soil, the pore-water pressure, u_w, and the pore-air pressure, u_a, are both identified, although the pore-air pressure was not measured for any of the work described in this thesis. However, in both cases, the value of the confining pressure provided the upper boundary for the excess pore-water pressure value.

In the oscillating box, the situation was somewhat different. No confining pressure was applied laterally (although K_0 conditions are present), since the walls of the box were rigid, while the top of the box was open to the atmosphere. Therefore, hydrostatic conditions existed in those soil specimens which, initially, were not being subjected to oscillatory motion, and the pore-water pressure at any depth was then

dependent on the total vertical geostatic stress at that point. In this case, vertical geostatic stress, σ_z, is given by:

$$\sigma_z = \gamma z \qquad [5.1]$$

where γ is the saturated unit weight of the soil specimen, and z is the depth at which the total vertical geostatic stress, σ_z, was to be measured. When the box was oscillated, excess pore-water pressures were generated, in accordance with the fundamental principles of pore-water pressure change in a soil element, as outlined extensively in Chapter 2. However, the excess pore-water pressures at any point can only rise to the limiting value of the vertical geostatic stress at that point. Therefore, the maximum excess pore-water pressure, $u_{w,max}$, that can be generated at any point is given by:

$$u_{w,\max} = \gamma z \qquad [5.2]$$

With the interior of the box 0.25m in depth, and the unit weight of any saturated sand used estimated at 20 kN/m^3, it follows from Equation [5.2] that the maximum excess pore-water pressure that can be measured in the box is approximately 5 kPa. This occurs at the bottom of the box, where the value of z is greatest, when the box is completely filled with fully saturated soil.

The vertical geostatic stress is not constant with depth, since a soil will generally become denser with increasing values of z. For unit weights which vary continuously with depth, the vertical geostatic stress may be calculated from:

$$\sigma_z = \int_0^z \gamma . dz \qquad [5.3]$$

where the unit weight, γ, is a linear function of the depth, z. In a stratified soil, where unit weights vary for different strata, the vertical geostatic stress will be given by:

$$\sigma_z = \sum \gamma . \Delta z \qquad [5.4]$$

where the unit weights, γ, of strata of thickness Δz are summed over the entire depth under consideration in order to establish the vertical geostatic stress. However, whichever form is chosen for the calculation of the vertical geostatic stress at a given depth, the value obtained is the maximum level to which excess pore-water pressure can rise at that depth. If the excess pore-water pressure reaches the value of the total vertical geostatic stress (i.e. the vertical *effective* geostatic stress = 0), then liquefaction will occur at that depth.

With reference to Equation [5.3], it was assumed that, over a depth of 0.25 m as existed in the oscillating box, the densification that would occur was not deemed significant enough for a relationship expressing γ as a function of z to be sought. However, as will be seen in the next Section, consideration of strata of differing unit weights was at the centre of the research programme using the oscillating box.

5.2 MEASUREMENT OF SOIL PROPERTIES

5.2.1 Introduction

For the purposes of the oscillating box test programme, Hostun sand was not used. Instead, in an attempt to broaden the scope of the current work, naturally-deposited Swansea Bay sand was used. When the sand was extracted from the coastal environment, care was taken to ensure that the sand mass was taken from as high above the high water mark as possible, in order that wind action might play a part in the natural regarding of the particles.

In order to calculate the unit weight, γ, of the fully saturated specimen to be used in the oscillating box, the specific gravity, G_s, the moisture content, w, and the initial void ratio, e_0, needed to be determined. The unit weight, γ, could then be established from:

$$\gamma = \frac{G_s(1+w)}{(1+e_0)}\gamma_w \qquad [5.5]$$

where γ_w is the unit weight of water (1000 kN/m^3). To determine the void ratio, the familiar phase relation was used, namely:

$$G_s w = S_{r0} e_0 \qquad [5.6]$$

With the initial degree of saturation, S_{r0}, set at 1.00, and G_s and w determined according to BS1377, the initial void ratio, e_0, could be found. Full saturation was achieved by first preparing a triaxial specimen of the sand, and the backpressuring to 400 kPa for 1 hour. Based on the details, both empirical and theoretical, presented in Section 3.3, this backpressure value was deemed to be sufficient to produce a value of S_{r0} of 1.00.

Knowledge of the values of all of the aforementioned phase properties formed the foundation upon which the remainder of the work in this thesis could be constructed.

5.2.2 Measurement of the Soil Properties

The results of the tests conducted to determine the phase properties G_s and w for Swansea Bay sand are now presented. The procedures for establishing these properties have been outlined previously in Section 3.3 and will not be repeated here.

Specific Gravity, G_s

Three tests were conducted, each following the same procedure as outlined in BS1377, and each given the prefix 'GX'. The results of these three tests are given in Table 5.1 below.

Test No.	G_s
GX-1	2.58
GX-2	2.58
GX-3	2.57

***Table 5.1** – Determination of the Specific Gravity for Naturally-Deposited Swansea Bay Sand*

Averaging between the values obtained, the specific gravity of Swansea Bay sand is established as 2.58. It can be seen that the value for the specific gravity obtained here is higher than the value of 2.56 obtained for Hostun sand (Chapter 3). This is due to the Swansea Bay sand not being sieved prior to the testing programme. Instead, the sand was extracted from high above the high water mark, and so it was assumed that wind action would play some role in the natural re-grading of the particles.

Moisture Content, w

In order to establish the moisture content for the naturally-deposited Swansea Bay sand, specimens were prepared in for testing in the triaxial apparatus, according to the procedure outlined in Chapter 3. The specimen was then backpressured to 400 kPa for 1 hour. With reference to the empirical and theoretical details presented in Section 3.3, this was considered sufficient to produce full saturation.

As with the specific gravity, the procedure for determining the moisture content, w, of a given sand specimen is comprehensively described in BS1377. Five tests were conducted, each carrying the prefix 'MX'. The results of these five tests are summarised in Table 5.2 overleaf.

Test No.	w
MX-1	0.2819
MX-3	0.2638
MX-4	0.2746
MX-5	0.2964
MX-6	0.2720

***Table 5.2** – Determination of Moisture Content for Naturally-Deposited Swansea Bay Sand*

Averaging the five results obtained from Table 5.2, the moisture content, w, for the Swansea Bay sand is 0.2777. This result, along with the value for the specific gravity, G_s, will now be used to calculate the initial void ratio, e_0, of the sand.

Initial Void Ratio, e_0

With the initial degree of saturation, S_{r0}, equal to 1.00, and the specific gravity, G_s, and moisture content, w, established earlier in this Section, the initial void ratio, e_0, could be determined from Equation [5.6]:

$$e_0 = \frac{G_s w}{S_{r0}} = \frac{(2.56)(0.2777)}{1.00} = 0.7109 = 0.71 \text{ (to 2 decimal places)}$$

This is the initial void ratio of specimens prepared for testing in the triaxial apparatus, using the modifications extensively described in Chapter 3, including the modified upper platen. There, sand was introduced into the specimen mould through a funnel inserted into the platen. Sand particles were therefore permitted to fall, under their own weight, into the sample mould. Provided no means of densification is introduced, the specimen was assumed to retain the void ratio, generated throughout the preparation phase, into the subsequent test. During testing, the void ratio would change, but the product of the void ratio at any instant and the degree of saturation at the same instant would always be constant in an undrained test.

For the oscillating box, a similar system was used. There was, of course, no requirement for a platen, although sand particles were allowed to fall, under their own gravity, into the box. The walls were rigid, so the scope for particle disturbance is greatly reduced. Care was taken, however, to ensure that the rate at which Swansea Bay sand particles were introduced into the oscillating box was kept as close as

possible to the rate at which Hostun sand particles were pluviated into the triaxial mould for the testing programme described in Chapter 3.

Here, the author has attempted to maintain consistency in the overall research programme, where the merits of employing partially saturated soil as a means of liquefaction mitigation are being investigated. In the triaxial tests described in Chapter 3, an effort was made to modify the triaxial apparatus to produce a specimen by similar means as would be achieved in the field. The situation here was very similar, where the sand was allowed to fall, under the influence of gravity, into the box.

Although laborious for a container of internal dimensions 300 mm x 200 mm x 250 mm, these precautions ensured that the pre-determined values of the moisture content, w, and the initial void ratio, e_0, were maintained as fully as possible. Therefore, due consideration of these issues ensured that the quality of the results obtained were not deemed to be unnecessarily compromised.

Determination of the Unit Weight, γ

Having established reliable values for the specific gravity, G_s, moisture content, w, and initial void ratio, e_0, as they apply to the Swansea Bay sand specimens prepared as described previously, determination of the unit weight, γ, is now possible. The saturated unit weight of the sand is given by:

$$\gamma = \frac{G_s(1+w)}{1+e}\gamma_w \qquad [5.7]$$

where γ_w is the unit weight of water (10 kN/m^3). Therefore, substituting values already obtained:

$$\gamma = \frac{(2.58)(1.2777)}{(1.7109)}\cdot(10) = 19.26 \text{ kN/m}^3 \qquad [5.8]$$

Note the difference between this value of the unit weight, γ, and that for Hostun sand, as determined in Chapter 3. This difference indicates that, for a given volume of each, the Swansea Bay sand would have the greater mass while, for a given mass, the Hostun sand would occupy the greater volume.

5.2.3 Measurement of the Excess Pore-Water Pressure

In the triaxial test programme, a number of quantities were measured, in an attempt to completely describe the behaviour of the soil when subjected to applied cyclic loading. These included:

- axial displacement during loading and unloading which, in turn, led to the determination of the engineering strain;
- axial load, as applied through the loading ram and modified upper platen;
- confining pressure; and
- excess pore-water pressure, which permitted an effective stress analysis to be conducted.

This array of measurable physical properties accounted for the detail with which the results and conclusions from the triaxial test programme were presented. However, in the oscillating box, only the excess pore-water pressure was measured directly.

As described in Section 5.1, the highest value to which the excess pore-water pressure can rise is equal to the vertical geostatic stress, or overburden pressure. In the oscillating box, neglecting the small degrees of densification that will occur due to overlying layers of soil, the vertical geostatic stress at any depth z is given by:

$$\sigma_c = \gamma z \qquad [5.9]$$

where γ is the unit weight of the soil, measured in kN/m^3. It has already been established that the unit weight of saturated Swansea Bay sand, which was the soil employed in the oscillating box test programme, is 19.26 kN/m^3. Therefore, since the maximum thickness that was set for the Swansea Bay specimen was 200mm (= 0.20m). Then, the maximum vertical geostatic stress that can be obtained is:

$$\sigma_c = (19.26)(0.20) = 3.852 \text{ kN/m}^2 \text{ (or kPa)}$$

The excess pore-water pressure at a pre-determined depth was estimated by means of a manometer tube of 4mm bore, inserted vertically down into the centre of the sand sub-layer under consideration. When the box was oscillated, the water in the manometer tube rose to a maximum, and then receded as dissipation of these pressures took place during the subsequent consolidation process. The system thus

returned to hydrostatic equilibrium. The excess pore-water pressure, u_e, was related to the height, h, reached by the manometer tube by the familiar expression from fundamental fluid mechanics:

$$u_e = \rho g h \qquad [5.10]$$

where ρ is the density of water at standard temperature and pressure conditions, which were assumed throughout this testing programme, and g is the acceleration due to gravity. The density of water was taken as $1000 kg/m^3$, while g, as in all work contained in this thesis, was taken to be $9.81 m/s^2$.

Although the determination of excess pore-water pressures by means of a manometer tube may appear crude, this method does have one significant advantage over using an electronic transducer and a data logger. The data logger, which was available for all research detailed in this thesis, did not give a continuous reading of the quantity being logged; instead, it provided an instantaneous reading once every second. This meant that maximum values of the excess pore-water pressure may have been missed.

The manometer tube gives a continuous reading, although it also requires some care in setting up. While it was not anticipated that the frequency of oscillation of the box would have been sufficient to dislodge the manometer, care was taken to ensure that the opening to the tube remained at the correct height in the specimen. Any vertical movement in the manometer may have given rise to erroneous readings.

Therefore, the manometer was fastened to a rigid crossbeam, which straddled the width of the box, and was fastened to both sides. Movement of the manometer tube, whether laterally or vertically, was thus avoided, and the readings of excess pore-water pressure obtained could then be considered as reliable as the equipment would permit.

5.3 SPECIMEN PREPARATION

5.3.1 Introduction

In this Section, attention will be given to method by which the test specimen was prepared inside the oscillating box. The method of preparation will be shown to be similar to that for the triaxial test specimens discussed in Chapters 3 and 4. However, unlike the triaxial apparatus, no further modifications of the oscillating box were required. This is because the box had rigid walls, and so the specimen was far less prone to disturbance during the preparation phase.

5.3.2 Preparation of the Sand Specimen

Chapter 3 detailed at some length how loose sand specimens were prepared within the triaxial apparatus, by means of the modifications discussed therein. The method of pluviating the sand through air and into a pre-prepared triaxial mould was described at considerable length.

For the tests conducted using the oscillating box, the method of specimen preparation was essentially identical, despite the fact that a different sand (Swansea Bay rather than Hostun) was used for this current investigation. Sand grains were allowed to fall, through air, from a hand-held spatula and into the box, thus creating a test specimen of the highest available initial void ratio, e_0, (e_{max} = 0.71, Section 5.2). Care was taken throughout the specimen preparation procedure to ensure that:

- the spatula was held as close to the existing surface of the sand, so that the sand particles were unable to accrue sufficient kinetic energy to disturb and densify the sand particles already in place; also
- that the surface of the sand was kept as level as possible at all times; and
- that contact with the rigid walls of the oscillating box was avoided wherever possible. Even though the walls of the box were rigid, thus rendering the specimen far less prone to disturbance when compared to the situation in the triaxial apparatus, the author was aware of the unwanted effects that an unnecessary disturbance of the box might produce.

Preparation of the sand specimen continued until the specimen reached the required depth of 200mm. Gentle screeding was performed on the surface of the specimen at

intervals of 40mm; the significance of this figure will be discussed in the next Section. The purpose of screeding was to ensure that the surface of the specimen was kept as level as possible. However, with all aforementioned precautions followed, such action was infrequent.

While this method of preparation may appear laborious, such precautions were necessary to ensure that the specimen was of the highest possible quality. The time required to prepare the specimen of the required 200mm depth was approximately three hours.

5.3.3 Saturation of the Sand Specimen

Once the test specimen had been satisfactorily prepared, it was necessary to introduce water into the voids. With reference to Figures 5.1 and 5.2 (Section 5.1), this was achieved by means of a rigid water inlet pipe, fixed to the base of the oscillating box with silicon grease. Water passed through this pipe and into the specimen from a reservoir, the upper surface of which was maintained at a height of approximately 100mm above the wetting front, as observed through the walls of the oscillating box. This small pressure head ensured that the hydraulic gradient was not sufficient to disturb the sand particles, thereby adversely affecting the void ratio. A constant head was maintained in the reservoir by constant refilling to the required height. The time required for the wetting front to reach the upper surface of the sand specimen was approximately 2½ hours. The arrangement described above is illustrated in Figure 5.3 below.

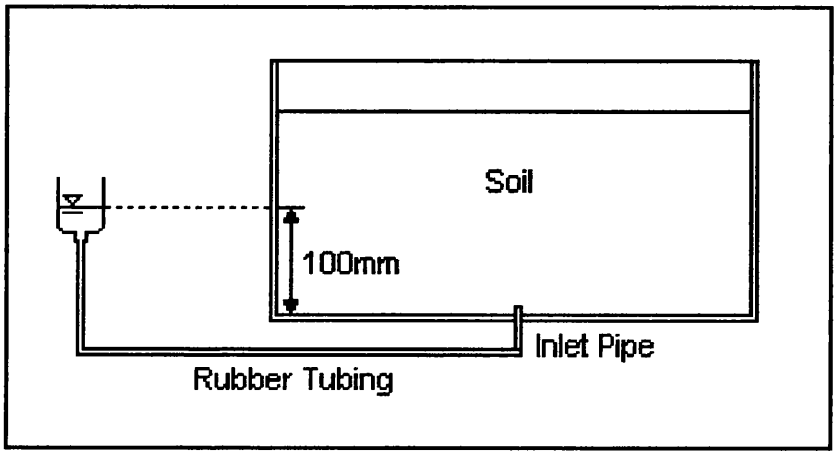

***Figure 5.3** – Saturation of the Specimen Within the Oscillating Box*

5.3.4 Installation of the Manometers

Two manometers were employed during the oscillating box test programme, which will be discussed at greater length in the next Section. These were installed within the apparatus before the box was filled with sand.

The manometers, which consisted of two transparent tubes of 4mm bore, were mounted on a crossbeam which straddled the width of the oscillating box at the open face. The manometers extended to the depth required by the test in question; lines were drawn across the entire width of the box, at both ends, at those depths at which excess pore-water pressures were to be monitored. Careful visual inspection from either end of the box then ensured that the openings to the manometers were as close as possible to the required depth.

The manometers were installed a distance of 25mm apart, and as close to the centre of the specimen as possible, when viewed from the horizontal plane. The close proximity of the manometers to each other ensured that limited head and eye movement was required when simultaneously recording the heights of the water in the tubes. The scope for error in this particular aspect of the test procedure is thus reduced to a minimum.

Two metric rules were mounted alongside the manometers. The zero point on both these rules coincided with where the surface of the specimen was to be, namely 200mm above the base of the box. Above this height, the manometer tubes were marked in 2mm intervals, to aid in the recording of the excess pore-water pressures. At this point, both manometers were open to the atmosphere.

On saturating the soil in the box, water rose up the manometer tubes as the wetting front approached the surface of the specimen. This gave further visual confirmation of the position of the upper water level. When the water level reached 0mm on the mounted metric rules, and after a short time period which permitted equilibrium conditions to be reached, the specimen was deemed to be saturated, providing visual inspection confirmed this observation.

Being mounted to a fixed crossbeam, the manometers were not susceptible to lateral movement as the box was oscillated. Lateral or even vertical movement of the manometers might have moved the manometers to regions where estimations of the excess pore-water pressures were not required. This, quite clearly, would have significantly reduced the quality of the results obtained from this testing programme.

5.3.5 Sources of Error

There are, as with all experimental apparatus, certain sources of error which are present in the oscillating box system. These will now be specifically considered.

The specimen is the oscillating box is 200mm thick. The height of the box is 250mm; the difference of 50mm ensures that material is not lost over the sides of the box during testing. However, while solving this problem, the difficulty of reading water heights in the manometer tubes which extended to shallow depths emerged. As will be seen in the next section, excess pore-water pressures for depths above 80mm in the specimen generally produce water heights of less than 80mm in the manometers when the oscillations are applied. It has already been stated that the difference between the top of the box and the top of the specimen is 50mm which means that, for observing the water heights, two options are available. These are;

- observing the water heights through the side walls of the box; or
- looking downward and at an angle to the manometer tubes, in order to ensure an unimpeded view of the manometers.

Both of these methods were seen to have disadvantages. For example, movements of soil and water near to the side walls of the box, when it is at the extreme of an oscillation, was seen to impede the view of the manometers. Looking downwards and at an angle to the manometers will, quite clearly, increase the possibility of parallax errors. However, it was deemed by the author that that latter option was preferable, simply because an unimpeded view of the manometers was of paramount importance, since these were the only means of understanding the response of the soil for this particular test programme.

When water is seeping upward through the soil matrix during the preparation phase, it does so under the influence of a hydraulic gradient, which is defined as the loss of pressure head per unit length. If the hydraulic gradient is less than 1.00, then linear conditions are assumed to exist. However, this does not infer that the wetting front is horizontal. In fact, the wetting front will have a slight protuberance directly over the exit point of the inlet pipe. As water seeps through the pores of the soil, further hydraulic gradients will be set up be set up between this protuberance and the remainder of the wetting front. These gradients will act in such a way that the wetting front is brought to equilibrium as it moves further up the specimen. In other words, these gradients will work to bring the wetting front horizontal.

When the wetting front emerged at the surface of the specimen, it was seen that wetting of the surface particles was essentially uniform. Equilibrium was confirmed by the position of the water in the manometer tubes. However, it should be noted that the head between the water reservoir and the wetting front was not maintained at 100mm, but is gradually reduced as the surface is approached. This ensures that water fills all regions of the specimen instead of collecting at the surface.

Finally, the vibratory effect produced when oscillations are being applied to the box enables the soil particles to settle into a denser, more stable configuration. Visual inspection of the specimen confirms this, as the surface is seen to subside as shaking continues. As excess pore-water pressures dissipate, so the specimen consolidates. During the pre-testing investigations, it was seen that, for a fully saturated specimen, the consolidation observed was approximately 13mm after 30 cycles, where each cycle had a maximum magnitude of acceleration of 0.1g. For an oscillating box specimen divided into five sub-layers, as was the case for this research programme, this represents a drop of 2.6mm per sub-layer of 40mm thickness. As the manometers extended to the centre of these sub-layers, it was deemed that, while such a decrease in volume might have an effect on the values of excess pore-water pressure produced, it would not adversely affect the overall trend that was expected to emerge. Therefore, errors due to such changes and subsidence of the surface were neglected.

5.4 THE OSCILLATING BOX TEST PROGRAMME

5.4.1 Introduction

Previously in this Chapter, the specifications of the oscillating box have been thoroughly detailed. The phase properties of the Swansea Bay sand, which was used in the test programme, have also been discussed fully. In this Section, the structure of the research programme conducted using the oscillating box with this sand will be laid out.

5.4.2 The Motion of the Oscillating Box

As described earlier in this Chapter, the oscillating box is a single-degree-of-freedom (SDOF) system, where motion of the box is constrained all directions other than laterally by guides beneath a supporting metal plate. However, the analysis of the soil specimen itself is not a SDOF problem. Here, since excess pore-water pressures are being estimated with depth and, since shear waves propagated in the vertical direction, the soil itself is considered as a one-dimensional system in the vertical direction.

This movement of the box is provided by a motor and speed controller combination, and connected to the metal plate by means of a rigid steel rod. For further information relating to the specifications of the box, the reader is referred to Section 5.2, while a mathematical treatment of the forced, undamped motions, which are produced by the motor/speed controller, is provided by Kramer (1996).

The motion of the oscillating box may be conveniently described by the equations governing simple harmonic (circular) motion. In this theory, the linear acceleration of a single-degree-of-freedom system, such as the oscillating box, is given by:

$$a = -\omega^2 x \qquad [5.11]$$

where a is the acceleration of the system, ω is the angular (circular) frequency of the motion (i.e. oscillations per second), and x is the displacement from the equilibrium position of the motion. The minus sign is present since a retarding acceleration always acts toward the equilibrium position.

For the oscillating box, the maximum amplitude of the motion was 0.1m, while the circular frequency was set for convenience at π radians per second (i.e. one full oscillation every two seconds). Then, the maximum linear acceleration of the system, which occurs at the point of maximum amplitude of the motion, is given by:

$$a = (\pi)(\pi)(0.1) \qquad = 0.987 \text{ m/s}^2$$

In terms of the known value of the acceleration due to gravity, g, this acceleration may be stated as $a = 0.1g$.

Following a period of experimentation, the details of which will not be included here, it was deemed that, with this magnitude of acceleration, a test consisting of 30 cycles, each having this magnitude of linear acceleration, was sufficient for the excess pore-water pressure at any point within the specimen to rise to its peak value, and then dissipate, so that this pressure returned to within 10% of its original hydrostatic levels. The time for each test was therefore set at 60 seconds.

5.4.3 The Test Programme

The Test Programme consisted of 18 tests, each conducted on Swansea Bay sand specimens prepared in the manner detailed earlier in this Chapter, and each subjected to 30 cycles of one-dimensional simple harmonic oscillations, as described above.

In each of the 18 tests, the specimens were carefully subdivided into 5 sub-layers, each of 40mm thickness. The reason behind gently screeding the specimen at this level, and multiples thereof, may now be understood.

Sub-layers may be saturated or partially saturated, depending on the test conducted. Partially saturated sub-layers were treated with zeolite prior to saturation. To obtain a fully saturated sub-layer, the sand constituting this sub-layer was pluviated into the oscillating box in the manner already described, without previously being mixed with the zeolite powder. Water was then introduced into the system which, under the action of an upward hydraulic gradient, completely filled the voids within these sub-layers.

To obtain a partially saturated sub-layer, zeolite was mixed thoroughly with the sand. It was shown in Chapter 3 that a volume of zeolite, equal to 2% of the total

volume of the sub-layer, would produce a sufficiently low initial degree of saturation, S_{r0}, within this sub-layer for the effects of the partial saturation to be observed. The total volume, V_l, of the sub-layer, in millimetres, is given by:

$$V_l = (300)(200)(40) = 2{,}400{,}000 mm^3$$

2% of this volume is 48,000 mm^3, which in turn is equal to 48 cm^3 (cubic centimetres, or cc's).

Of the 18 tests conducted in this programme, 3 were 'control' tests, in which the excess pore-water pressure at the centre of each of the five saturated sub-layers was determined. In the remaining 15 tests, the same five excess pore-water pressures were established, but for each of the five sub-layers being partially saturated in turn. Therefore, not only was the excess pore-water pressure in the partially saturated sub-layer estimated, but the pore-water pressures in other sub-layers were also determined. This permitted a comprehensive profile of the excess pore-water pressures within such a deposit to be established, so that the effect of the partially saturated sub-layer on surrounding fully saturated sub-layers may be reliably modelled.

Test Nomenclature

In order to identify them as being a part of the current research, each of the 18 tests in this programme was given a 'BX' prefix. Numbering of the tests was sequential, except where tests were not conducted for the reasons stated.

The five sub-layers within the soil specimen were labelled from L-1 to L-5, depending on their depth. Table 5.1 below illustrates the depth at which each sub-layer was located.

Sub-Layer	Depth
L-1	0 mm (surface) to 40 mm
L-2	40 mm to 80 mm
L-3	80 mm to 120 mm
L-4	120 mm to 160 mm
L-5	160 mm to 200 mm

***Table 5.1** – Sub-Layers in Oscillating Box Specimen*

Table 5.2 summarises the 18 tests that were conducted for the purposes of this research. The first column gives the test number, according to the nomenclature stated above. In the second column, those sub-layers that remained totally saturated throughout the given test are listed. The third column gives the sub-layer affected by partial saturation. The sub-layers from which excess pore-water measurements were taken are given in the fourth column. A maximum of two excess pore-water pressure measurements, from differing sub-levels, were taken for each test. Each series of excess pore-water pressure measurements required a separate manometer tube.

Test	Full Sat. Sub-Layers	Part. Sat. Sub-Layers	Pore Pressure From
BX-2 (Fig 5.4)	All	None	L-1 & L-2
BX-3 (Fig 5.4)	All	None	L-3 & L-4
BX-5 (Fig 5.4)	All	None	L-5
BX-6 (Fig 5.5)	L-1, L-2, L-3, L-4	L-5	L-1 & L-2
BX-7 (Fig 5.5)	L-1, L-2, L-3, L-4	L-5	L-3 & L-4
BX-8 (Fig 5.5)	L-1, L-2, L-3, L-4	L-5	L-5
BX-9 (Fig 5.6)	L-1, L-2, L-3, L-5	L-4	L-1 & L-2
BX-10 (Fig 5.6)	L-1, L-2, L-3, L-5	L-4	L-3 & L-4
BX-11 (Fig 5.6)	L-1, L-2, L-3, L-5	L-4	L-5
BX-12 (Fig 5.7)	L-1, L-2, L-4, L-5	L-3	L-1 & L-2
BX-13 (Fig 5.7)	L-1, L-2, L-4, L-5	L-3	L-3 & L-4
BX-15 (Fig 5.7)	L-1, L-2, L-4, L-5	L-3	L-5
BX-16 (Fig 5.8)	L-1, L-3, L-4, L-5	L-2	L-1 & L-2
BX-17 (Fig 5.8)	L-1, L-3, L-4, L-5	L-2	L-3 & L-4
BX-18 (Fig 5.8)	L-1, L-3, L-4, L-5	L-2	L-5
BX-19 (Fig 5.9)	L-2, L-3, L-4, L-5	L-1	L-1 & L-2
BX-20 (Fig 5.9)	L-2, L-3, L-4, L-5	L-1	L-3 & L-4
BX-21 (Fig 5.9)	L-2, L-3, L-4, L-5	L-1	L-5

***Table 5.2** – Summary of the Test Programme for the Oscillating Box*

Notes:

- Test BX-1 was used as a 'dummy' test, to permit familiarity with the test procedure.
- Test BX-4 was aborted due to failure in saturating the specimen. This failure was caused by aggregations of sand blocking the interior of the water inlet pipe.
- Test BX-14 was aborted due to accidental specimen disturbance.

5.4.4 The Test Method

This sub-Section summarises the method used when completing each of the 18 tests outlined above.

- The two manometer tubes were set inside the oscillating box with their lower ends at the required depths.
- The specimen was prepared using the procedure outlined earlier.
- The upper surfaces of each of the five sub-levels were carefully screeded at intervals of 40 mm
- Where partial saturation was to be introduced into a given sub-layer, the sand was mixed thoroughly with 48 cubic centimetres of zeolite (2% by volume), before being pluviated through air and into the oscillating box. Aggregations of zeolite were avoided at all times by grounding the zeolite powder.
- Water was introduced through the inlet pipe and into the specimen at 200mm depth. At this point, every attempt was made to maintain a pressure head of 100mm between the upper level of the reservoir, and the wetting front inside the oscillating box.
- The pressure head was reduced by 20mm when visual inspection of the specimen indicated that a sub-layer had been saturated.
- Once it as deemed that the wetting front had reached all parts of the surface of the specimen, the upper level of the reservoir was brought level with the top of the specimen.
- A further ten minutes was allowed before shaking for all sub-layers, particularly the one containing the zeolite, to reach equilibrium.
- Once this time had elapsed, the reservoir was sealed from the atmosphere. It was important to ensure that no air was trapped above the reservoir.
- Shaking of the box then commenced at the required frequency.
- Measurements were taken of the height that the water had reached in the manometer tubes. These measurements were taken approximately at six-second intervals. The time taken for the 30 cycles, with a frequency of π radians per second, was 60 seconds, allowing a maximum of 10 readings of water height reached to be taken for each sub-layer.
- On removal from the oscillating box, the sand used was washed to remove any zeolite residue, and then allowed to dry in air.

Several precautions needed to be observed so that the test programme could be conducted in as reliable a manner as was possible. Firstly, before each test, it was necessary to ensure that sand had not become trapped inside the water inlet pipe. Such an obstruction would lead to an unacceptable period required for saturation of the specimen.

Once the wetting front had visibly covered the entire extent of the surface of the specimen, the upper level of the reservoir was set to this level, to prevent any water flowing either to or from the specimen. Prior to the application of the oscillations, the reservoir was sealed, so that it did not, in effect, become a third manometer tube. Sealing the reservoir ensured that, given the incompressibility of water, it acted as an extension of a pore space, and was therefore subject to the same physical phenomena that existed throughout the remainder of the specimen.

5.5 THE OSCILLATING BOX TEST RESULTS

5.5.1 Introduction

In this Section, the results from the test programme using the oscillating box are presented. The reader is referred to Table 5.2 in the previous Section for a summary of the test programme, and the nomenclature employed. For ease of reference, the results from the current testing programme will be presented in the same order as detailed in Table 5.2.

For each test, two sets of readings for the excess pore-water pressure were taken. The manometer tubes from which these values were determined were placed side by side and 25mm apart on the crossbeam of the oscillating box, with each having its own millimetre scale. This arrangement is discussed further in Section 5.3, which focused on the method of specimen preparation, and also on the manner in which the two manometer tubes were set at their respective depths. Having the manometers in such close proximity to each other reduced the scope for error during each six-second interval between heights being recorded. Thus, the quality of the results obtained was maintained throughout the test programme.

For each test, the heights that the water reached in the manometer tubes is presented in raw form. The manometer tubes were marked with horizontal lines at intervals of 20mm, for increased ease of reference. As stated above, and also in the previous Section, readings of water height were taken every six seconds. The excess pore-water pressures, u_e, at heights, h, were calculated from the familiar expression:

$$u_e = \rho g h \qquad [5.12]$$

where ρ is the density of water at standard temperature and pressure conditions, and has a value of 1000kg/m^3, while g is the acceleration due to gravity, taken to be 9.81m/s^2.

In addition, time histories of the excess pore-water pressures are given. These are plots of the evolution of the excess pore-water pressure with time over the 60-second duration of each test. From these plots, approximate values of maxima may be obtained. These values will subsequently be used in the work outlined in Chapter 6.

5.5.2 Tests BX-2, BX-3, and BX-5

In these tests, all sub-layers were fully saturated.

Water Heights (mm)

Test Details		Time Elapsed (seconds)										
No.	**Sub-layer**	**0**	**6**	**12**	**18**	**24**	**30**	**36**	**42**	**48**	**54**	**60**
BX-2	L-1	0	1	2	2	2	1	1	0	0	0	0
BX-2	L-2	0	14	33	31	24	17	12	9	7	5	2
BX-3	L-3	0	31	76	104	103	90	71	50	29	11	4
BX-3	L-4	0	87	142	142	135	111	82	56	25	12	5
BX-5	L-5	0	136	190	194	194	179	141	96	44	16	6

Table 5.3 *– Water Heights Reached in Tests BX-2, BX-3, and BX-5*

Excess Pore-Water Pressures (kPa)

Test Details		Time Elapsed (seconds)										
No.	**Sub-layer**	**0**	**6**	**12**	**18**	**24**	**30**	**36**	**42**	**48**	**54**	**60**
BX-2	L-1	0.00	0.01	0.02	0.02	0.02	0.01	0.01	0.00	0.00	0.00	0.00
BX-2	L-2	0.00	0.14	0.32	0.30	0.24	0.17	0.12	0.09	0.07	0.05	0.02
BX-3	L-3	0.00	0.30	0.75	1.02	1.01	0.88	0.70	0.49	0.28	0.11	0.04
BX-3	L-4	0.00	0.85	1.39	1.39	1.32	1.09	0.80	0.55	0.25	0.12	0.05
BX-5	L-5	0.00	1.33	1.86	1.90	1.90	1.76	1.38	0.94	0.43	0.16	0.06

Table 5.4 *– Excess Pore-Water Pressures in Tests BX-2, BX-3, and BX-5*

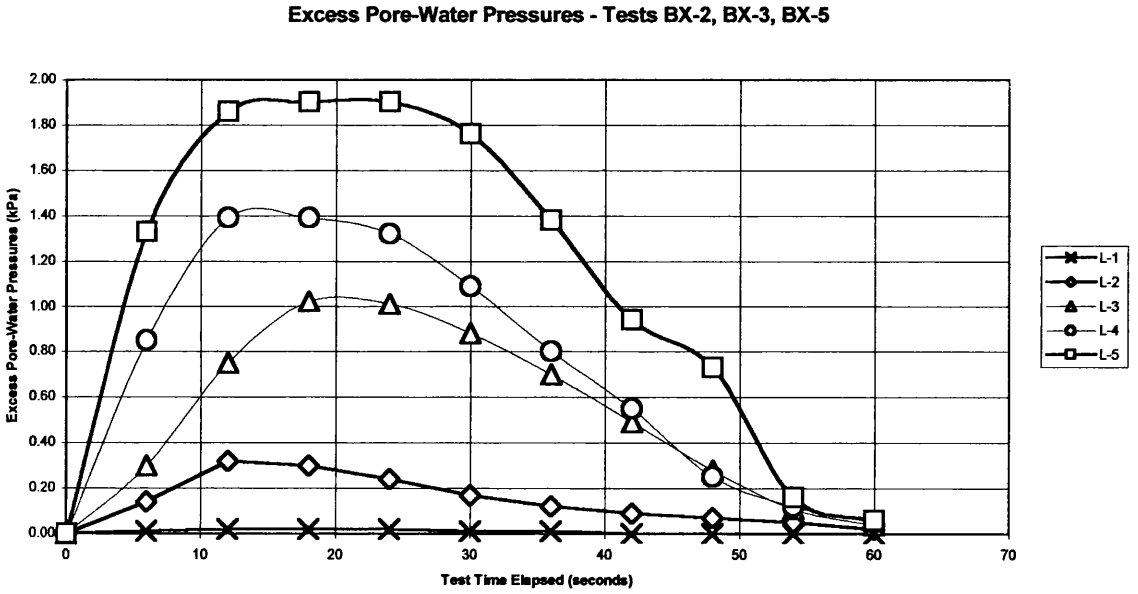

Figure 5.4 *– Excess Pore-Water Pressures in Tests BX-2, BX-3, and BX-5*

5.5.3 Tests BX-6, BX-7, BX-8

Here, sub-layer L-5 (depth 160mm to 200mm) was partially saturated.

Water Heights (mm)

Test Details		Time Elapsed (seconds)										
No.	**Sub-layer**	**0**	**6**	**12**	**18**	**24**	**30**	**36**	**42**	**48**	**54**	**60**
BX-6	L-1	0	0	1	2	1	2	1	1	0	0	0
BX-6	L-2	0	29	37	34	29	23	18	13	10	7	3
BX-7	L-3	0	45	99	102	100	88	65	46	33	18	8
BX-7	L-4	0	81	128	137	123	98	80	61	41	28	11
BX-8	L-5	0	77	140	144	143	127	103	70	43	22	7

***Table 5.5** – Water Heights Reached in Tests BX-6, BX-7, and BX-8*

Excess Pore-Water Pressures (kPa)

Test Details		Time Elapsed (seconds)										
No.	**Sub-layer**	**0**	**6**	**12**	**18**	**24**	**30**	**36**	**42**	**48**	**54**	**60**
BX-6	L-1	0.00	0.00	0.01	0.02	0.01	0.02	0.01	0.01	0.00	0.00	0.00
BX-6	L-2	0.00	0.28	0.36	0.33	0.28	0.23	0.18	0.13	0.10	0.07	0.03
BX-7	L-3	0.00	0.44	0.97	1.00	0.98	0.86	0.64	0.45	0.32	0.18	0.08
BX-7	L-4	0.00	0.79	1.26	1.34	1.21	0.96	0.78	0.60	0.40	0.27	0.11
BX-8	L-5	0.00	0.76	1.37	1.41	1.40	1.25	1.01	0.69	0.42	0.22	0.07

***Table 5.6** – Excess Pore-Water Pressures in Tests BX-6, BX-7, and BX-8*

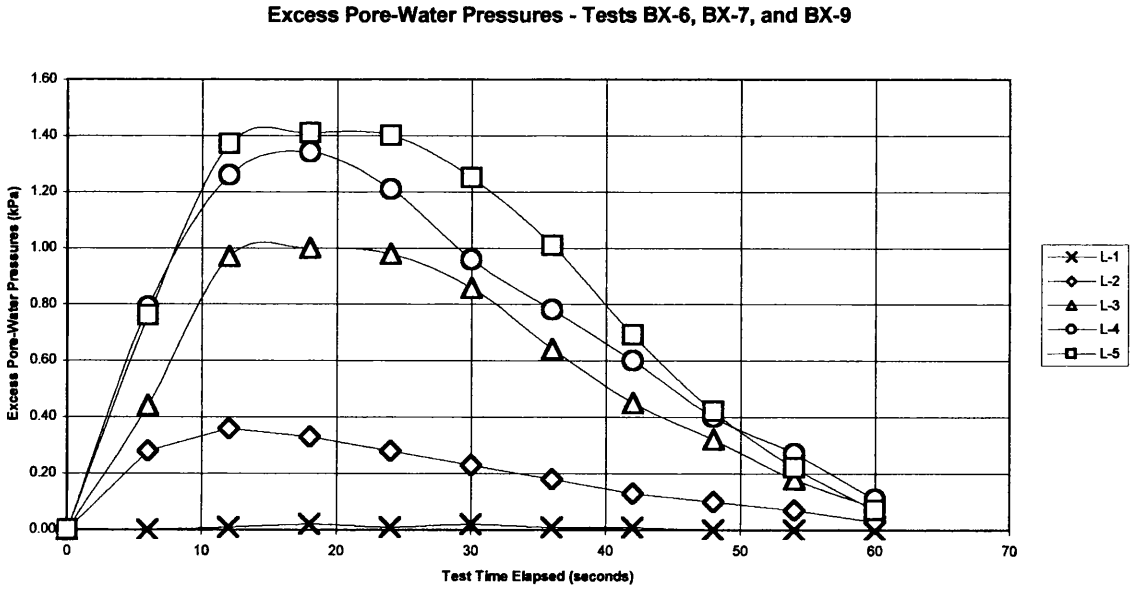

***Figure 5.5** – Excess Pore-Water Pressures in Tests BX-6, BX-7, and BX-8*

5.5.4 Tests BX-9, BX-10, and BX-11

Here, sub layer L-4 (depth 120mm to 160mm) was partially saturated.

Water Heights (mm)

Test Details		Time Elapsed (seconds)										
No.	**Sub-layer**	**0**	**6**	**12**	**18**	**24**	**30**	**36**	**42**	**48**	**54**	**60**
BX-9	L-1	0	0	2	2	2	1	1	0	0	0	0
BX-9	L-2	0	34	41	41	37	31	24	18	11	7	2
BX-10	L-3	0	79	108	106	90	76	62	47	33	20	6
BX-10	L-4	0	74	119	126	124	110	90	72	49	30	9
BX-11	L-5	0	132	177	178	154	127	103	84	62	44	22

***Table 5.7** – Water Heights Reached in Tests BX-9, BX-10, and BX-11*

Excess Pore-Water Pressures (kPa)

Test Details		Time Elapsed (seconds)										
No.	**Sub-layer**	**0**	**6**	**12**	**18**	**24**	**30**	**36**	**42**	**48**	**54**	**60**
BX-9	L-1	0.00	0.00	0.02	0.02	0.02	0.01	0.01	0.00	0.00	0.00	0.00
BX-9	L-2	0.00	0.33	0.40	0.40	0.36	0.30	0.24	0.18	0.11	0.07	0.02
BX-10	L-3	0.00	0.77	1.06	1.04	0.88	0.75	0.61	0.46	0.32	0.20	0.06
BX-10	L-4	0.00	0.73	1.17	1.24	1.22	1.08	0.89	0.71	0.48	0.29	0.09
BX-11	L-5	0.00	1.29	1.74	1.75	1.51	1.25	1.01	0.82	0.61	0.43	0.22

***Table 5.8** – Excess Pore-Water Pressures in Tests BX-9, BX-10, and BX-11*

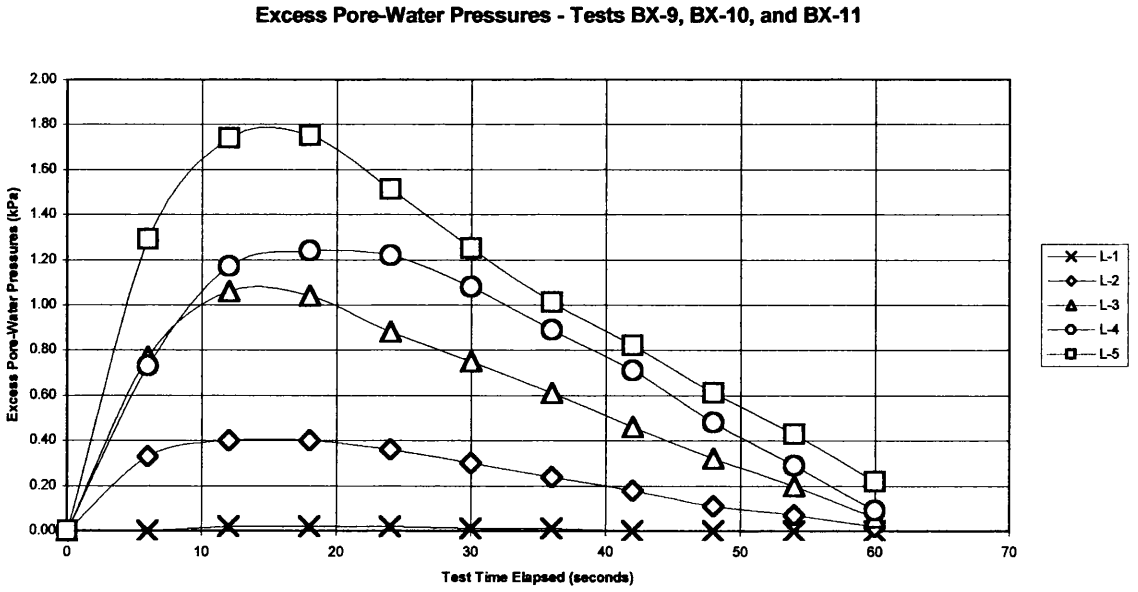

***Figure 5.6** – Excess Pore-Water Pressures in Tests BX-9, BX-10, and BX-11*

5.5.5 Tests BX-12, BX-13, and BX-15

Here, sub-layer L-3 (depth 80mm to 120mm) is partially saturated.

Water Heights (mm)

Test Details		Time Elapsed (seconds)										
No.	**Sub-layer**	**0**	**6**	**12**	**18**	**24**	**30**	**36**	**42**	**48**	**54**	**60**
BX-12	L-1	0	1	2	2	1	1	1	1	0	0	0
BX-12	L-2	0	37	41	41	36	31	25	19	13	8	3
BX-13	L-3	0	53	84	85	84	58	34	21	11	8	5
BX-13	L-4	0	85	144	145	144	116	86	62	27	17	14
BX-15	L-5	0	157	188	186	167	143	110	87	56	36	15

Table 5.9 *– Water Heights Reached in Tests BX-12, BX-13, and BX-15*

Excess Pore-Water Pressures (kPa)

Test Details		Time Elapsed (seconds)										
No.	**Sub-layer**	**0**	**6**	**12**	**18**	**24**	**30**	**36**	**42**	**48**	**54**	**60**
BX-12	L-1	0.00	0.01	0.02	0.02	0.01	0.01	0.01	0.01	0.00	0.00	0.00
BX-12	L-2	0.00	0.36	0.40	0.40	0.35	0.30	0.25	0.19	0.13	0.08	0.03
BX-13	L-3	0.00	0.52	0.83	0.84	0.83	0.57	0.34	0.21	0.11	0.08	0.05
BX-13	L-4	0.00	0.84	1.42	1.43	1.42	1.14	0.85	0.61	0.27	0.17	0.14
BX-15	L-5	0.00	1.54	1.84	1.82	1.64	1.40	1.08	0.85	0.55	0.35	0.15

Table 5.10 *– Excess Pore-Water Pressures in Tests BX-12, BX-13, and BX-15*

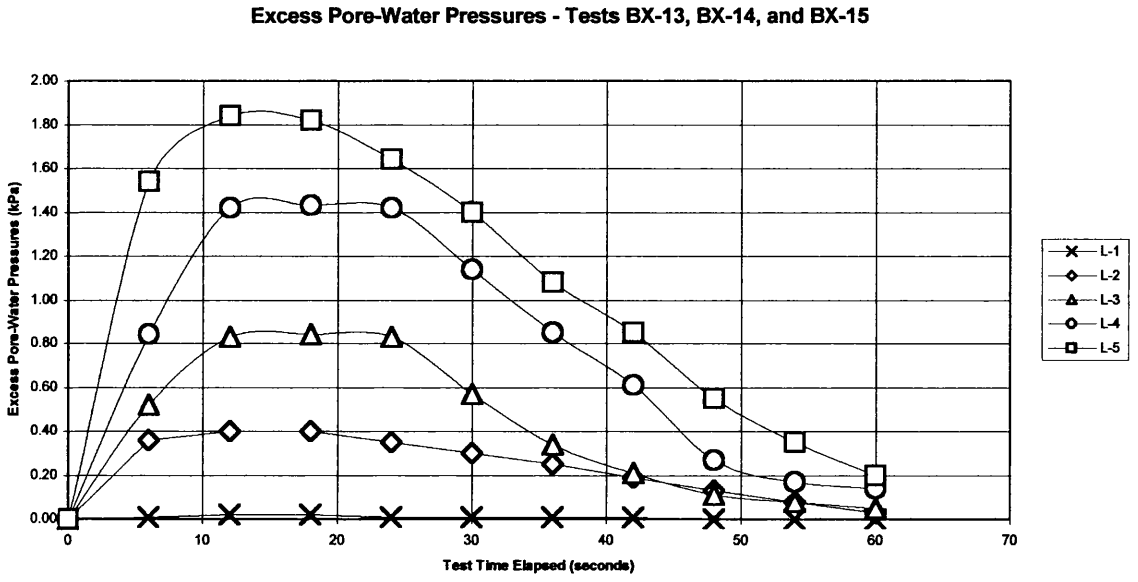

Figure 5.7 *– Excess Pore-Water Pressures in Tests BX-12, BX-13, and BX-15*

5.5.6 Tests BX-16, BX-17, and BX-18

Here, sub-layer L-2 (depth 40mm to 80mm) is partially saturated.

Water Heights (mm)

Test Details		Time Elapsed (seconds)										
No.	**Sub-layer**	**0**	**6**	**12**	**18**	**24**	**30**	**36**	**42**	**48**	**54**	**60**
BX-16	L-1	0	1	2	2	2	1	1	1	0	0	0
BX-16	L-2	0	18	28	31	29	25	18	14	7	6	3
BX-17	L-3	0	73	94	100	99	83	69	50	31	16	4
BX-17	L-4	0	109	138	138	115	89	74	51	33	19	6
BX-18	L-5	0	141	188	191	180	153	127	101	63	39	11

Table 5.11 *– Water Heights Reached in Tests BX-16, BX-17, and BX-18*

Excess Pore-Water Pressures (kPa)

Test Details		Time Elapsed (seconds)										
No.	**Sub-layer**	**0**	**6**	**12**	**18**	**24**	**30**	**36**	**42**	**48**	**54**	**60**
BX-16	L-1	0.00	0.01	0.02	0.02	0.02	0.01	0.01	0.01	0.00	0.00	0.00
BX-16	L-2	0.00	0.18	0.28	0.30	0.29	0.25	0.18	0.14	0.07	0.06	0.03
BX-17	L-3	0.00	0.72	0.92	0.98	0.97	0.81	0.68	0.49	0.30	0.16	0.04
BX-17	L-4	0.00	1.07	1.35	1.35	1.13	0.87	0.73	0.50	0.32	0.19	0.06
BX-18	L-5	0.00	1.38	1.84	1.87	1.77	1.50	1.25	0.99	0.62	0.38	0.11

Table 5.12 *– Excess Pore-Water Pressures in Tests BX-16, BX-17, and BX-18*

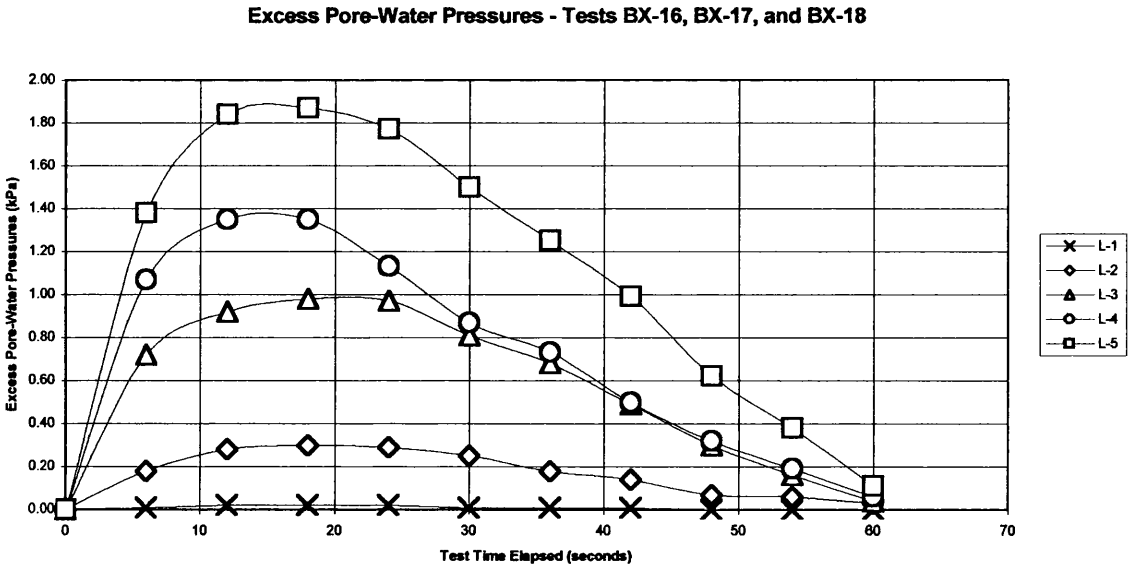

Figure 5.8 *– Excess Pore-Water Pressures in Tests BX-16, BX-17, and BX-18*

5.5.7 Tests BX-19, BX-20, and BX-21

Here, the uppermost sub-layer L-1 (depth 0mm to 40mm) is partially saturated.

Water Heights (mm)

Test Details		Time Elapsed (seconds)										
No.	**Sub-layer**	**0**	**6**	**12**	**18**	**24**	**30**	**36**	**42**	**48**	**54**	**60**
BX-19	L-1	0	0	1	1	2	2	1	1	0	0	0
BX-19	L-2	0	30	39	39	37	31	26	20	14	7	3
BX-20	L-3	0	73	102	100	87	73	54	42	27	16	4
BX-20	L-4	0	103	139	138	121	106	88	67	47	26	8
BX-21	L-5	0	145	193	177	151	124	101	82	60	41	18

Table 5.13 *– Water Heights Reached in Tests BX-19, BX-20, and BX-21*

Excess Pore-Water Pressures (kPa)

Test Details		Time Elapsed (seconds)										
No.	**Sub-layer**	**0**	**6**	**12**	**18**	**24**	**30**	**36**	**42**	**48**	**54**	**60**
BX-19	L-1	0.00	0.00	0.01	0.01	0.02	0.02	0.01	0.01	0.00	0.00	0.00
BX-19	L-2	0.00	0.29	0.38	0.38	0.36	0.30	0.26	0.20	0.14	0.07	0.03
BX-20	L-3	0.00	0.72	1.00	0.98	0.85	0.72	0.53	0.41	0.26	0.16	0.04
BX-20	L-4	0.00	1.01	1.36	1.35	1.19	1.04	0.86	0.66	0.46	0.26	0.08
BX-21	L-5	0.00	1.42	1.89	1.74	1.48	1.22	0.99	0.80	0.59	0.40	0.18

Table 5.14 *– Excess Pore-Water Pressures in Tests BX-19, BX-20, and BX-21*

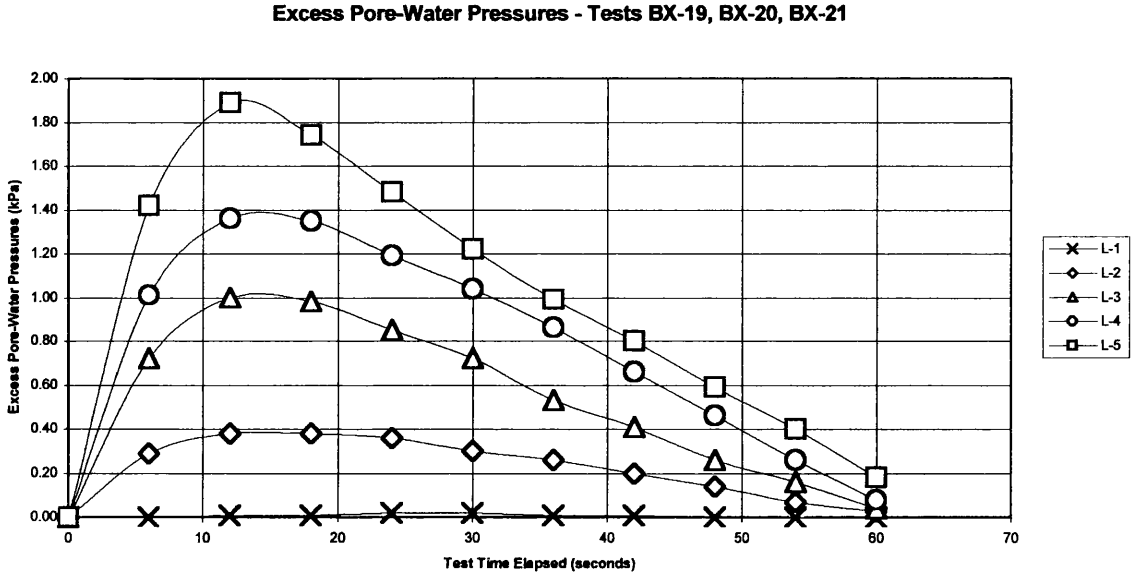

Figure 5.9 *– Excess Pore-Water Pressures in Tests BX-19, BX-20, and BX-21*

5.6 POST-PROCESSING AND CONCLUSIONS

5.6.1 A Summary of the Work

This Chapter focused on a qualitative test programme conducted using the so-called oscillating box system. The system was described as single-degree-of-freedom (SDOF), although the analysis of the Swansea Bay sand specimen placed inside the rigid box could be considered as a one-dimensional problem in the vertical direction. Rollins and Seed (1990) summarised similar work conducted by Yoshimi and Tokimatsu (1977) in which the influence of a surface load was investigated.

The programme consisted of 18 tests, in each of which the sand specimen was divided into five sub-layers. Each layer was of thickness 40mm, and each was treated with zeolite to produce partial saturation within that sub-layer. The pore-water pressure response of all layers, when the box was subjected to cyclic loading, was then analysed using simple manometer tubes. The results of this test programme were detailed in the previous Section.

The method by which the Swansea Bay specimens were prepared was also included in this Section, as well as the method by which the excess pore-water pressures were recorded. All relevant spatial dimensions of the oscillating box were explicitly stated, as were anticipated sources of error.

5.6.2 Analysis of Pore-Water Pressure Response

Tables 5.15 to 5.20 below detail the maximum excess pore-water pressure recorded in each test. This pressure is expressed in terms of the normalised pore-water pressure ratio r_0, which is the ratio of the maximum pore-water pressure recorded at a given depth (u_e) to the maximum obtainable pore-water pressure at that depth ($u_{e,max}$). The depths indicated are those at which manometer tubes were inserted. Shaded entries indicate levels at which partial saturation was introduced.

Sub-Layer	Unit Wt.	Depth (m)	$u_{e,max}$ (kPa)	u_e (kPa)	r_0
L-1	19.26	0.02	0.39	0.02	0.05
L-2	19.26	0.06	1.16	0.33	0.28
L-3	19.26	0.10	1.93	1.03	0.53
L-4	19.26	0.14	2.70	1.40	0.52
L-5	19.26	0.18	3.47	1.90	0.55

***Table 5.15** – Values of r_0 with all Sub-Layers Saturated (No Partial Saturation)*

Sub-Layer	Unit Wt.	Depth (m)	$u_{e,max}$ (kPa)	u_e (kPa)	r_0
L-1	19.26	0.02	0.39	0.02	0.05
L-2	19.26	0.06	1.16	0.37	0.32
L-3	19.26	0.10	1.93	1.00	0.52
L-4	19.26	0.14	2.70	1.46	0.54
L-5	18.87	0.18	3.47	1.41	0.41

***Table 5.16** – Values of r_0 with Sub-Layer L-5 Partially Saturated*

Sub-Layer	Unit Wt.	Depth (m)	$u_{e,max}$ (kPa)	u_e (kPa)	r_0
L-1	19.26	0.02	0.39	0.02	0.05
L-2	19.26	0.06	1.16	0.43	0.37
L-3	19.26	0.10	1.93	1.08	0.56
L-4	18.87	0.14	2.70	1.27	0.47
L-5	19.26	0.18	3.47	1.75	0.51

***Table 5.17** – Values of r_0 with Sub-Layer L-4 Partially Saturated*

Sub-Layer	Unit Wt.	Depth (m)	$u_{e,max}$ (kPa)	u_e (kPa)	r_0
L-1	19.26	0.02	0.39	0.02	0.05
L-2	19.26	0.06	1.16	0.41	0.35
L-3	18.87	0.10	1.93	0.81	0.42
L-4	19.26	0.14	2.70	1.34	0.50
L-5	19.26	0.18	3.47	1.85	0.53

***Table 5.18** – Values of r_0 with Sub-Layer L-3 Partially Saturated*

Sub-Layer	Unit Wt.	Depth (m)	$u_{e,max}$ (kPa)	u_e (kPa)	r_0
L-1	19.26	0.02	0.39	0.02	0.05
L-2	18.87	0.06	1.16	0.30	0.26
L-3	19.26	0.10	1.93	0.98	0.51
L-4	19.26	0.14	2.70	1.36	0.50
L-5	19.26	0.18	3.47	1.87	0.54

***Table 5.19** – Values of r_0 with Sub-Layer L-2 Partially Saturated*

Sub-Layer	Unit Wt.	Depth (m)	$u_{e,max}$ (kPa)	u_e (kPa)	r_0
L-1	18.87	0.02	0.39	0.02	0.05
L-2	19.26	0.06	1.16	0.38	0.33
L-3	19.26	0.10	1.93	1.00	0.51
L-4	19.26	0.14	2.70	1.37	0.51
L-5	19.26	0.18	3.47	1.89	0.54

***Table 5.20** – Values of r_0 with Sub-Layer L-1 Partially Saturated*

A comparison between the values of r_0 in each of the partially saturated layers, and the same ration for the fully saturated case (Table 5.15) is given in Table 5.21 below. The percentage changes in the values of r_0 are also indicated.

Sub-Layer	r_0 (fully saturated)	r_0 (partially saturated)	% Change
L-1	0.05	0.05	**0.00**
L-2	0.28	0.26	**-7%**
L-3	0.53	0.42	**-26%**
L-4	0.52	0.47	**-11%**
L-5	0.55	0.41	**-34%**

***Table 5.21** – Comparison of r_0 data*

From Table 5.21, it can seen that the percentage decrease in r_0 generally increases with increasing depth, indicating the positive effect, in terms of liquefaction mitigation, of introducing a partially saturated soil stratum into a fully saturated soil matrix.

Although these results were obtained from a test programme that is somewhat more qualitative that that presented in Chapter 4 for the triaxial test, the data does suggest that the aforementioned conclusion, namely that partial saturation can reduce the potential for deleterious rises in excess pore-water pressures, and therefore be considered as a viable method of liquefaction mitigation, is valid.

The contribution made by the vibrations induced in the system by the motor is not clear. However, it should be recognised that the frequency used for all tests was the same, and so the effect of these secondary motions on each test would be deemed to produce no significant changes in the actual trends produced. Nevertheless, small errors may be present in the observed magnitudes of the excess pore-water pressures produced during testing.

CHAPTER 6

CLOSING REMARKS

6.1 CLOSING REMARKS

6.1.1 Introduction

In this Section, a closing summary of the work will be presented. General conclusions will also be quoted. However, for detailed information, the reader is directed to the relevant Chapter, where a Section outlining all relevant conclusions is included. The exceptions are Chapters 1 and 2, which contain the Opening Remarks and Liquefaction literature review respectively.

This Section also includes details of the author's recommendations for further research into the subject of using partially saturated soil as a means of liquefaction mitigation.

6.1.2 Closing Remarks

This work focused on the viability of using partially saturated soil as a means of liquefaction mitigation in engineering practice. This principle was suggested by Pietruszczak and Pande (e.g. Pietruszczak and Pande, 1995 & 1996), and the ideas presented therein form the basis of the current research.

In the opening remarks contained in Chapter 1, the objectives, layout, and scope of the work are presented. Chapter 2 contains an extensive literature review on the subject of liquefaction, and it is here that the terms and principles which are used in modern engineering practice are introduced. The primary mechanism for the development of liquefaction, namely rises in excess pore-water pressures in granular soils, was thoroughly discussed. The literature review also contained the details of a case study in order to illustrate the catastrophic effects that liquefaction can cause. This case study centred on the aftermath of the Hyogo-ken Nanbu earthquake which seriously disrupted the port facilities in the Japanese city of Kobe in 1995. The details of the resulting devastation to shoreline structures helped to provide the justification for the current work.

Chapters 3 and 4 outlined the test programme conducted in order to ascertain the viability of employing partial saturation as a means of liquefaction mitigation i.e. a process which significantly reduces the scope for deleterious rises in excess pore-water pressures. The test programme consisted of a series of undrained one-way cyclic tests on Hostun sand, a granular soil which is known for its susceptibility to liquefaction. Chapter 3 outlined the modifications to the triaxial apparatus that were

required in order to conduct this test programme effectively, as well as introducing a new technique of specimen preparation by means of a redesigned upper platen and clamp which was designed to be attached to the frame of the triaxial apparatus. Preliminary tests clearly indicated that the modified upper platen was capable of producing sand specimens with a high void ratio, a necessary condition for any soil to be susceptible to liquefaction effects.

Partial saturation was achieved by means of zeolite, a chemical which releases oxygen during reaction with water. It was found that 2% of zeolite by total volume of the specimen was capable of producing an initial degree of saturation, S_{r0}, of approximately 0.90. It was demonstrated in Chapter 4 that such a degree of saturation had a markedly negative effect on the capacity for pore-water pressures to rise within a granular specimen. With these observation, it was concluded that even a slight decrease in the degree of saturation could indeed inhibit the development of excess pore-water pressures in a granular soil, resulting in turn in a reduction in the liquefaction potential.

Chapter 5 outlined the results from a test programme using an oscillating box, which is a single-degree-of-freedom system designed to simulate the subsurface conditions present during an earthquake. The logical progression from triaxial testing to more dynamic investigations is clear; in both test programmes, however, the specimens were prepared by dry pluviation through air. The box, which was made from clear perspex to assist qualitative observation, was oscillated with an amplitude of 0.1*g*, while the specimen was of 200mm depth. The test specimen was composed of naturally-deposited Swansea Bay sand, as opposed to the Hostun sand described in Chapters 3 and 4, in order that the scope of the overall project may be broadened. Two manometer tubes, mounted onto a fixed crossbeam, allowed excess pore-water pressures within the specimen to be monitored. Initially, the water in the specimen, including that in the tubes, was in the hydrostatic condition. The results from this second test programme indicated, once again, that excess pore-water pressures could indeed be inhibited through the introduction of partial saturation. It was also demonstrated that the effect of introducing partial saturation also has an effect on the surrounding, unaffected soil. This was due to the increase in matric suction in the specimen when the partial saturation was introduced. The matric suction, which is a tensile stress, reduced the capability of the soil specimen to undergo shear strain. Strain compatibility conditions suggest, therefore, that neighbouring soil was also

affected, explaining the slight reduction in excess pore-water pressures at these secondary locations.

6.1.3 Recommendations for Further Research

Here, the main aspects of the work will be considered separately. This permits ease of reference to other parts of the thesis.

Partial Saturation (Chapters 3 and 4)

The theory and application of partial saturation in soils is an ongoing area of development within geotechnical engineering. The importance of partially saturated soils in engineering applications is now being recognised, and further innovative work is expected.

With reference to liquefaction mitigation, however, the use of partially saturated soil has received limited attention. Although this current work is expected to add positively to the body of knowledge already in existence, more sophisticated investigations will need to be conducted in order that a unified approach for the practicing engineer may be developed. However, the current work clearly indicates that a slight decrease in the degree of saturation will significantly inhibit rises in excess pore-water pressures, the primary mechanism behind liquefaction in the field.

Zeolite (Chapter 3)

Zeolite is a chemical in powder form which, on contact with water, undergoes an irreversible chemical transition. Although the British Zeolite Association has confirmed that zeolite has been used in environmental projects, its viability in terms of liquefaction mitigation has yet to be assessed in full.

This current work does, however, indicate that zeolite does indeed produce partial saturation within a granular soil.

Modified Upper Platen and Clamp (Chapter 3)

The design for the modified upper platen and clamp has, to the knowledge of the author, not been reported elsewhere in the technical literature. Although its success for the purposes of the current work has been clearly demonstrated, its effectiveness

as a universal alternative or replacement for existing coarse-grained specimen preparation methods will need to be assessed.

The Oscillating Box (Chapter 5)

The oscillating box system described in Chapter 5 has been used elsewhere, for example by Yoshimi and Tokimatsu (1977). Although the test programme was highly qualitative in nature, it should be stated that engineering principles were followed in both cases, thereby adding to the reliability of the respective results obtained.

Final remark

This work has been undertaken assuming that partial saturation can be maintained over a long period. This may however not be possible by injection of zeolite. New technology to achieve long-term partial saturation will have to be developed in due course.

REFERENCES

ADALIER, K., ELGAMAL, A.W., and **MARTIN, R.** (1998), "Foundation Liquefaction Countermeasures for Earth Embankments," Vol. 124, No.6, *Journal of Geotechnical and Geoenvironmental Engineering*, A.S.C.E., pp. 500-517.

ANDERSEN, A., and **BJERRUM, L.** (1968), "Slides in Subaqueous Slopes in Loose Sand and Silt," Publication 81, *Norwegian Geotechnical Institute*, Publication 8, Oslo, pp. 34-37.

ANDRUS, R.D., and **STOKOE, K.H., II** (2000), "Liquefaction Resistance of Soils from Shear Wave Velocity," *Journal of Geotechnical and Geoenvironmental Engineering*," Vol. 126, No.11, pp. 1015-1025.

BAEZ, J. I., and **HENRY, J. F.** (1993), "Reduction of Liquefaction Potential by Compaction Grouting at Pinopolis West Dam, SC.," *Geotechnical Practice in dam Rehabilitation*, pp. 493-506.

BARTLETT, S.F., and **YOUD, T.L.** (1995), "Empirical Prediction of Liquefaction-Induced Lateral Spread," *Journal of Geotechnical Engineering*, A.S.C.E., Vol. 121, No. 4, pp. 316-329.

BERRILL, J.B., CHRISTENSEN, S.A., KEENAN, R.P., OKADA, W., and **PETTINGA, J.R.** (2001), "Case Study of Lateral Spreading Forces on a Piled Foundation, *Géotechnique*, Vol. 51, No. 6, pp. 501-517.

BEVAN, D. J. (1997), "The Use of Dynamic Compaction to Remove/Reduce Risks due to Collapse Compression and Seismicity in Silty Fine Sands at

Smelter Site in Iran," *Ground Improvement Geosystems*, pp. 45-53, June 1997.

BISHOP, A.W. (1959), "The Principle of Effective Stress," lecture delivered in Oslo, Norway, in 1955 and published in Teknisk Ukeblad, Vol. 106, No. 39, pp. 859-863.

BISHOP, A.W. (1961), "The Measurement of Pore Pressures in the Triaxial Test," *Proceedings*, Conference on Pore Pressure and Suction in Soils, Butterworths, London.

BISHOP, A.W., and **BLIGHT, G.E.** (1963), "Some Aspects of Effective Stress in Saturated and Unsaturated Soils," *Geotechnique*, Vol.13, No.3, pp. 177-197.

BISHOP, A. W., and **HENKEL, D. J.** (1957), "The Measurement of Soil Properties in the Triaxial Test," Second Edition, Edward Arnold (Publishers) Ltd., London.

BLAZQUEZ, R.M., **KRIZEK, R.J.**, and **BAZANT, Z.P.** (1980), "Site Factors Controlling Liquefaction", *Journal of the Geotechnical Engineering Division*, A.S.C.E., Vol. 106(7), pp. 785-801.

BLIGHT, G.E. (1961), "Strength and Consolidation Characteristics of Compacted Soils," thesis presented to the University of London in partial fulfilment of the requirements of the degree of Doctor of Philosophy.

BOUCKOVALAS, G., **WHITMAN, R.V.**, and **MARR, W.A.**, (1984), "Permanent Displacement of Sand with Cyclic Loading," Journal of Geotechnical Engineering, Vol. 110, No.11, pp. 1606-1628.

BOULANGER, R.W., and **HAYDEN, R.F.** (1995), "Aspects of Compaction Grouting of Liquefiable Soil," *Journal of Geotechnical Engineering*, A.S.C.E., Vol. 121, No. 12, pp. 844-855.

BOULANGER, R.W., MEJIA, L.H., and **IDRISS, I.M.** (1997), "Liquefaction at Moss Landing During Loma Prieta Earthquake," Journal of Geotechnical and Geoenvironmental Engineering, A.S.C.E., Vol. 123, No. 5, pp. 453-467.

BOULANGER, R.W., and **SEED, R.B.** (1995), "Liquefaction of Sand Under Bidirectional Monotonic and Cyclic Loading," *Journal of Geotechnical Engineering*, A.S.C.E., Vol. 121, No. 12, pp. 870-878.

BOUSSINESQ, J. (1885), "Application des potentiels à l'étudé de l'équilibre et de mouvement des solides élastiques," Gauthier-Villard, Paris.

BRITISH STANDARDS INSTITUTION, "Methods of Test for Soils for Civil Engineering Purposes," BS 1377.

BROMS, B.B. (1980) "Soil Sampling in Europe: State-of-the-Art," *Journal of the Geotechnical Engineering Division*, A.S.C.E., GT1, Vol. 106, Paper 15199, pp. 1108-1136.

CALIFORNIA DIVISION OF MINES AND GEOLOGY (1992), "Draft Guidelines: Liquefaction Hazard Zones," Sacramento, California.

CASAGRANDE, A. (1936), "Characteristics of Cohesionless Soils Affecting the Stability of Slopes and Earth Fills", *Journal of the Boston Society of Civil Engineers*.

CASAGRANDE, A. (1976), "Liquefaction and Cyclic Mobility of Sands: A Critical Review," Harvard Soil Mechanics, Series 88, Harvard University, Cambridge, Massachusetts.

CASTRO, G. (1969), "Liquefaction of Sands," thesis presented to Harvard University, Cambridge, Massachusetts, in partial fulfilment of the requirements of the degree of Doctor of Philosophy.

CASTRO, G., and **POULOS, S.J.** (1977), "Factors Affecting Liquefaction and Cyclic Mobility", *Journal of the Geotechnical Engineering Division*, A.S.C.E., Vol.103, No GT6, pp. 501-517.

CASTRO, G., SEED, R.B., KELLER, T.O., and **SEED, H.B.** (1992), "Steady-State Strength Analysis of Lower San Fernando Dam Slide," Journal of Geotechnical Engineering, A.S.C.E., Vol. 118, No. 3, pp. 406-427.

CHRISTIAN, J. T. (1980), "Probabilistic Soil Dynamics: State of the Art," *Journal of the Geotechnical Engineering Division*, ASCE, Vol. 106(4), pp. 385-397.

COPP, D.M. (1996), "The Preparation of Partially Saturated Sand Samples," thesis submitted to the University of Swansea in partial fulfilment of the requirements of the degree of M.Sc.

DAVILA, R.S., SEGO, D.C., and **ROBERTSON, P.K.** (1992), "Undisturbed Sampling of Sandy Soil by Freezing," *Canadian Geotechnical Conference Proceedings*, Totonto, pp.13A-1 to 13A-10.

DAVIS, R.O., and **BERRILL, J.B.** (1998), "Energy Dissipation and Liquefaction at Port Island, Kobe," *Bulletin*, New Zealand National Society for Earthquake Engineering, Waikanae, New Zealand, Vol. 31, pp. 31-50.

DESAI, C.S. (2000), "Evaluation of Liquefaction Using Disturbed State and Energy Approaches," *Journal of Geotechnical and Geoenvironmental Engineering*, A.S.C.E., Vol. 126, No. 7, pp. 618-631.

DIKMEN, S.U., and **GHABOUSSI, J.** (1984), "Effective Stress Analysis of Seismic Response and Liquefaction," *Journal of Geotechnical Engineering*, A.S.C.E., Vol.110(5), pp. 628-644.

DOANH, T., IBRAIM, E., DUBUJET, P., MATIOTTI, R., and **HERLE, I.** (1999), "Static Liquefaction of Very Loose Hostun RF Sand: Experiments and

Modelling," *Physics and Mechanics of Soil Liquefaction*, Lade & Yamamuro (eds.), Balkema, Rotterdam.

DONALD, I.B. (1961), "The Mechanical Properties of Saturated and Partially Saturated Soils with Special Reference to Negative Pore Water Pressure," thesis submitted to the University of London in partial fulfilment of the requirements of the degree of Doctor of Philosophy.

DORSEY, N.E. (1940), "Properties of Ordinary Water Substances'" American Chemical Society, Mono. Series, Reinhold, New York.

DYVIK, R., BERRE, T., LACASSE, S., and **RAADIM, B.** (1987), "Comparison of Truly Undrained and Constant Volume Direct Simple Shear Tests," *Geotechnique*, Vol. 37, No. 1, pp. 3-10.

EDUPRO CIVIL SYSTEMS LTD., *ProShake Computer Software User's Manual*, Version 1.1.

ELGAMAL, A.W., ZEGHAL, M., and **PARRA, E.** (1996), "Liquefaction of Reclaimed Island in Kobe, Japan", *Journal of Geotechnical Engineering*, A.S.C.E., Vol. 122, No. GT1, pp. 39-49.

ELGAMAL, A.W., PARRA, E., YANG, Z., DOBRY, R., ZEGHAL, M. (1999), "Liquefaction Constitutive Model," *Physics and Mechanics of Soil Liquefaction*, Balkema, Rotterdam.

ELLIS, E.A., SOGA, K., BRANSBY, M.F., and **SATO, M.** (2000), "Resonant Column Testing of Sands with Different Viscosity Pore Fluids," *Journal of Geotechnical Engineering*, A.S.C.E., Vol. 126, No. 1, pp. 10-17.

EVANS, M.D., and **ZHOU, S.** (1995), "Liquefaction Behaviour of Sand-Gravel Composites," *Journal of Geotechnical Engineering*, A.S.C.E., Vol. 121, No. 3, pp. 287-298.

FELLENIUS, B. (1955), "The Landslide at Guntorp," *Geotechnique*, Vol. 5, No. 1, pp. 120-125.

FIEGEL, G.L., and **KUTTER, B.L.** (1994), "Liquefaction Mechanism for Layered Soils," *Journal of Geotechnical Engineering*, A.S.C.E., Vol. 120, No. 4, pp. 737-755.

FINN, W.D.L., EMERY, J.J., and **GUPTA, Y.P.** (1971), "Liquefaction of Large Samples of Saturated Sand on a Shaking Table," *Proceedings*, 1st Canadian Conference on earthquake Engineering, Vancouver, Canada, pp. 97-110.

FINN, W.D.L., LEE, K.W., and **MARTIN, G.R.** (1975), "Stress Strain Relations for Sand in Simple Shear," presented at the A.S.C.E. Annual Convention and Cexpo '75, held at Denver, Colorado, November 3-7, 1975.

FINN, W.D.L., LEE, K.W., and **MARTIN, G.R.** (1977), "An Effective Stress Model for Liquefaction," *Journal of the Geotechnical Engineering Division*, A.S.C.E., Vol. 103, No. GT6, pp. 517-533

FINN, W.D.L., PICKERING, D.J., and **BRANSBY, P.L.** (1971a), "Sand Liquefaction in Triaxial and Simple Shear Tests," *Journal of the Soil Mechanics and Foundations Division*, A.S.C.E., Vol. 97, No. SM4, Proc. Paper 8039, pp. 639-659.

FINN, W.D.L., PICKERING, D.J., and **BRANSBY, P.L.** (1971b), "Effect of Strain History on Liquefaction of Sand," *Journal of the Soil Mechanics and Foundations Division*, A.S.C.E., Vol. 96, No. SM6, Proc. Paper 7670, pp. 1917-1934.

FLAVIGNY, E., DESURES, J., and **PALAYER, B.** (1990), "Le Sable Hostun RF," *Revue Française de Géotechnique*, Volume 53, pp. 67-69.

FOURIE, A.B., HOFMANN, B.A., MIKULA, R.J., LORD, E.R.F., and **ROBERTSON, P.K.** (2001), "Partially Saturated Tailings Sand below the Phreatic Surface," *Géotechnique*, Vol. 51, No. 7, pp 577-585.

FREDLUND, D.G., and **MORGANSTERN, N.R.** (1976), "Constitutive Relations for Volume Change in Unsaturated Soils," Canadian Geotechnical Journal, Vol.13, No.3, pp. 261-276.

FREDLUND, D.G., and **MORGANSTERN, N.R.** (1977), "Stress State Variables for Unsaturated Soils," Journal of the Geotechnical Engineering Division, Vol. 103, No. GT5, pp. 447-466.

FREDLUND, D.G., and **RAHARDJO, H.** (1993), "Soil Mechanics for Unsaturated Soils," John Wiley & Sons, Inc.

FREDLUND, D.G., MORGANSTERN, N.R., and **WIDGER, R.A.** (1978), "The Shear Strength of Unsaturated Soils," *Canadian Geotechnical Journal*, Vol. 15, No. 3, pp. 313-321.

GOHL, W.B., JEFFERIES, M.G., HOWIE, J.A., and **DIGGLE, D.** (2000), "Explosive Compaction: Design, Implementation, and Effectiveness," *Géotechnique*, Vol. 50, No. 6, pp. 657-665.

GHABOUSSI, J., and **DIKMEN, S. U.** (1981), "Liquefaction Analysis for Multidirectional Shaking," *Journal of the Geotechnical Engineering Division*, ASCE, Vol. 107(5), pp. 605-627.

HACHEY, J.E., PLUM, R.L., BYRNE, R.J., KILIAN, A.P., and **JENKINS, D.V.** (1994), "Blast Densification of a Thick, Loose Debris Flow at Mt. St. Helen's, Washington," *Proceedings*, Vertical and Horizontal Deformations of Foundations and Embankments, Geotechnical Special Publication No. 40, A.S.C.E., College Station, Texas, pp. 502-512.

HASHEMI, H.T., and **SLIEPCEVICH, C.M.** (1973), "Effect of Seepage Stream of Artificial Soil Freezing," *Proceedings*, Ground Freezing Conference, Developments in Geotechnical Engineering, Vol. 28, pp.189-201.

HAZEN, A. (1920), "Hydraulic Fill Dams", *Transactions*, A.S.C.E., Vol. 83, Paper No. 1458, pp.1713-1745.

HEALY, A.K. (1963), "Preliminary Investigations Into the Liquefaction of Sand," *Research Report R63-29*, Department of Civil Engineering, Massachusetts Institute of Technology, Cambridge, Massachusetts.

HICKS, M.A., and **BOUGHRAROV, R.** (1998), "Finite Element Analysis of the Nerlerk Underwater Berm Failure," *Géotechnique*, Vol. 48, No. 2, pp. 169-185.

HOFMANN, B.A. (1997), "In-Situ Ground Freezing to Obtain Undisturbed Samples of Loose Sand for Liquefaction Assessment," thesis submitted to the University of Alberta, Edmonton, in partial fulfilment of the Degree of Doctor of Philosophy.

HOFFMAN, B.A., SEGO, D.C., ROBERTSON, P.K. (1998), "Feasibility of In-Situ Ground Freezing to Obtain Undisturbed Samples of Loose Sand," paper submitted to A.S.C.E.

HOUGH, B.K. (1957), "Basic Soils Engineering," Ronald Press, New York.

HRYCIW, R. D., VITTON, S., and **THOMANN, T. G.** (1990), "Liquefaction and Flow failure During Seismic Exploration," *Journal of Geotechnical Engineering*, ASCE, Vol.116, No. 12, pp. 1881-1889.

IAI, S., and **BARDET, J.P.** (2001), "Plane Strain Instability of Saturated Elasto-Plastic Soils," *Géotechnique*, Vol. 51, No. 5, pp. 389-398.

ISHIHARA, K. (1984), "Post-Earthquake Failure of a Tailings Dam due to Liquefaction of the Pond Deposit", *Proceedings, International Conference on Case Histories in Geotechnical Engineering*, University of Missouri, St. Louis, Vol. 3, pp. 1129-1143.

ISHIHARA, K. (1993), "Liquefaction and Flow Failure During Earthquakes," *Géotechnique*, Vol. 43, No. 3, pp. 351-415.

ISHIHARA, K., KAWASE, Y., and **NAKAJIMA, M.** (1980), "Liquefaction Characteristics of Sand Deposits at an Oil Tank Site during the 1978 Miyagiken-Oki Earthquake," *Soils and Foundations*, Tokyo, Vol. 20, No. 2, pp. 97-111.

JAMIOLKOWSKI, M., and **LO PRESTI, D.C.F.** (1990), "Correlation between Liquefaction Resistance and Shear Wave Velocity," *Soils and Foundations*, Vol. 32, No. 2, pp. 145-148.

JEFFERIES, M.G., (1999), "A Critical State View of Liquefaction," *Physics and Mechanics of Soil Liquefaction*, Balkema, Rotterdam.

JOER, H.A., LANIER, J., and **FAHEY, M.** (1998), "Deformation of Granular Materials due to Rotation of the Principal Axes," *Géotechnique*, Vol. 48, No.5, pp. 605-619.

JUANG, C.H., CHEN, C.J., and **JIANG, T.** (2001), "Probabilistic Framework for Liquefaction Potential by Shear Wave Velocity," *Journal of Geotechnical and Geoenvironmental Engineering*, Vol. 127, No. 8, pp. 670-678.

JUANG, C.H., CHEN, C.J., TANG, W.H., and **ROSOWSKY, D.V.** (2000 a), "CPT-Based Liquefaction Analysis, Part 1: Determination of Limit State Function," *Géotechnique*, Vol. 50, No. 5, pp. 583-592.

JUANG, C.H., CHEN, C.J., ROSOWSKY, D.V., and **TANG, W.H.** (2000 b), "CPT-Based Liquefaction Analysis, Part 2: Reliability for Design," *Géotechnique*, Vol. 50, No. 5, pp. 593-599.

KAGAWA, T., and **LELAND, M.K., Jnr.** (1981), "Modeling the Liquefaction Process", *Journal of the Geotechnical Engineering Division*, A.S.C.E., Vol 107(12), pp. 1593-1607.

KARSTUNEN, M., and **PANDE, G.N.** (1994), "On the Mechanical Response of Gassy Clays: Some Theoretical Considerations," *Numerical Methods in Geotechnical Engineering*, Balkema, Rotterdam.

KAWAKAMI and **ASADA** (1966), "Damage to Ground and Earth Structures Caused by the Niigata Earthquake of June 16, 1964," Soils and Foundations, Vol. 6, No. 1, pp. 14-30.

KERWIN, S.T., and **STONE, J.J.** (1997), "Liquefaction Failure and Remediation: King Harbor, Redondo Beach, California," *Journal of Geotechnical and Geoenvironmental Engineering*, Vol. 123, No. 8, pp. 760-769.

KISHIDA, H. (1965), "Damage of Reinforced Concrete Buildings in Niigata City with Special Reference to Foundation Engineering", *Soils and Foundations*, Vol. 6, No.1.

KO, K.-Y., and **DEWOOLKAR, M.M.** (1999), "Modeling Liquefaction in Centrifuges," *Physics and Mechanics of Soil Liquefaction*, Balkema, Rotterdam.

KOGAMI, T., and **KUBU, K.**, "The Behaviour of Soil During Vibration", *Proceedings, 3rd International Conference on Soil Mechanics and Foundation Engineering*, Zurich, Volume 1, pp. 152-155.

KOKOSHU, T. (1999), "Water-Film on Liquefied Sand and its Effects on Lateral Spreads," Journal of Geotechnical and Geoenvironmental Engineering, A.S.C.E., Vol. 125, No. 10, pp. 817-826.

KONRAD, J.M., and **MORGANSTERN, N.R.** (1980), "A Mechanistic Theory of Ice Lens Formation in Fine Grained Soils," *Canadian Geotechnical Journal*, Vol. 17, pp. 473-486.

KOVACS, W.D., and **LEO, E.** (1981), "Cyclic Simple Shear of Large-Scale Samples," *Proceedings*, International Conference on recent Advances in Geotechnical Earthquake Engineering and Soil Dynamics, St. Louis, Missouri, Vol. 3, pp. 897-907.

KRAMER, S. L. (1988), "Triggering of Liquefaction Flow Slides in Coastal Soil Deposits," *Engineering Geology*, Vol. 26, No. 1, pp. 17-31.

KRAMER, S.L. (1996), "Geotechnical Earthquake Engineering", *Prentice-Hall Series in Civil Engineering and Engineering Mechanics.*

KRAMER, S. L., and **SEED, H. B.** (1988), "Initiation of Soil Liquefaction Under Static Loading Conditions," *Journal of Geotechnical Engineering*, ASCE, Vol. 114, No. 4, pp. 412-430.

KRISHNASWAMY, N.R., and **ISAAC, N.T.** (1995), "Liquefaction Analysis of Saturated Reinforced Granular Soils," *Journal of Geotechnical Engineering*, A.S.C.E., Vol. 121, No. 9, pp. 645-651.

LADD, R.S. (1977), "Specimen Preparation and Cyclic Stability of Sands," *Journal of the Geotechnical Engineering Division*, ASCE, Vol. 103, No. GT6, pp. 535-547.

LADD, R.S. (1978), "Preparing Test Specimens Using Undercompaction," *Geotechnical Testing Journal*, Vol. 1, No. 1, pp. 16-23.

LADE, P. V. (1992), "Static Instability and Liquefaction of Loose Fine Sandy Slopes," *Journal of Geotechnical Engineering*, ASCE, Vol. 118, No. 1, pp. 51-71.

LADE, P. V. (1999), "Instability of Granular Materials," *Physics and Mechanics of Soil Liquefaction*, A. A. Balkema (Publishers), Rotterdam, pp. 3-16.

LAMBE, T.W. (1967), "Stress Path Method," *Journal of the Soil Mechanics and Foundations Division*, A.S.C.E., Vol. 93, No. SM6.

LEE, K.L., and **SEED, H.B.** (1967), "Cyclic Stress Conditions Causing Liquefaction of Sand," Journal of the Soil Mechanics and Foundations Division, A.S.C.E., Vol. 93, No. SM1, Proc. Paper 5058, pp. 47-70.

LIU, H., and **QIAO, T.** (1984), "Liquefaction Potential on Saturated Sand During Earthquakes," 8th World Conference of Earthquake Engineering, I.A.E.E., Vol. 3, pp. 199-206.

MADABHUSHI, S.P.G., and **SCHOFIELD, A.N.** (1993), "Centrifuge Modelling of Tower Structures on Saturated Sands Subjected to Earthquake Perturbations," *Géotechnique*, Vol. 43, No. 4, pp. 555-565.

MARCUSON, W.F., III (1978), "Definition of Terms Related to Liquefaction," *Journal of the Geotechnical Engineering Division*, A.S.C.E., Vol. 104, No. 9, pp. 1197-1200.

MARTIN, J.R., II, and **CLOUGH, G.W.** (1994), "Seismic Parameters from Liquefaction Evidence," *Journal of Geotechnical Engineering*, A.S.C.E., Vol. 120, No. 8, pp. 1345-1361.

MATSUI, T. (1994), "Major Onshore and Offshore Projects in the Osaka Bay Area," *Proceedings*, 4th International Offshore and Polar Engineering Conference, Osaka, Japan, Vol. I, pp. 8-17.

MENESES-LOJA, J., and **ISHIHARA, K.** (2000), "Flow Failure of Saturated Sand Under Simultaneous Monotonic and Cyclic Stresses," *Journal of Geotechnical and Geoenvironmental Engineering*, A.S.C.E., Vol. 126, No. 2, pp. 131-138.

MOGAMI, T., and **KABU, K.** (1953), "The Behaviour of Soil During Vibration," *Proceedings*, 3rd International Conference on Soil Mechanics and Foundation Engineering, Zurich, Vol.1, pp.152-155.

MOHAMAD, R., and **DOBRY, R.** (1986), "Undrained Monotonic and Cyclic Triaxial Strength of Sand," *Journal of Geotechnical Engineering*, Vol. 112, No. 10, pp. 941-958.

MORGANSTERN, N.R. (1979), "Properties of Compacted Soils," contribution to Panel Discussion, Session IV, *Proceedings of the 6th Pan-American Conference of Soil Mechanics and Foundations Engineering*, Lima, Peru, Vol. 3, pp. 349-354.

MULILIS, J.P. (1975), "The Effects of Method of Sample Preparation on the Cyclic Stress-Strain Behaviour of Sand," thesis presented to the University of California at Berkeley, California, in partial fulfilment of the degree of Doctor of Philosophy.

NEMAT-NASSER, S., and **TAKAHASHI, K.** (1984), "Liquefaction and Fabric of Sand," *Journal of Geotechnical Engineering*, ASCE, Vol. 110(9), pp. 1291-1306.

NORRIS, G., **SIDDHARTAN, R.**, **ZAFIR, Z.**, and **MADHU, R.** (1997), "Liquefaction and Residual Strength of Sands from Drained Triaxial Tests," *Journal of Geotechnical and Geoenvironmental Engineering*, A.S.C.E., Vol. 123, No. 3, pp. 220-228.

ODA, M. (1972), "The Mechanism of Fabric Changes During the Compressional Deformation of Sand," *Soils and Foundations*, Vol. 12, pp. 1-18.

OLSEN, S.M., **STARK, T.D.**, **WALTON, W.H.**, and **CASTRO, G.** (2000), "1907 Static Liquefaction Flow Failure of the North Dike of the Wachusett Dam," *Journal of Geotechnical and Geoenvironmental Engineering*, Vol. 126, No. 12, pp. 1184-1193.

PEACOCK, W.H., and **SEED, H.B.** (1968), "Sand Liquefaction under Cyclic Loading Simple Shear Conditions," *Journal of the Soil Mechanics and Foundations Division*, ASCE, Vol. 94, No. SM3, Proc. Paper 5957, pp. 689-708.

PECK, R.B. (1979), "Liquefaction Potential – Science Versus Practice", *Journal of the Geotechnical Engineering Division*, ASCE, Vol. 105, No. GT3, pp. 393-398.

PIETRUSZCZAK, S. (1994), "A Continuum Theory of Granular Media Partially Saturated with a Viscous Fluid," *International Journal for Numerical and Analytical Methods in Geomechanics*, Vol. 18, pp. 93-105.

PIETRUSZCZAK, S., and **OULAPOUR, M.** (1999), "Assessment of Dynamic Stability of Foundations on Saturated Sandy Soils," *Journal of Geotechnical and Geoenvironmental Engineering*, A.S.C.E., Vol. 125, No. 7, pp. 576-582.

PIETRUSZCZAK, S., and **PANDE, G.N.** (1995), "On the Mechanical Response of Partially Saturated Soils at Low and High Degrees of Saturation," *Numerical Models in Geomechanics (NUMOG V)*, Balkema, Rotterdam.

PIETRUSZCZAK, S., and **PANDE, G.N.** (1996), "Constitutive Relations for Partially Saturated Soils Containing Gas Inclusions", *Journal of Geotechnical Engineering*, A.S.C.E., Vol. 122, No. 1, pp. 50-59.

PILGRIM, N.K. (1998), "Earthquake-Related Deformation Beneath Gently Inclined Ground," *Géotechnique*, Vol. 48, No. 2, pp. 187-199.

POLITO, C.P., and **MARTIN, J.R., II** (2001), "Effects of Nonplastic Fines on the Liquefaction Resistance of Sands," *Journal of Geotechnical and Geoenvironmental Engineering*, A.S.C.E., Vol. 127, No. 5, pp. 408-415.

POULOS, H.G., and **DAVIS, E.H.** (1974), "Elastic Solutions for Soil and Rock Mechanics," John Wiley and Sons Inc., New York.

PYKE, R. (1979), "Non-Linear Models for Irregular Cyclic Loadings", *Journal of the Geotechnical Engineering Division*, A.S.C.E., Vol. 105, No. GT6, Proc. Paper 14642, pp. 715-726.

RAUCH, A.F., and **MARTIN, J.R. II** (2000), "EPOLLS Model for Predicting Average Displacements on Lateral Spreads," *Journal of Geotechnical and Geoenvironmental Engineering*, Vol. 126, No. 4, pp. 360-371.

ROBERTSON, P.K., **HOFMANN, B.A.**, and **LIST, B.R.** (1995), "CANLEX (Canadian Liquefaction Experiment): A One-Year Update," *Proceedings*, 3rd International Conference on Recent Advances in Geotechnical Earthquake Engineering Soil Dynamics, St. Louis, pp. 815-823.

RODEBUSH, W.H., and **BUSSWELL, A.M.** (1958), "Properties of Water Substances," Highway Res. Board Special Report No.40.

ROLLINS, K.M., and **SEED, H.B.** (1990), "Influence of Buildings on Potential Liquefaction Damage," *Journal of Geotechnical Engineering*, A.S.C.E., Vol.116, pp. 165-185.

ROY, D., **CAMPANELLA, R.G.**, **BYRNE, P.M.**, and **HUGHES, J.M.O.** (1996), "Strain Level and Uncertainty of Liquefaction Related Index Tests," *Uncertainty in the Geologic Environment: From Theory to Practice*, Geotechnical Special Publication, Vol. 2, No. 58, Shackleford, Nelson, and Roth (eds.), A.S.C.E., New York, pp. 1143-1162.

SANGER, F.J., and **SAYLES, F.H.** (1979), "Thermal and Rheological Computations for Artificially Frozen Ground Construction," *Engineering Geology*, Vol. 13, pp. 311-337.

SASSA, S., and **SEKIGUCHI, H.** (2001), "Analysis of Wave-Induced Liquefaction of Sand Beds," *Géotechnique,* Vol. 51, No. 2, pp. 115-126.

SASSA, S., SEKIGUCHI, H., and **MIYAMOTU, J.** (2001), "Analysis of Progressive Liquefaction as a Moving Boundary Problem," *Géotechnique*, Vol. 51, No. 10, pp. 847-857.

SEED, H.B. (1968), "Landslides During Earthquakes due to Soil Liquefaction," 4th Terzaghi Lecture, *Proceedings*, A.S.C.E., New York, No. SM-5, pp. 1053-1122.

SEED, H.B. (1979), "Soil Liquefaction and Cyclic Mobility Evaluation for Level Ground During Earthquakes", *Journal of the Geotechnical Engineering Division*, A.S.C.E., Vol. 105(2), pp. 201-255.

SEED, H.B., and **IDRISS, I.M.** (1967), "Analysis of Soil Liquefaction: Niigata Earthquake", *Journal of the Soil Mechanics and Foundations Division*, A.S.C.E., Vol. 93, No.SM3, Proc. Paper 5233, pp. 83-108.

SEED, H.B., and **IDRISS, I.M.** (1982), "Ground Motions and Soil Liquefaction During Earthquakes," Earthquake Engineering Research Institute Monograph, 134p.

SEED, H.B., IDRISS, I.M., and **ARANGO, I.** (1983), "Evaluation of Liquefaction Potential Using Field Performance Data," *Journal of Geotechnical Engineering*, A.S.C.E., Vol. 109, No.3, pp. 458-482.

SEED, H.B., and **LEE, K.L.** (1966), "Liquefaction of Saturated Sands During Cyclic Loading," *Journal of the Soil Mechanics and Foundations Division*, ASCE, Vol. 92, No. SM6, pp. 105-134.

SEED, H.B., and **PEACOCK, W.H.** (1971), "Test Procedures for Measuring Soil Liquefaction Characteristics", *Journal of the Soil Mechanics and Foundations Division*, A.S.C.E., Vol. 97, No. SM8, pp. 1099-1119.

SEED, H.B., SINGH, M., CHAN, C.K., and **VILELA, T.F.** (1982), "Considerations in Undisturbed Sampling of Sands," *Journal of the*

Geotechnical Engineering Division, A.S.C.E., No. GT2, Vol. 108, pp. 265-283.

SEED, H.B., and **WILSON, S.D.** (1967), "The Turnagain Heights Landslide, Anchorage, Alaska", *Journal of the Soil Mechanics and Foundations Division*, A.S.C.E., No. SM4, Proc. Paper 5320, pp. 325-353.

SEGO, D.C., HOFMANN, B.A., ROBERTSON, P.K., and **WRIDE, C.E.** (1999), "Undisturbed Sampling of Loose Sand Using In-Situ Ground Freezing," *Physics and Mechanics of Soil Liquefaction*, Balkema, Rotterdam.

SILLS, G.C., WHEELER, S.J., THOMAS, S.D., and **GARDNER, T.N.** (1991), "Behaviour of Offshore Soils Containing Gas Bubbles," *Geotechnique*, Vol. 41, No. 2, pp. 227-241.

SILVER, M.L., and **SEED, H.B.** (1971a), "Deformation Characteristics of Sands Under Cyclic Loading," *Journal of the Soil Mechanics and Foundations Division*, A.S.C.E., Vol. 97, No. SM8, Proc. Paper 8334, pp. 1081-1098.

SILVER, M.L., and **SEED, H.B.** (1971b), "Volume Changes in Sands During Cyclic Loading," Journal of the Soil Mechanics and Foundations Division, A.S.C.E., Vol. 97, No. SM9, Proc Paper 8354, pp. 1171-1182.

SKEMPTON, A.W. (1956), "The Pore Pressure Coefficients A and B," *Geotechnique*, Volume 4, pp. 143-147.

SOLYMAR, Z.V., and **REED, D.J.** (1986), "A Comparison of Foundation Compaction Techniques," *Canadian Geotechnical Journal*, Volume 23, No.3, pp. 271-280.

STARK, T.D., and **OLSEN, S.M.** (1995), "Liquefaction Resistance Using CPT and Field Case Histories," *Journal of Geotechnical Engineering*, A.S.C.E., Vol. 121, No. 12, pp. 856-869.

STILLEY, A.N. (1982), "Compaction Grouting for Foundation Stabilization," *Proceedings*, A.S.C.E. Specialty Conference on Grouting in Geotechnical Engineering, New Orleans, Louisiana, pp. 923-937.

TABODA-URTUZUASTEGUI, V.M., and **DOBRY, R.** (1998), "Centrifuge Modeling of earthquake-Induced Lateral Spreading in Sand," *Journal and Geotechnical and Geoenvironmental Engineering*, A.S.C.E., Vol. 124, No. 12, pp. 1195-1206.

TERZAGHI, K. (1936), "The Shear Resistance of Saturated Soils," *Proceedings*, First International Conference on Soil Mechanics and Foundations Engineering, Vol. 1, pp. 54-56.

TERZAGHI, K. (1956), "Varieties of Submarine Slope Failures," *Proceedings*, 8th Texas Conference on Soil Mechanics and Foundations Engineering, pp 1-41.

THEVANAYAGAM, S., and **MOHAN, S.** (2000), "Intergranular State Variables and Stress-Strain Behaviour of Silty Sands," *Géotechnique*, Vol. 50, No. 1, pp. 1-23.

TIMOSHENKO, S.P., and **GOODIER, J.N.** (1951), "Theory of Plasticity," 2nd Edition, McGraw-Hill (Publishers), New York.

TOKIMATSU, K., **KOJIMA, H.**, **KUWAYAMA, S.**, **ABE, A.**, and **MIDORIKAWA, S.** (1994), "Liquefaction-Induced Damage to Buildings in 1990 Luzon Earthquake," *Journal of Geotechnical Engineering*, A.S.C.E., Vol. 120, No. 2, pp. 290-307.

TSATSANIFOS, C.P., and **SARMA, S.K.** (1982), "Pore Pressure Rise During Cyclic Loading of Sands", *Journal of the Geotechnical Engineering Division*, A.S.C.E., Vol. 108(2), pp. 315-319.

VAID, Y. P., and **CHERN, J. C.** (1983), "Effect of Static Shear on Resistance of Liquefaction," *Soils and Foundations*, Vol. 23, No. 1, pp. 47-60.

VAID, Y.P., and **THOMAS, J.** (1995), "Liquefaction and Post-Liquefaction Behavior of Sand," *Journal of Geotechnical Engineering*, A.S.C.E., Vol. 121, No. 2, pp. 163-173.

VASQUEZ-HERRERA, A., and **DOBRY, R.** (1989), "The Behaviour of Undrained Contractive Sand and its Effects on Seismic Liquefaction Flow Failures of Earth Structures," Contract No. 86-003, Department of Army, U.S. Army Corps of Engineers, Washington D.C.

WANG, G., and **SASSA, K.** (2001), "Factors Affecting Rainfall-Induced Flowslides in Laboratory Flume Tests," *Géotechnique*, Vol. 51, No. 7, pp. 587-599.

WANG, W. (1979), "Some Findings on Soil Liquefaction," Water Conservancy and Hydroelectric Power Institute, Beijing, China.

WARNER, J. (1982), "Compaction Grouting – The First Thirty Years", *Proceedings*, A.S.C.E. Speciality Conference on Grouting in Geotechnical Engineering, New Orleans, Louisiana, pp. 694-707.

WATANABE, T. (1966), "Damage to Oil Refinery Plants and a Building on Compacted Ground by the Niigata Earthquake and their Restoration," *Soils and Foundations*, Tokyo, Vol. 6(2), pp. 86-99.

WHEELER, S.J. (1988), "A Conceptual Model for Soils Containing Large Gas Bubbles," *Geotechnique*, Vol. 38, No. 3, pp. 389-397.

WILSON, D.W., **BOULANGER, R.W.**, and **KUTTER, B.L.** (2000), "Observed Seismic Lateral Resistance of Liquefying Sand," *Journal of Geotechnical and Geoenvironmental Engineering*, A.S.C.E., Vol. 126, No. 10, pp. 898-906.

YOSHIMI, Y.K., TOMIMATSU, K., KANEKO, O., and **MAKIHARA, Y.** (1994), "Undrained Cyclic Shear Strength of a Dense Niigata Sand," *Soils and Foundations*, Vol. 24, No. 4, pp. 131-145.

YOUD, T.L., and **HOOSE, S.N.** (1977), "Liquefaction Susceptibility and Geologic Setting," *Proceedings, 6th World Conference on Earthquake Engineering*, New Delhi, India, Vol. 3, pp. 2189-2194.

YOUD, T.L., and **HOOSE, S.N.** (1978), "Historic Ground Failures in Northern California Triggered by Earthquakes," U.S. Geological Survey Professional Paper 993.

YOUD, T.L., and **IDRISS, I.M.,** eds. (1997), "NCEER Workshop on Evaluation of Liquefaction Resistance of Soils," *Technical Report NCEER-97-0022*, National Center for Earthquake Engineering Research, State University of New York, Buffalo.

YOUD, T.L., IDRISS, I.M., ANDRUS, R.D., ARANGO, I., CASTRO, G., CHRISTIAN, J.T., DOBRY, R., FINN, W.D.L., HARDER, L.F. Jnr., HYNES, M.E., ISHIHARA, K., KOESTER, J.P., LIAO, S.S.C., MARCUSON, W.F. III, MARTIN G.R., MITCHELL, J.K. , MORIWAKI, Y., POWER, M.S., ROBERTSON, P.K., SEED, R.B., STOKOE, K.H. II (2001), "Liquefaction Resistance of Soils: Summary Report from the 1996 NCEER and 1998 NCEER/NSF Workshops on Evaluation of Liquefaction Resistance of Soils, Journal of Geotechnical and Geoenvironmental Engineering, Vol. 127, No. 4, pp 297-313.

ZENG, X., and **ARULANANDAN, K.** (1995), "Modeling Lateral Sliding of Slope due to Liquefaction," *Journal of Geotechnical Engineering*," A.S.C.E., Vol. 121, No. 11, pp. 814-816.

ZHANG, L. (1998), "Assessment of Liquefaction Potential using Optimum Seeking Method," *Journal of Geotechnical and Geoenvironmental Engineering*, A.S.C.E., Vol. 124, No. 8, pp. 739-748.

ON-LINE REFERENCES

www.geotechnics.com

Website of Geotechnics America Ltd., soil improvement specialists (U.S.A.).

www.eeri.org

Website of the Earthquake Engineering Research Institute.

www.haywardbaker.com

Soil Improvement Specialists (U.S.A.). This website provides more technical information on the more common methods of liquefaction mitigation in the field.

www.nisee.berkeley.edu

Website of Berkeley University, California, U.S.A.

www.liquefaction.com

Specialised liquefaction information site, maintained by Richard Olsen Ph.D.

www.bza.org

Website of the British Zeolite Association